ISSN O248451X

CENTRE NATIONAL DE LA RECHERCHE SCIENTIFIQUE

LABORATOIRE D'AEROTHERMIQUE

R 94-4

Rarefied gas flow simulation based on quasi gas dynamic equations

Tatiana ELIZAROVA, Irina GRAUR,
Jean-Claude LENGRAND et Amer CHPOUN

Août 1994

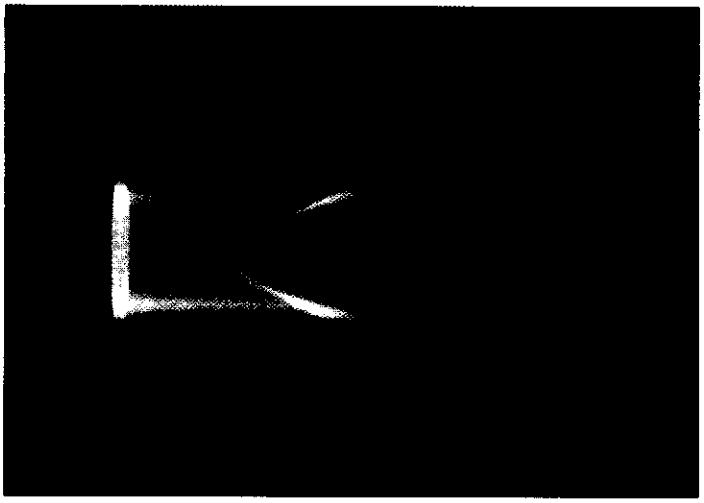

4 ter, route des Gardes
F-92190 MEUDON

Tél. Standard CNRS (1) 45 07 50 50
Tél. Aérothermique (1) 45 07 51 57
Fax Aérothermique (1) 45 07 58 20

ISSN O248451X

R 94-4

Rarefied gas flow simulation based on quasi gas dynamic equations

Tatiana ELIZAROVA, Irina GRAUR,
Jean-Claude LENGRAND et Amer CHPOUN

Août 1994

Rarefied Gas Flow Simulation Based on Quasi Gas Dynamic Equations

Elizarova T.G.[1], Graur I.A.[1], Lengrand J.C.[2], Chpoun A.[2]

[1] Institute for Mathematical Modelling, Russian Academy of Science
Miusskaya sq.4a, Moscow 125047, Russia

[2] Laboratoire d'Aérothermique du CNRS
4 ter, route des gardes, 92190 Meudon, France

August 16, 1994

Abstract

The treatment of rarefied gas flows by means of equations based on the mechanics of continuum media is desirable because solving such equations requires less computational resources than methods based on a molecular description. The present work aims at clarifying the domain of validity of two continuum approaches by comparing their results to a reference given by a Direct Simulation Monte Carlo method (DSMC). The first continuum approach is based on the usual Navier-Stokes (NS) equations. The second one is based on the Quasi-Gas-Dynamic (QGD) equations which are derived from Boltzmann equation with an additional diffusion term. The present paper includes a self-consistent presentation of QGD equations. The flow around a flat plate has been considered for a freestream Mach number varying from 1.5 to 20 and a wall temperature taken successively equal to freestream and stagnation temperatures. A criterion is proposed for the validity of the continuum approaches.

1 Introduction

The treatment of rarefied gas flows by means of equations based on the mechanics of continuum media is desirable because solving such equations requires less computational resources than methods based on a molecular description.

A popular way of handling rarefied flow problems consists in solving Navier-Stokes (NS) equations with modified boundary conditions (BCs) to account for velocity slip and temperature jump. Using Burnett equations is expected to lead to better results when the degree of non-equilibrium increases. However Burnett equations suffer from a number of disadvantages : they are considerably more complicated and there is no appropriate theory for writing their BCs. Furthermore there is little evidence that they bring any significant improvement compared with NS equations for problems of practical interest. Both Burnett and NS equations can be considered as approximate models derived from Boltzmann equation using different orders of approximations.

Starting from 1951 in papers by Sloskin [8], Valander [9], Alexeev [10], Klimontovich [11], [12] and Elizarova & Chetverushkin [13], [14] equations of the gas dynamical type, usually called generalized NS equations were constructed based on different hypotheses. These models differ from the NS model by the structure of the second order differential terms. They were used both for developing computational algorithms and were also considered as independent mathematical models in hydrodynamics.

In this paper, one type of generalized NS model — Quasi Gas Dynamic (QGD) equations — is presented. QGD equations were originally constructed based on a kinetical model for the distribution function and were successively used for creating stable numerical methods for viscous supersonic flows. Computational schemes obtained were called kinetical-consistent finite-difference (KCFD) schemes [14]. The possibility of applying kinetical-consistent finite-difference schemes based directly on a finite-difference approximation of kinetical equations is considered in [23] and [24] for slightly rarefied gases. Now we consider QGD system of equations as a specific mathematical model for gas flows simulation.

A number of theoretical results have already been obtained in [19, 16, 17] for QGD equations. Particularly, the connection between QGD and NS was established. It was shown that for a stationary case, NS equations are the asymptotic limit of QGD equations for $\tau \longrightarrow 0$, where τ is a characteristic collisional time. In a non-stationary case, NS equations are the asymptotic limit of the so-called generalized QGD equations. The latter differ from QGD equations by an additional mixed space and time derivation of the second order. For QGD system the increase of the full thermodynamic entropy was demonstrated and the expression of the dissipation function was found. These properties must actually be confirmed for any equation system that pretends to describe gas dynamic flows. All these results have been presented in [20].

Application of QGD equations to the shock-wave problem was investigated theoretically in [15]. It was shown that the solution is smooth in a stationary case. For the case of negligibly small heat conductivity the increase of full entropy was proved. Some results for

the numerical simulation of the problem of stationary shock-wave structure are discussed in [22], [21], where results obtained for QGD model, NS model, kinetical model simulations and some experimental data are compared. It was shown that QGD model approximately describes the shock-wave structure in a wide range of Mach numbers. For low Mach numbers data obtained by NS, QGD and kinetical models are just similar. As Mach number increases, the NS model loses its stability while QGD equations continue to provide gas dynamical profiles, although approximately.

Recently a quasi hydrodynamic system of equations, similar to the QGD system, was constructed for incompressible viscous flows [25]. The corresponding dissipation function was found and the theorem about the decrease of mechanical energy was proved.

In the present paper QGD equations are presented. A comparison between numerical solutions of QGD and NS equations is made in the range of moderate Knudsen numbers, i.e. under conditions where the difference between the mentioned systems is not very small. As reference data the results given by a Direct Simulation Monte Carlo method (DSMC) [28] are used.

The test-problem retained was the flow around a semi-infinite sharp flat plane parallel to the direction of the freestream. A systematic study was carried out by varying the freestream Mach number M_1 from 1.5 to 20 and setting the wall temperature T_w equal successively to the freestream temperature T_1 and to the freestream stagnation temperature T_0. Particular attention was paid to using consistent physical modeling in all approaches considered : monoatomic hard-sphere gas with full accommodation at the wall, resulting in a viscosity law $\mu \propto T^{0.5}$ and a Prandtl number equal to $Pr = 2/3$.

Because the problem considered does not introduce any length scale except the freestream mean free path, the abscissa along the plate is directly related to any parameter that characterizes usually the degree of rarefaction of the flow : Reynolds number Re, rarefaction parameter $\bar{V}$, interaction parameter χ, Knudsen number Kn, etc. In other words considering different abscissae along the plate is equivalent to considering different rarefaction levels.

The objective of the work reported herein was to examine whether QGD equations brought some improvement compared with NS equations for the treatment of rarefied flows. More specifically, the objective was to define a criterion for the validity of QGD and NS sets of equations. The present report is also an opportunity to give a self-consistent presentation of QGD equations.

2 Quasi Gas Dynamic model

2.1 Short presentation of QGD equations

For a quasi-stationary flow (i.e. varying slowly with time), the QGD system was written in an invariant form [19, 16] as

$$\rho_t + div\rho\vec{u} = div\tau(div\rho\vec{u} \otimes \vec{u} + \vec{\nabla}p) \tag{1}$$

$$\begin{gathered}(\rho\vec{u})_t + div(\rho\vec{u} \otimes \vec{u}) + \vec{\nabla}p = \\ = div\tau(div\rho\vec{u} \otimes \vec{u} \otimes \vec{u} + (\vec{\nabla} \otimes p\vec{u}) + (\vec{\nabla} \otimes p\vec{u})^T) + \nabla\tau div(p\vec{u})\end{gathered} \tag{2}$$

$$E_t + div((E+p)\vec{u}) = div\tau(div(E+2p)\vec{u} \otimes \vec{u} + \vec{\nabla}(p(E+p)/\rho)) \tag{3}$$

Considering a perfect-gas we add

$$E = \rho(\vec{u}^2/2 + \varepsilon),\ \varepsilon = p/\rho(\gamma - 1),\ p = \rho RT \tag{4}$$

Adding finally the initial and boundary conditions, we obtain a closed system of equations which describes the space-time evolution of the macroscopic parameters of the gas: $\vec{u}$ - velocity, ρ - density, p - pressure, E - total energy. T is the temperature, ε the internal energy and $\gamma = C_p/C_v$ is the specific heat ratio. The transport phenomena appear in the equations through a local characteristic time τ. Additional terms would be present to describe a general unsteady flow.

Eqs.1 - 3 can be obtained by averaging over molecular velocities a model kinetical equation in the form

$$f_t + (\vec{\xi}\nabla)f - (\vec{\xi}\nabla)\tau(\vec{\xi}\nabla)f = \mathcal{J}(f, f') \tag{5}$$

where $f = f(\vec{x}, \xi, t)$ is the one-particle distribution function that depends on space coordinates $\vec{x}$, molecular velocities $\vec{\xi}$ and time t. The right-hand side term is the collision integral $\mathcal{J}$. The procedure is illustrated in Appendix 1 for a 1-D flow.

In this paper we will not present in detail how Eq.5 was obtained. An equation like 5 was first obtained by Elizarova and Chetverushkin [13] by describing the molecular motion as a cyclic process of free flight and instantaneous maxwellization. For the phase of collisionless moving, they have expanded the distribution function into a Taylor series for the parameter $\xi\tau$. The diffusive-like term in Eq. 5 was obtained as a result of usual gradient expansion for space derivations. In the gas dynamic limit this term must remain small compared with the convection term. A similar additional term appears in the Fokker-Planck's equation that describes the diffusion motion of the heavy particles within a gas of light particles (brownian motion) [3].

Eq. 5 allows to derive macroscopic QGD equations that include viscosity and heat transfer even when the closure of the system is based on the equilibrium distribution function instead of a special "Navier-Stokes" expression for f. Dissipative terms in QGD equations appear when averaging the relaxation term in the form $(\vec{\xi}\nabla)\tau(\vec{\xi}\nabla)f$. In other words the structure of viscous and heat-conductive terms in 1– 3 is defined by the diffusive term in Eq.5.

The presence of this additional term in Eq. 5 allows to obtain QGD system that is not only closely connected to NS equations but also presents a number of advantages.

2.2 Relation between QGD and NS set of equations

Let NS equations be written as

$$\rho_t + div\rho\vec{u} = 0 \tag{6}$$

$$(\rho\vec{u})_t + div(\rho\vec{u}\otimes\vec{u}) + \vec{\nabla}p = div\sigma_{NS} \tag{7}$$

$$E_t + div((E+p)\vec{u}) = div\kappa\vec{\nabla}T + div\vec{u}\sigma_{NS} \tag{8}$$

where σ_{NS} is the NS shear-stress tensor, and κ is the thermal conductivity.

$$\sigma_{NS} = \mu((\vec{\nabla}\otimes\vec{u}) + (\vec{\nabla}\otimes\vec{u})^T - 2/3\mathcal{I}div\vec{u}). \tag{9}$$

and $\mathcal{I}$ is the unit-tensor.

The shear-stress tensor in Eq.2 of QGD system can be written in a form similar to Eq.9

$$\sigma_{QGD} = \tau(div\rho\vec{u}\otimes\vec{u}\otimes\vec{u} + (\vec{\nabla}\otimes p\vec{u}) + (\vec{\nabla}\otimes p\vec{u})^T + \mathcal{I}div(p\vec{u})). \tag{10}$$

With these notations the impulse equations for NS and QGD systems are formally identical and have the classical form of Eq.7.

For QGD system, an equation corresponding to the NS equation of entropy balance was found [19] :

$$(\rho S)_t + div(\rho S\vec{u}) = div\tau div(\rho S\vec{u}\otimes\vec{u}) + div(\tau S\nabla p) + div\left(\kappa\frac{\nabla T}{T}\right) + \frac{\Phi_{QGD}}{T} + \kappa\left(\frac{\nabla T}{T}\right)^2, \tag{11}$$

where $S = c_v\ln(p/\rho^\gamma) + \text{cste}$ is the specific entropy and

$$\Phi_{QGD} = \Phi_{NS} + \tau\frac{p}{\rho^2}(div\rho\vec{u})^2 + \frac{\tau}{\rho}(\rho(\vec{u}\nabla)\vec{u} + \vec{\nabla}p)^2 + \frac{\tau}{\rho\varepsilon}(\rho(\vec{u}\nabla)\varepsilon + pdiv\vec{u})^2. \tag{12}$$

is the dissipation function. It appears as the sum of NS dissipation function and the squares of left-hand side terms of classical Euler equations in stationary case each of them being multiplied by positive coefficients. The consequence of Eq.11 is the non-decreasing character of the full thermodynamic entropy in an adiabatic system described by QGD equations.

QGD equations differ from NS equations by the structure of the dissipative terms in the right-hand side of impulse and energy equations and by the presence of a divergence term in the right-hand side of the continuity equation. It was shown in [19] that these differences

are small in the stationary case. They are of the order $O(\tau^2)$. For the non-stationary case the same result was proved for generalized QGD system. If the classical boundary layer approximations are introduced, QGD system reduces to Prandtl equations [14].

As already mentioned, the continuity equation in QGD system has additional space derivatives of higher order than the corresponding NS equation. This is the reason why QGD system requires an additional boundary condition (BC). That additional BC was applied to the pressure gradient normal to the wall in the form

$$\partial p/\partial n = 0. \tag{13}$$

This relation is classical in the boundary layer approximation and in the derivation of slip BCs. This kind of additional BC is sometimes used in practice for the numerical solution of NS equations although it is not formally required.

As will be shown in section 2.3, the condition ($\tau \rightarrow 0$) that makes QGD equations reduce to NS equations corresponds to small Knudsen numbers. The numerical work that will be presented later confirms that QGD and NS results coincide for small values of Kn, and demonstrates that for moderate values of Kn, QGD results are closer to the reference DSMC results.

2.3 Relations with actual gas properties

Asymptotical convergence QGD system to NS one for small τ was obtained in [19] by identifying $\mu = p\tau$ and $\kappa = C_p p\tau$, where μ and κ denote viscosity and heat conductivity, respectively. This results in a Prandtl number $Pr = \mu C_p/\kappa$ necessarily equal to unity.

Generalization of the equation system (1) - (3) for the case $Pr \neq 1$ may be done by introducing the Prandtl number Pr in the term of Eq. 3, that looks like the heat diffusion term in the energy equation in NS system. This will be illustrated here for the one-dimensional case. The right-hand side of Eq.3 writes

$$\frac{\partial}{\partial x}\tau\frac{\partial}{\partial x}u^2(E+\frac{5}{2}p) + \frac{\gamma}{\gamma-1}\frac{\partial}{\partial x}\frac{p}{\rho}\tau\frac{\partial p}{\partial x} + \frac{\gamma}{\gamma-1}\frac{\partial}{\partial x}p\tau\frac{\partial p/\rho}{\partial x} \tag{14}$$

whereas the right-hand side of Eq.8 writes

$$\frac{\partial}{\partial x}\frac{4}{3}p\tau\frac{\partial}{\partial x}\frac{u^2}{2} + \frac{\gamma Pr^{-1}}{\gamma-1}\frac{\partial}{\partial x}p\tau\frac{\partial p/\rho}{\partial x}.$$

The last term in expression 14 is multiplied by Pr^{-1} to make it identical to the corresponding term in NS equations. In invariant form, the same operation applied to Eq.3 leads to the energy equation

$$E_t + div((E+p)\vec{u}) = div\tau(div(E+2p)\vec{u}\otimes\vec{u} + \vec{\nabla}\frac{p\vec{u}^2}{2}) + \frac{\gamma}{\gamma-1}div\tau\frac{p}{\rho}\nabla p + \frac{\gamma Pr^{-1}}{\gamma-1}div\tau p\nabla\frac{p}{\rho}. \tag{15}$$

After the above introduction of the Prandtl number, the results relative to the entropy remain valid.

To ensure consistency with the actual gas viscosity, τ should thus be taken equal to

$$\tau = \mu/p. \tag{16}$$

It is useful to relate τ to quantities that characterize the flow from a molecular point of view. Using Bird's relation [7] between viscosity and mean free path λ

$$\lambda = \frac{\mu}{\rho\sqrt{2\pi RT}} \times \frac{2(7-2\omega)(5-2\omega)}{15} \tag{17}$$

the equation of state $p = \rho RT$, and the mean thermal speed $\overline{c'} = \sqrt{8RT/\pi}$, one gets

$$\tau = \frac{\lambda}{\sqrt{RT}} \times \frac{15\sqrt{2\pi}}{2(7-2\omega)(5-2\omega)} = \frac{\lambda}{\overline{c'}} \times \frac{30}{(7-2\omega)(5-2\omega)} \tag{18}$$

where R is the perfect-gas constant. Eq.17 is a generalization of the usual expression for a hard-sphere gas ($\mu \propto T^{1/2}$) to a Variable Hard Sphere (VHS) gas whose viscosity law is $\mu \propto T^{\omega}$. Realistic values of ω fall between 0.5 and 1. τ is then interpreted as

$$\tau = \frac{1}{\nu} \times \frac{30}{(7-2\omega)(5-2\omega)} \tag{19}$$

where ν denotes the molecular collision frequency. The last factor in Eq.19 ranges from 1.25 (for $\omega = 0.5$) to 2 (for $\omega = 1$). τ had been related quantitatively to the physical gas properties (Eq.16). Now it is also interpreted clearly as the local mean collisional time multiplied by a constant of the order of unity that depends only on the intermolecular potential.

3 QGD equations for the 2D plane flow around a flat plate

3.1 System of equations

After introducing the modification to account for a non-unity Prandtl number, the system of QGD equations for a 2D flows in the (x, y) plane writes :

$$\frac{\partial \rho}{\partial t} + \frac{\partial \rho u}{\partial x} + \frac{\partial \rho v}{\partial y} = \frac{\partial}{\partial x}\tau\frac{\partial}{\partial x}(\rho u^2 + p) + \frac{\partial}{\partial y}\tau\frac{\partial}{\partial y}(\rho v^2 + p)$$
$$+\frac{\partial}{\partial x}\tau\frac{\partial}{\partial y}\rho uv + \frac{\partial}{\partial y}\tau\frac{\partial}{\partial x}\rho uv \tag{20}$$

$$\frac{\partial \rho u}{\partial t} + \frac{\partial}{\partial x}(\rho u^2 + p) + \frac{\partial \rho uv}{\partial y} = \frac{\partial}{\partial x}\tau\frac{\partial}{\partial x}(\rho u^3 + 3pu) + \frac{\partial}{\partial y}\tau\frac{\partial}{\partial y}(\rho uv^2 + pu)$$
$$+\frac{\partial}{\partial x}\tau\frac{\partial}{\partial y}(\rho u^2 v) + \frac{\partial}{\partial y}\tau\frac{\partial}{\partial x}(\rho u^2 v) + \frac{\partial}{\partial x}\tau\frac{\partial}{\partial y}pv + \frac{\partial}{\partial y}\tau\frac{\partial}{\partial x}pv \tag{21}$$

$$\frac{\partial \rho v}{\partial t} + \frac{\partial}{\partial y}(\rho v^2 + p) + \frac{\partial \rho uv}{\partial x} = \frac{\partial}{\partial y}\tau\frac{\partial}{\partial y}(\rho v^3 + 3pv) + \frac{\partial}{\partial x}\tau\frac{\partial}{\partial x}(\rho vu^2 + pv)$$
$$+\frac{\partial}{\partial x}\tau\frac{\partial}{\partial y}(\rho uv^2) + \frac{\partial}{\partial y}\tau\frac{\partial}{\partial x}(\rho uv^2) + \frac{\partial}{\partial x}\tau\frac{\partial}{\partial y}pu + \frac{\partial}{\partial y}\tau\frac{\partial}{\partial x}pu \tag{22}$$

$$\frac{\partial E}{\partial t} + \frac{\partial}{\partial x}u(E + p) + \frac{\partial}{\partial y}v(E + p) =$$
$$\frac{\partial}{\partial x}\tau\frac{\partial}{\partial x}u^2(E + 2.5p) + \frac{\partial}{\partial y}\tau\frac{\partial}{\partial y}v^2(E + 2.5p) + \frac{\partial}{\partial x}\tau\frac{\partial}{\partial x}\frac{v^2 p}{2} + \frac{\partial}{\partial y}\tau\frac{\partial}{\partial y}\frac{u^2 p}{2} +$$
$$\frac{\gamma}{\gamma - 1}(\frac{\partial}{\partial x}\frac{p}{\rho}\tau\frac{\partial p}{\partial x} + \frac{\partial}{\partial y}\frac{p}{\rho}\tau\frac{\partial p}{\partial y}) + \frac{\gamma Pr^{-1}}{\gamma - 1}(\frac{\partial}{\partial x}p\tau\frac{\partial}{\partial x}\frac{p}{\rho} + \frac{\partial}{\partial y}p\tau\frac{\partial}{\partial y}\frac{p}{\rho})$$
$$+\frac{\partial}{\partial x}\tau\frac{\partial}{\partial y}uv(E + 2p) + \frac{\partial}{\partial y}\tau\frac{\partial}{\partial x}uv(E + 2p) \tag{23}$$

where u and v are the components of the velocity-vector. The equations of state and the expression for the specific internal energy (Eq.4) close the system of Eqs.(20) – (23). The expression of τ is given by the relation Eq.16 with $\mu(T) = \mu_1(T/T_1)^\omega$. Subscript 1 refers to reference conditions. Assuming a power-law viscosity-temperature relationship is not required for QGD equations themselves. However, this is required for consistency with the DSMC calculations based on VHS model.

3.2 Boundary conditions on the solid wall

Even if a flow is expected to be correctly modeled by macroscopic equations, there exists a layer of fluid along the wall where the flow is far from equilibrium because molecules re-emitted by the wall and molecules from within the flow have not suffered enough collisions to reach thermal equilibrium. The thickness of this layer — the Knudsen layer — is of the order of a few mean free paths. This region should be described by kinetical models.

To avoid this difficulty and to remain in the framework of gas dynamic equations one can implement special boundary conditions (BCs) on the solid wall for tangential velocity and for temperature. These conditions — so-called slip conditions — must been constructed in such a way that the flow parameters on the external boundary of the Knudsen layer coincide with the ones resulting from kinetical equations applied to the Knudsen layer. Based on some approximations (e.g. linear variation of flow parameters near the wall) one finds the values for tangential velocity u_s and temperature T_s to be prescribed as BCs on the wall when solving the macroscopic equations for the whole flowfield. These values do not coincide with the real velocity and temperature of the gas near the solid wall as they would be obtained by using kinetical models.

Different expressions of the slip BCs can be found in the literature [2], [4], [3], but all of them have the same structure and differ essentially in the values of the numerical coefficients. In [2] the slip conditions are written as

$$u_s = 1.012\left(\frac{2\mu}{\rho\sqrt{2RT}}\frac{\partial u}{\partial y}\right)_s + 0.84\left(\frac{\mu}{\rho T}\frac{\partial T}{\partial x}\right)_s, \tag{24}$$

$$v_s = 0, \tag{25}$$

$$T_s - T_w = 1.173\frac{\sqrt{\pi}}{2R}\left(\frac{1}{\sqrt{2RT}}\frac{\kappa}{\rho}\frac{\partial T}{\partial y}\right)_s, \tag{26}$$

where T_w denotes wall temperature. These conditions were obtained by Kogan using the $\tau-$ approximation for Boltzmann equation, assuming full accommodation, $Pr = 1$ and $\gamma = 5/3$. We introduce

$$\kappa = \frac{\mu C_p}{Pr}, \qquad \text{and} \qquad \frac{C_p}{R} = \frac{\gamma}{\gamma - 1}$$

and Eq.26 becomes

$$T_s - T_w = 1.173\frac{\gamma}{(\gamma - \frac{1}{2})Pr} \times \left(\frac{\mu}{\rho\sqrt{8RT/\pi}}\frac{\partial T}{\partial y}\right)_s. \tag{27}$$

This expression is retained even for other values of Pr and γ. In the present case, it was used for $Pr = 2/3$ and $\gamma = 5/3$.

Kogan's boundary conditions have been obtained by matching the solution of Boltzmann equation in the Knudsen layer to the solution of the macroscopic equations supposed to be NS equations. A similar treatment should be done for the QGD system, by matching the solutions of QGD equations and kinetical equations on the boundary of the Knudsen layer. This appears to be a difficult task that should be regarded independently.

Because this has not been done, it seems natural to use the same slip BCs for QGD equations as for NS equations. These conditions have a long history and were proved to

be correct for a number of different practical problems. The asymptotic convergence of QGD system toward NS one gives some support to using the same BCs.

An additional support is found when comparing the shear stress tensor and the energy flux on the boundary for these two models.

Shear stress for a plate located along x direction is determined by the σ^{xy} component of the shear stress tensor. According to Eq.9 and Eq.10 for the two models under consideration one obtains

$$\sigma^{xy}{}_{NS} = \mu(\frac{\partial u}{\partial y} + \frac{\partial v}{\partial x}) \tag{28}$$

$$\sigma^{xy}{}_{QGD} = \tau(\frac{\partial pu}{\partial y} + \frac{\partial pv}{\partial x} + \frac{\partial \rho u^2 v}{\partial x} + \frac{\partial \rho v^2 u}{\partial y}) \tag{29}$$

Accounting for the BCs

$$v = 0, \qquad \frac{\partial p}{\partial y} = 0 \tag{30}$$

and for the relation $\mu = p\tau$, one gets

$$\sigma^{xy}{}_{QGD} = \sigma^{xy}{}_{NS} \tag{31}$$

and shear stresses in both models are formally equal. The same is true for energy transfer. According to Eq. 3 and 8 energy fluxes normal to the plate write

$$Q^y{}_{NS} = -(E+p)v + \mu\frac{\partial}{\partial y}\frac{u^2}{2} + \frac{\gamma Pr^{-1}}{\gamma - 1}\mu\frac{\partial p/\rho}{\partial y} + \frac{4}{3}\mu v\frac{\partial v}{\partial y} - \frac{2}{3}\mu v\frac{\partial u}{\partial x} + \mu u\frac{\partial v}{\partial x} \tag{32}$$

$$\begin{aligned} Q^y{}_{QGD} \;=\; & -(E+p)v + \tau\frac{\partial}{\partial y}v^2(E+2.5p) + \tau\frac{\partial}{\partial y}\frac{u^2 p}{2} + \frac{\gamma}{\gamma-1}\frac{p}{\rho}\tau\frac{\partial p}{\partial y} + \\ & \frac{\gamma Pr^{-1}}{\gamma-1}p\tau\frac{\partial}{\partial y}\frac{p}{\rho} + \tau\frac{\partial}{\partial x}uv(E+2p) \end{aligned} \tag{33}$$

Taking into account Eq.30 and $\mu = p\tau$ one gets

$$Q^y{}_{NS} = Q^y{}_{QGD}.$$

A relation of the same type is also obtained for QGD and NS density fluxes normal to the wall. According to Eqs. 1 and 6 normal density fluxes write

$$W^y{}_{NS} = -\rho v, \qquad \text{and } W^y{}_{QGD} = -\rho v + \tau\frac{\partial}{\partial y}(\rho v^2 + p).$$

Note,that NS continuity equation includes only convective mass transfer, and QGD continuity equation includes convective and molecular mass transfer together [8], [9].

Taking into account Eq.30 yields $W^y{}_{NS} = W^y{}_{QGD}$.

So in both systems of equations normal components of shear stress tensor and full energy flux to the wall are formally equal and they are related to the gradients by the classical relations

$$\sigma^{xy} = \left(\mu \frac{\partial u}{\partial y}\right)_s \tag{34}$$

and

$$q = \left(\kappa \frac{\partial T}{\partial y}\right)_s + \left(\mu u \frac{\partial u}{\partial y}\right)_s \tag{35}$$

for QGD as well as for NS equations. Here the condition of small τ is not necessary, but the additional BC $\partial p/\partial y = 0$ (Eq.13) is essential. The above results are useful to extract wall quantities from the calculation results. Simultaneously they bring an additional support to using the same BCs for QGD and NS equations.

3.3 Dimensionless quantities

To solve the system of Eqs. (20) - (23) it is convenient to rewrite it in a non-dimensional form by introducing scaling quantities for all dimensional variables. The corresponding scaling quantities are taken in the freestream region : mean free path λ_1, density ρ_1, sound velocity $a_1 = \sqrt{\gamma R T_1}$, temperature T_1. So we have the following relations between adimensional and dimensional variables ("tilda" refers to dimensionless quantities).

$$\rho = \tilde{\rho}\rho_1, \qquad p = \tilde{p}\rho_1 {a_1}^2, \qquad T = \tilde{T}T_1$$

$$a = \tilde{a}a_1, \qquad x = \tilde{x}\lambda_1, \qquad t = \tilde{t}\lambda_1/a_1, \tag{36}$$

$$u = \tilde{u}a_1, \qquad v = \tilde{v}a_1, \qquad \tau = \tilde{\tau}\lambda_1/a_1, \qquad E = \tilde{E}\rho_1 {a_1}^2$$

After having introduced non-dimensional quantities, the form of equations 20–23 does not changed. We now drop the "tilda" sign. It is useful to express dimensionless quantities like

$$\text{pressure } p = \rho T/\gamma,$$

$$\text{sound velocity } a = \sqrt{T},$$

$$\text{mean free path } \lambda = \frac{T^{\omega-1/2}}{\rho} = \frac{(p\gamma)^{\omega-1/2}}{\rho^{\omega+1/2}}$$

$$\text{local relaxation time } \tau = \frac{\mu}{p} = \frac{\lambda}{a} \times \frac{15\sqrt{2\pi\gamma}}{2(7-2\omega)(5-2\omega)} = \frac{(\gamma p)^{\omega-1}}{\rho^{\omega}} \times \frac{15\sqrt{2\pi\gamma}}{2(7-2\omega)(5-2\omega)}$$

$$\text{shear stress (reduced by } \rho_1 a_1^2) : \quad \sigma^{xy} = p\tau\frac{\partial u}{\partial y}$$

$$\text{energy flux (reduced by } \rho_1 a_1^3) : \quad q = \frac{1}{Pr(\gamma-1)}(p\tau\frac{\partial T}{\partial y})_s + p\tau u\frac{\partial u}{\partial y}$$

The freestream conditions write

$$\rho_1 = 1, \quad p_1 = 1/\gamma, \quad u_1 = M_1, \quad T_1 = 1, \quad T_0 = 1 + \frac{\gamma-1}{2}M_1^2$$

Boundary conditions 24 and 26 can be rewritten in dimensionless variables as

$$u_s = 1.012\sqrt{\frac{2}{\gamma}}\left(\tau\sqrt{T}\frac{\partial u}{\partial y}\right)_s + \frac{0.84}{\gamma}\left(\tau\frac{\partial T}{\partial x}\right)_s \tag{37}$$

$$v_s = 0 \tag{38}$$

$$T_s - T_w = 1.173\frac{1}{(\gamma-1)Pr} \times \sqrt{\frac{\gamma\pi}{8}}\left(\tau\sqrt{\frac{\partial T}{\partial y}}\right)_s \tag{39}$$

3.4 Computational algorithm

A finite-difference scheme was constructed based on the dimensionless form of Eqs.20–23 with space accuracy of the order $O(h^2)$ (centered scheme), where h characterizes space discretization.

The code uses a finite-volume approach [5] with a centered approximation for all space derivatives including convective terms. The flow parameters are calculated in the nodes of the computational grid, and the fluxes are calculated in the centered point between the nodes. The symmetry plane and the plate surface are placed in the centered points.

The 2-D computational domain is limited

- by the plane $y = 0$ that contains the plate. The leading edge is located at $x = 0$. Symmetry conditions are applied for $x < 0$ and boundary conditions in the form Eqs.13 and 37–39 and are applied along the plate ($x > 0$);

- by the plane $x = x_{min} < 0$ ahead of the leading edge, where freestream conditions are prescribed;
- by the planes $y = y_{max} > 0$ and $x = x_{max} > 0$ where "soft" conditions are prescribed : $\text{grad}(f) = 0$, with $f = (\rho, u, p, E)$.

y_{max} is taken sufficiently large for the upper boundary to be located entirely in the undisturbed freestream.

A rectangular non-uniform grid is used with steps δx and δy. The smallest space step is found near the plate leading edge ($\delta x = \delta x_{min}$ and $\delta y = \delta y_{min}$). Between adjacent cells, δx and δy increase by constant factors f_x and f_y respectively.

Equations are solved as algebraic expressions and nonlinear values were taken from the previous time step. The steady-state solution is obtained as a limit of a time-evolving process. The time step is chosen from the Courant stability condition

$$\Delta t = \alpha \min(h/V)$$

where $V = a + \sqrt{u^2 + v^2}$ and $h = \min(\delta x, \delta y)$.

Coefficient α was chosen experimentally in the range $0.01 - 0.1$. To be more correct, the stability condition should be written as

$$\Delta t \times \frac{a}{h} + \Delta t \times \frac{Re}{h^2} \leq 1/2.$$

The computation was stopped when the steady-state solution was achieved, according to the criterion

$$\varepsilon = \frac{1}{N_x N_y} \sum \frac{\rho^{j+1} - \rho^j}{\Delta t} \leq 0.001 \tag{40}$$

The numerical method used in the present work was probably not the most efficient one, but the objective was to examine the validity domain of QGD equations rather than optimizing their numerical solution. The code that will be described in section 4.3 for solving NS equations is more robust and efficient. Applying similar methods would enable us to solve QGD equations more efficiently.

The structure of the dissipation terms makes stability properties better for QGD equations than for NS ones in their numerical solutions. This was demonstrated by carrying out additional NS calculations :

For $M_1 = 1.5$, 2 and 5 and $T_w = T_0$, NS system was computed with the same scheme (explicit centered scheme) as QGD one, using the same grids and time steps. For $M_1 = 1.5$ and $M_1 = 2$ convergence was virtually identical, but for $M_1 = 5$ convergence was reached for QGD and not for NS equations.

When solving QGD equations (as for NS ones), oscillations appeared for high Mach numbers in regions with strong gradients. As a rule this problem is overcome by decreasing the order of precision of the numerical scheme. In the present calculations, with the above-mentioned scheme, the onset of fluctuations is visible on density profiles in the shock region at $M_1 = 10$, $T_w = T_0$ and computations for $M_1 = 20$ failed. For QGD equations, decreasing the order of precision of the numerical scheme can be achieved as follows.

QGD equations include a characteristic time τ equal to μ/p where $\mu \approx \rho\lambda a$, where a is the velocity of sound. To overcome the problem of oscillations, τ is expressed as

$$\tau = \frac{1}{p}(\mu + \mu') \text{ where } \mu' = \beta\rho h a$$

in some of the dissipation terms. h is the local space step, β is a smallest possible parameter that ensures the stability of the solution. This is equivalent to introducing an artificial viscosity, similar to that implemented in KCFD schemes[13, 14].

In the present computations, this method was used for $M_1 = 20$ ($\beta = 0.15$ for $T_w = T_0$, and $\beta = 0.1$ for $T_w = T_1$).

4 Computational work

4.1 Flow conditions

The test-problem retained for the present work is the flow around a semi-infinite sharp flat plane parallel to the direction of the freestream. A systematic study was carried out by varying the freestream Mach number M_1 from 1.5 to 20 and setting the wall temperature T_w equal successively to the freestream temperature T_1 and to the freestream stagnation temperature T_0.

As explained in section 3.3, the code for QGD equations uses dimensionless quantities. However, the codes used to solve NS equations and the code for DSMC simulation use dimensional quantities. Dimensional quantities had thus to be chosen to characterize the flow conditions. Note that the dimensional quantities have been introduced just for convenience in NS and DSMC calculations. They are somewhat arbitrary.

The flowing gas was supposed to be Argon characterized by
molar mass : $\mathcal{M} = 0.039948$ kg/mole, molecular mass : $m = 6.634 \times 10^{-26}$ kg/molecule,
perfect-gas constant : $R = 208.121$ joule/(kg.K)
viscosity : $\mu(T) = \mu_{ref} \times (T/T_{ref})^{\omega}$ with $\omega = 0.5$ and $\mu_{ref} = 2.125 \times 10^{-5}$ Pa.s at $T_{ref} = 273$ K
specific heat ratio : $\gamma = 5/3$, Prandtl number : $Pr = 2/3$.

The viscosity law was chosen to be consistent with the VHS model used in DSMC calculations (here in the particular case of hard-sphere molecules). The three numerical methods used were also consistent in modeling the gas/surface interaction : diffuse reflection with perfect accommodation at T_w was assumed.

The freestream was characterized by
temperature : $T_1 = 273\,\mathrm{K}$, number density $n_1 = 1.716 \times 10^{18}$ molecules/m^3 resulting in density $\rho_1 = 1.138 \times 10^{-7}\,\mathrm{kg/m^3}$, pressure $p_1 = 6.466 \times 10^{-3}\,\mathrm{Pa}$, sound velocity $a_1 = 307.7\,\mathrm{m/s}$.

Density was chosen to correspond to a mean free path $\lambda_1 = 1\,\mathrm{m}$ (Eq.17). Collision frequency was equal to $\nu_1 = 380.4\,\mathrm{s}^{-1}$ and mean collisional time was $1/\nu_1 = 2.629 \times 10^{-3}\,\mathrm{s}$.

Although the problem considered is relative to a semi-infinite flat plate, practical calculations were carried out for a plate of length approximately equal to 100 meters (or 100 mean free paths) This allowed to cover the range of Knudsen numbers larger than 0.01.

Five values of the Mach number were considered. For each of them, two values of the wall temperature were considered, namely $T_w = T_0$, where T_0 is the stagnation temperature in the freestream conditions (nearly adiabatic case) and $T_w = T_1$. Table 1 presents a number of parameters relative to the different flow conditions. It includes the value of a Reynolds number Re_w based on wall temperature rather than on freestream temperature. It includes also quantities $\rho_1 V_1^2$ and $\rho_1 V_1 C_p(T_0 - T_1)$. The first one is used to normalize the wall skin-friction and get the skin-friction coefficient $C_f/2 = \sigma^{xy}/(\rho_1 V_1^2)$ whereas the second one is used to normalize the wall heat transfer in the case $T_w = T_1$ and to get the heat transfer coefficient (Stanton number) defined as $St = C_h = q/(\rho_1 V_1 C_p(T_0 - T_w))$. In the near-adiabatic case ($T_w = T_0$), thermal flux is not considered.

In QGD calculations, wall quantities $C_f/2$ and St are derived from the dimensionless variables defined in section 3.3 by

$$\frac{C_f}{2} = \frac{1}{M_1^2}\left(\tilde{p}\tilde{\tau}\frac{\partial \tilde{u}}{\partial \tilde{y}}\right)_s$$

and

$$C_h = St = \frac{1}{PrM_1(\tilde{T}_0 - 1)}\left(\tilde{p}\tilde{\tau}\frac{\partial \tilde{T}}{\partial \tilde{y}}\right)_s + \frac{\gamma - 1}{M_1(\tilde{T}_0 - 1)}\left(\tilde{p}\tilde{\tau}\tilde{u}\frac{\partial \tilde{u}}{\partial \tilde{y}}\right)_s .$$

For reference, it is useful to calculate the free molecular limits of the momentum and energy exchange between the gas and the plate. Values of the nondimensionalized normal momentum exchange p/p_1, tangential momentum exchange $C_f = \sigma^{xy}/(\rho_1 V_1^2)$ and energy flux $C_h = q/(\rho_1 V_1 C_p(T_0 - T_w))$ are given in Table 2 as calculated by combining classical formulae (e.g. in Bird [1]) for the incident molecular flux $()_i$ and the reflected flux $()_r$. Again perfect accommodation at T_w was assumed. Note that Reynolds analogy $C_f/2 = C_h$ can be formally demonstrated in free molecular regime for $T_w = T_1$.

4.2 QGD calculations

QGD calculations were carried out, based on the equations and on the numerical procedure described in section 3. The flow parameters were those indicated in section 4.1 : five values

Mach number M_1	1.5	2	5	10	20
Stagnation temperature T_0 (K)	477.8	637.0	2548	9373	36673
Velocity V_1 (m/s)	461.6	615.5	1538.7	3077	6155
Reynolds number $Re_1 = \rho_1 V_1 L/\mu(T_1)$	247.2	329.6	824.1	1648.1	3296
Rarefaction parameter $\bar{V} = M_1/\sqrt{Re_1}$	0.095	0.110	0.174	0.246	0.348
Reynolds number[a] $Re_w = \rho_1 V_1 L/\mu(T_w)$	186.9	215.8	269.7	281.3	284.4
$\rho_1 V_1^2$ (Pa)	0.02425	0.04311	0.26944	1.07775	4.31099
$\rho_1 V_1 C_p(T_0 - T_1)$ (W/m^2)	5.597	13.266	207.29	1658	13270
The present values of the parameters are based on $L = 100$ meters					
[a] Re_w calculated for $T_w = T_0$. Note that $Re_w = Re_1$ if $T_w = T_1$.					

Table 1: Flow parameters

Mach number M_1	1.5	2	5	10	20
Incident flux					
p_i/p_1	0.5	0.5	0.5	0.5	0.5
$\sigma_i^{xy}/(\rho_1 V_1^2)$	0.206	0.155	0.062	0.031	0.015
$q_i/(\rho_1 V_1 C_p(T_0 - T_w))$	0.426	0.247	0.068	0.032	0.016
Cold wall $T_w = T_1$					
Reflected flux					
p_r/p_1	0.5	0.5	0.5	0.5	0.5
$\sigma_r^{xy}/(\rho_1 V_1^2)$	0	0	0	0	0
$q_r/(\rho_1 V_1 C_p(T_0 - T_w))$	0.22	0.093	0.006	0.0007416	0.00009271
Total Flux					
p/p_1	1	1	1	1	1
$C_f/2 = C_h = \sigma^{xy}/(\rho_1 V_1^2)$	0.206	0.155	0.062	0.031	0.015
Hot wall $T_w = T_0$					
Reflected flux					
p_r/p_1	0.661	0.764	1.528	2.930	5.795
$\sigma_r^{xy}/(\rho_1 V_1^2)$	0	0	0	0	0
Total Flux					
p/p_1	1.161	1.264	2.028	3.430	6.295
$C_f/2 = \sigma^{xy}/(\rho_1 V_1^2)$	0.206	0.155	0.062	0.031	0.015

Table 2: Free molecular limit of wall transfers

of Mach number M_1 were combined with two values of wall temperature T_w, resulting in 10 test-cases. The name of the result files corresponding to the calculations, as well as a number of computational parameters are given in Table 3. Calculations at $M_1 = 5$ were repeated for two different grids to check the influence of space discretization. The quantities contained in the output files are listed below :

Flowfield : x, y, u, v, w, p, T, M
Wall quantities : $x, y, p, T, C_f/2, C_h, u$

In the wall quantities, T differs from T_w by the temperature jump, and u differs from zero by the velocity slip. The space distributions of density ρ, temperature T, Mach number M and $u-$component of velocity are plotted in figures that are described in section B. Note that ρ, T, u are reduced by their corresponding freestream value. They are denoted as R,T.M,U in the figures.

Results obtained at $M_1 = 5$ with two values of h are plotted in a similar way in Figs.73 and 74. The full lines are relative to $h_{\min} = 0.7$ and the dotted lines to $h_{\min} = 0.2$. The calculation with the fine grid was limited to a smaller domain. The agreement between the two calculations is excellent. The main discrepancy occurs near the downstream boundary of the domain (thus indicating the extent of its zone of influence). The differences that are visible on the iso-density lines appear in a region of weak gradients, where the position of the isolines is very sensitive to small variations in the function to be plotted. A similar grid sensitivity study was carried out for $M_1 = 2$ and both wall temperatures.

Wall quantities and profiles of some flow quantities are plotted together with results obtained by NS and DSMC calculations and will be commented upon later.

These figures include also comparisons of results obtained at $M_1 = 2, 5$ and $T_w = T_0, T_1$ a) by QGD model with slip BCs, b) by QGD with no-slip BCs and c) by DSMC as a reference.

4.3 DSMC and NS calculations

Results obtained by solving QGD equations were compared with DSMC results considered as a reference. In order to see whether QGD equations brought an improvement over usual NS equations, the solutions of the latter were also obtained for comparison purpose.

DSMC calculations were carried out for the tests-cases presented before. The computer code DISIRAF (DIrect SImulation of RArefied gas Flows) had been developed before at the Laboratoire d'Aérothermique du CNRS. It has been already used in Ref.[28] and described in Ref.[26]. It is based on the ideas of Bird [1]. The molecular interaction model was the VHS model. Consistency with QGD calculations was ensured by the relation between viscosity and reference collisional cross-section [7]

$$\mu = \frac{15}{8}\sqrt{\frac{\pi}{2}}\frac{m\sqrt{2\,k\,T/m}}{(2-\alpha)^{\alpha}\,\Gamma(4-\alpha)\,\sigma_{ref}}\left(\frac{T}{T_{ref}}\right)^{\alpha},$$

Near-adiabatic case $T_w = T_0$					
M_1	1.5	2	5	10	20
$\tilde{h}_{\min}$	0.7	0.7	0.7	0.7	0.7
$\tilde{h}_{\max}$	5.46	1.62	1.62	1.62	1.62
α	0.08	0.07	0.05	0.03	0.01
$\Delta\tilde{t}$	2.2×10^{-2}	1.6×10^{-2}	5.6×10^{-3}	1.7×10^{-3}	2.9×10^{-4}
N_{iter}	8100	7000	9300	16500	57200
$(N_x \times N_y)_{\text{grid}}$	55×44	102×91	102×91	102×91	102×56
Output files					
flowfield	m1t0f	m2t0f	m5t0f	m10t0f	m20t0f
wall	m1t0w	m2t0w	m5t0w	m10t0w	m20t0w
Cold wall $T_w = T_1$					
M_1	1.5	2	5	10	20
$\tilde{h}_{\min}$	0.7	0.7	0.7	0.7	0.7
$\tilde{h}_{\max}$	5.46	1.62	1.62	1.62	1.62
α	0.09	0.07	0.05	0.03	0.01
$\Delta\tilde{t}$	2.5×10^{-2}	1.6×10^{-2}	5.7×10^{-3}	1.8×10^{-3}	3.1×10^{-4}
N_{iter}	6400	7600	11400	21500	76000
$(N_x \times N_y)_{\text{grid}}$	55×44	102×91	102×91	102×91	102×56
Output files					
flowfield	m1t1f	m2t1f	m5t1f	m10t1f	m20t1f
wall	m1t1w	m2t1w	m5t1w	m10t1w	m20t1w
Fine grid					
M_1	5	5			
T_w	$= T_0$	$= T_1$			
$\tilde{h}_{\min}$	0.2	0.2			
$\tilde{h}_{\max}$	1.1	1.1			
α	0.01	0.01			
$\Delta\tilde{t}$	3.2×10^{-3}	3.3×10^{-3}			
N_{iter}	34600	39600			
$(N_x \times N_y)_{\text{grid}}$	89×71	89×71			
Output files					
flowfield	m5t00f	m5t11f			
wall	m5t00w	m5t11w			

Table 3: conditions of QGD calculations

where $\alpha = \omega - 1/2$ is taken equal to 0 in the present case (hard-sphere molecules). This resulted in a molecular diameter $d_{ref} = \sqrt{\sigma_{ref}/\pi} = 3.622 \times 10^{-10}$ m at $T_{ref} = 273$ K. Although the code allows for mixtures of polyatomic molecules, it was used here for a pure gas of monoatomic molecules. The correct molecular frequency was ensured by using the NTC (No Time Counter) algorithm.

The number of real molecules simulated by a computational molecule (the *weight* of the molecule) was variable. In a given cell, it was taken equal to $(n_{\rm approx} V_{\rm cell})/10$, where $n_{\rm approx}$ was a estimation of the local density and $V_{\rm cell}$ the volume of the cell. The following procedure was used. In a first calculation, $n_{\rm approx}$ was taken equal to n_1. This resulted in a number of molecules per cell variable from a few units to a few tens of units. A flowfield was calculated in these conditions, based on a small number of samples. The resulting density was used as a better estimate of n to readjust the *weight* of the molecules. Then a new calculation was launched. The number of molecules per cell was found to be nearly constant (9–11) and the results were retained.

The computational grids were constructed in the same way as for QGD calculations, except that the spacing δx was constant and equal to $\delta x_{\rm min}$ ahead of the leading edge. Different grids were used to check the sensitivity of the results to the grid parameters, and to adjust the computational domain to the extent of the region disturbed by the presence of the plate. The parameters of the grids are given in Table 4. They include the extent of the computational domain ($x_{\rm min} < x < x_{\rm max}$, $0 < y < y_{\rm max}$), the number of cells N_x along the plate, the number of cells N_y in the normal direction and the total number of cells. Note that $y_{\rm max} = \delta y_{\rm min} \times (f_y^{N_y} - 1)/(f_y - 1)$ and $x_{\rm max} = \delta x_{\rm min} \times (f_x^{N_x} - 1)/(f_x - 1)$. The factor $f = f_x = f_y$ by which the size is increased between adjacent cells was equal to 1.05.

Preliminary calculations indicated that taking $x_{\rm min} = -5$ was not sufficient to capture the upstream influence of the plate when $M_1 = 1.5$ in the near-adiabatic case, whereas $x_{\rm max} = -10$ was sufficient. This value was retained for all calculations. Remember that all length are expressed in meters (or reduced by $\lambda_1 = 1$ meter).

Molecules were injected through the upstream and lateral boundaries. The plate ($y = 0, x > 0$) was considered as a diffusely reflecting surface with perfect accommodation at wall temperature T_w. The plane ($y = 0, x < 0$) was considered as a specularly reflecting surface. For low values of M_1, molecules were also injected through the downstream boundaries with distribution functions corresponding to freestream parameters. For high values of M_1, the inward flow-rate of molecules is negligibly small and injection through the downstream boundary could have been indifferently set or removed. However it was found necessary to remove it to avoid *underflows*.

Calculations required usually less than 3 Megabytes of memory, except those based on grid C that required 5.3 Megabytes. Approximately 20–25 million molecular collisions were calculated in one hour of CPU time on a IBM 3090 computer.

The time step δt was sufficiently small to ensure $\nu \times \delta t < 1$ in each cell, where ν is the collision frequency of a molecule, estimated from the local macroscopic flow parameters [7]

Grid	A	B	C	D	E
$x_{\max}$	105	123	103	123	123
$y_{\max}$	105	123	61	68	51
$(\delta x)_{\min} = (\delta y)_{\min}$	0.5	0.5	0.25	0.5	0.5
$(\delta x)_{\max}$	5.461	6.321	5.148	6.321	6.321
$(\delta y)_{\max}$	5.461	6.321	3.161	3.696	2.896
n_x	50	53	63	53	53
n_y	50	53	53	42	37
Number of cells	3500	3869	5459	3066	2701
Injection through downstream boundary	no	yes	yes	yes	no

Table 4: Parameters of computational grids used for DSMC

$$\nu = \sqrt{\frac{8}{\pi}}(2-\alpha)^{\alpha}\Gamma(2-\alpha) \times n\,\sigma_{ref}\sqrt{\frac{2kT}{m}}\left(\frac{T_{ref}}{T}\right)^{\alpha}.$$

Calculations were first performed for the near-adiabatic case $T_w = T_0$. Some parameters that characterize the computations are given in Table 5.

The test-cases corresponding to $M_1 = 1.5, 2, 5$ and 10 were treated using grid A (runs A2, A4, A6, A8, respectively). It was suspected that the inadequate downstream boundary condition could affect a significant part of the flowfield.

Therefore calculations for $M_1 = 1.5$ were repeated with grid B that covered a larger domain and was associated with downstream injection (run B2). Comparing results indicated that a region of length $30\,\lambda_1$ ahead of the trailing edge was affected for run A2 (Fig.76). This run was further completed to reduce statistical fluctuations and is further referred to as B5. For run B5, the extent of the affected region is probably smaller, due to a better downstream condition (injection of molecules). Therefore results B5 are expected to be unaffected by the downstream boundary condition at least for $x < 90\,\lambda_1$. They required 97 mn of CPU time. The steady-state was considered to be reached when the number of molecules in the computational domain became nearly constant. This was achieved for $t_{\text{stat}} = 2\,\text{s}$ (i.e. 7.5 the aerodynamic time $x_{\max}/V_1$) and sampling of the flowfield was done at each time step between $t = 2\,\text{s}$ and $t = 4.47\,\text{s}$. So 45% of the computational time was used to reach steady-state and 55% to gather statistical information.

In the same way, calculations for the near-adiabatic case at $M_1 = 2$ were repeated with grid B (run B4). Results are unaffected by the downstream boundary condition up to $x = 90\,\lambda_1$.

In the same way, calculations for the near-adiabatic cases at $M_1 = 5$ and $M_1 = 10$ were repeated with grid D (run D3 and D2, respectively). Results are unaffected by the

downstream boundary condition up to $x = 90\,\lambda_1$. Grid D is identical to grid B, except for a smaller extent in the y direction, which is sufficient at the Mach numbers considered here.

The near-adiabatic test-case at $M_1 = 20$ was calculated using grid E that differs from grid D by an even smaller extent in the y direction (run E2). Furthermore, molecular injection through the downstream boundary was negligibly small and provoked *underflows*. It was formally removed.

To check for a possible influence of space discretization, the near-adiabatic test-case at $M_1 = 10$ was recalculated with grid C which differs from the previous ones by a smaller extent in the x and y direction and by a cell size smaller by a factor of 2. The results (run C2) exhibit no difference when compared with those of run D2, except for the influence of the downstream boundary that occurs for a smaller value of x, due to the smaller value of $x_{\max}$. This is clearly evidence in Fig.75 where wall quantities are plotted.

Finally, the test-cases for the cold wall were calculated. Typical parameters of the calculations are also given in Table 5.

For comparison, the same test-cases were also treated on the basis of the usual Navier-Stokes (NS) equations. The code used a finite-volume upwind implicit method with flux-vector-splitting of Steger and Warming. Artificial viscosity was introduced. Velocity slip and temperature jump were used as boundary conditions along the wall, in a form derived from Ref.[6] by assuming full accommodation and neglecting the $x-$derivative of temperature in velocity slip :

$$u_s = \left(\frac{\mu\sqrt{\pi}}{\rho\sqrt{2RT}} \frac{\partial u}{\partial y} \right)_s \tag{41}$$

$$v_s = 0, \tag{42}$$

$$T_s - T_w = \frac{\sqrt{\pi}}{2R} \left(\frac{1}{\sqrt{2RT}} \frac{\kappa}{\rho} \frac{\partial T}{\partial y} \right)_s . \tag{43}$$

These conditions are slightly different from that retained for QGD equations (Eqs.24–26).

The results obtained by solving NS equations and by the DSMC method are plotted as the isolines of density, temperature, Mach number and u-component of velocity for the different test-cases.

4.4 Discussion

Numerical results show that for small Knudsen numbers (i.e. large abscissas) NS and QGD models give the same results. This is consistent with the fact that NS equations are the asymptotic limit of QGD equations for $Kn \to 0$ [19]. This is also the confirmation of the validity of NS boundary conditions used in the present QGD calculations.

First calculations (grid A)						
Run	A2	A4	A6	A8		
M_1	1.5	2	5	10		
T_w	T_0	T_0	T_0	T_0		
Grid	A	A	A	A		
δt (ms)	1	1	0.7	0.4		
t_{stat} (s)	0.7	0.7	0.5	0.3		
t_{final} (s)	2.3	2.93	1.2	1.58		
Output files						
flowfield	pleflda2	pleflda4	pleflda6	pleflda8		
wall	plewala2	plewala4	plewala6	plewala8		
Near-adiabatic case $T_w = T_0$						
Run	B5	B4	D3	D2	E2	C2
M_1	1.5	2	5	10	20	10
T_w	T_0	T_0	T_0	T_0	T_0	T_0
Grid	B	B	D	D	E	C
δt (ms)	1	1	0.5	0.4	0.15	0.4
t_{stat} (s)	2	0.7	0.5	0.25	0.1	0.25
t_{final} (s)	4.47	5.05	1.8	1.5	1.1	1.6
CPU time	97 mn	98 mn	54 mn	54 mn	83 mn	108 mn
Output files						
flowfield	l1t0f	l2t0f	l5t0f	l10t0f	l20t0f	
wall	l1t0w	l2t0w	l5t0w	l10t0w	l20t0w	
Cold wall $T_w = T_1$						
Run	B8	B7	D6	D7	E4	
M_1	1.5	2	5	10	20	
T_w	T_1	T_1	T_1	T_1	T_1	
Grid	B	B	D	D	E	
δt (ms)	1	1	0.5	0.2	0.15	
t_{stat} (s)	2	1	0.3	0.15	0.1	
t_{final} (s)	5.3	2.53	1.95	1.22	1.03	
CPU time	108 mn	54 mn	54 mn	83 mn	83 mn	
Output files						
flowfield	l1t1f	l1t1f	l5t1f	l10t1f	l20t1f	
wall	l1t1w	l2t1w	l5t1w	l10t1w	l20t1w	

Table 5: Characteristic parameters of the runs

Values of $M/\sqrt{Re_x}$ (and x/λ) at breakdown of continuum models					
M	1.5	2	5	10	20
$T_w = T_0$	0.95 (1)	0.78 (2)	0.66 (7)	0.78 (10)	1.00 (12)
$T_w = T_\infty$	0.67 (2)	0.64 (3)	0.45 (15)	0.39 (40)	0.45 (60)

Table 6: Breakdown of continuum models

The additional BC $\partial p/\partial n$ is not restrictive compared with NS equations, where this condition is not prescribed. This is demonstrated by considering the pressure profiles perpendicular to the plate (cf. figures for $M_1 = 2, 10, 20$ and both wall temperatures). Far from the leading edge, NS results exhibit actually a zero pressure gradient at the wall, even for the cold wall. Close to the leading edge, NS and QGD profiles exhibit nearly identical non-zero pressure gradients, the additional BC in QGD affects the solution only at a few wall-nearest grid points. DSMC results exhibit also zero pressure gradients for the hot wall and large pressure gradients for large values of M_1 in the cold wall cases. However these gradients affect only the Knudsen layer that is not claimed to be treated exactly by the continuum approach. This domain is treated approximately in continuum approaches by implementing slip BCs.

For small Mach numbers both continuum models come rapidly to close agreement with DSMC. However the region near the trailing edge is affected by the differences in formulating the downstream boundary conditions. The upstream influence of BC is particularly important in NS calculations for small Mach numbers.

As M increases, discrepancies appear near the leading edge of the plate. Both these discrepancies and the extent of the region where they appear increase with increasing M. QGD results are generally closer to DSMC than NS ones. This is due to additional dissipation in QGD model. The ratio of additional terms in QGD to the NS one in the right-hand side of Eq.2 is proportional to M^2. So the difference between QGD and NS increases with M. Thus QGD equations can be considered as an improvement, compared with the usual NS equations in the domain of large M in slip-flow regimes.

However, both continuum models depart from DSMC at approximately the same abscissas x. The values of $M/\sqrt{Re_x}$ corresponding to those abscissas (as taken from the C_f distributions) are given in Table 6. They range from ≈ 0.5 ($T_w = T_\infty$) to ≈ 1 ($T_w = T_0$).

This parameter that can be interpreted as a Knudsen number based on the boundary layer thickness $Kn_\delta = \lambda_\infty/\delta$ appears to be a basis for an approximate validity criterion for continuum approaches in a wide range of wall temperatures and freestream Mach numbers.

QGD results obtained for slip BCs and no slip BCs, respectively, show that

- no slip BCs result in a strong overestimation of p, C_f and C_h in the immediate vicinity of the leading edge;

- there is no visible difference in the distribution of these wall quantities for values of x sufficiently large to satisfy the just mentioned criterion (which means that the gradients $\partial u/\partial y$ and $\partial T/\partial y$ are the same for both BCs);
- for all cases investigated, using no slip BCs results in an overestimation of the distance between the shock and the plate. Similar conclusions are expected for NS equations. Thus for a correct description of the flowfield, slip BCs are required.

4.5 Conclusions

It results from the present work that

- QGD equations can be considered as a model for the description of viscous gas flows.
- The results support the proposed BCs for QGD model, consisting of usual NS boundary conditions completed by an additional one.
- Under some conditions, QGD equations bring significant improvement compared with NS ones. Otherwise QGD and NS results tend to collapse together.
- For small values of M, continuum models are valid except in the immediate vicinity of the leading edge.
- More generally, a criterion based on $M_1/\sqrt{Re_\infty}$ can be proposed for the validity of the continuum approach in a wide range of Mach number and temperature ratio.
- Using slip BCs in continuum approaches is desirable.

A Derivation of the 1-D QGD equations

For illustration purpose, QGD equations are derived here for the case of 1D plane gas flow along x-axis. Molecule velocities $\vec{\xi} = (\xi_1, \xi_2, \xi_3,)$ write

$$\xi_1 = u + c_1,$$

$$\xi_2 = c_2,$$

$$\xi_3 = c_3,$$

where u is the macroscopic velocity along x -axis, $\vec{c} = (c_1, c_2, c_3)$ is the thermal velocity of the molecules.

Equation 5 writes

$$\frac{\partial f}{\partial t} + \xi_1 \frac{\partial f}{\partial x} - \xi_1 \frac{\partial}{\partial x} \tau \xi_1 \frac{\partial f}{\partial x} = \mathcal{J}. \tag{44}$$

Macroscopic equations are derived by multiplying Eq.44 successively by summation invariants

$$\varphi(\vec{\xi}) = 1, \vec{\xi}, \vec{\xi}^2/2$$

and integrating over molecule velocities $\vec{\xi}$. Conservation of mass, momentum and energy during collisions results in the following equation for the collision integral

$$\int \mathcal{J} \varphi(\vec{\xi}) d\vec{\xi} = 0. \tag{45}$$

A.1 Density equation

According to the definition

$$\rho = \int f d\vec{\xi}, \tag{46}$$

averaging the different terms of Eq.44 gives successively

$$\int \frac{\partial f}{\partial t} d\vec{\xi} = \frac{\partial}{\partial t} \int f d\vec{\xi} = \frac{\partial}{\partial t} \rho, \tag{47}$$

$$\int \frac{\partial f}{\partial x} \xi_1 d\vec{\xi} = \frac{\partial}{\partial x} \int (u + c_1) f d\vec{\xi} = \frac{\partial}{\partial x} \int u f d\vec{\xi} = \frac{\partial}{\partial x} \rho u. \tag{48}$$

Here the relation

$$\int c_i f d\vec{\xi} = 0 \tag{49}$$

was used. For the last left-hand side term of Eq.44 one has

$$\int \xi_1 \frac{\partial}{\partial x} \tau \xi_1 \frac{\partial f}{\partial x} d\vec{\xi} = \frac{\partial}{\partial x} \tau \frac{\partial}{\partial x} \int {\xi_1}^2 f d\vec{\xi} = \frac{\partial}{\partial x} \tau \frac{\partial}{\partial x} \int (u + c_1)^2 f d\vec{\xi} = \frac{\partial}{\partial x} \tau \frac{\partial}{\partial x} (\rho u^2 + p). \quad (50)$$

Here relation 49 was used and pressure p was introduced as

$$p = \int {c_i}^2 f d\vec{\xi} = 1/3 \int ({c_1}^2 + {c_2}^2 + {c_3}^2) f d\vec{\xi}. \quad (51)$$

Combining expressions 45, 47, 48 and 50 yields the first equation of the QGD system in the form

$$\frac{\partial \rho}{\partial t} + \frac{\partial \rho u}{\partial x} = \frac{\partial}{\partial x} \tau \frac{\partial}{\partial x} (\rho u^2 + p). \quad (52)$$

A.2 Momentum equation

Let Eq.44 be multiplied by ξ_1 and integrated over $\vec{\xi}$. According to Eqs.48 and 49 one has

$$\int \xi_1 \frac{\partial}{\partial t} f d\vec{\xi} = \frac{\partial}{\partial t} \rho u, \quad (53)$$

$$\int {\xi_1}^2 \frac{\partial}{\partial x} f d\vec{\xi} = \frac{\partial}{\partial x} (\rho u^2 + p). \quad (54)$$

The diffusive-like term writes

$$\begin{aligned} \int {\xi_1}^2 \frac{\partial}{\partial x} \tau \xi_1 \frac{\partial f}{\partial x} d\vec{\xi} &= \frac{\partial}{\partial x} \tau \frac{\partial}{\partial x} \int {\xi_1}^3 f d\vec{\xi} = \frac{\partial}{\partial x} \tau \frac{\partial}{\partial x} \int (u + c_1)^3 f d\vec{\xi} \\ &= \frac{\partial}{\partial x} \tau \frac{\partial}{\partial x} \int (u^3 + 3u^2 c_1 + 3u {c_1}^2 + {c_1}^3) f d\vec{\xi} = \frac{\partial}{\partial x} \tau \frac{\partial}{\partial x} (\rho u^3 + 3pu) \quad (55) \end{aligned}$$

Here equations 49 and 51 have been used. Combining equations 45, 53, 54 and 55 yields the second equation of the QGD system in the form

$$\frac{\partial \rho u}{\partial t} + \frac{\partial \rho u^2 + p}{\partial x} = \frac{\partial}{\partial x} \tau \frac{\partial}{\partial x} (\rho u^3 + 3pu). \quad (56)$$

A.3 Energy equation

Total energy for a monoatomic gas is defined as

$$E = \frac{1}{2}\int \vec{\xi}^2 f d\vec{\xi}. \tag{57}$$

Averaging Eq.44 with weight $\vec{\xi}^2/2$ successively for each term results in

$$\int \frac{\vec{\xi}^2}{2}\frac{\partial}{\partial t} f d\vec{\xi} = \frac{\partial E}{\partial t}, \tag{58}$$

$$\begin{aligned}\int \frac{\partial}{\partial x} f\xi_1 \frac{{\xi_1}^2+{\xi_2}^2+{\xi_3}^2}{2} d\vec{\xi} &= \frac{\partial}{\partial x}\int u\frac{{\xi_1}^2+{\xi_2}^2+{\xi_3}^2}{2} f d\vec{\xi} + \frac{\partial}{\partial x}\int c_1 \frac{(c_1+u)^2+{c_2}^2+{c_3}^2}{2} f d\vec{\xi} \\ &= \frac{\partial}{\partial x} uE + \frac{\partial}{\partial x} up. \end{aligned} \tag{59}$$

Here we have used relation 49 and

$$\int c_i {c_j}^2 f d\vec{\xi} = 0. \tag{60}$$

The dissipative-like terms in the total energy equation are thus obtained as

$$\begin{aligned}\int \frac{\vec{\xi}^2}{2}\xi_1 \frac{\partial}{\partial x}\tau\xi_1\frac{\partial f}{\partial x} d\vec{\xi} &= \frac{\partial}{\partial x}\tau\frac{\partial}{\partial x}\int \frac{\vec{\xi}^2}{2}{\xi_1}^2 f d\vec{\xi} = \frac{\partial}{\partial x}\tau\frac{\partial}{\partial x}\int (u+c_1)^2\frac{(c_1+u)^2+{c_2}^2+{c_3}^2}{2} f d\vec{\xi} \\ &= \frac{\partial}{\partial x}\tau\frac{\partial}{\partial x}\int u^2\frac{(c_1+u)^2+{c_2}^2+{c_3}^2}{2} f d\vec{\xi} \\ &\quad + \frac{\partial}{\partial x}\tau\frac{\partial}{\partial x}\int 2uc_1\frac{(c_1+u)^2+{c_2}^2+{c_3}^2}{2} f d\vec{\xi} \\ &\quad + \frac{\partial}{\partial x}\tau\frac{\partial}{\partial x}\int {c_1}^2\frac{(c_1+u)^2+{c_2}^2+{c_3}^2}{2} f d\vec{\xi} \\ &= \frac{\partial}{\partial x}\tau\frac{\partial}{\partial x}(u^2E + 2u^2p + \frac{u^2p}{2} + \int \frac{{c_1}^2}{2}\frac{{c_1}^2+{c_2}^2+{c_3}^2}{2} f d\vec{\xi}). \end{aligned}$$

To find the last integral we suppose that the distribution function f has a locally-maxwellian form

$$f = f_0 = \frac{\rho}{(2\pi RT)^{3/2}}\exp\frac{-(\vec{\xi}-\vec{u})^2}{2RT} = \frac{\rho}{(2\pi RT)^{3/2}}\left(\exp\frac{-{c_1}^2}{2RT}\right)\left(\exp\frac{-{c_2}^2}{2RT}\right)\left(\exp\frac{-{c_3}^2}{2RT}\right). \tag{61}$$

Using this relation into the integral of the right-hand side, introducing variables

$$x = \frac{c_1}{\sqrt{2RT}}, \quad y = \frac{c_2}{\sqrt{2RT}}, \quad z = \frac{c_3}{\sqrt{2RT}}$$

and taking into account that

$$\int \exp(-x^2)dx = \sqrt{\pi}, \quad \int x^2 \exp(-x^2)dx = \sqrt{\pi}/2, \quad \int x^4 \exp(-x^2)dx = 3\sqrt{\pi}/4,$$

one has

$$\int \frac{{c_1}^2}{2} \frac{{c_1}^2 + {c_2}^2 + {c_3}^2}{2} f_0 dc_1 dc_2 dc_3 = \frac{5p^2}{2\rho}. \tag{62}$$

According to the previous relations, the dissipative-like terms in the energy equation appear as

$$\frac{\partial}{\partial x}\tau\frac{\partial}{\partial x}(u^2(E+2p) + \frac{u^2 p}{2} + \frac{5p^2}{2\rho}). \tag{63}$$

Considering that

$$\rho\varepsilon = \frac{p}{\gamma - 1} = \frac{3p}{2}$$

for $\gamma = 5/3$, one can rewrite the last expression in a form convenient for the calculation of non-monoatomic gas flows

$$\frac{u^2 p}{2} + \frac{5p^2}{2\rho} = \frac{p}{\rho}(\frac{\rho u^2}{2} + \rho\varepsilon + p) = \frac{p}{\rho}(E+p). \tag{64}$$

Combining together Eqs. 45, 58, 59 63 and 64 results in the last equation of the QGD system.

$$\frac{\partial E}{\partial t} + \frac{\partial u(E+p)}{\partial x} = \frac{\partial}{\partial x}\tau\frac{\partial}{\partial x}(u^2(E+2p) + \frac{p}{\rho}(E+p)). \tag{65}$$

B Description of figures

The distributions of wall quantities for $M_1 = 1.5, 2, 5, 10, 20$ are given in Figs.1–10 for $T_w = T_0$ and in Figs.11–21 for $T_w = T_1$. The figures include the distributions of

- pressure (and normal stress calculated by DSMC)
- skin-friction coefficient
- heat transfer coefficient (only for $T_w = T_1$)
- gas temperature along the wall.
- gas velocity along the wall (only for $M_1 = 20$)

In Figs.22–35, the profiles of flow parameters ρ, p, T, u against y at abscissas $x/\lambda = 10, 40, 80$ are plotted for $M_1 = 2, 10, 20$. For $M_1 = 5$, only density profiles are plotted.

In Figs.36–54, the isolines of a number of flow parameters (ρ, p, M, T, etc...) are plotted for $M_1 = 1.5, 2, 5, 10, 20$ and $T_w = T_0$, as obtained by DSMC, QGD and NS, respectively. Figures 55–72 contain the same information for $T_w = T_1$.

The results of the grid sensitivity studies carried out for QGD at $M_1 = 5$ for both values of T_w are presented in Figs.73 and 74.

The results of a similar study for DSMC at $M_1 = 10$ is presented in Fig.75.

In Fig.76, profiles of velocity, density, temperature as well as the distribution of wall parameters are plotted as obtained by DSMC using grids A and B, respectively. This figure makes clearly visible the extent of the region affected by the downstream boundary condition.

The comparison of results obtained using slip BC and no-slip BC, respectively for QGD model at $M_1 = 2$ and $M_1 = 5$ is presented in Figs.77–80 for $T_w = T_0$ and in Figs.81–84 for $T_w = T_1$. DSMC results are plotted in the same figures as a reference.

References

[1] Bird G.A.: Molecular Gas Dynamics, Clarendon Press, Oxford, 1976.

[2] Kogan M.N.:Rarefied gas dynamics, Ed.Nauka, Moscow, 1967.

[3] Lifshitz E.M., Pitaevsky L.P.: Physical kinetics, Ed.Nauka, Moscow, 1979.

[4] Shidlovsky V.P.: Introduction to the rarefied gas dynamics, Ed.Nauka, 1963, pp. 86 - 127.

[5] Samarsky A.A.: Theory of finite-difference schemes, Ed.Nauka, x1977.

[6] Schaaf S.A., Talbot L. : Mechanics or Rarefied Gases, Handbook of Supersonic Aerodynamics, section 16, NAVORD Report 1488, V.5, Feb.1959.

[7] Bird G.A. : Definition of Mean Free Path for Real Gases, Phys. of Fluids, Vol.26, pp.3222-3223, nov. 1983.

[8] Sloskin N.A.: About differential equations for gas flow. DAN USSR, 1951, v. 77, N 2, pp.205–208.

[9] Valander S.V.: Viscous gas dynamical equations. DAN USSR, 1951, v.78, N.1, pp. 25-27.

[10] Alexeev B.V.: Hydrodynamic equations in the kinetic theory of gases with chemical reactions. USSR J. Comput. Math. Phys. 1987, v.27, N 5, pp. 730-740.

[11] Klimontovich Yu.L.: About kinetical foundation for hydrodynamic equations with self diffusion. Letter to J. Tech. Phys., 1990, v. 16, N. 9, pp. 81-83.

[12] Klimontovitch Yu. L.: On the necessity and possibility of the united description of kinetic and hydrodynamic processes. J. Theoretical and mathematical physics, 1992, v.92, N 2, pp. 312 - 330.

[13] Elizarova T.G., Chetverushkin B.N.: Kinetic algorithms for calculating gas dynamic flows. J. Comput. Mathem. and Mathem. Phys. 1985, v.25, No 5, pp.164-169 (Printed in Great Britain).

[14] Elizarova T.G., Chetverushkin B.N.: Kinetically coordinated difference schemes for modelling flows of a viscous heat- conducting gas. J. Comput. Mathem. and Mathem. Phys., 1988, v. 28, No 6, pp. 64-75 (Printed in Great Britain).

[15] Elizarova T.G., Sheretov Yu.V.: About a shock wave-like solution properties for quasi gas dynamic equations, Preprint of Institute of Applied mathematics USSR, N 156, 1990.

[16] Sheretov Yu.V.: NS equations as asymptotic generalized QGD system. Preprint of Institute of Applied mathematics USSR, N 46, 1990.

[17] Sheretov Yu.V.: Entropy theorem for quasi gas dynamic equations, Preprint of Institute of Applied mathematics USSR, N 131, 1990.

[18] Antonov A.N., Elizarova T.G., Chetverushkin B.N., Sheretov Yu.V.: Numerical modelling of pulsating regimes accompanying supersonic flow round a hollow cylinder. USSR J. Comput. Math. Phys. Vol. 30, No 2, pp. 139-144, 1990.

[19] Elizarova T.G., Sheretov Yu.V.: The invariant form and asymptotic properties of a generalized quasi-gas-dynamic system. J. Comput. Mathem. and Math. Phys. 1991, v. 31, N 7, p.72-78 (Printed in Great Britain).

[20] Elizarova T.G., Chetverushkin B.N., Sheretov Yu.V.: Quasi-gas dynamic equations and computer simulation of viscous gas flows. Lecture Notes in Phys., N 414, Proc.13-Intern. Conf. on Numer. Meth. in Fluid Dynamics, Italy, Rome 1992, p.421-425.

[21] Elizarova T.G., Graur I.A., Sheretov Yu.V.: Quasi-gas dynamic equations and computer simulation of rarefied gas flows. 19th Intern. Symp. on Shock Waves, Marseille, 1993, 26 - 30 july.

[22] Graur I.A., Elizarova T.G., Sheretov Yu.V.: Shock structure simulation based on quasi-gas dynamic equations. Moscow, Nat.Cent. Math. Model. 1992, Preprint N 42.

[23] Abalakin I.V., Chetverushkin B.N.: Using kinetically- consistent difference schemes for prediction of slightly rarefied gas flows, J. Mathematical Modelling, v. 4, N 11, pp.19 - 35, 1992.

[24] Abalakin I.V., Chetverushkin B.N.: Kinetically- consistent finite difference schemes as a model for the flows of slightly rarefied gases, J. Mathematical Modelling, v. 5, N 5, pp.61 - 70, 1993.

[25] Sheretov Yu.V.: Theorem about the energy dissipation and exact solutions for system of quasi hydrodynamic equations, Russian Comput. Math. Phys. J ., 1994, v.34, N 3, pp.483-491.

[26] Skovorodko P.A., Lengrand J.C.: Computation of plume flow exhausting into a vacuum, including the corresponding viscous flow in the nozzle, Lab. d'Aérothermique du CNRS, Meudon, Fr., R 90-9 (1990).

[27] Chpoun A., Lengrand J.C., Heffner K.S.: Numerical and Experimental Investigation of Rarefied Compression Corner Flow. AIAA 27th Thermophysics Conference, July 6-8, 1992, Nashville,TN.

[28] Lengrand J.C., Chpoun A., Allègre J., Hériard-Dubreuilh X., Raffin M., Rarefied Hypersonic Flow over a Sharp Cone : DSMC, Navier-Stokes and Experimental Results, IUTAM Symposium on Aerothermochemistry of Spacecraft and Associated Hypersonic Flows, Marseille (Fr.), sept.1–4, 1992, Proceedings, Ed. Brun & Chikhaoui, pp.73–78, Marseille 1993.

Contents

Wall quantities

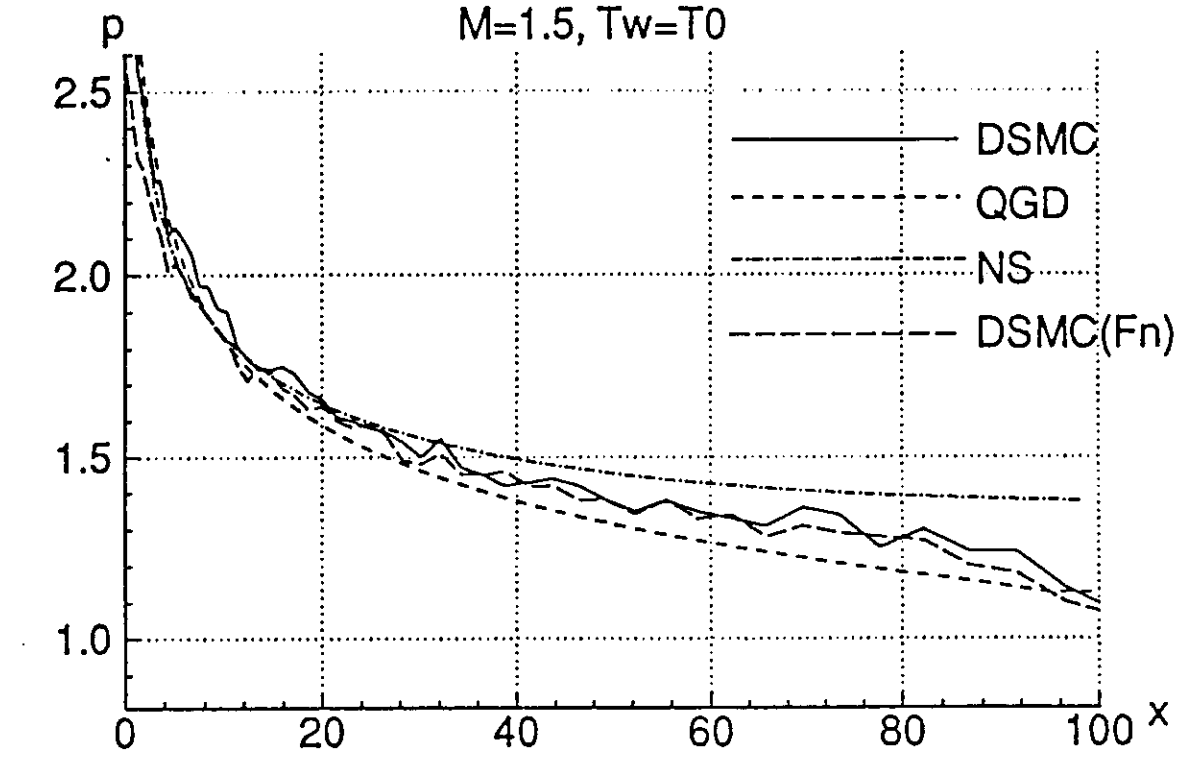
p
M=1.5, Tw=T0
2.5
2.0
1.5
1.0
0
20
40
60
80
100
x
DSMC
QGD
NS
DSMC(Fn)

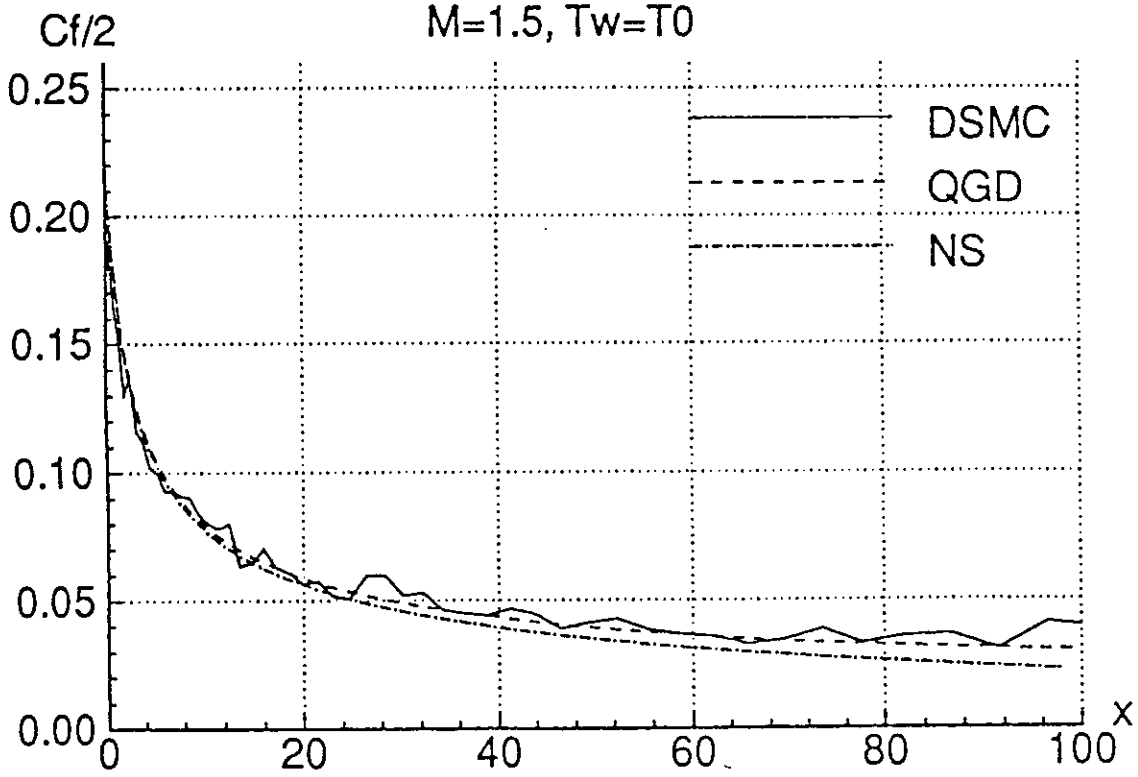
Cf/2
M=1.5, Tw=T0
0.25
0.20
0.15
0.10
0.05
0.00
0
20
40
60
80
100
x
DSMC
QGD
NS

Fig.1

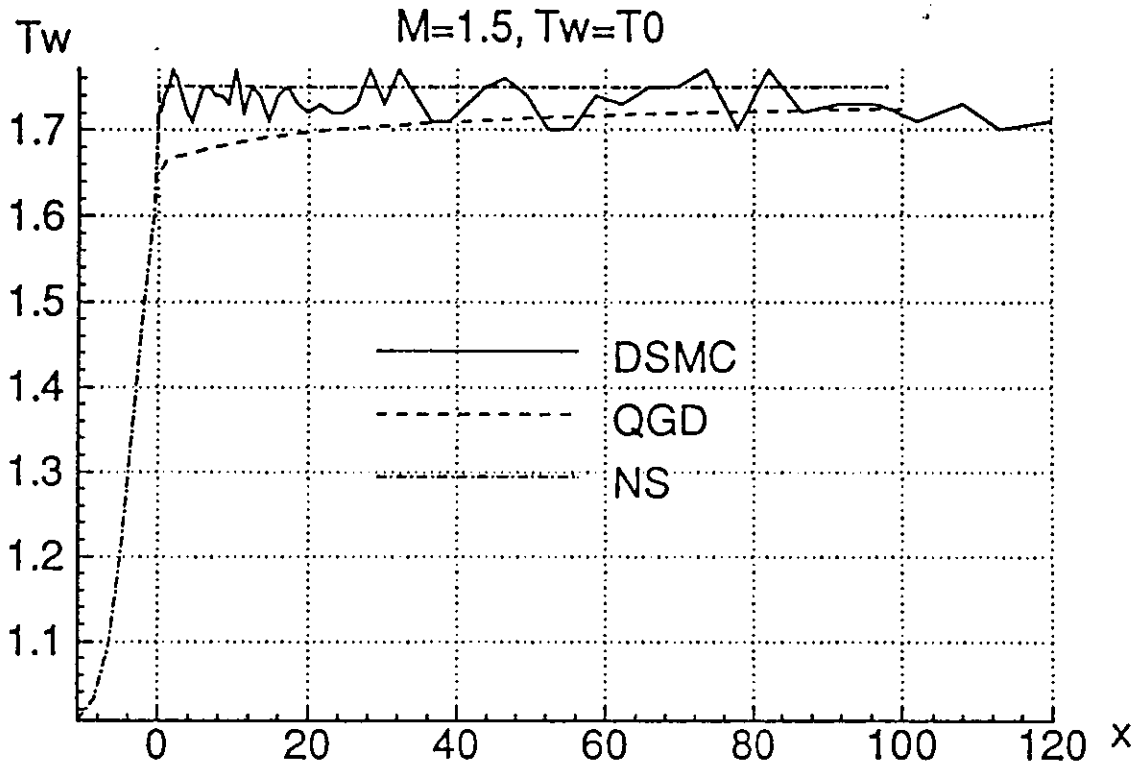

Fig.2

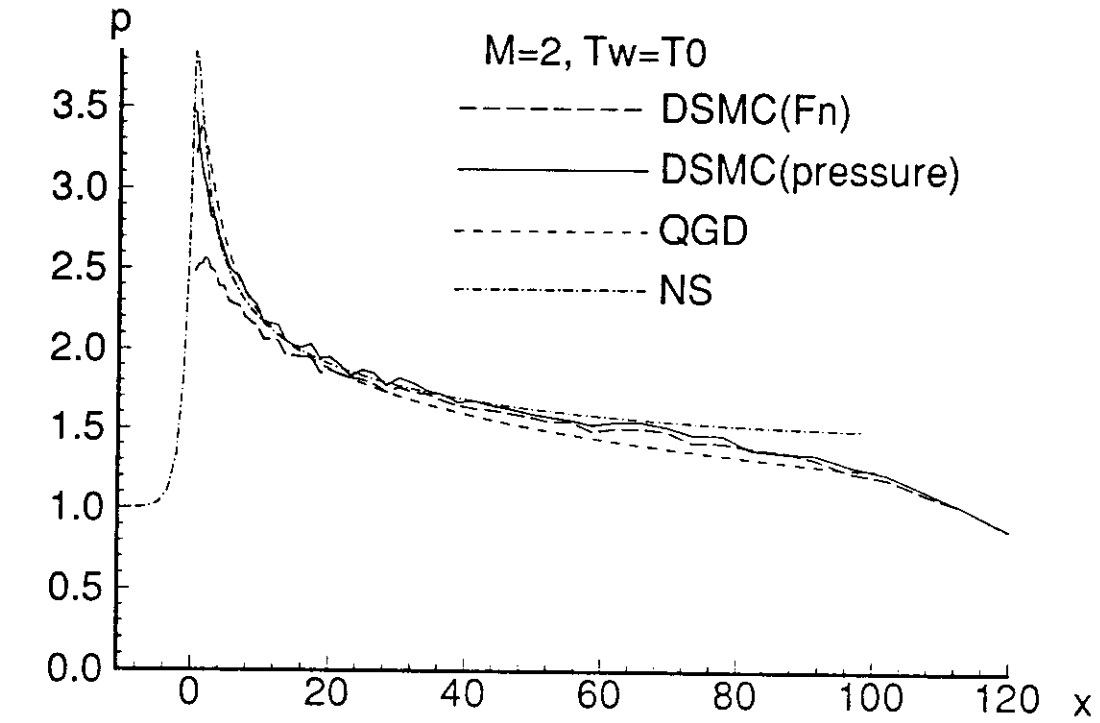
p
M=2, Tw=T0
DSMC(Fn)
DSMC(pressure)
QGD
NS
3.5
3.0
2.5
2.0
1.5
1.0
0.5
0.0
0
20
40
60
80
100
120
x

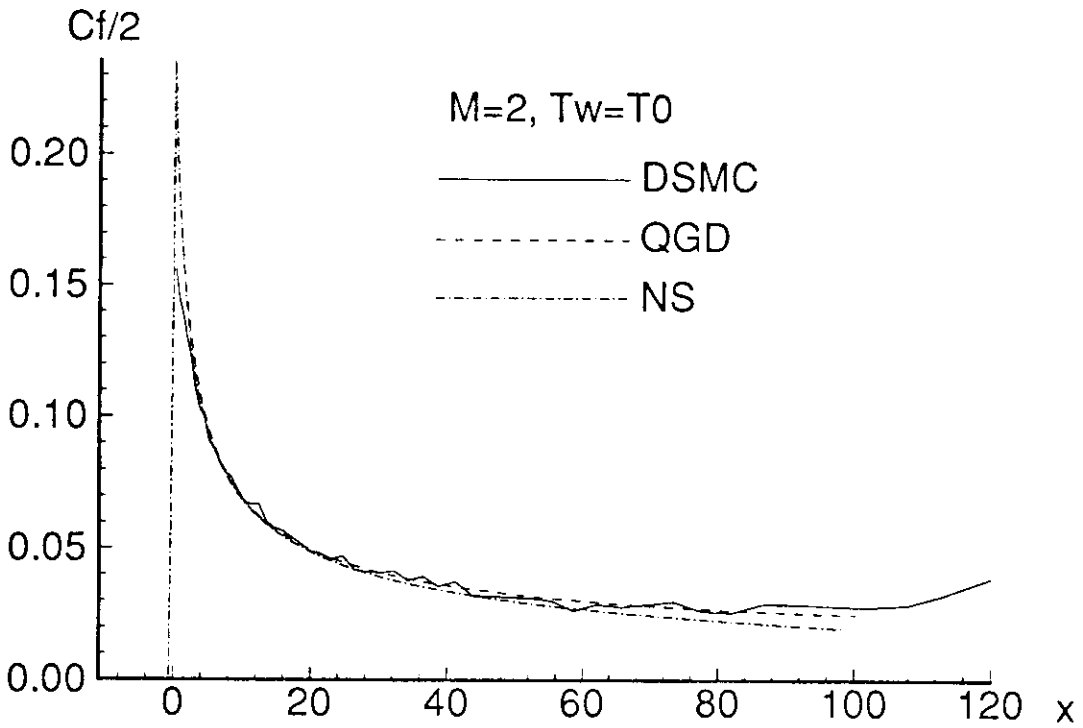
Cf/2
M=2, Tw=T0
DSMC
QGD
NS
0.20
0.15
0.10
0.05
0.00
0
20
40
60
80
100
120
x

Fig.3

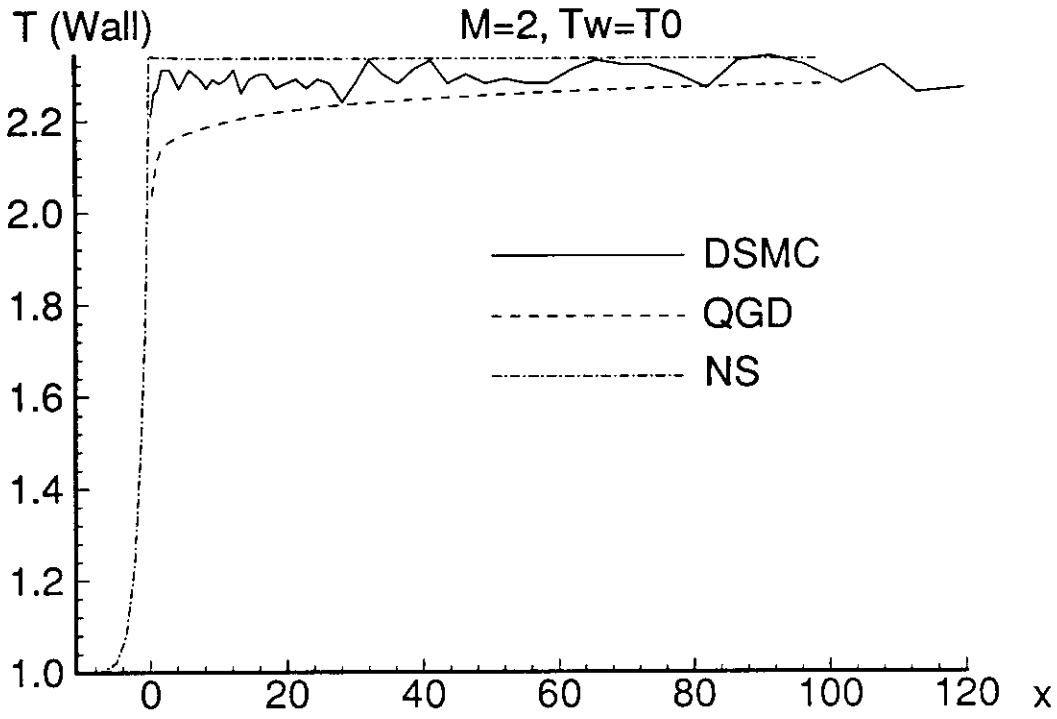
T (Wall)
M=2, Tw=T0
2.2
2.0
1.8
1.6
1.4
1.2
1.0
0
20
40
60
80
100
120
x
DSMC
QGD
NS

Fig.4

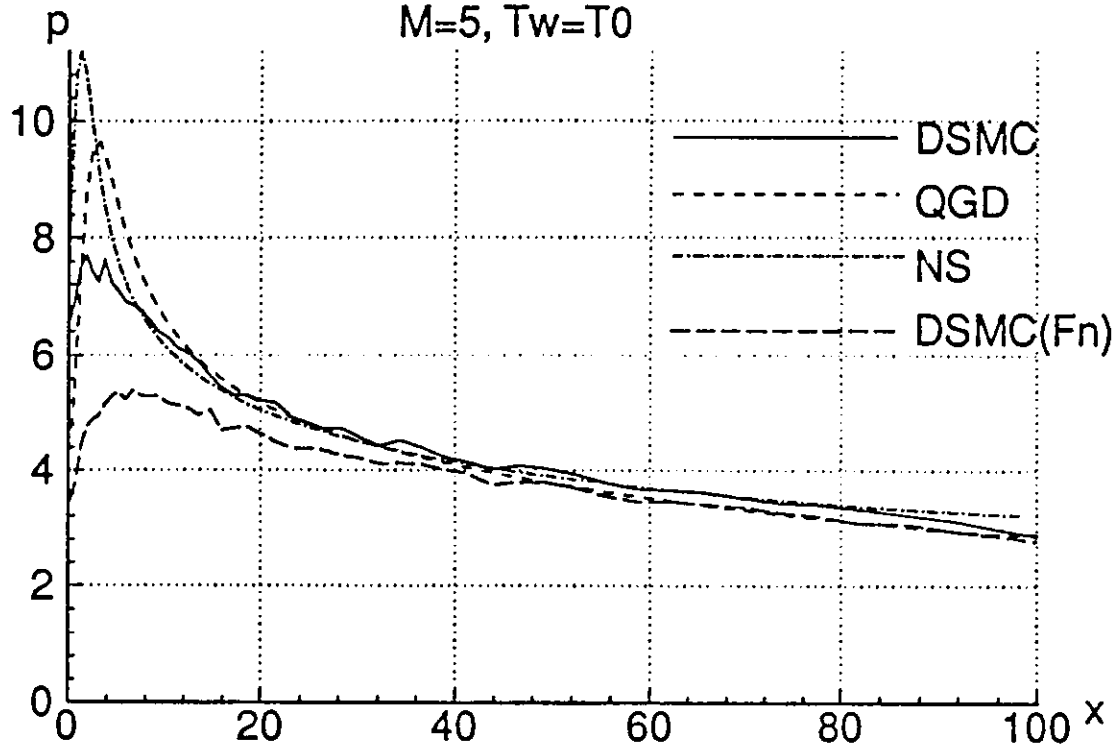
p
M=5, Tw=T0
10
8
6
4
2
0
0
20
40
60
80
100
x
DSMC
QGD
NS
DSMC(Fn)

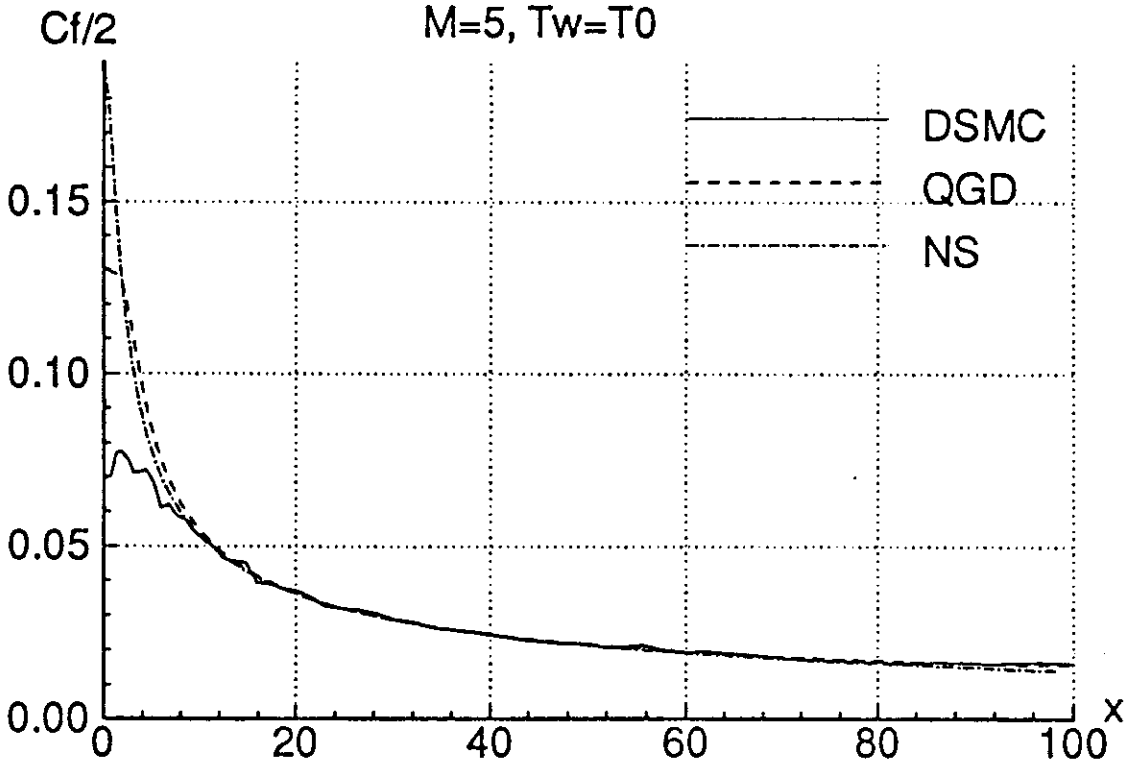
Cf/2
M=5, Tw=T0
0.15
0.10
0.05
0.00
0
20
40
60
80
100
x
DSMC
QGD
NS

Fig.5

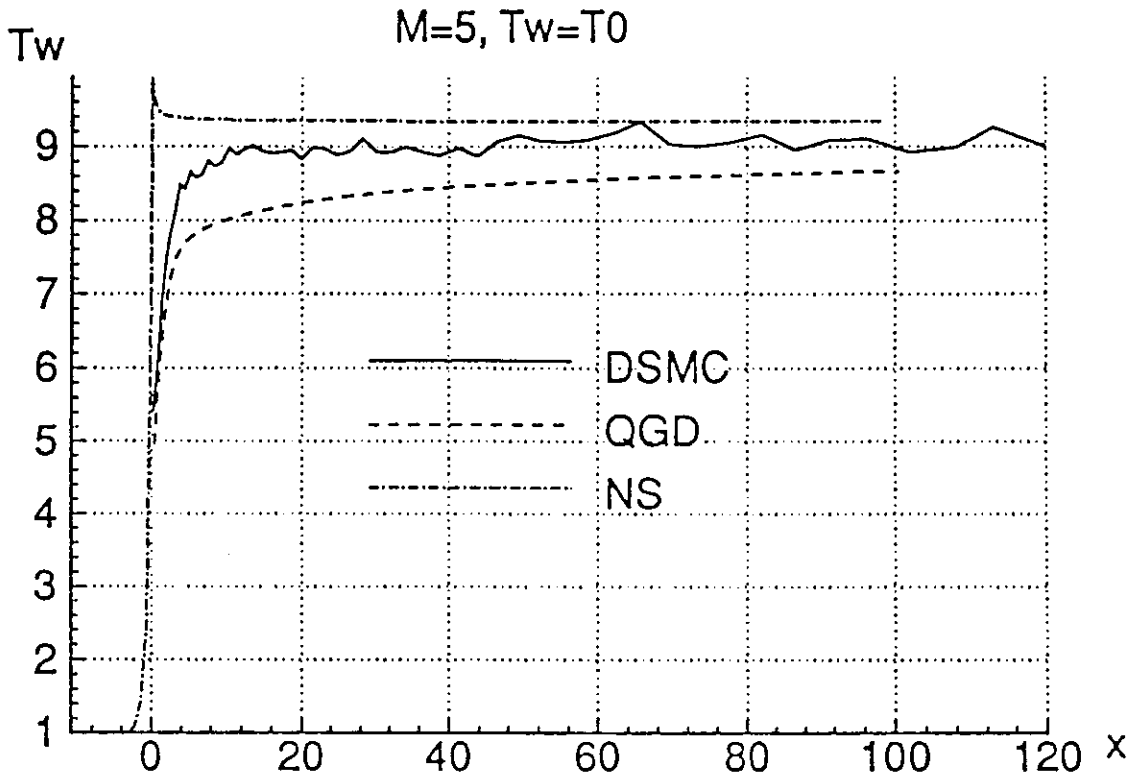

Fig.6

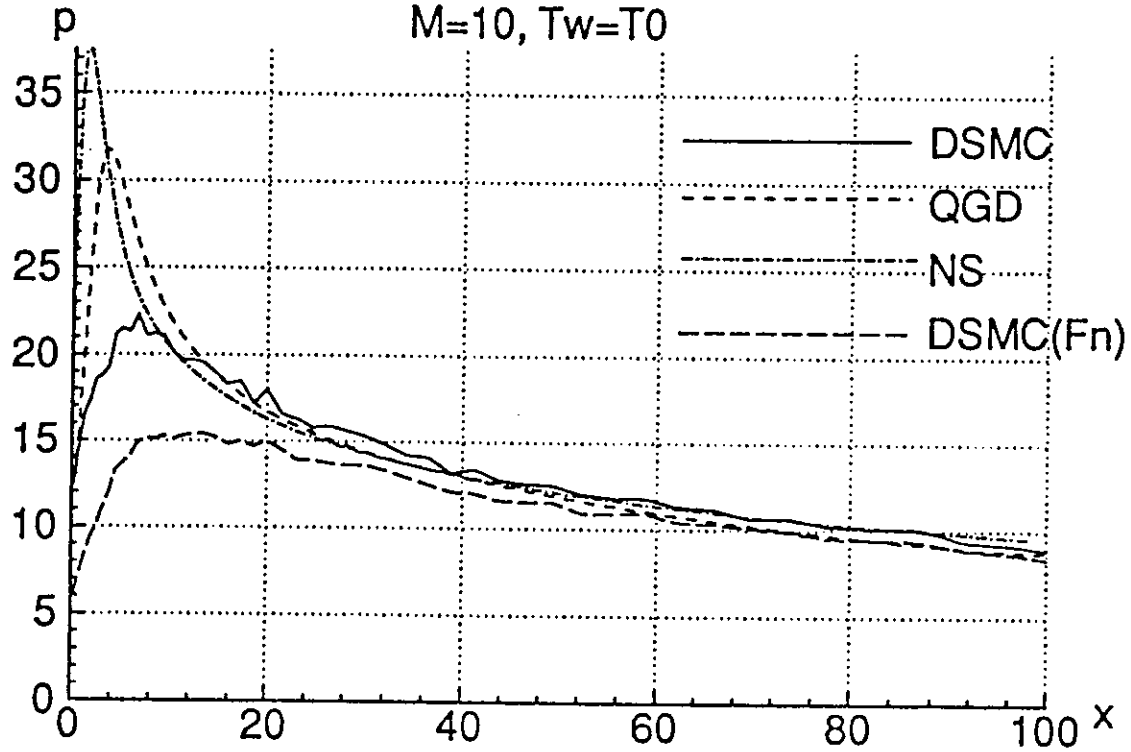
p
M=10, Tw=T0
35
30
25
20
15
10
5
0
0
20
40
60
80
100
x
DSMC
QGD
NS
DSMC(Fn)

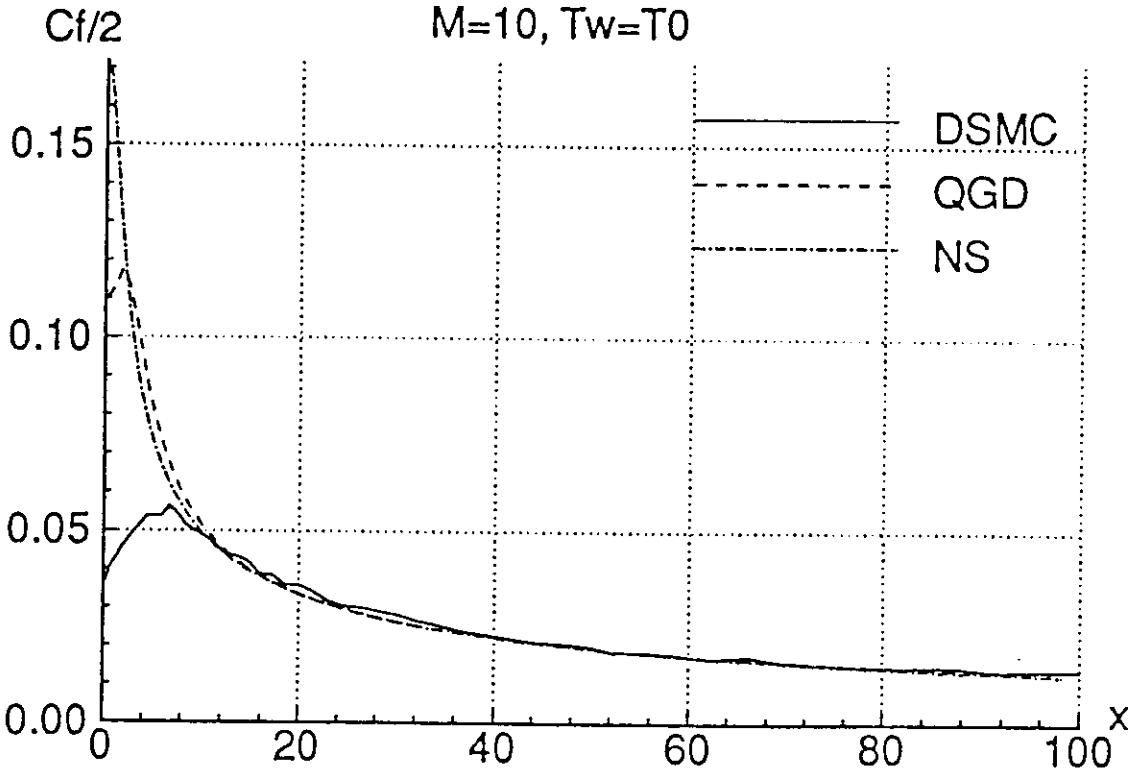
Cf/2
M=10, Tw=T0
0.15
0.10
0.05
0.00
0
20
40
60
80
100
x
DSMC
QGD
NS

Fig.7

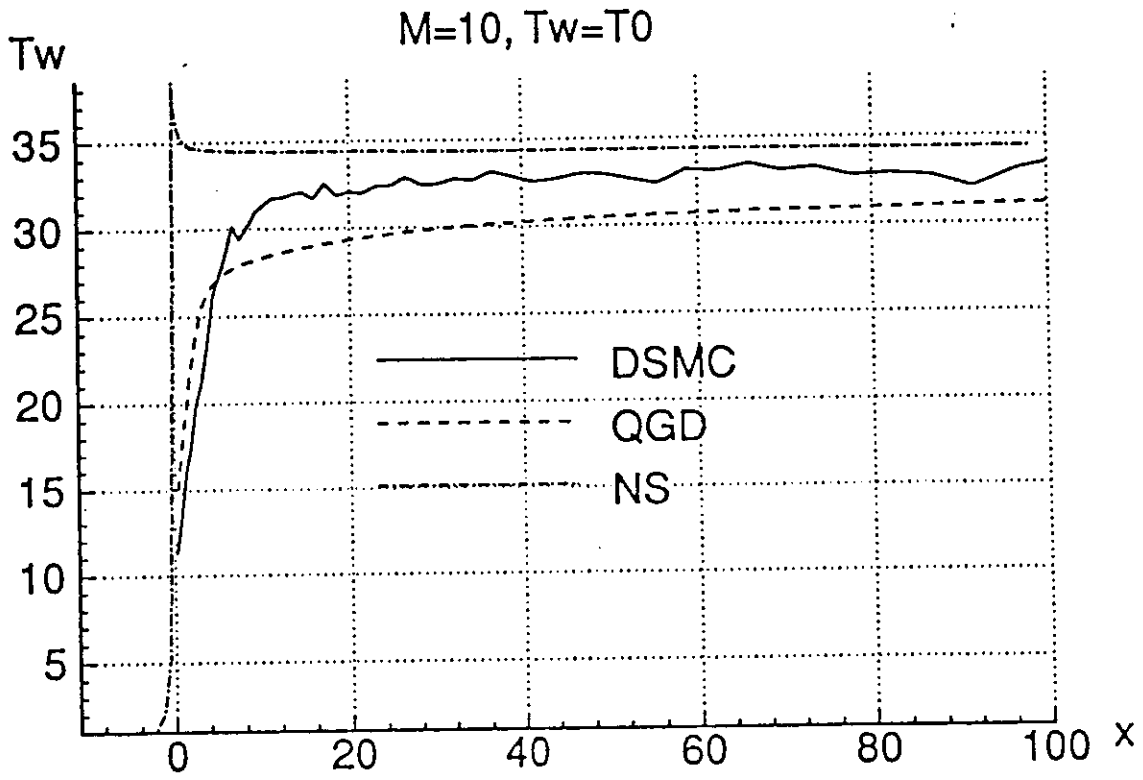

Fig.8

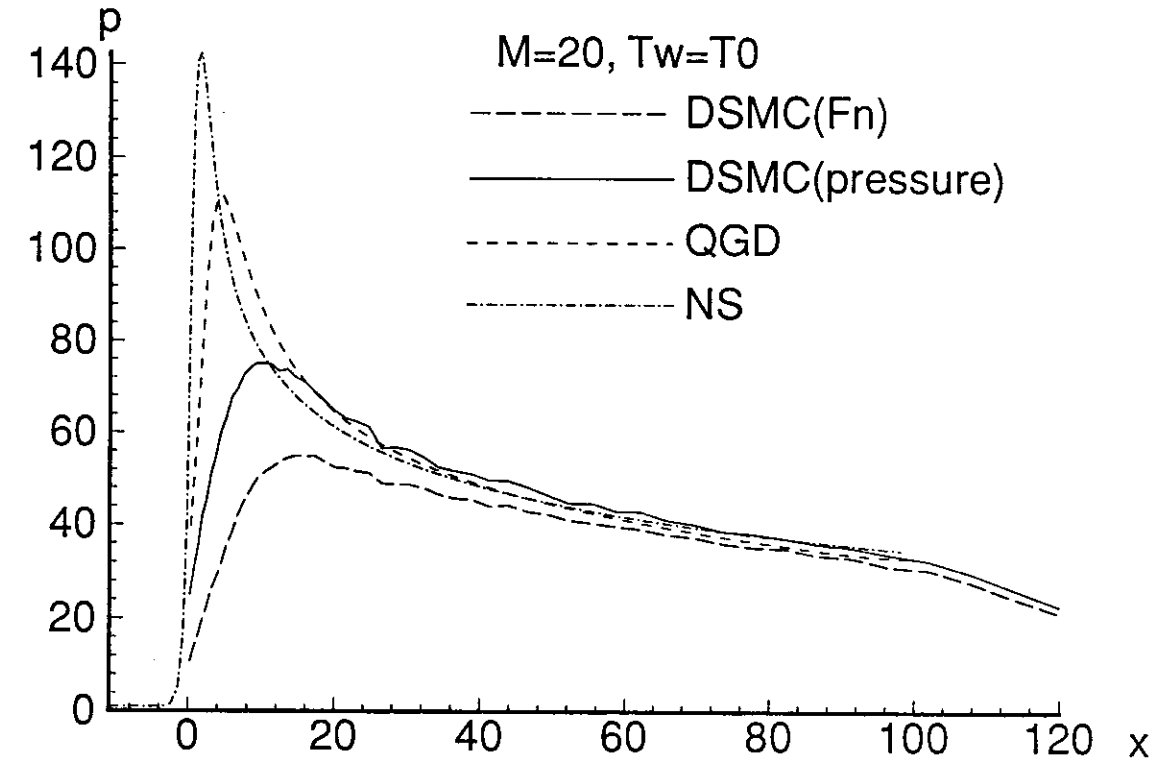
p
140
120
100
80
60
40
20
0
0
20
40
60
80
100
120
x
M=20, Tw=T0
DSMC(Fn)
DSMC(pressure)
QGD
NS

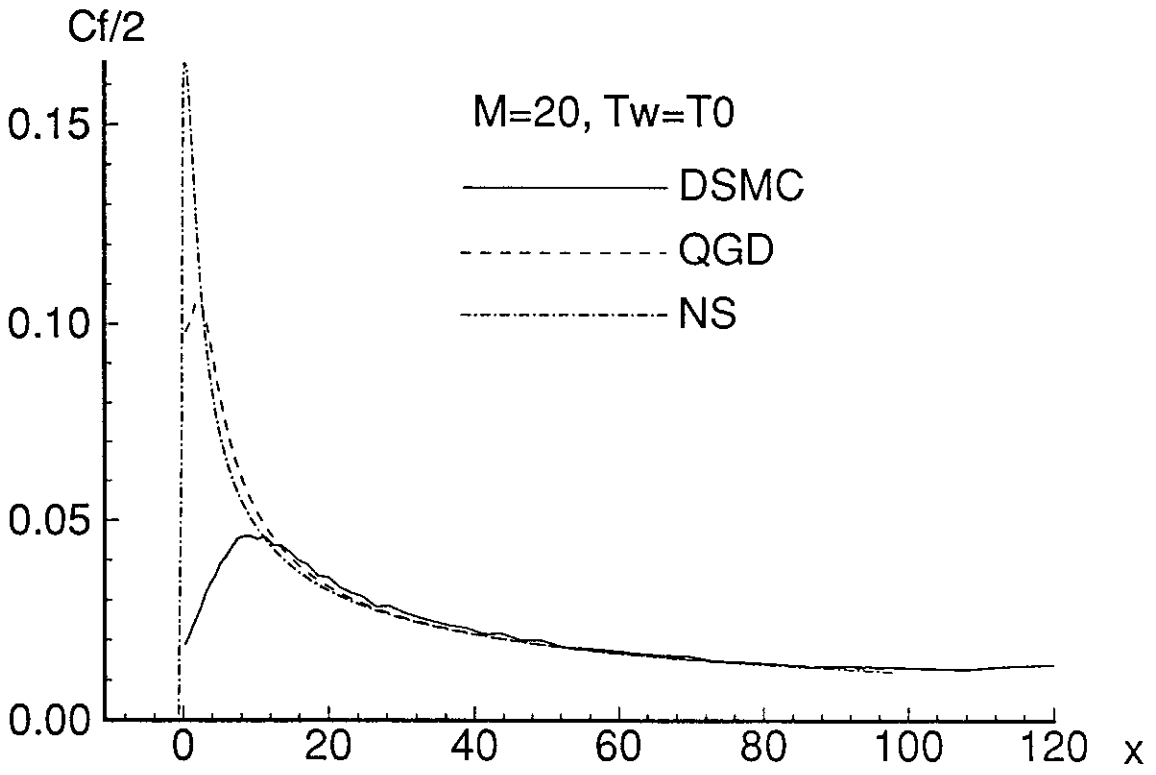
Cf/2
0.15
0.10
0.05
0.00
0
20
40
60
80
100
120
x
M=20, Tw=T0
DSMC
QGD
NS

Fig.9

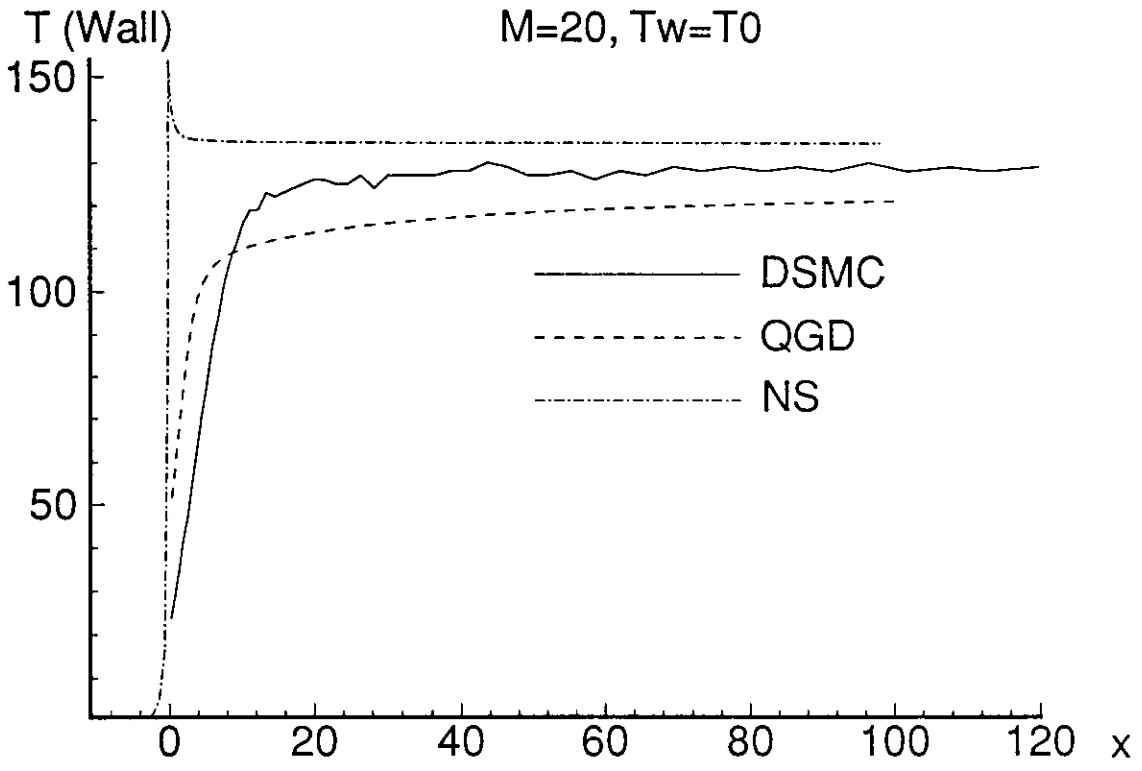
T (Wall)
M=20, Tw=T0
150
100
50
0
20
40
60
80
100
120
x
DSMC
QGD
NS

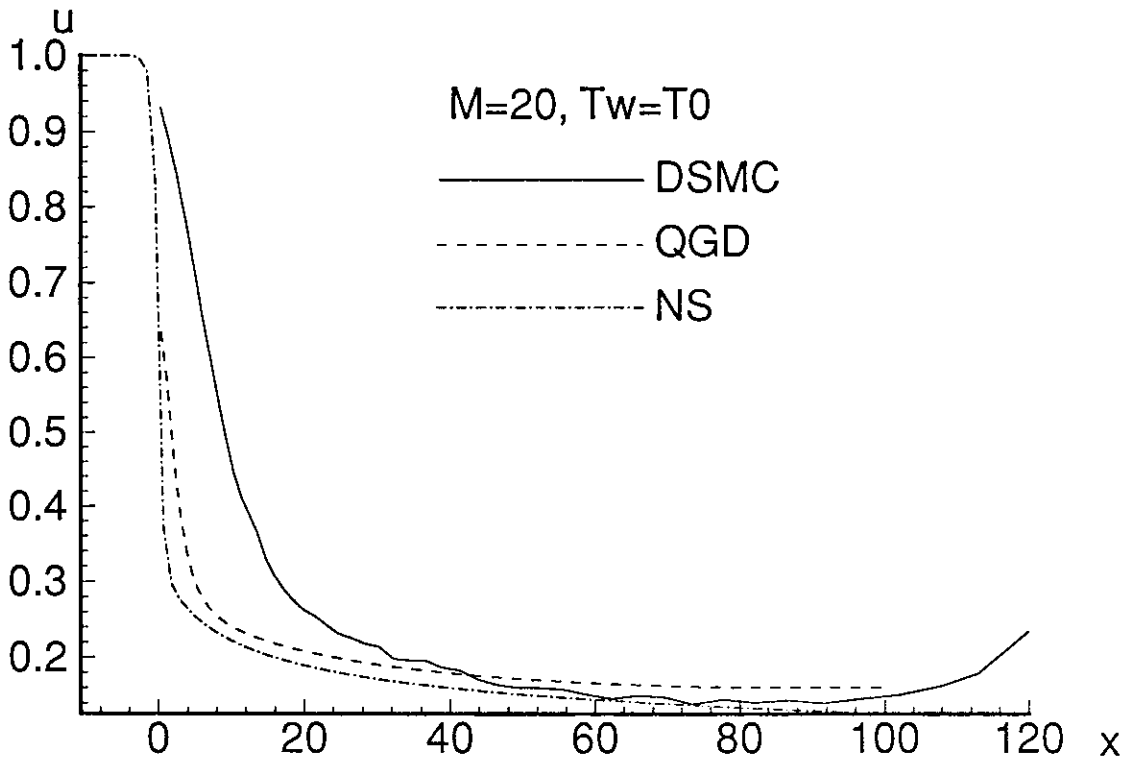
u
1.0
0.9
0.8
0.7
0.6
0.5
0.4
0.3
0.2
0
20
40
60
80
100
120
x
M=20, Tw=T0
DSMC
QGD
NS

Fig.10

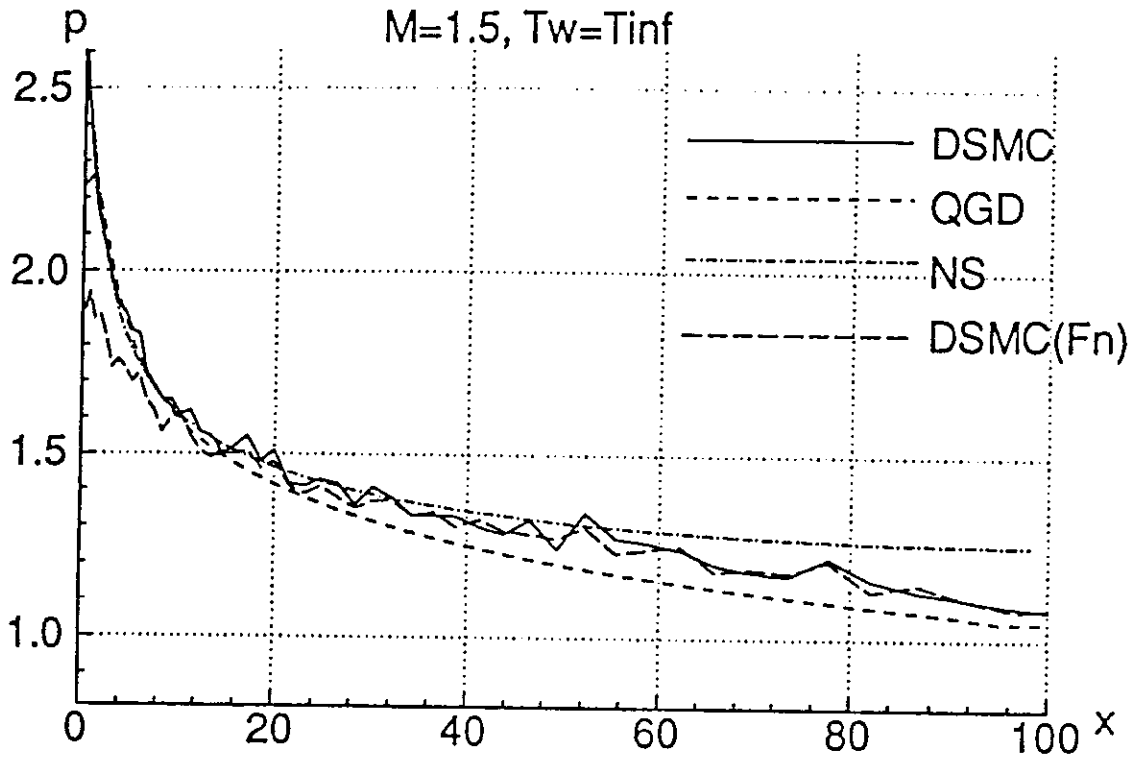
p
M=1.5, Tw=Tinf
2.5
2.0
1.5
1.0
0
20
40
60
80
100
x
DSMC
QGD
NS
DSMC(Fn)

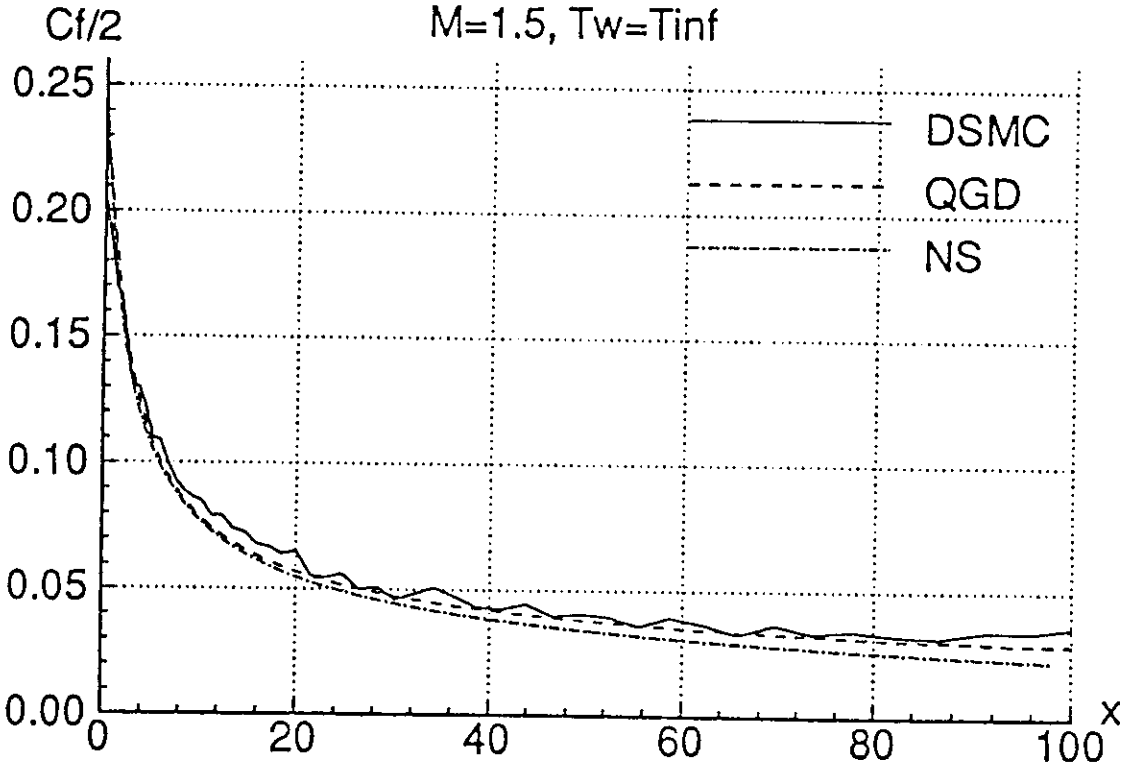
Cf/2
M=1.5, Tw=Tinf
0.25
0.20
0.15
0.10
0.05
0.00
0
20
40
60
80
100
x
DSMC
QGD
NS

Fig.11

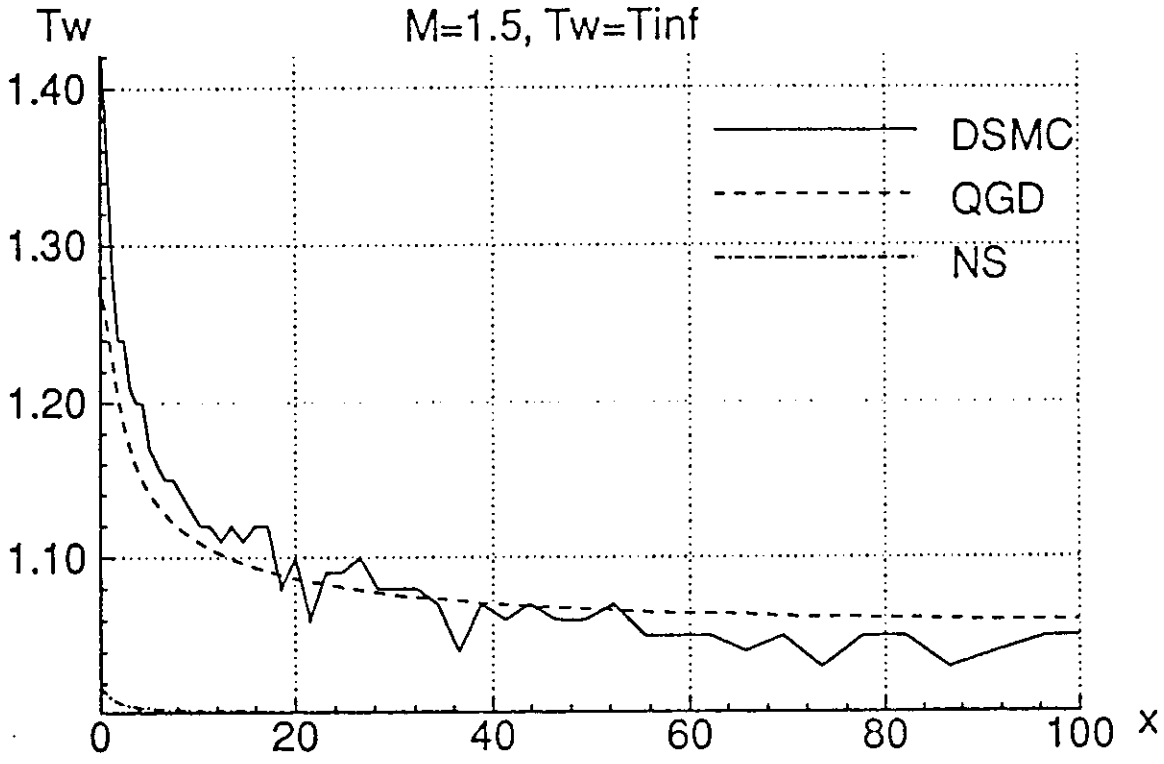
Tw
M=1.5, Tw=Tinf
1.40
1.30
1.20
1.10
DSMC
QGD
NS
0
20
40
60
80
100
x

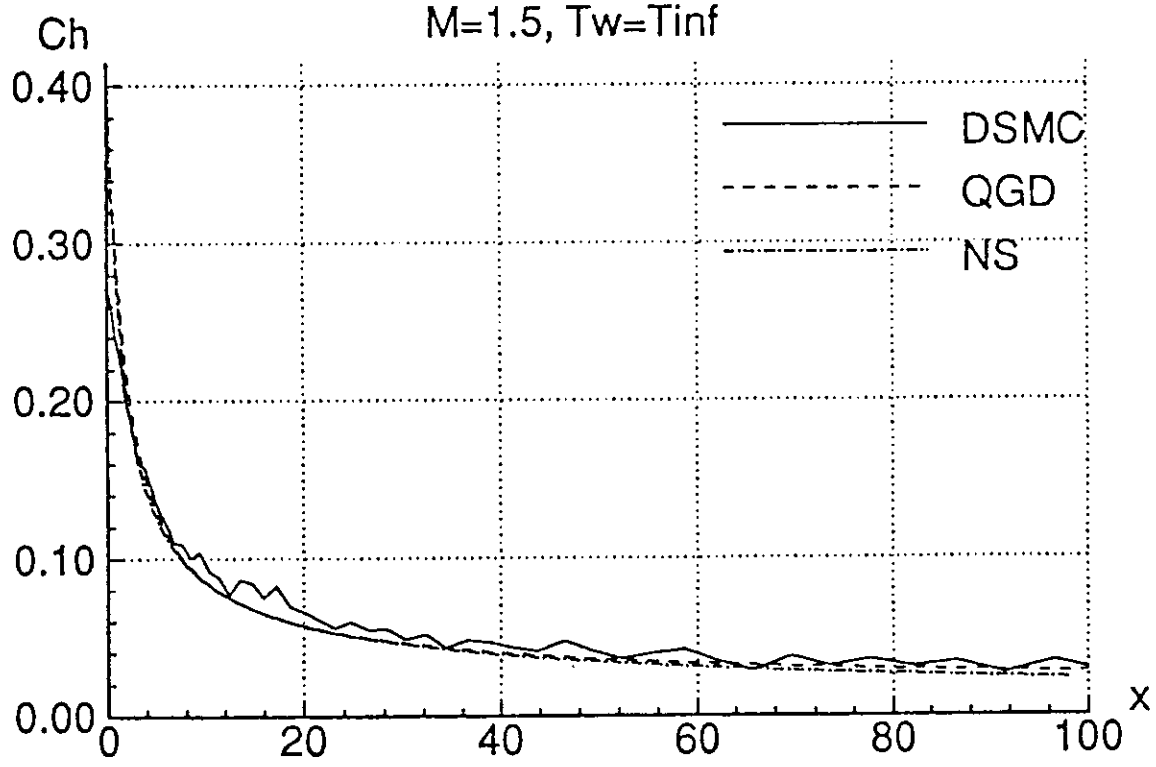
Ch
M=1.5, Tw=Tinf
0.40
0.30
0.20
0.10
0.00
DSMC
QGD
NS
0
20
40
60
80
100
x

Fig.12

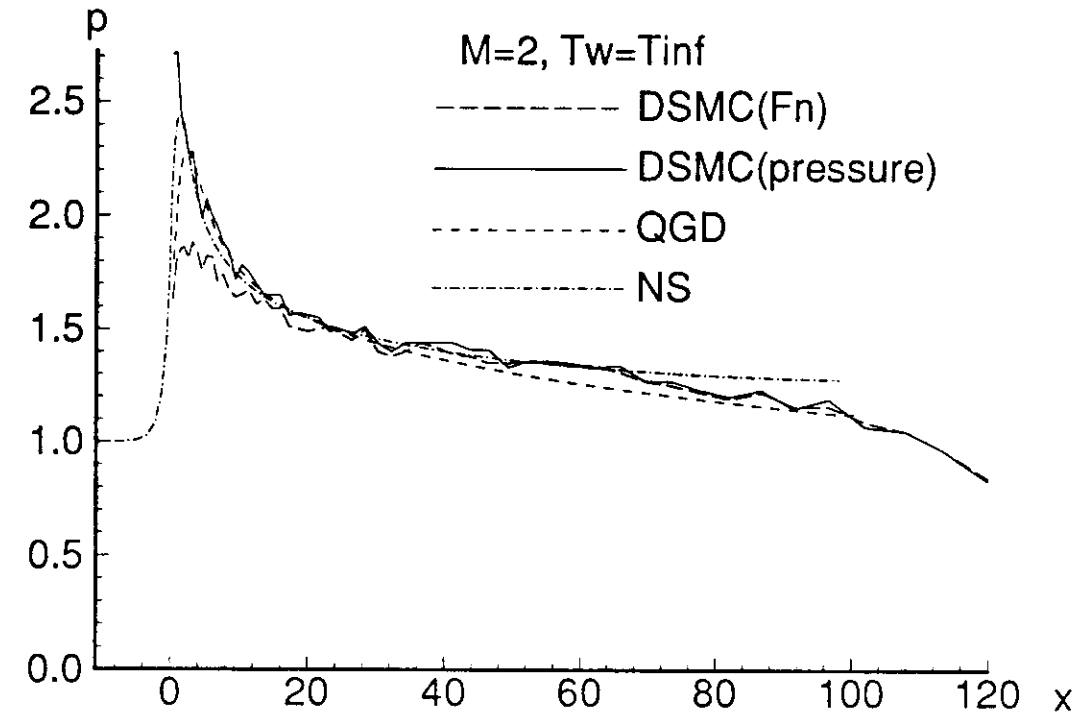
p
M=2, Tw=Tinf
DSMC(Fn)
DSMC(pressure)
QGD
NS
2.5
2.0
1.5
1.0
0.5
0.0
0
20
40
60
80
100
120
x

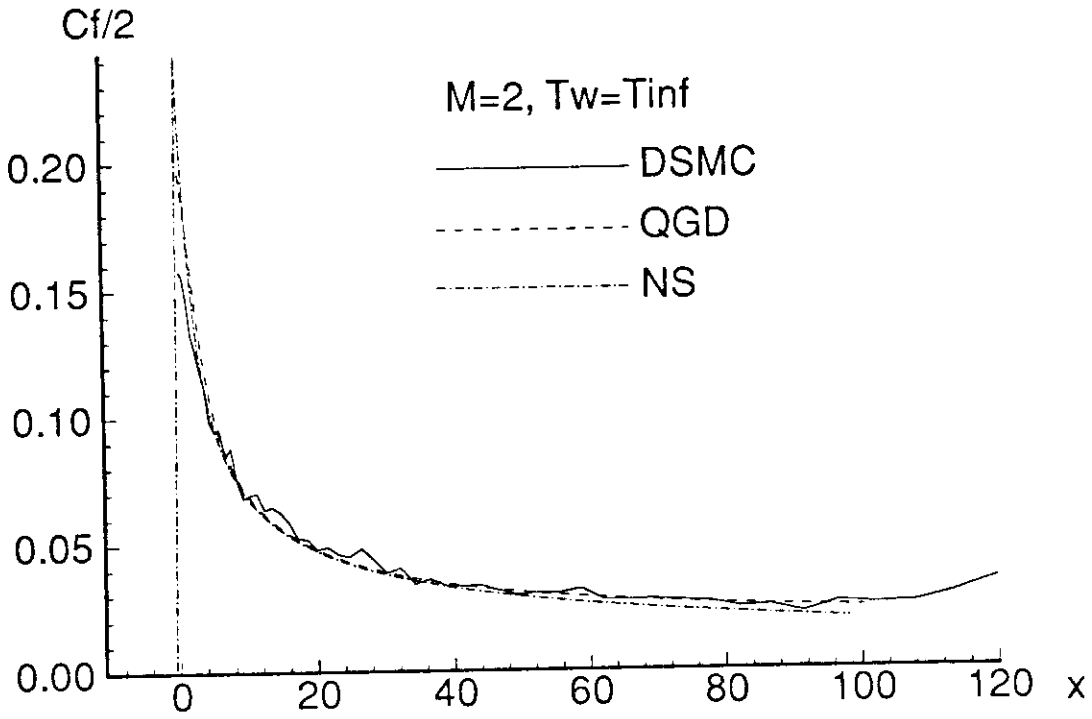
Cf/2
M=2, Tw=Tinf
DSMC
QGD
NS
0.20
0.15
0.10
0.05
0.00
0
20
40
60
80
100
120
x

Fig.13

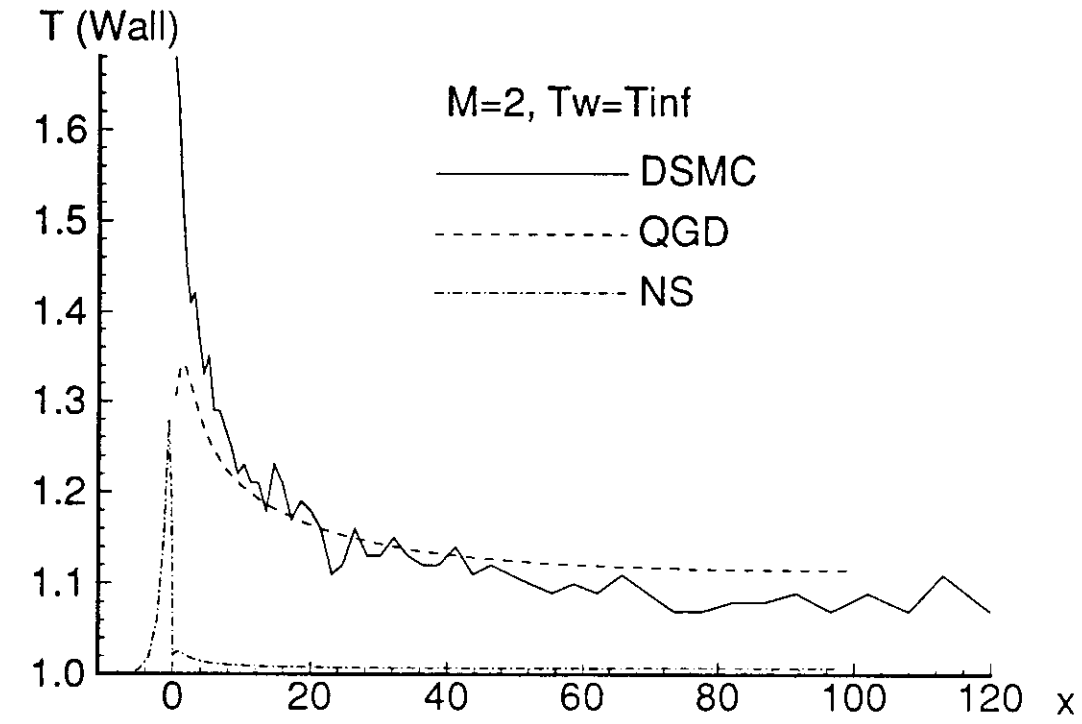
T (Wall)
M=2, Tw=Tinf
DSMC
QGD
NS
1.6
1.5
1.4
1.3
1.2
1.1
1.0
0
20
40
60
80
100
120
x

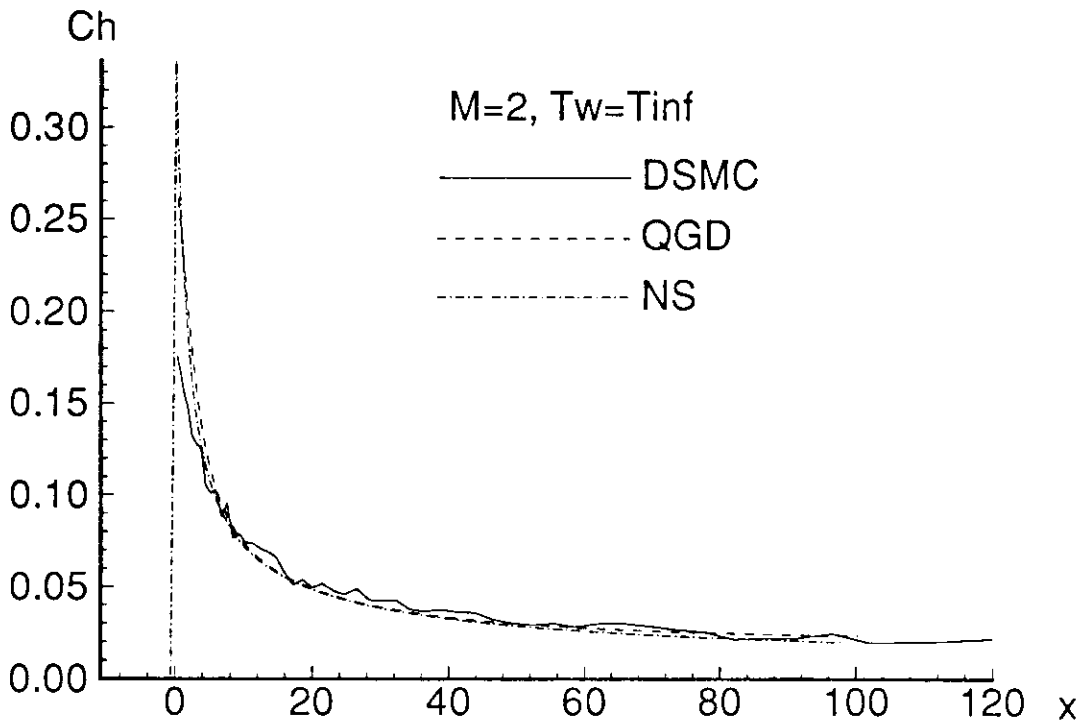
Ch
M=2, Tw=Tinf
DSMC
QGD
NS
0.30
0.25
0.20
0.15
0.10
0.05
0.00
0
20
40
60
80
100
120
x

Fig.14

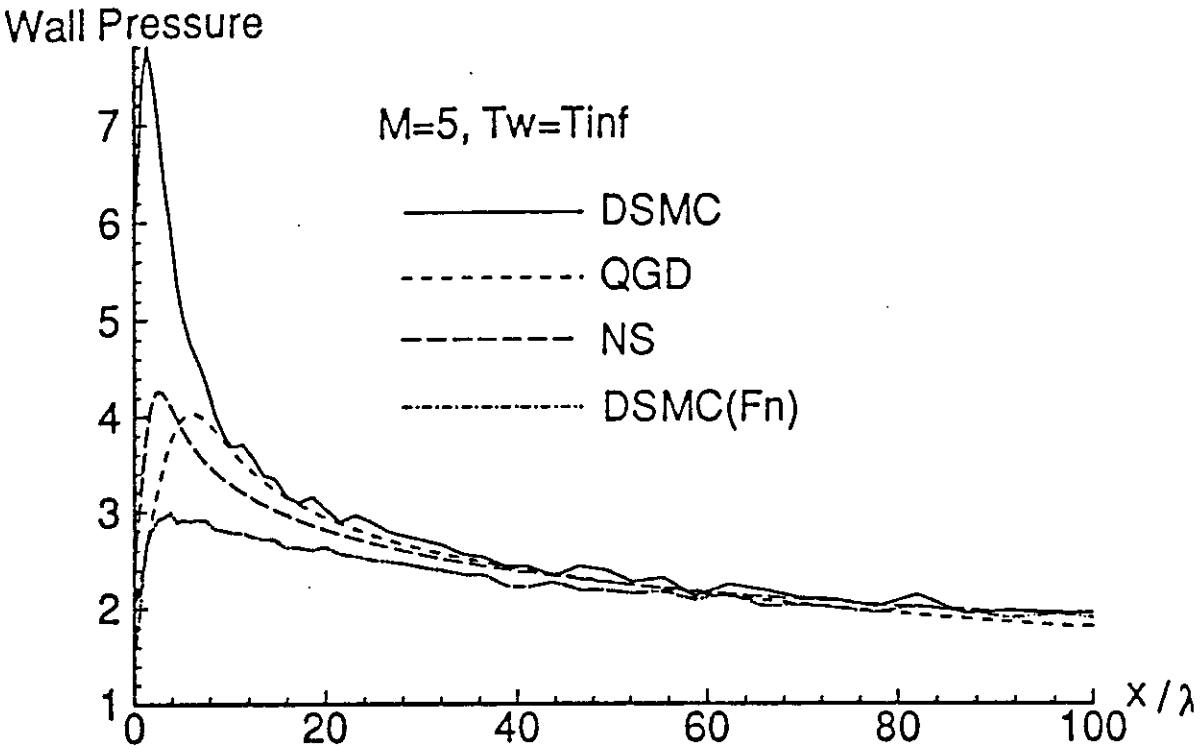
Wall Pressure
M=5, Tw=Tinf
DSMC
QGD
NS
DSMC(Fn)
7
6
5
4
3
2
1
0
20
40
60
80
100
X / λ

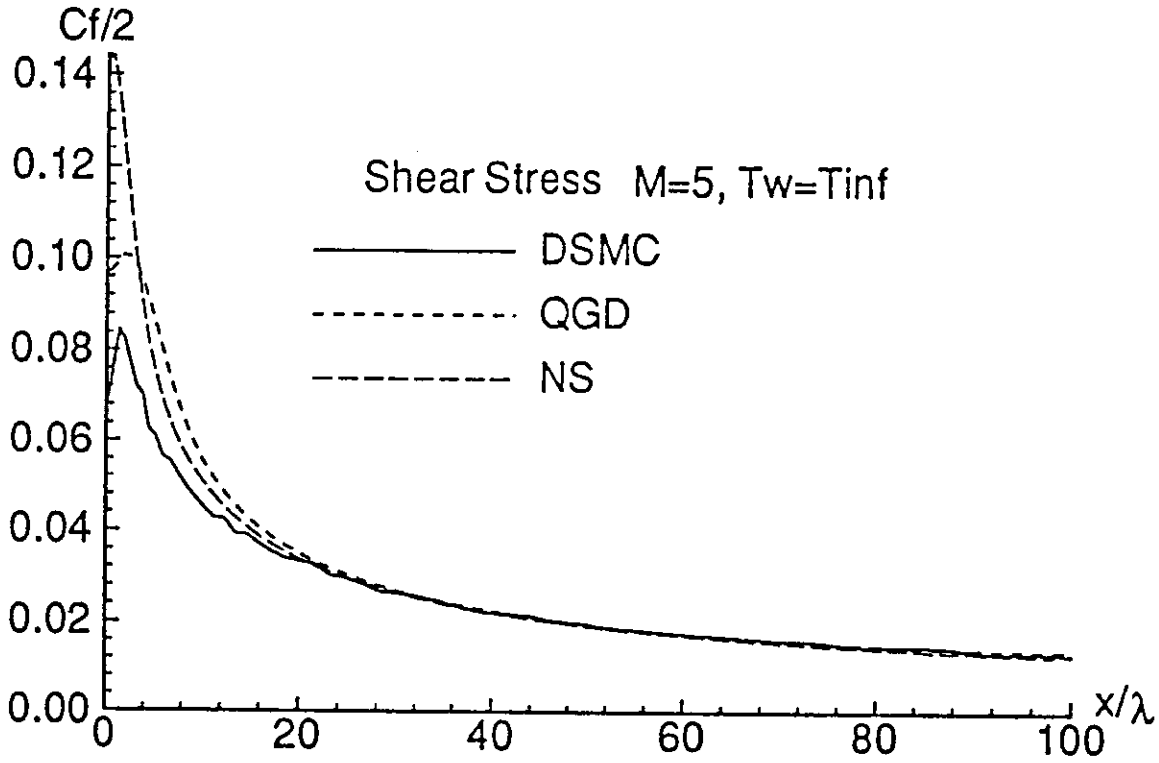
Cf/2
Shear Stress M=5, Tw=Tinf
DSMC
QGD
NS
0.14
0.12
0.10
0.08
0.06
0.04
0.02
0.00
0
20
40
60
80
100
x/λ

Fig.15

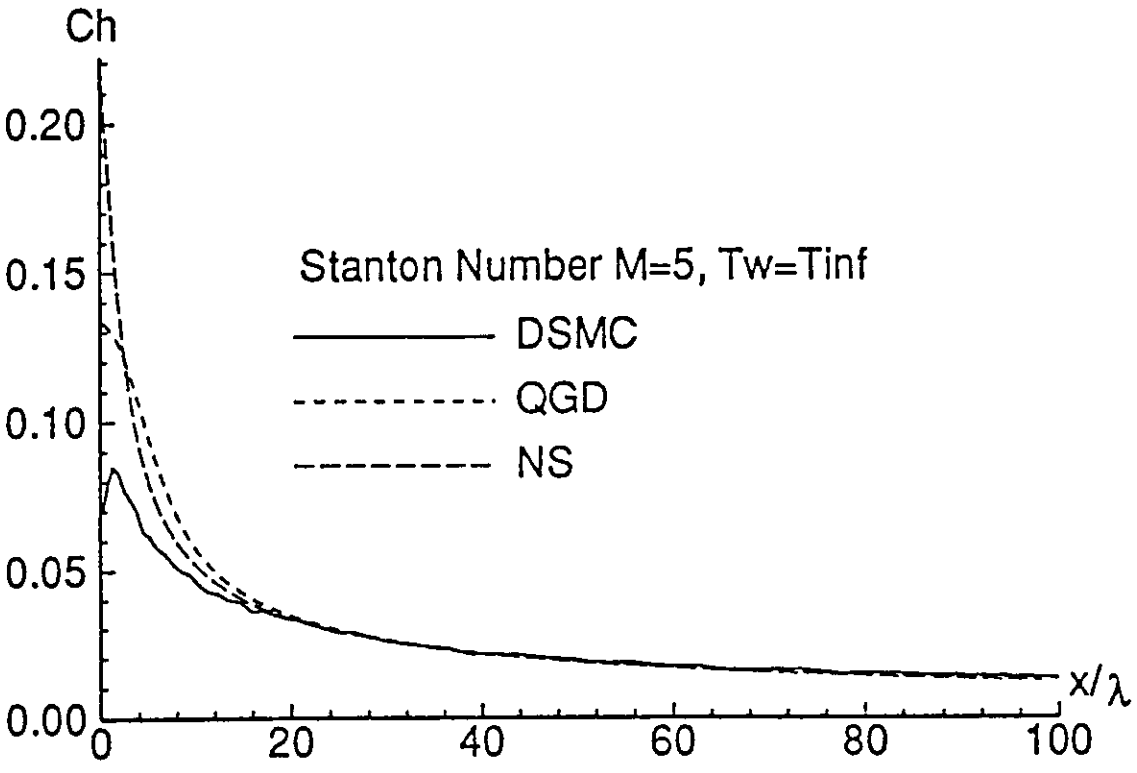
Ch
0.20
0.15
0.10
0.05
0.00
0
20
40
60
80
100
x/λ
Stanton Number M=5, Tw=Tinf
DSMC
QGD
NS

Fig.16

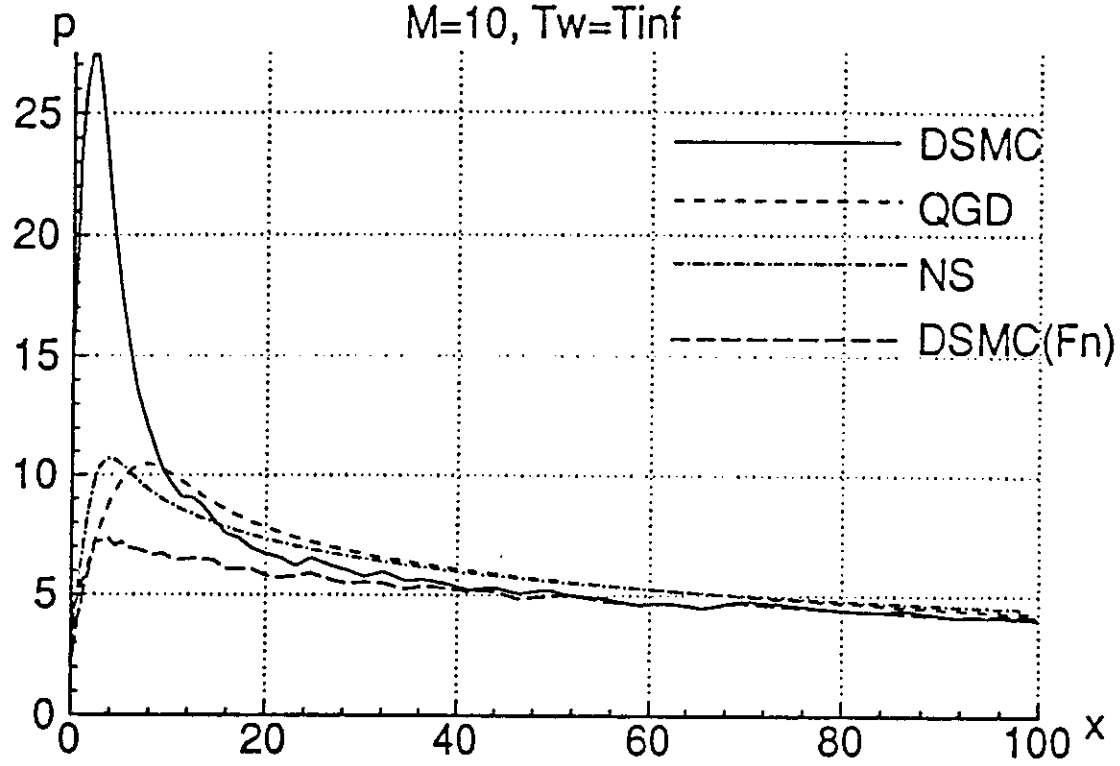
p
M=10, Tw=Tinf
25
20
15
10
5
0
0
20
40
60
80
100
x
DSMC
QGD
NS
DSMC(Fn)

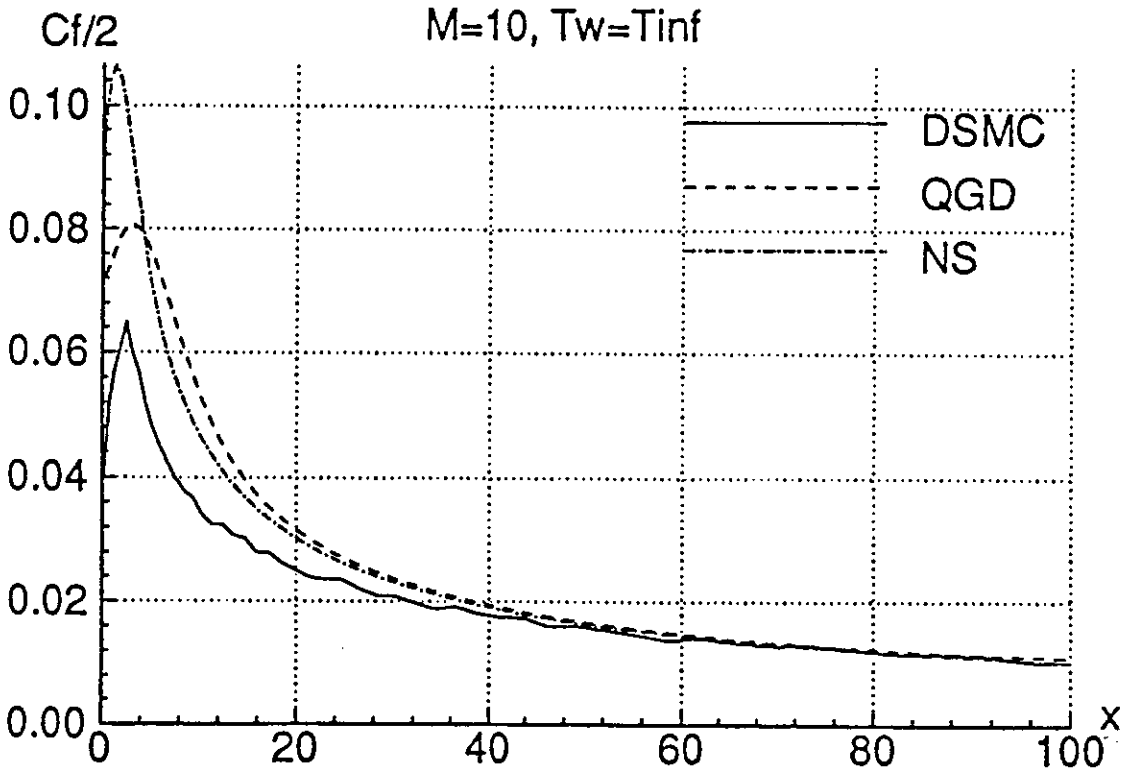
Cf/2
M=10, Tw=Tinf
0.10
0.08
0.06
0.04
0.02
0.00
0
20
40
60
80
100
x
DSMC
QGD
NS

Fig.17

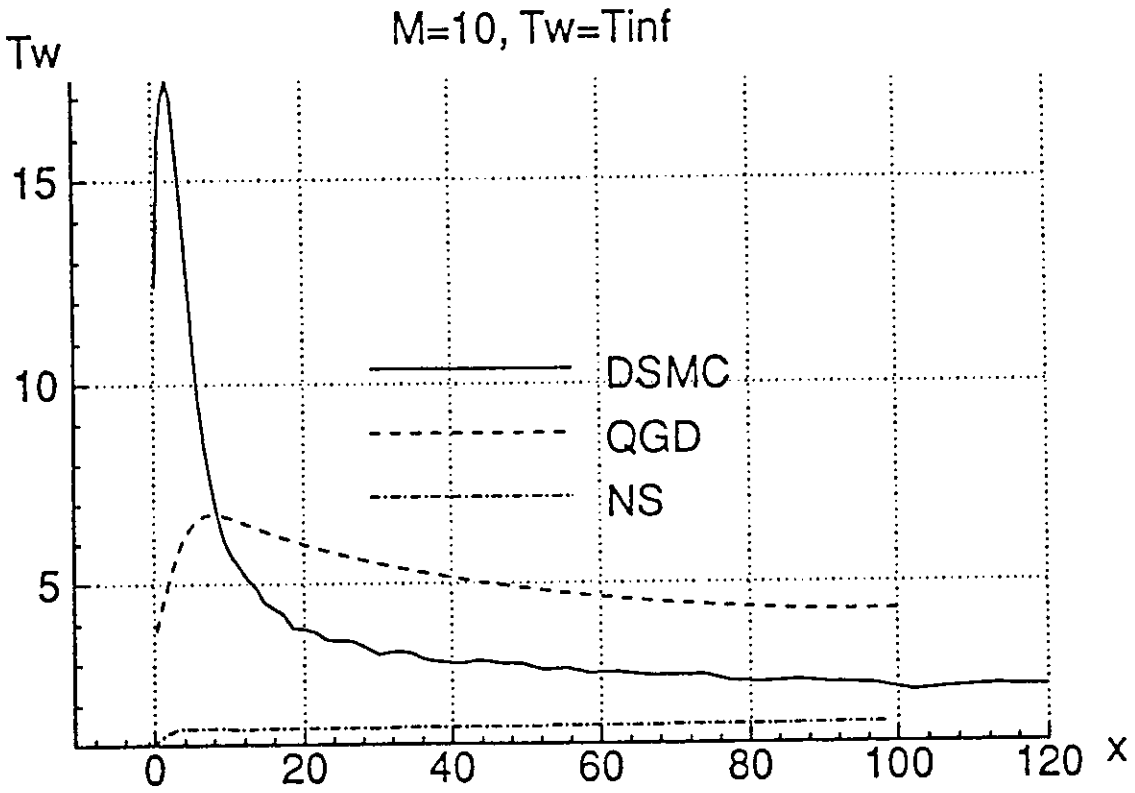
M=10, Tw=Tinf
Tw
15
10
5
0
20
40
60
80
100
120
x
DSMC
QGD
NS

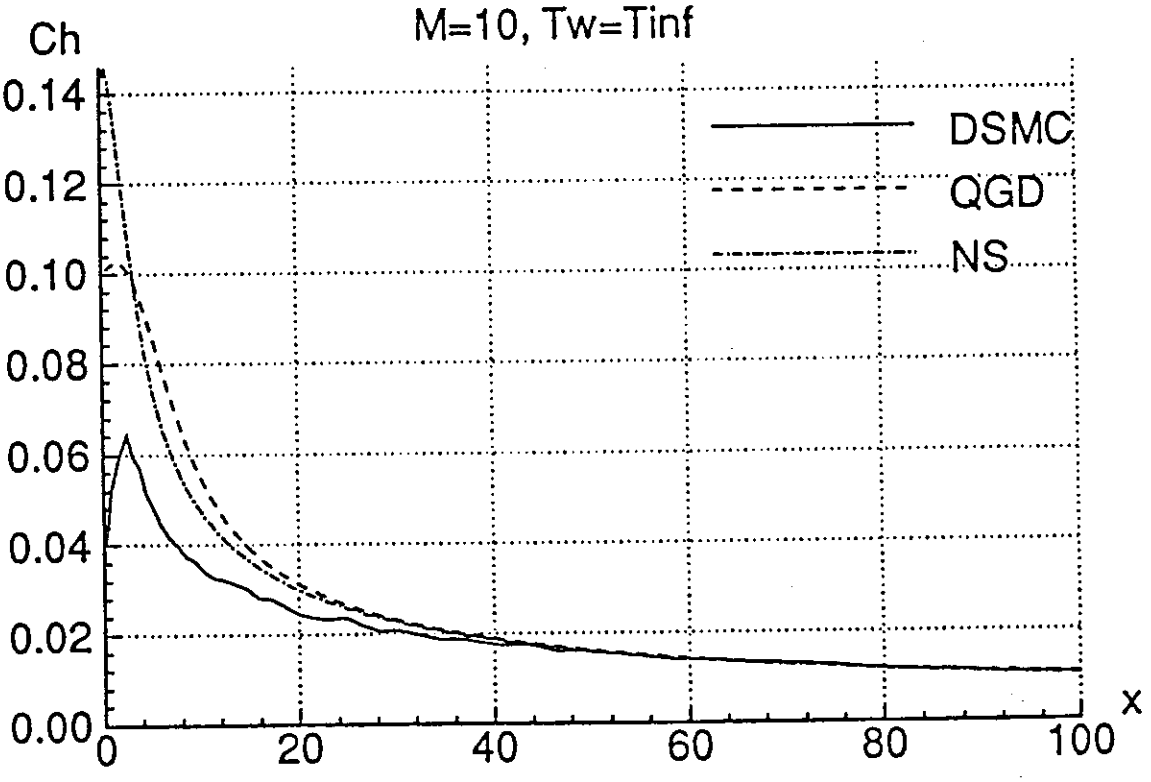
M=10, Tw=Tinf
Ch
0.14
0.12
0.10
0.08
0.06
0.04
0.02
0.00
0
20
40
60
80
100
x
DSMC
QGD
NS

Fig.18

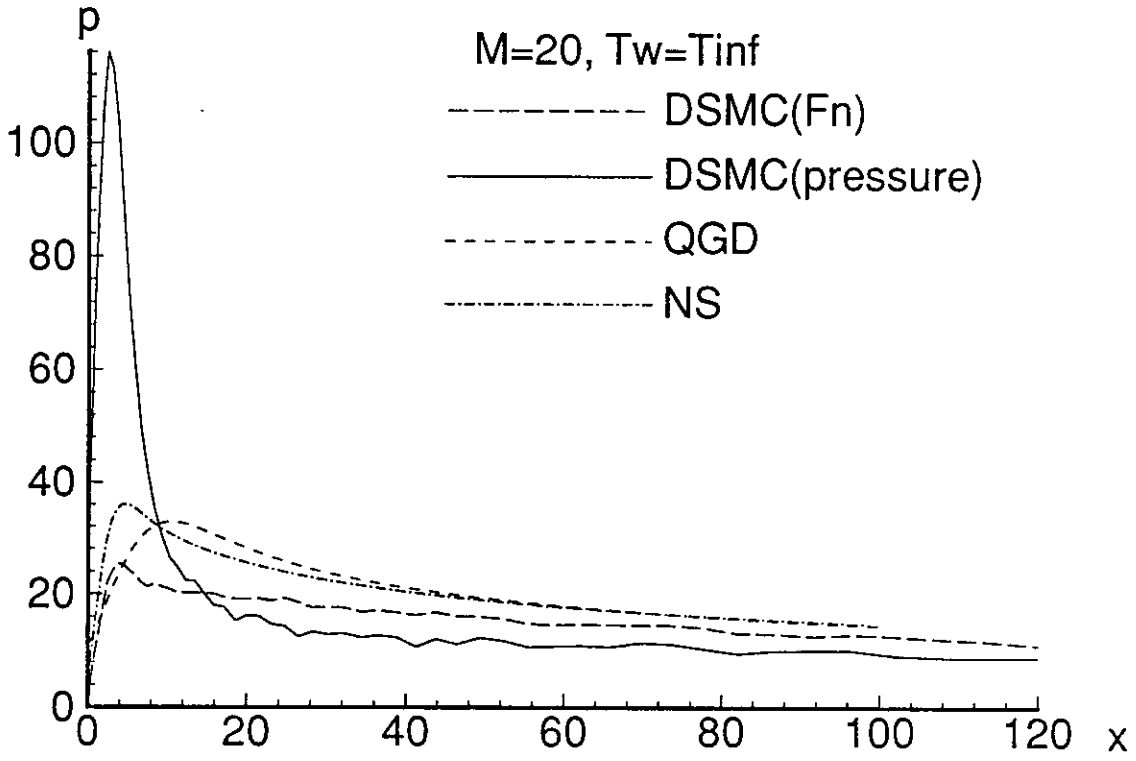
p
M=20, Tw=Tinf
DSMC(Fn)
DSMC(pressure)
QGD
NS
100
80
60
40
20
0
0
20
40
60
80
100
120
x

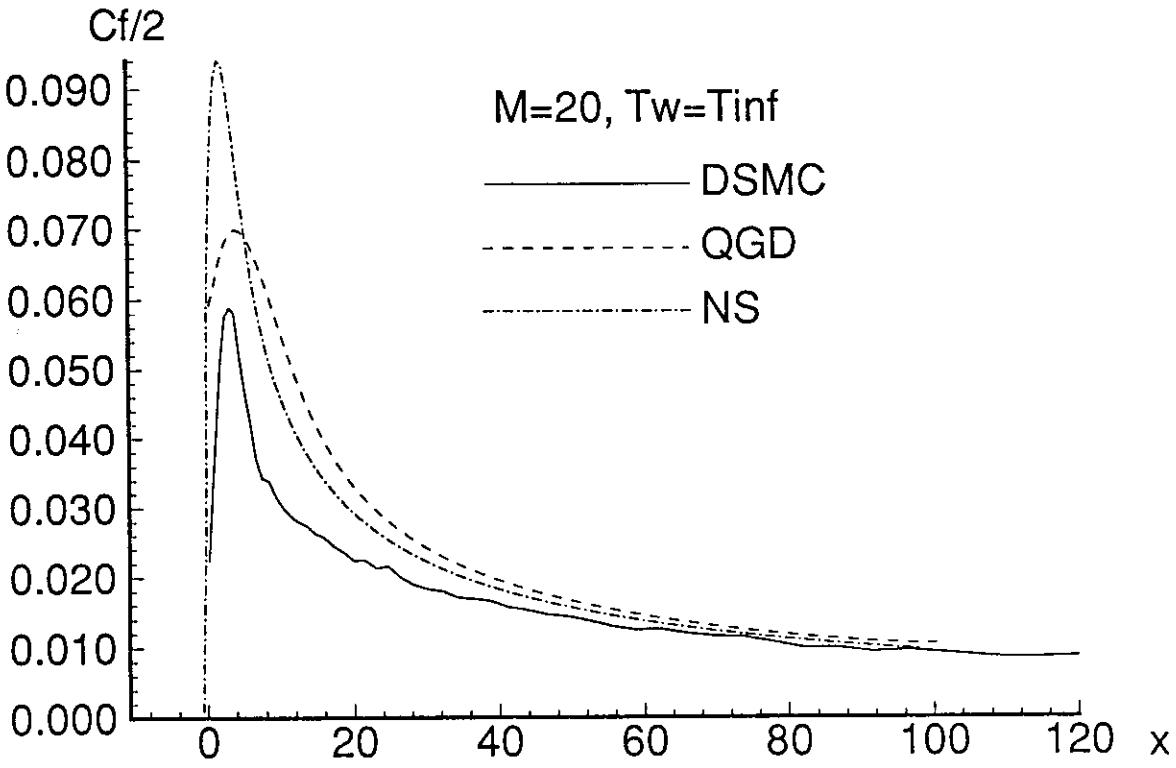
Cf/2
M=20, Tw=Tinf
DSMC
QGD
NS
0.090
0.080
0.070
0.060
0.050
0.040
0.030
0.020
0.010
0.000
0
20
40
60
80
100
120
x

Fig.19

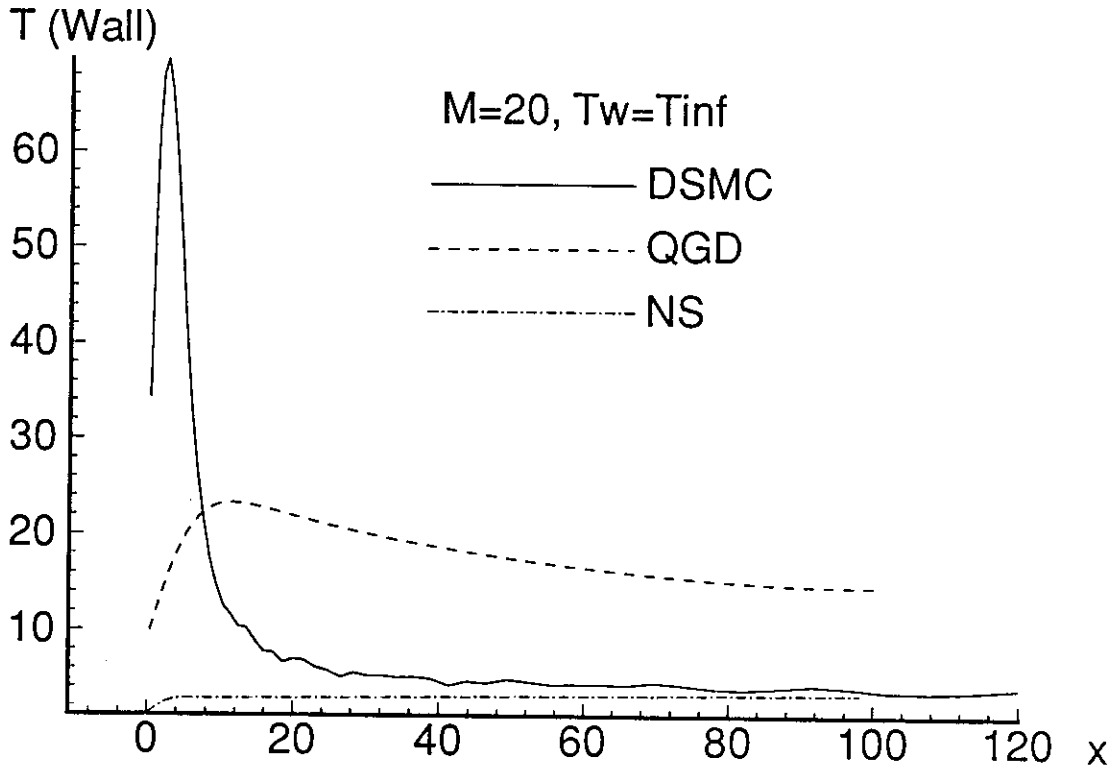
T (Wall)
M=20, Tw=Tinf
DSMC
QGD
NS
60
50
40
30
20
10
0
20
40
60
80
100
120
x

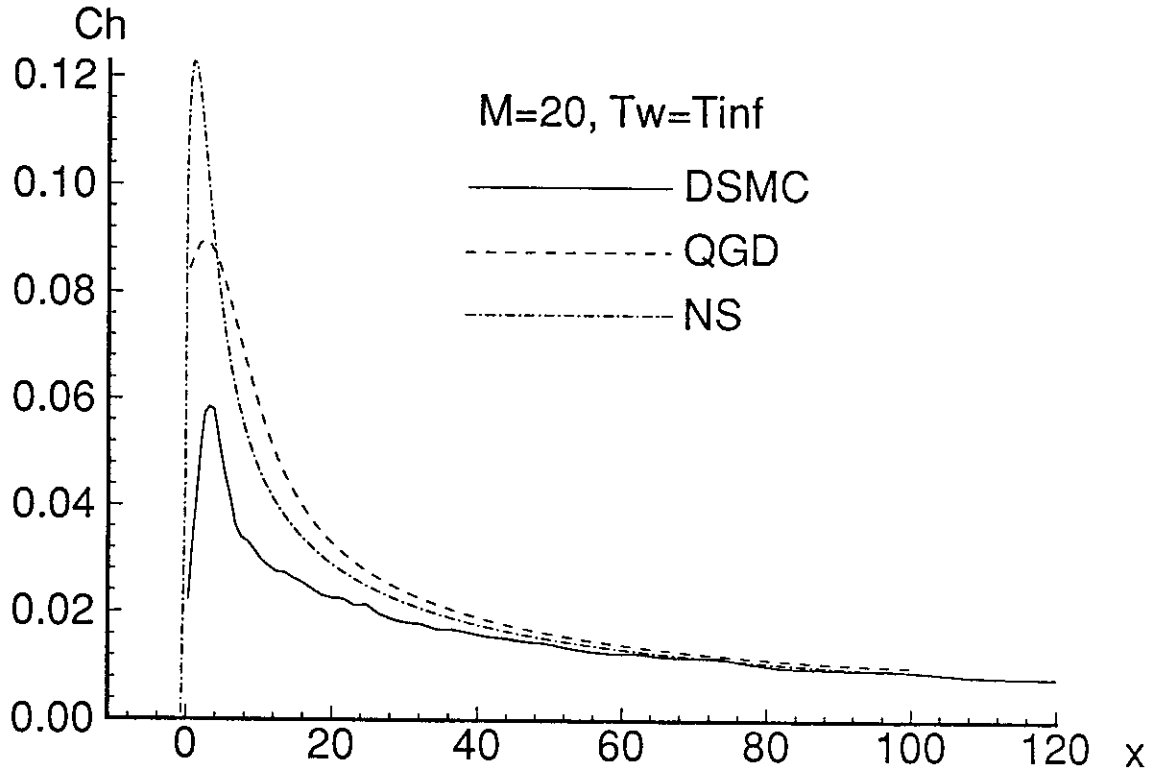
Ch
M=20, Tw=Tinf
DSMC
QGD
NS
0.12
0.10
0.08
0.06
0.04
0.02
0.00
0
20
40
60
80
100
120
x

Fig.20

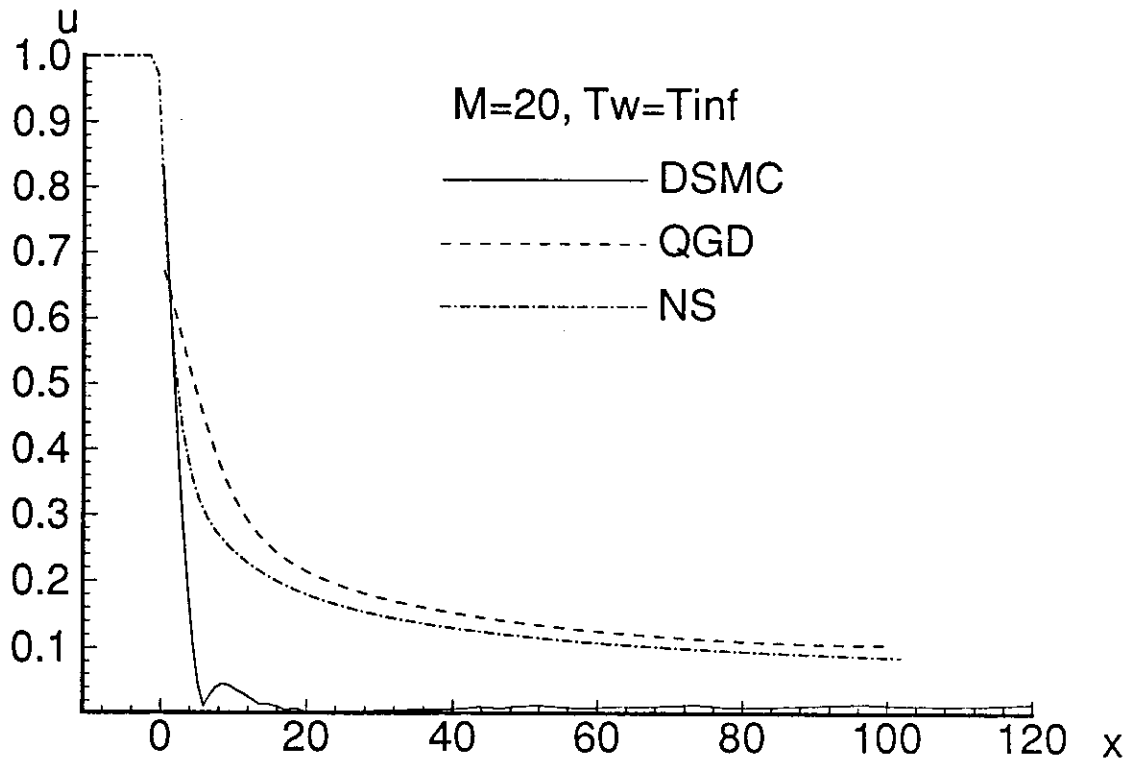
u
1.0
0.9
0.8
0.7
0.6
0.5
0.4
0.3
0.2
0.1
M=20, Tw=Tinf
DSMC
QGD
NS
0
20
40
60
80
100
120
x

Fig.21

Profiles

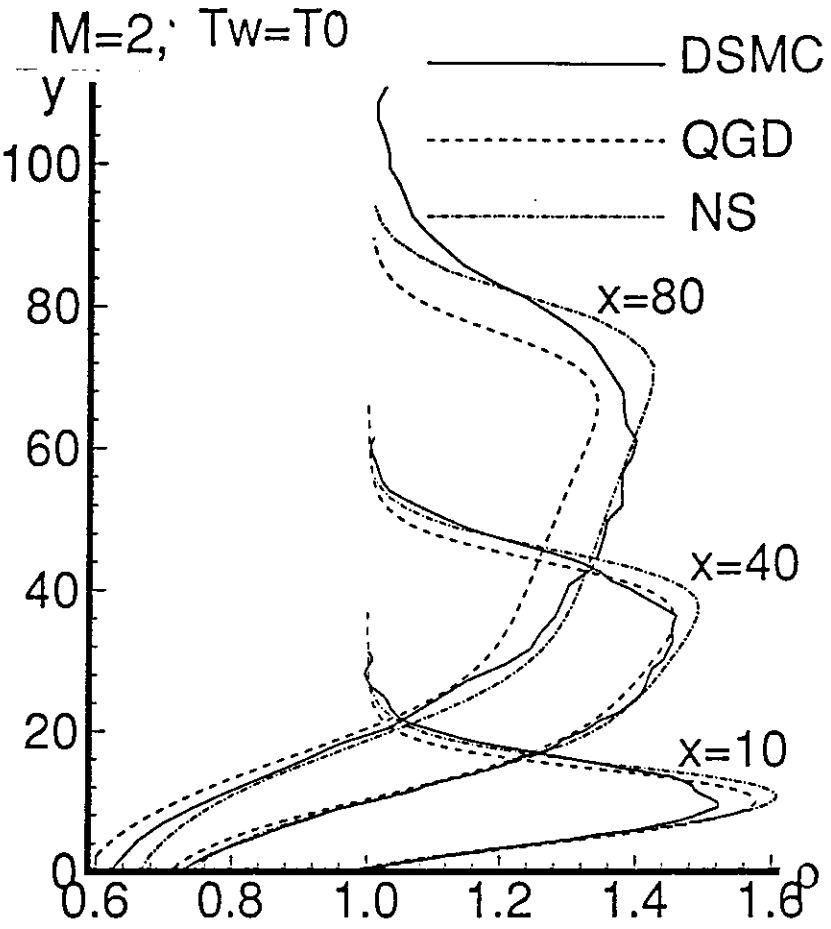
M=2, Tw=T0
DSMC
QGD
NS
y
100
80
60
40
20
0
x=80
x=40
x=10
0.6
0.8
1.0
1.2
1.4
1.6
p

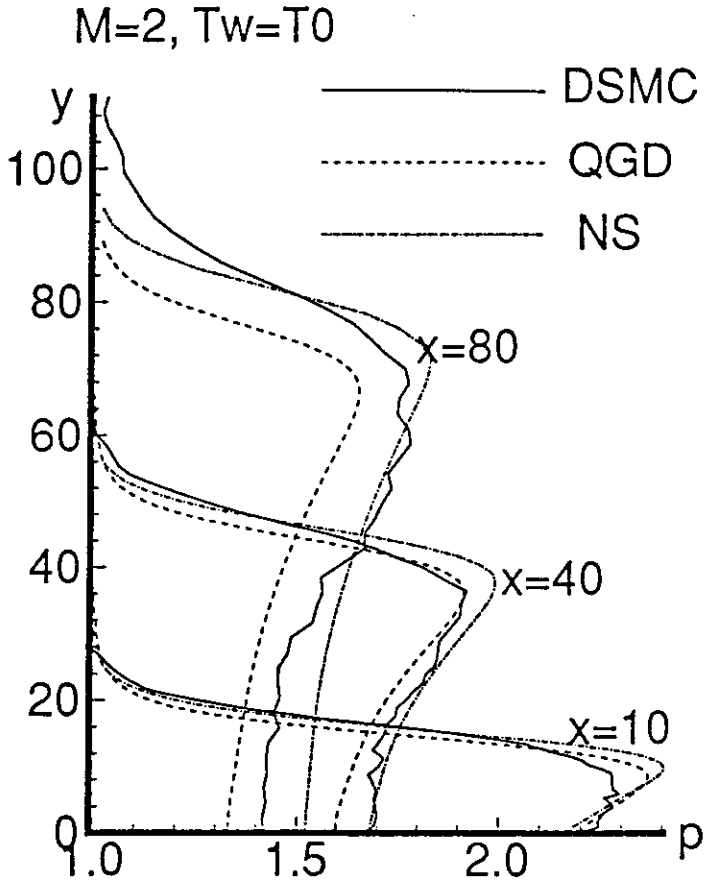
M=2, Tw=T0
DSMC
QGD
NS
y
100
80
60
40
20
0
x=80
x=40
x=10
1.0
1.5
2.0
p

Fig.22

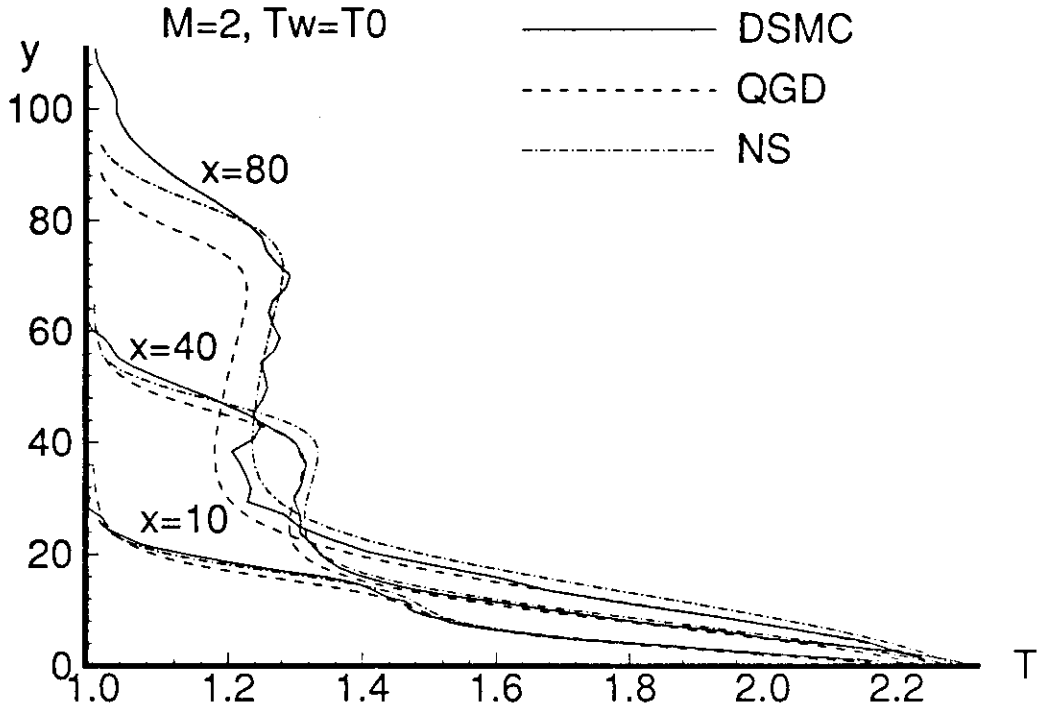
M=2, Tw=T0
DSMC
QGD
NS
y
100
80
60
40
20
0
x=80
x=40
x=10
1.0
1.2
1.4
1.6
1.8
2.0
2.2
T

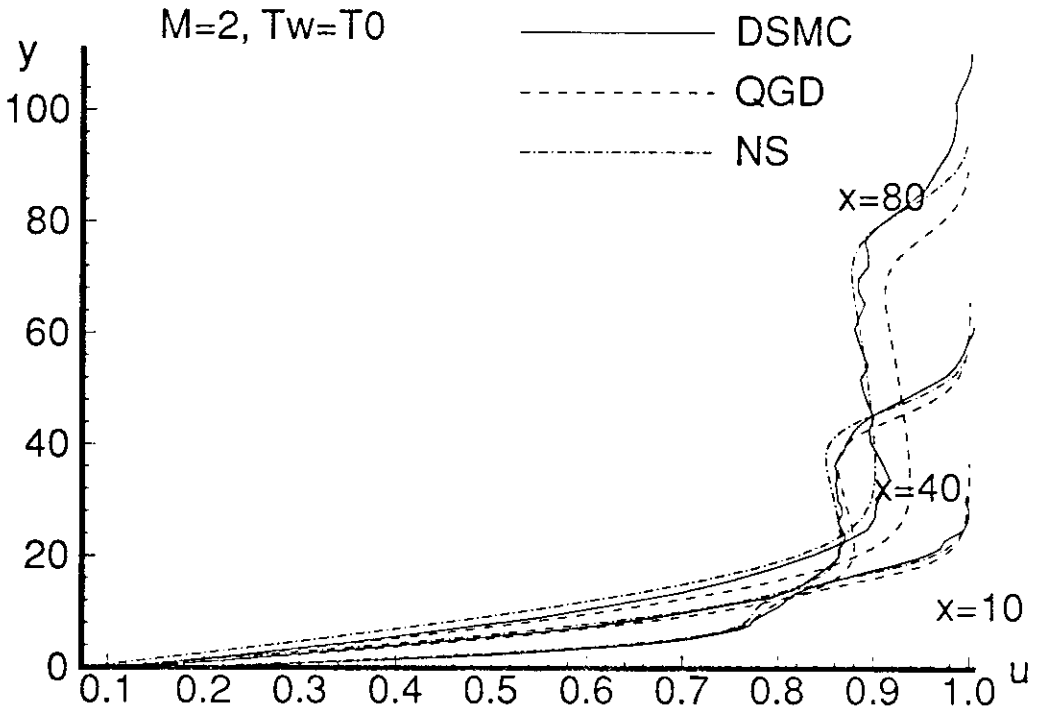
M=2, Tw=T0
DSMC
QGD
NS
y
100
80
60
40
20
0
x=80
x=40
x=10
0.1
0.2
0.3
0.4
0.5
0.6
0.7
0.8
0.9
1.0
u

Fig.23

$M_1 = 5, T_w = T_0$

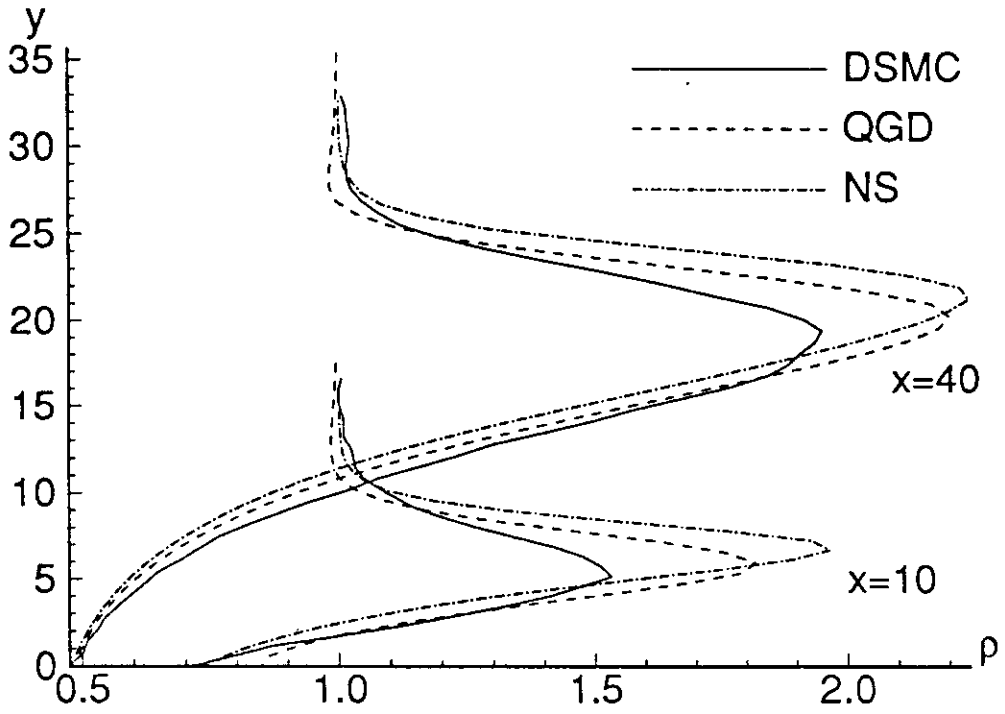

Fig.24

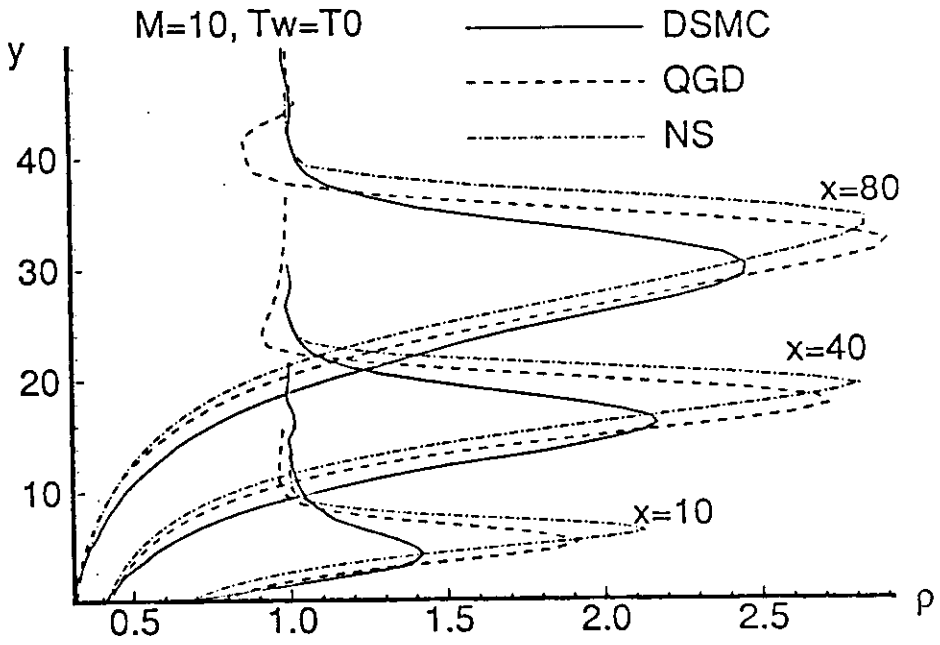
M=10, Tw=T0
DSMC
QGD
NS
y
40
30
20
10
x=80
x=40
x=10
0.5
1.0
1.5
2.0
2.5
ρ

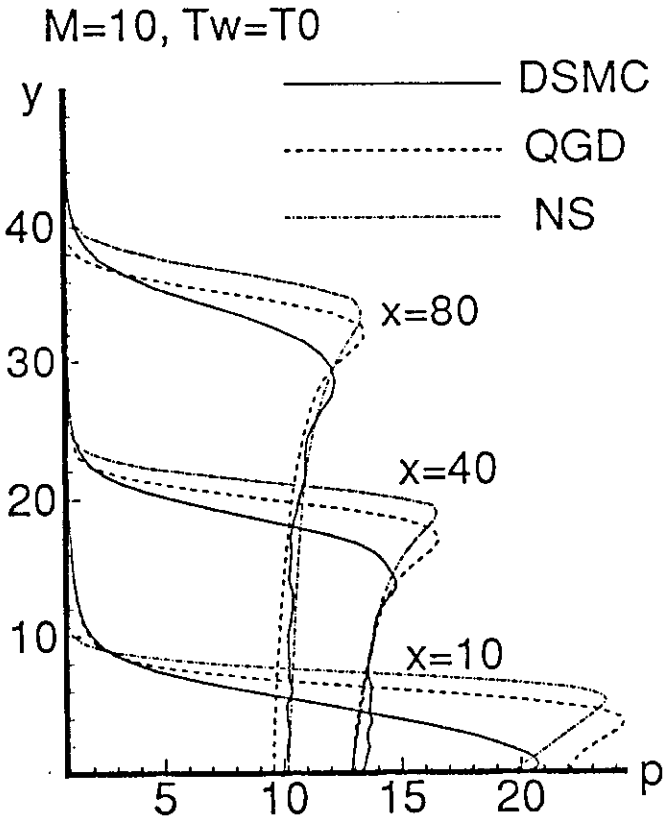
M=10, Tw=T0
DSMC
QGD
NS
y
40
30
20
10
x=80
x=40
x=10
5
10
15
20
p

Fig.25

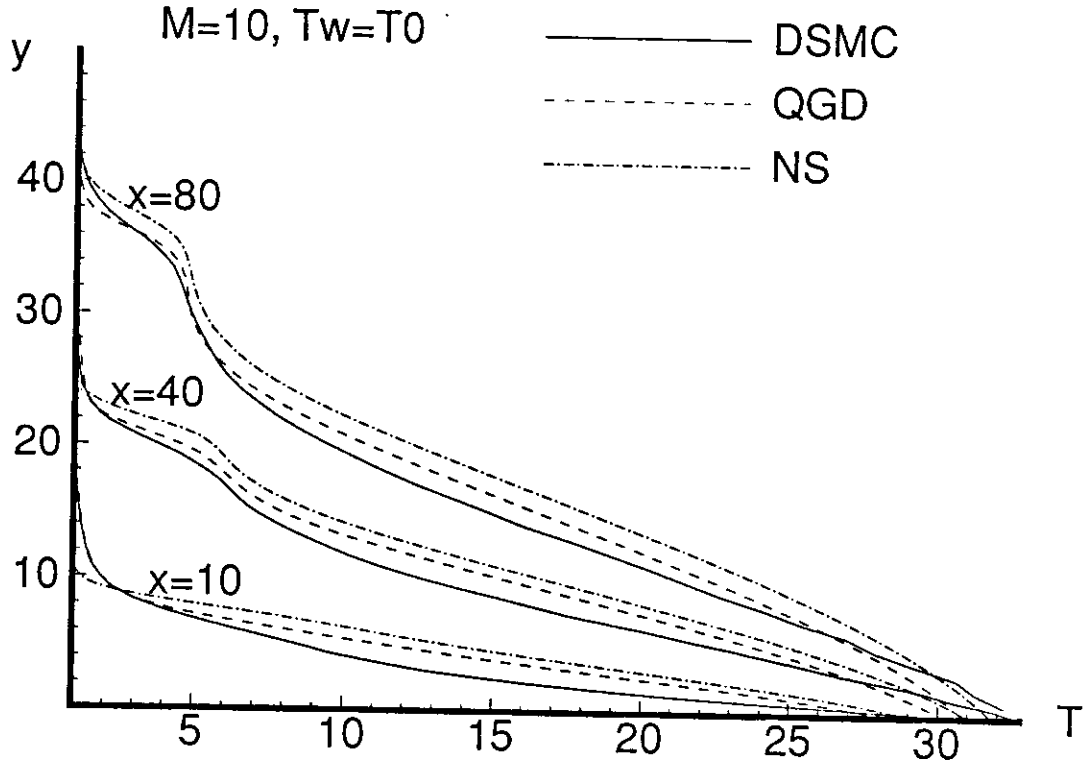
M=10, Tw=T0
DSMC
QGD
NS
y
40
30
20
10
x=80
x=40
x=10
5
10
15
20
25
30
T

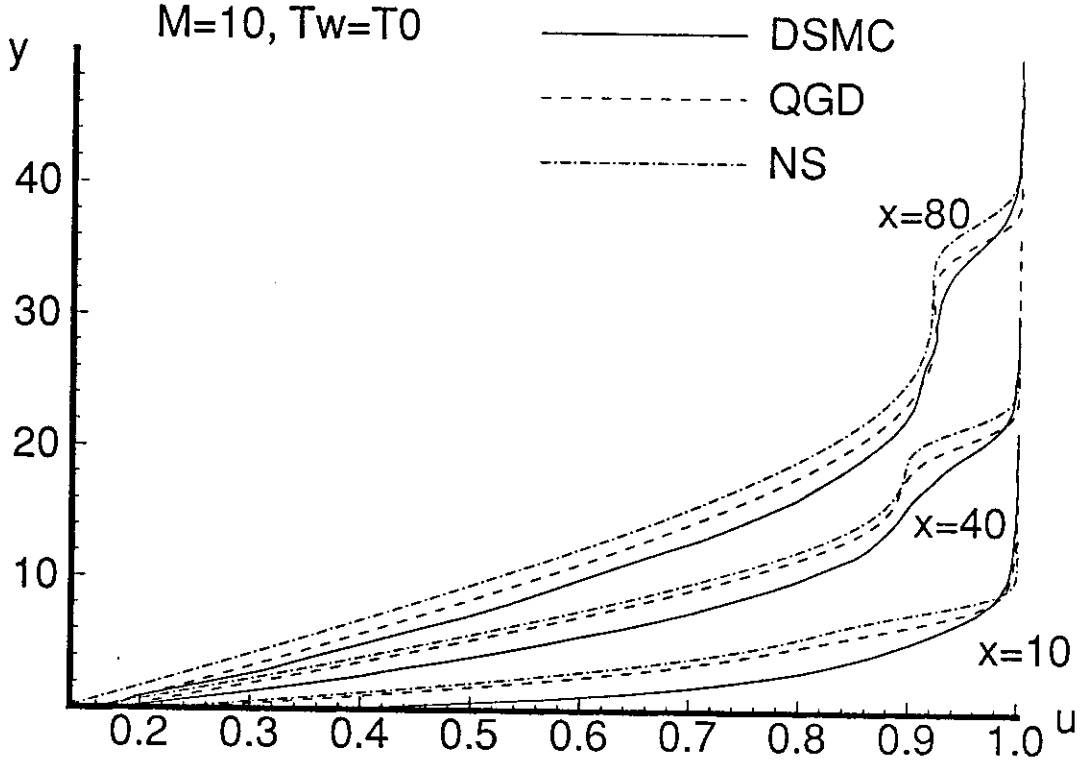
M=10, Tw=T0
DSMC
QGD
NS
y
40
30
20
10
x=80
x=40
x=10
0.2
0.3
0.4
0.5
0.6
0.7
0.8
0.9
1.0
u

Fig.26

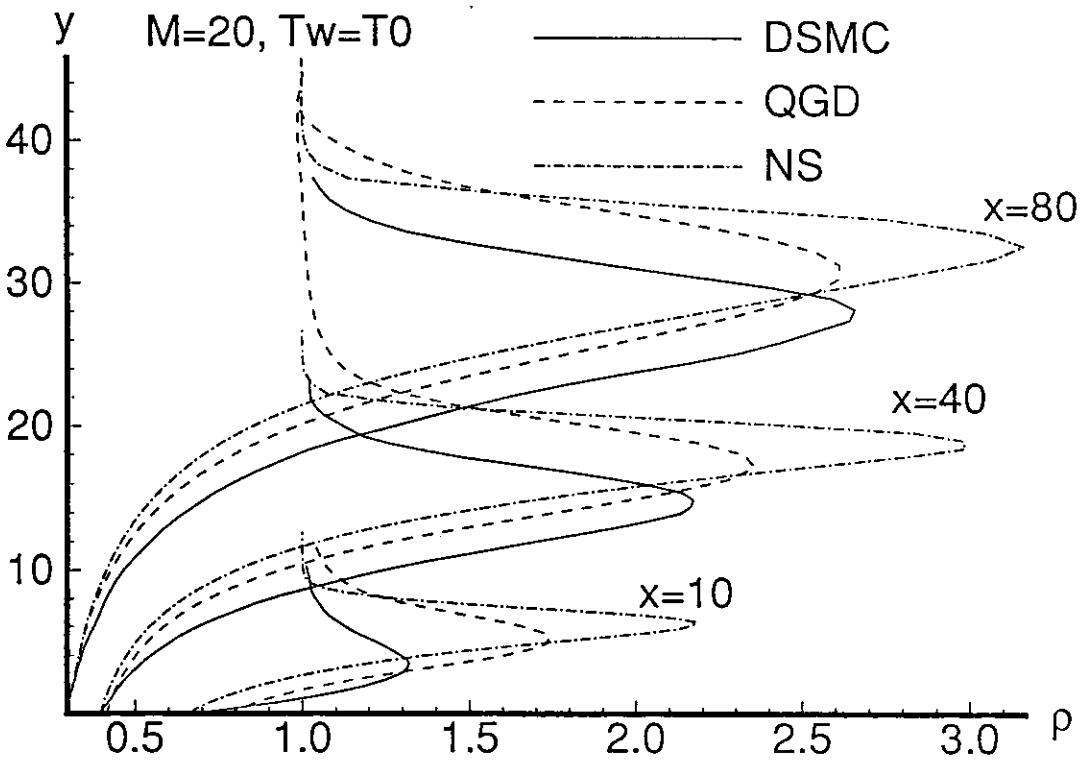
y
M=20, Tw=T0
DSMC
QGD
NS
40
30
20
10
x=80
x=40
x=10
0.5
1.0
1.5
2.0
2.5
3.0
p

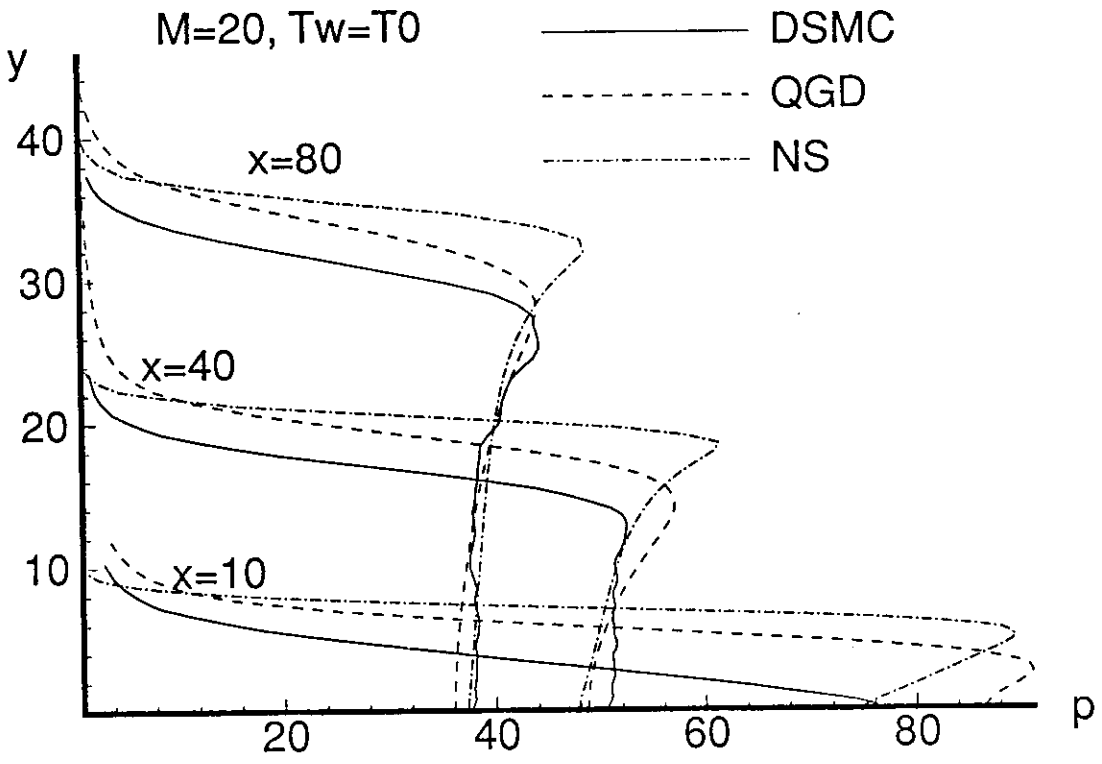
M=20, Tw=T0
DSMC
QGD
NS
y
40
30
20
10
x=80
x=40
x=10
20
40
60
80
p

Fig.27

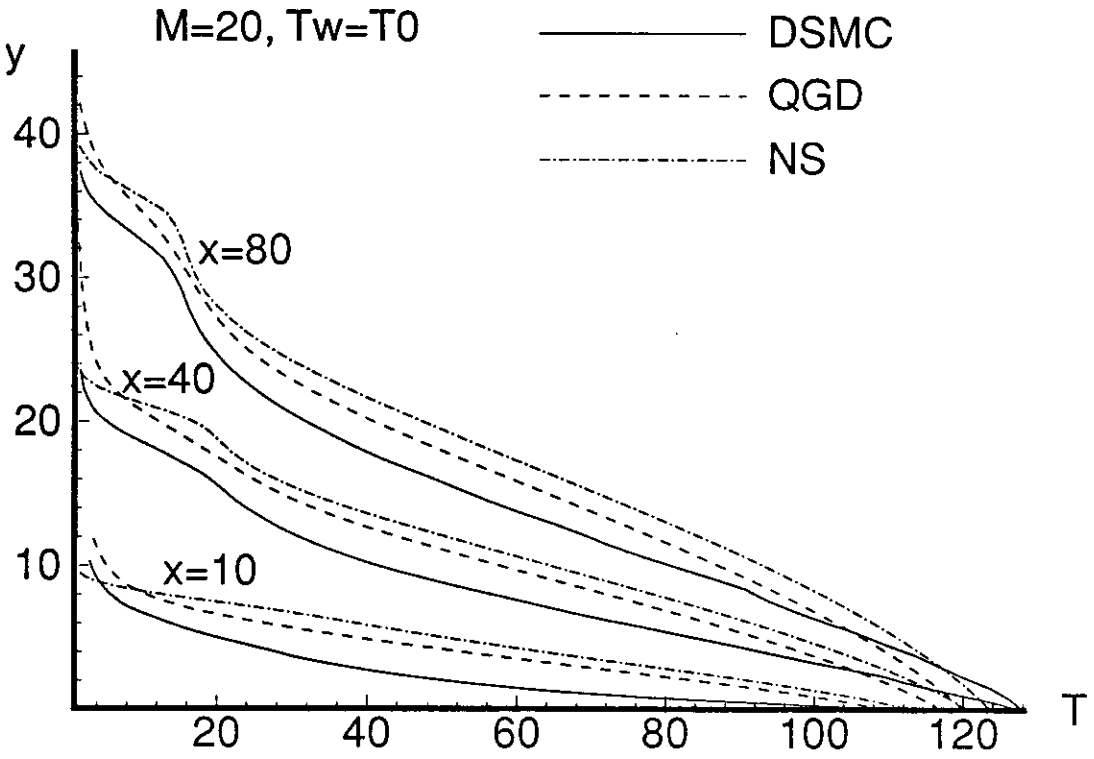
M=20, Tw=T0
DSMC
QGD
NS
y
40
30
20
10
x=80
x=40
x=10
20
40
60
80
100
120
T

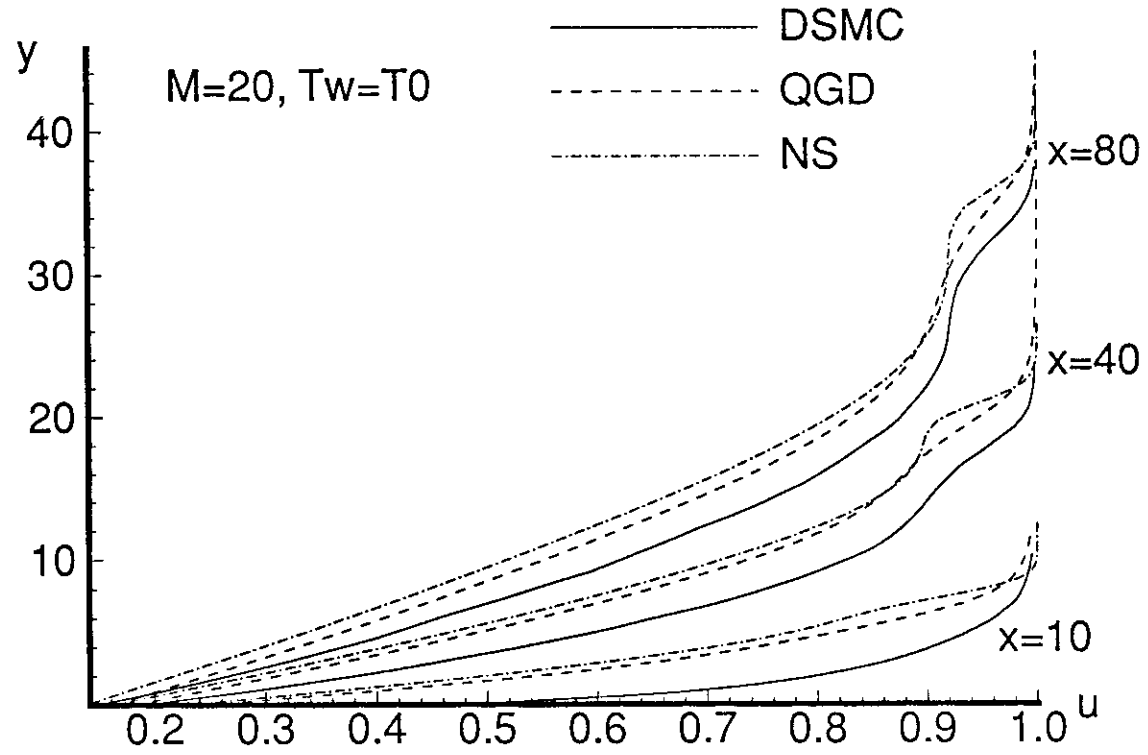
DSMC
QGD
NS
y
M=20, Tw=T0
40
30
20
10
x=80
x=40
x=10
0.2
0.3
0.4
0.5
0.6
0.7
0.8
0.9
1.0
u

Fig.28

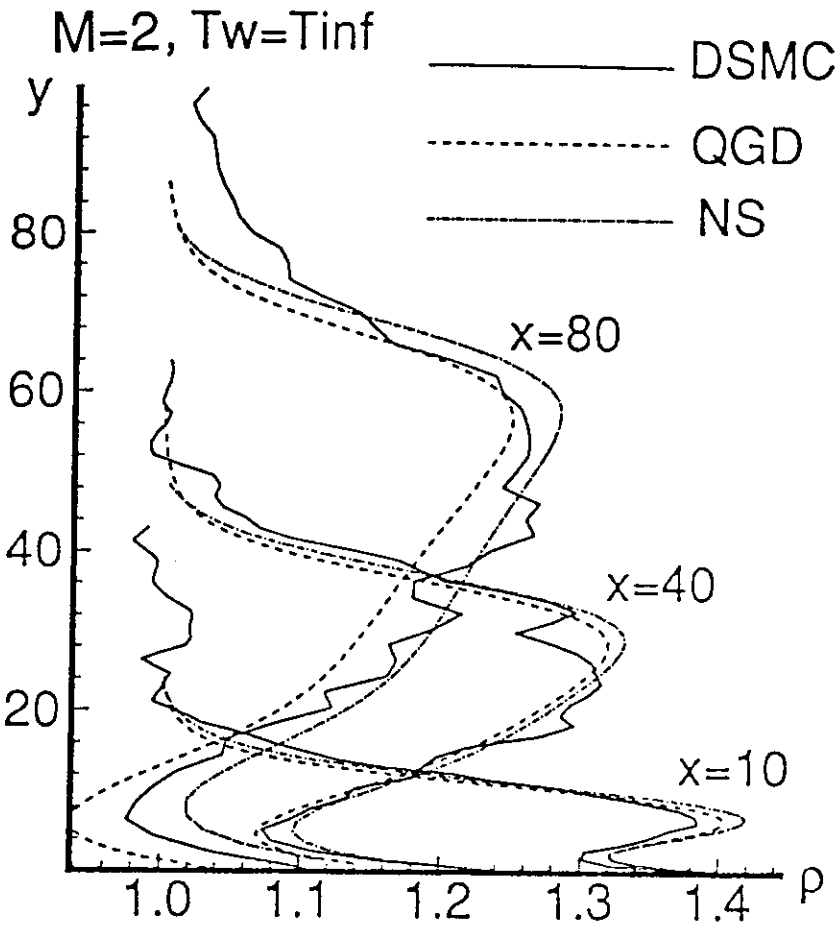
M=2, Tw=Tinf
DSMC
QGD
NS
y
80
60
40
20
x=80
x=40
x=10
1.0
1.1
1.2
1.3
1.4
ρ

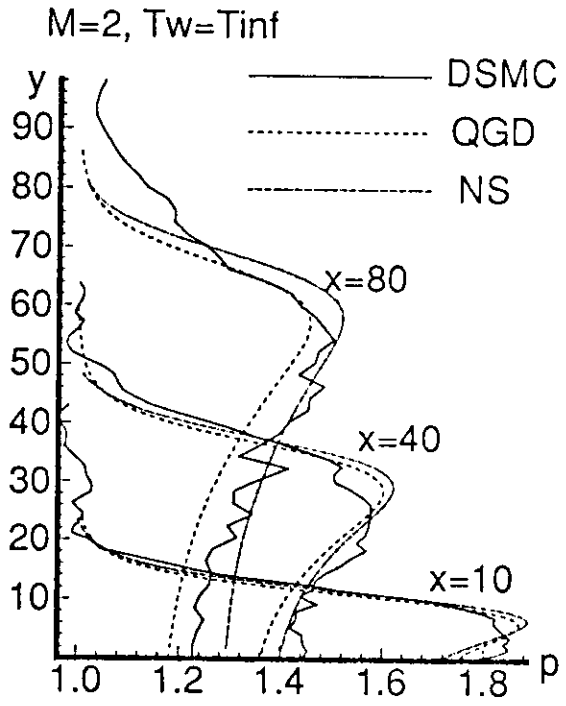
M=2, Tw=Tinf
DSMC
QGD
NS
y
90
80
70
60
50
40
30
20
10
x=80
x=40
x=10
1.0
1.2
1.4
1.6
1.8
p

Fig.29

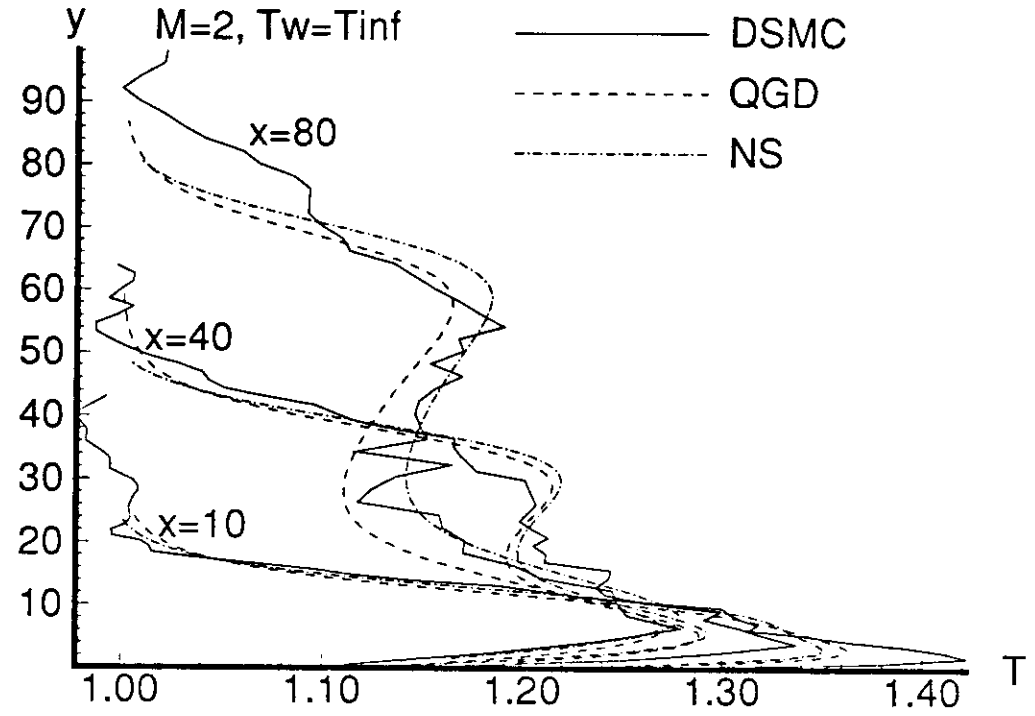
y
M=2, Tw=Tinf
DSMC
QGD
NS
x=80
x=40
x=10
90
80
70
60
50
40
30
20
10
1.00
1.10
1.20
1.30
1.40
T

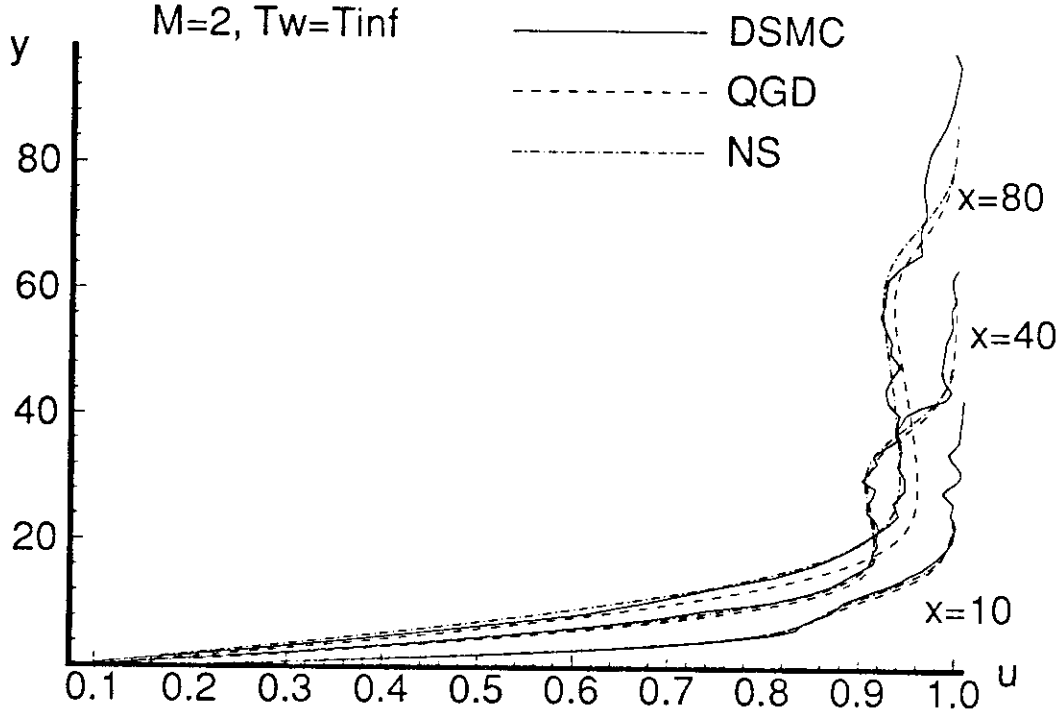
M=2, Tw=Tinf
y
DSMC
QGD
NS
x=80
x=40
x=10
80
60
40
20
0.1
0.2
0.3
0.4
0.5
0.6
0.7
0.8
0.9
1.0
u

Fig.30

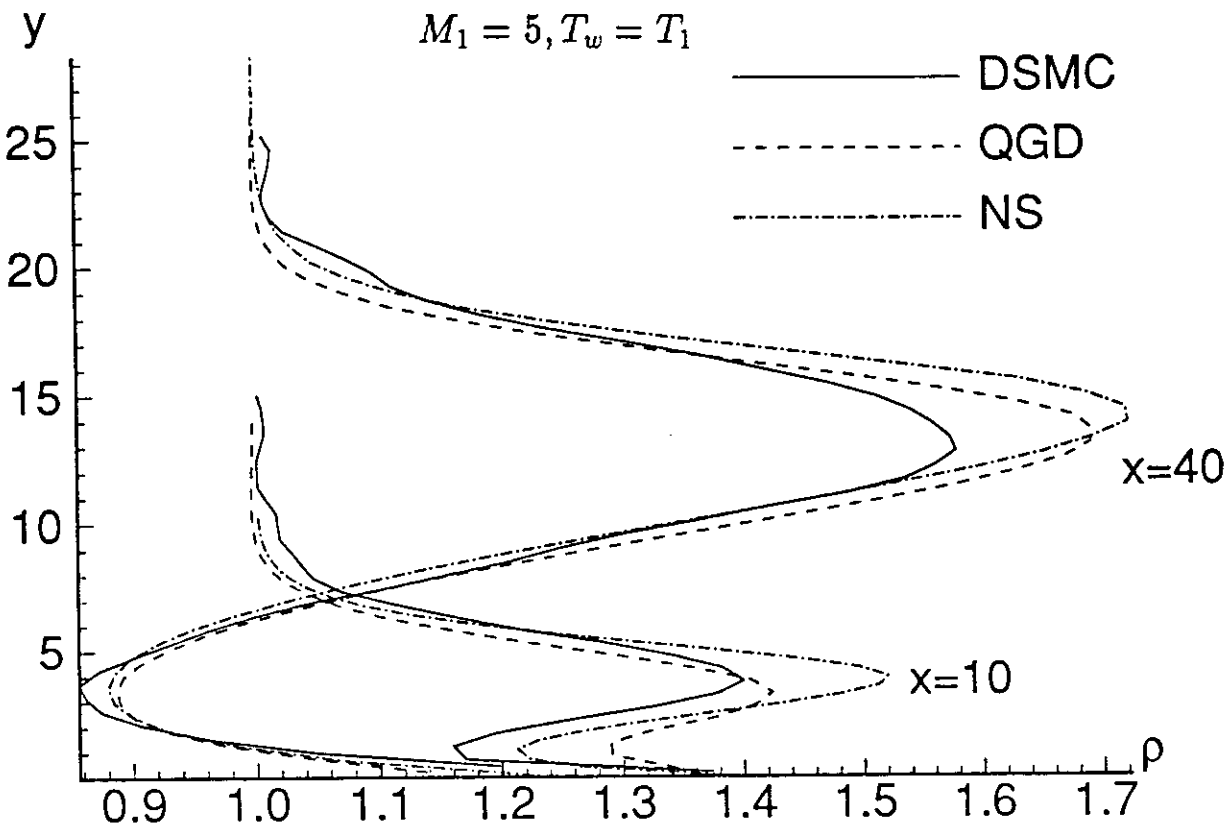
y
$M_1 = 5, T_w = T_1$
DSMC
QGD
NS
25
20
15
10
5
x=40
x=10
ρ
0.9
1.0
1.1
1.2
1.3
1.4
1.5
1.6
1.7

Fig.31

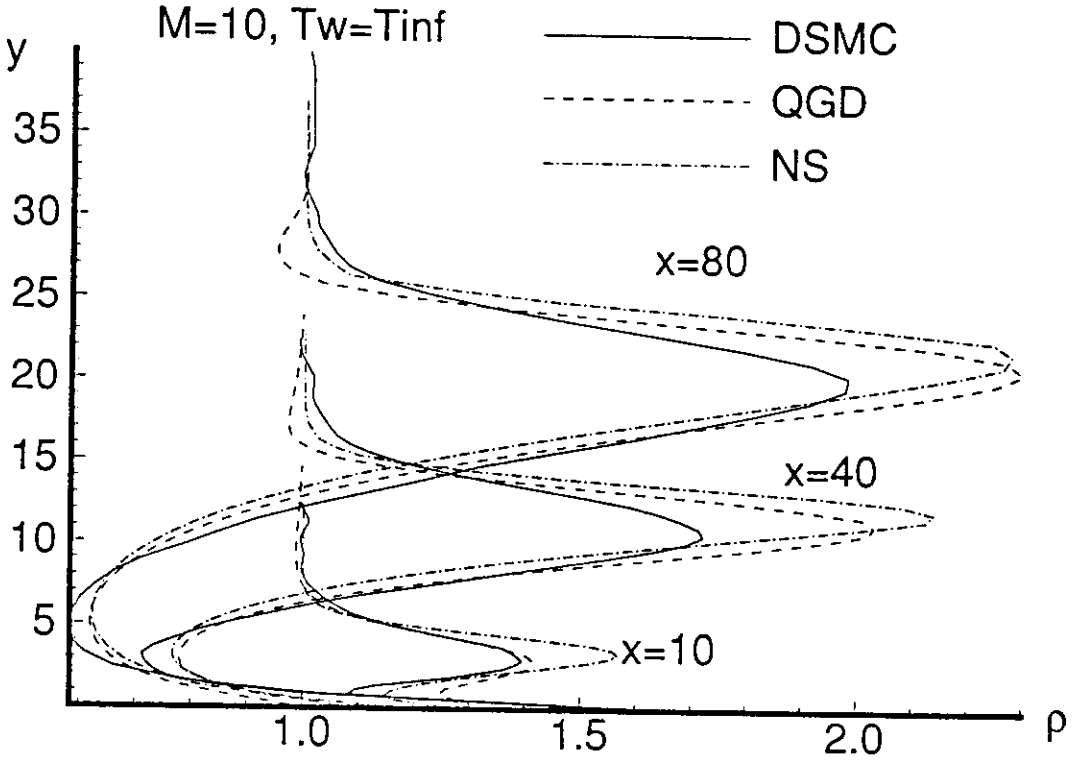
M=10, Tw=Tinf
DSMC
QGD
NS
y
35
30
25
20
15
10
5
x=80
x=40
x=10
1.0
1.5
2.0
ρ

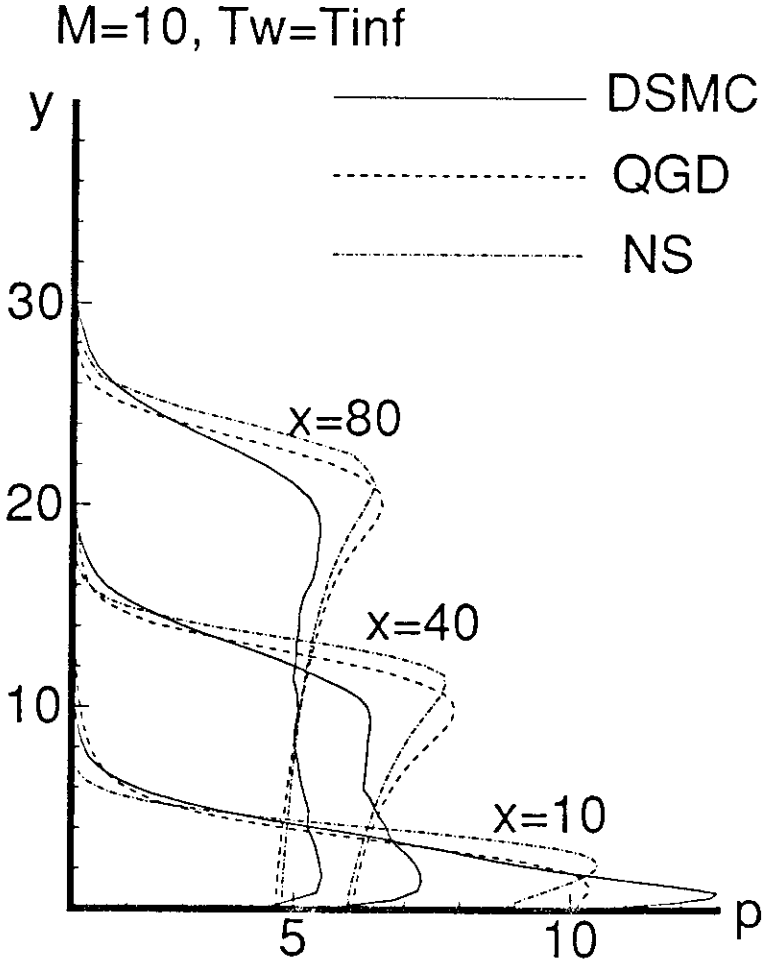
M=10, Tw=Tinf
DSMC
QGD
NS
y
30
20
10
x=80
x=40
x=10
5
10
p

Fig.32

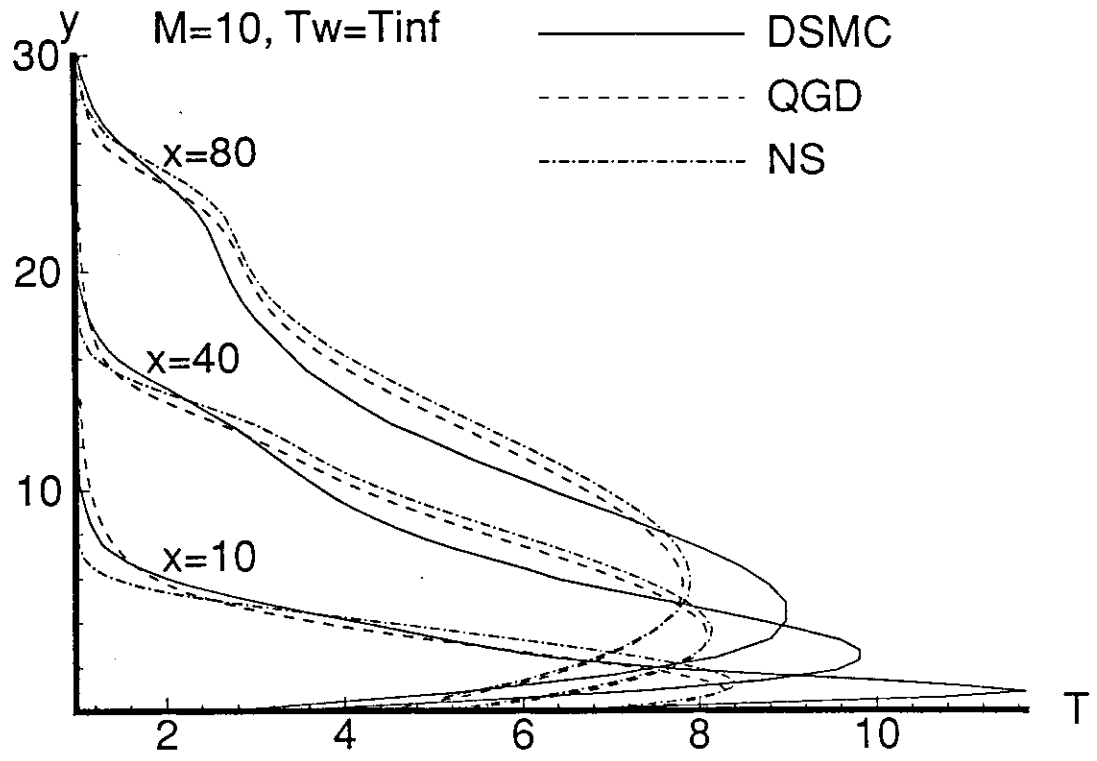
y
M=10, Tw=Tinf
DSMC
QGD
NS
30
20
10
x=80
x=40
x=10
2
4
6
8
10
T

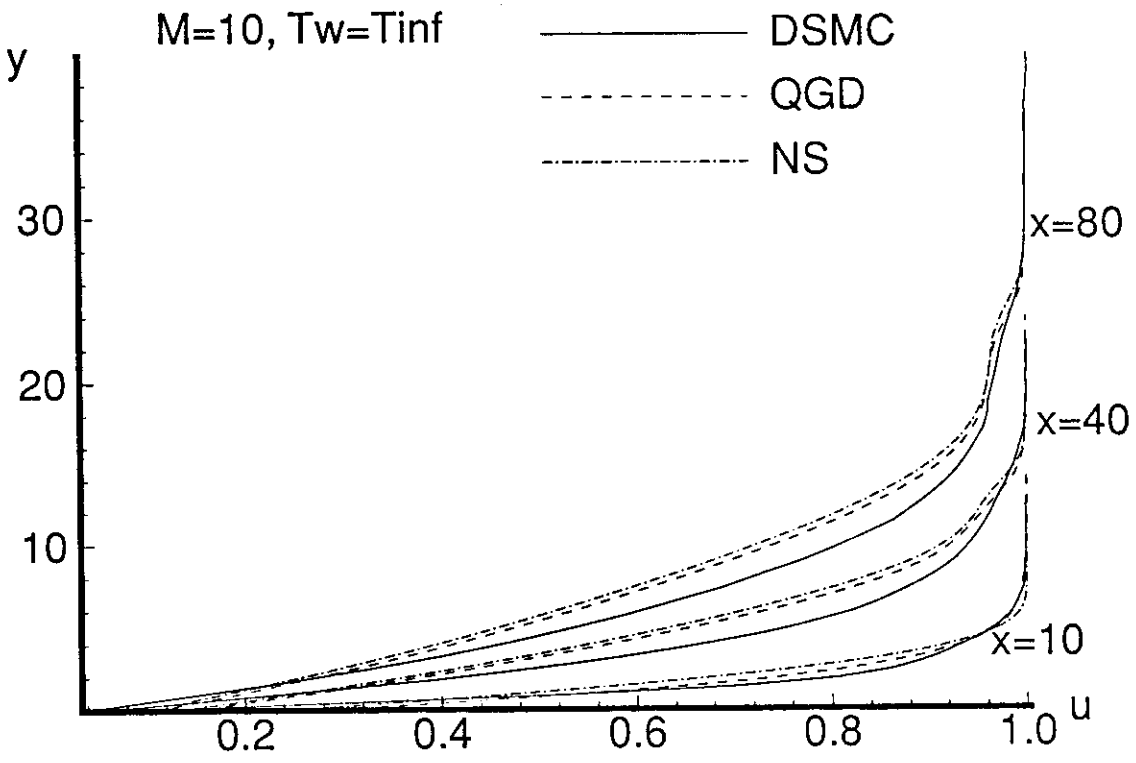
M=10, Tw=Tinf
DSMC
QGD
NS
y
30
20
10
x=80
x=40
x=10
0.2
0.4
0.6
0.8
1.0
u

Fig.33

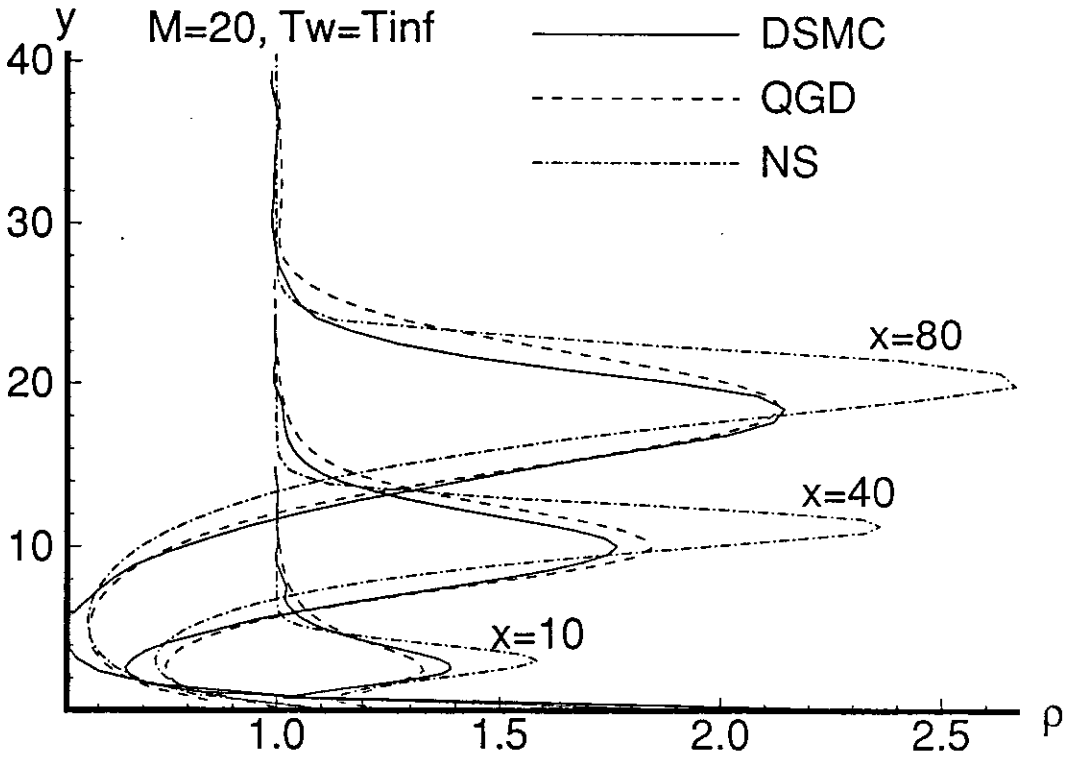
y
M=20, Tw=Tinf
DSMC
QGD
NS
40
30
20
10
x=80
x=40
x=10
1.0
1.5
2.0
2.5
ρ

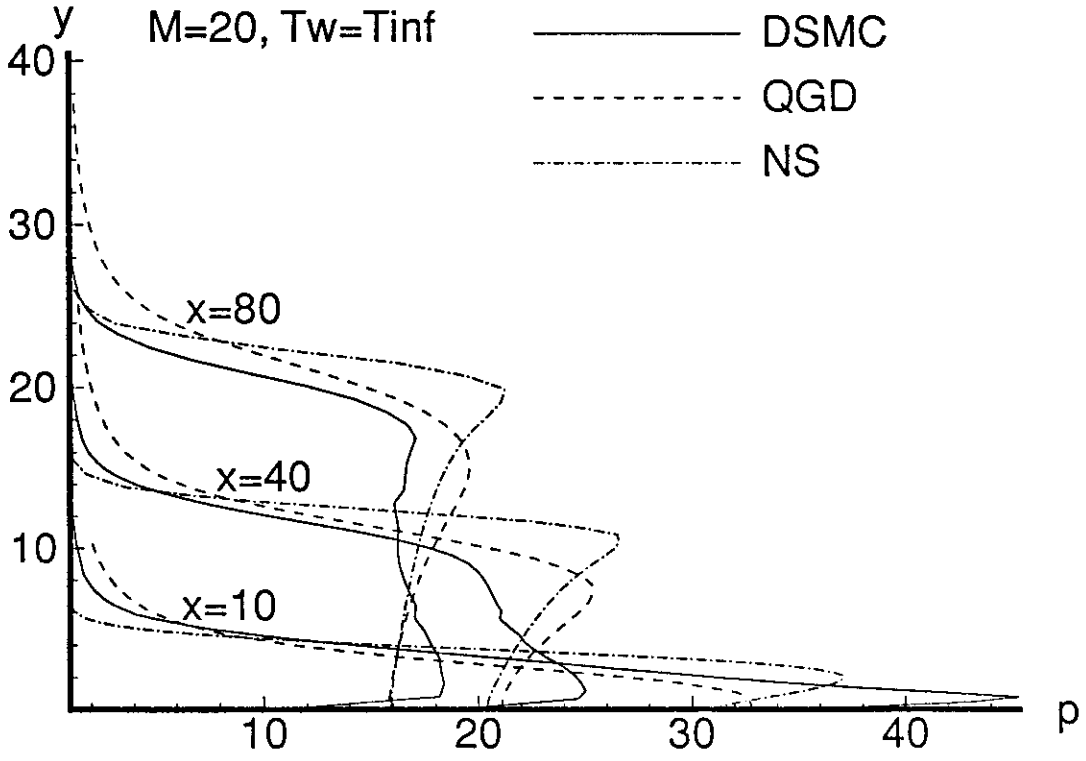
y
M=20, Tw=Tinf
DSMC
QGD
NS
40
30
20
10
x=80
x=40
x=10
10
20
30
40
p

Fig.34

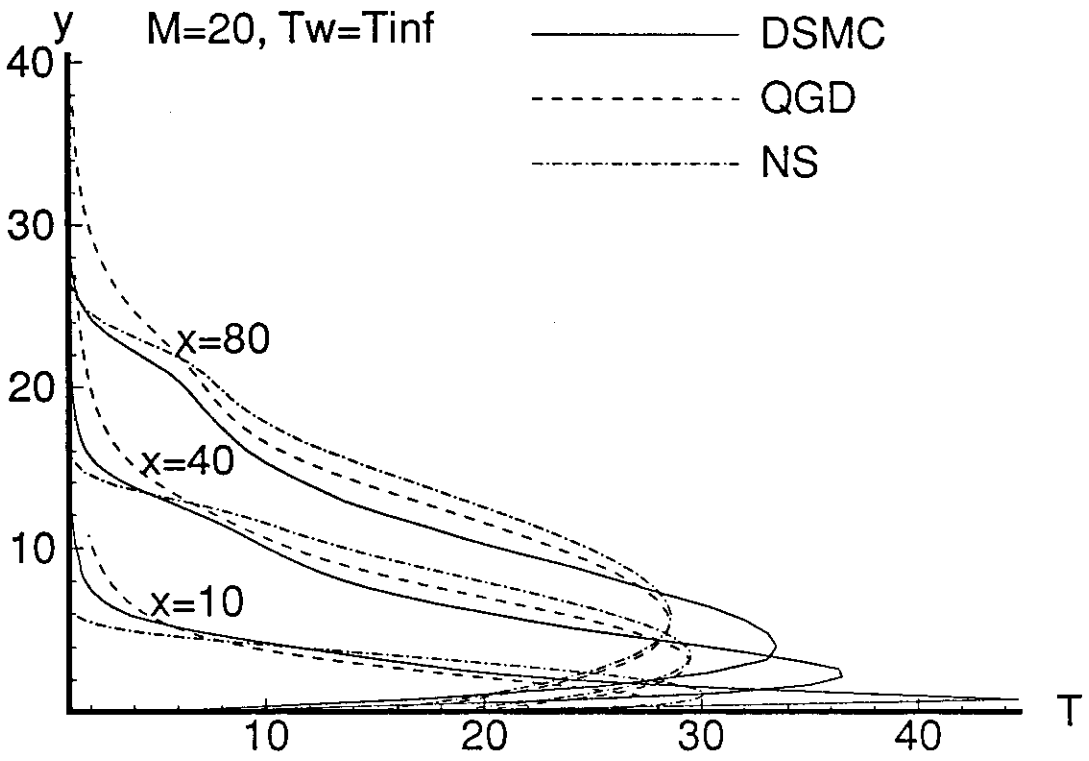
y
M=20, Tw=Tinf
DSMC
QGD
NS
40
30
20
10
x=80
x=40
x=10
10
20
30
40
T

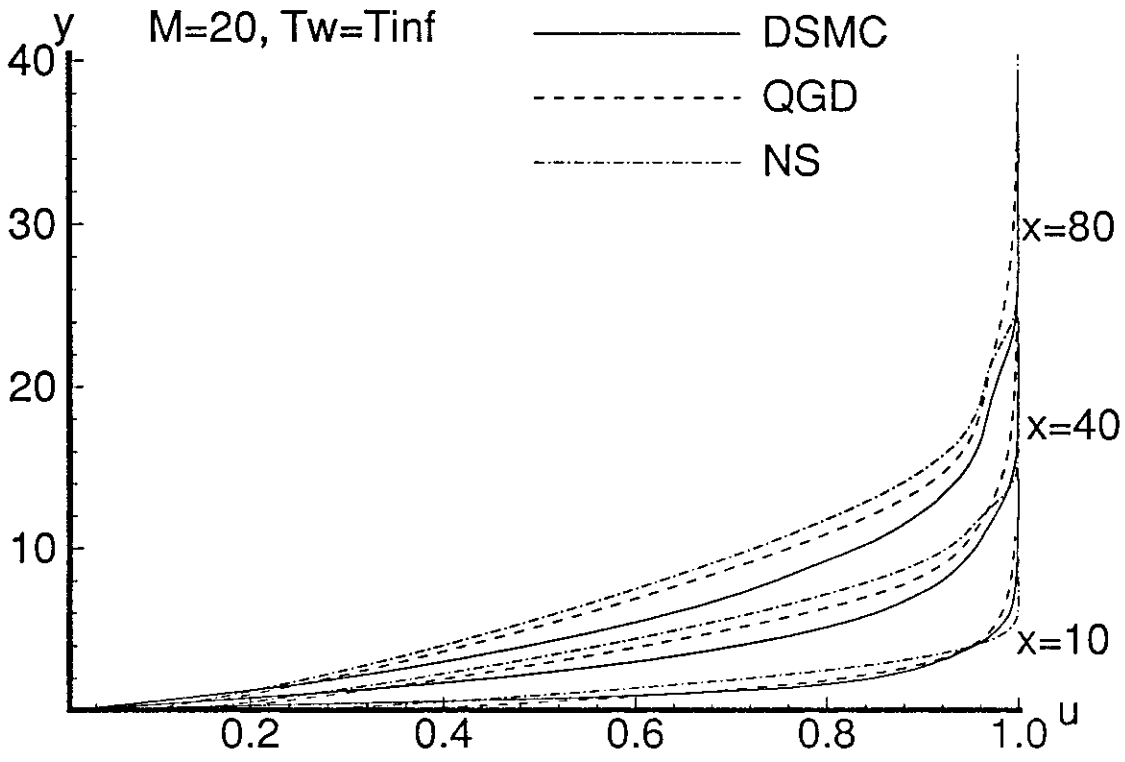
y
M=20, Tw=Tinf
DSMC
QGD
NS
40
30
20
10
x=80
x=40
x=10
0.2
0.4
0.6
0.8
1.0
u

Fig.35

Isolines

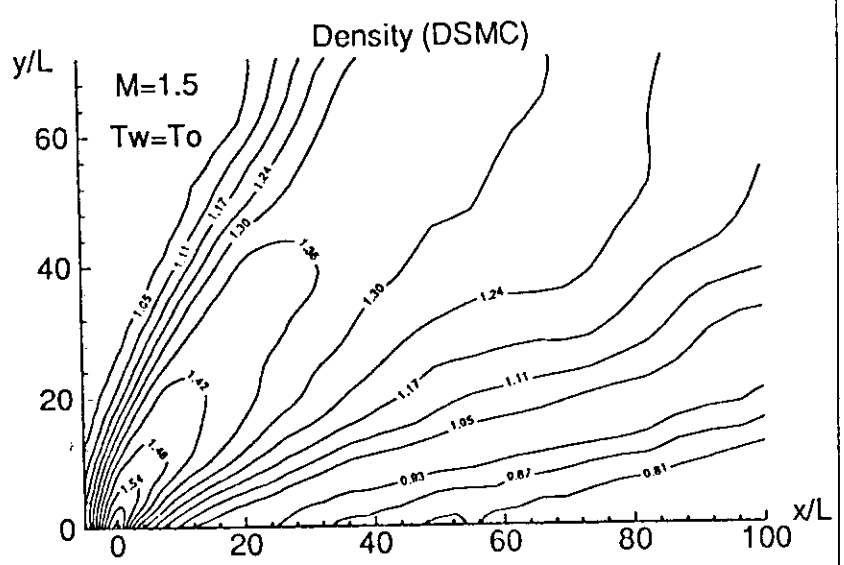
Density (DSMC)
M=1.5
Tw=To
y/L
x/L
0
20
40
60
80
100
1.05
1.11
1.17
1.24
1.30
1.36
1.43
1.48
1.54
1.30
1.24
1.17
1.11
1.05
0.99
0.93
0.87
0.81

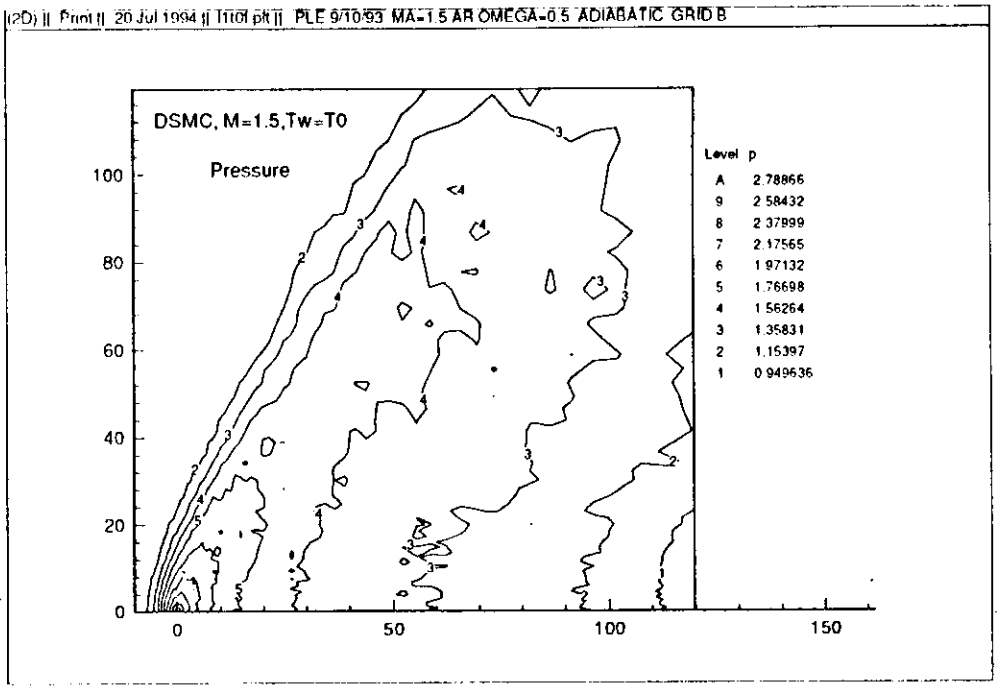
(2D) || Print || 20 Jul 1994 || 1110 plt || PLE 9/10/93 MA=1.5 AR OMEGA=0.5 ADIABATIC GRID B
DSMC, M=1.5,Tw=T0
Pressure
Level p
A 2.78866
9 2.58432
8 2.37999
7 2.17565
6 1.97132
5 1.76698
4 1.56264
3 1.35831
2 1.15397
1 0.949636
0
50
100
150

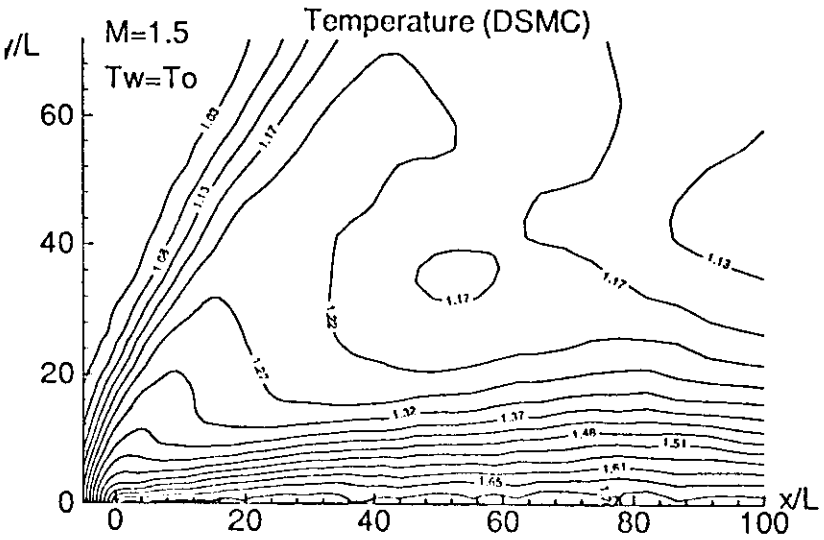
Temperature (DSMC)
M=1.5
Tw=To
y/L
x/L
0
20
40
60
80
100
1.05
1.09
1.13
1.17
1.22
1.32
1.37
1.46
1.51
1.61
1.65
1.17
1.13

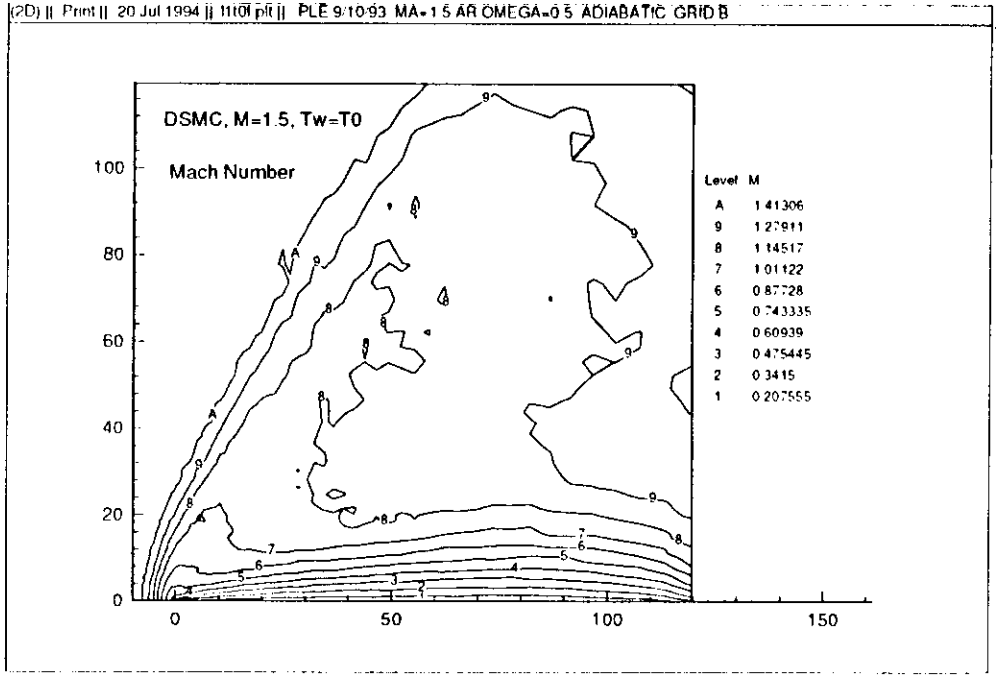
(2D) || Print || 20 Jul 1994 || 1110 plt || PLE 9/10/93 MA=1.5 AR OMEGA=0.5 ADIABATIC GRID B
DSMC, M=1.5, Tw=T0
Mach Number
Level M
A 1.41306
9 1.27911
8 1.14517
7 1.01122
6 0.87728
5 0.743335
4 0.60939
3 0.475445
2 0.3415
1 0.207555
0
50
100
150

Fig.36

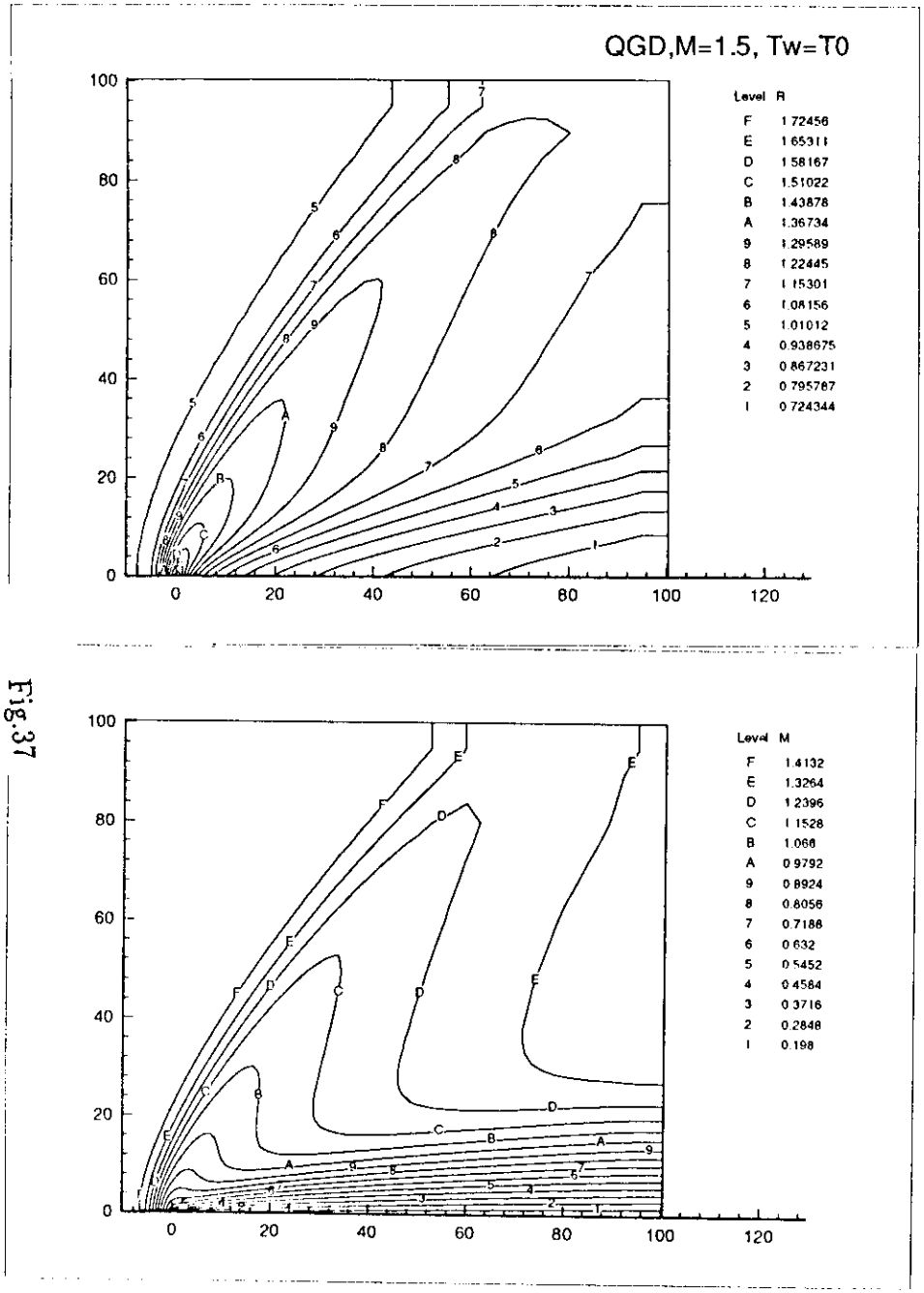
QGD,M=1.5, Tw=T0
Level R
F 1.72456
E 1.65311
D 1.58167
C 1.51022
B 1.43878
A 1.36734
9 1.29589
8 1.22445
7 1.15301
6 1.08156
5 1.01012
4 0.938675
3 0.867231
2 0.795787
1 0.724344
Level T
F 1.67875
E 1.6335
D 1.58825
C 1.543
B 1.49775
A 1.4525
9 1.40725
8 1.362
7 1.31675
6 1.2715
5 1.22625
4 1.181
3 1.13575
2 1.0905
1 1.04525
Level M
F 1.4132
E 1.3264
D 1.2396
C 1.1528
B 1.066
A 0.9792
9 0.8924
8 0.8056
7 0.7188
6 0.632
5 0.5452
4 0.4584
3 0.3716
2 0.2848
1 0.198
Level U
A 0.95
9 0.85
8 0.75
7 0.65
6 0.55
5 0.45
4 0.35
3 0.25
2 0.15
1 0.05

Fig.37

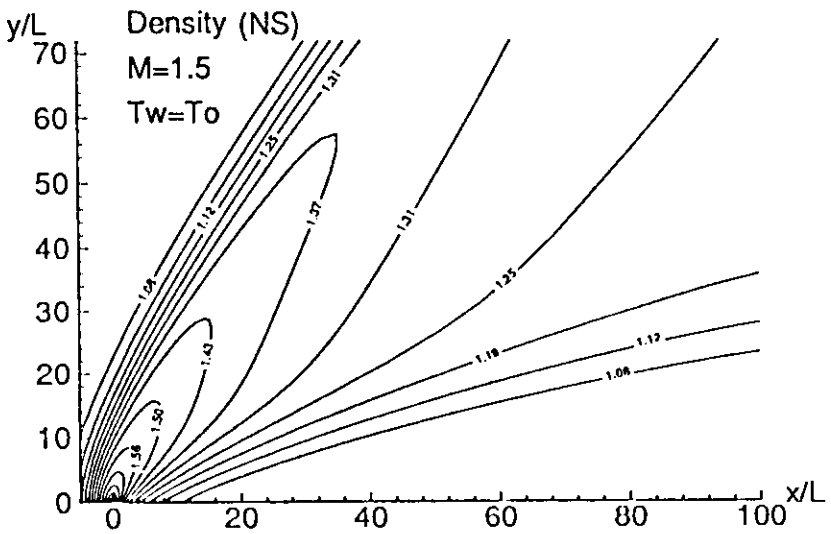
Density (NS)
M=1.5
Tw=To
y/L
x/L
0
10
20
30
40
50
60
70
0
20
40
60
80
100

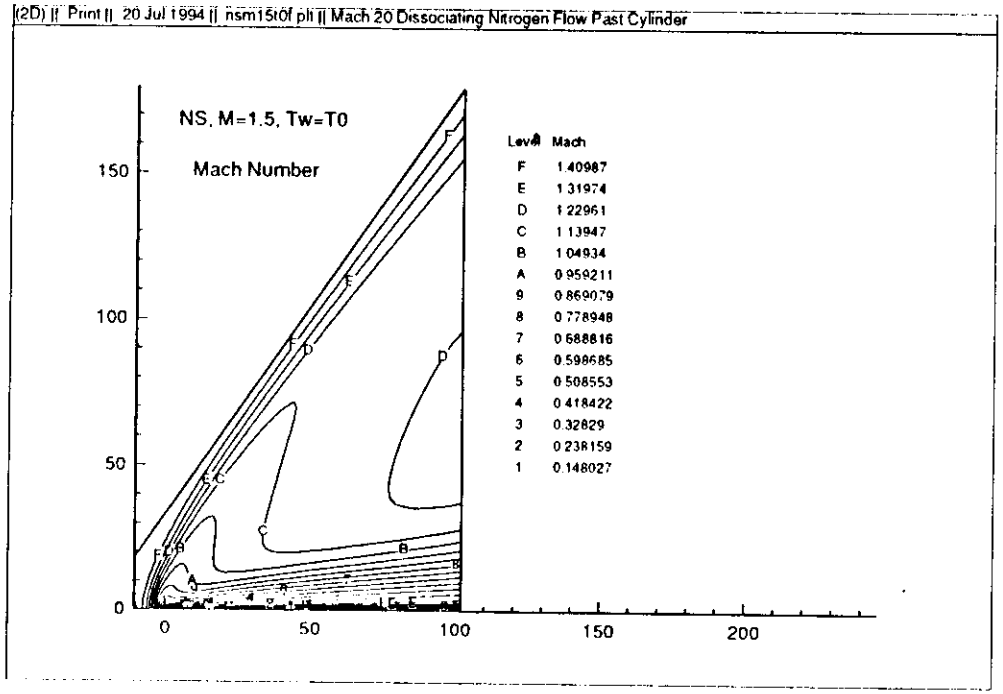
(2D) || Print || 20 Jul 1994 || nsm15t0f.plt || Mach 20 Dissociating Nitrogen Flow Past Cylinder
NS, M=1.5, Tw=T0
Mach Number
Level Mach
F 1.40987
E 1.31974
D 1.22961
C 1.13947
B 1.04934
A 0.959211
9 0.869079
8 0.778948
7 0.688816
6 0.598685
5 0.508553
4 0.418422
3 0.32829
2 0.238159
1 0.148027
0
50
100
150
200

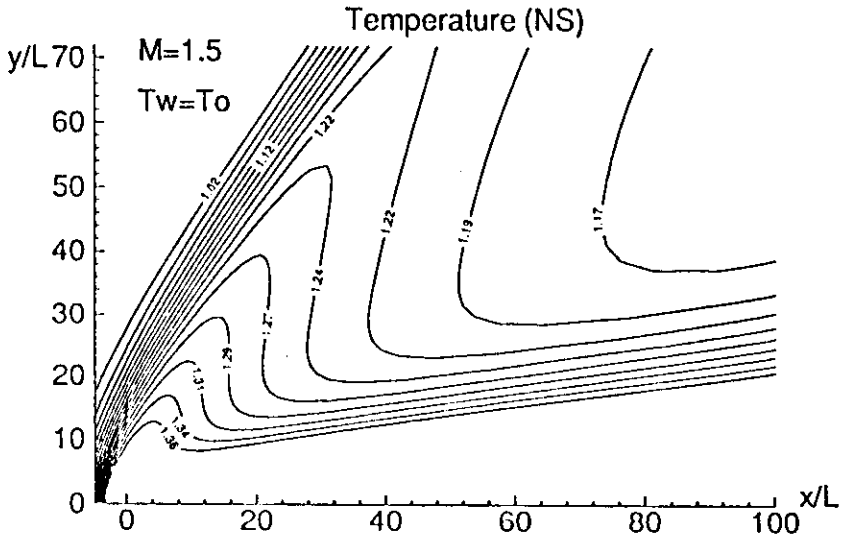
Temperature (NS)
M=1.5
Tw=To
y/L
x/L
0
10
20
30
40
50
60
70
0
20
40
60
80
100

Fig.38

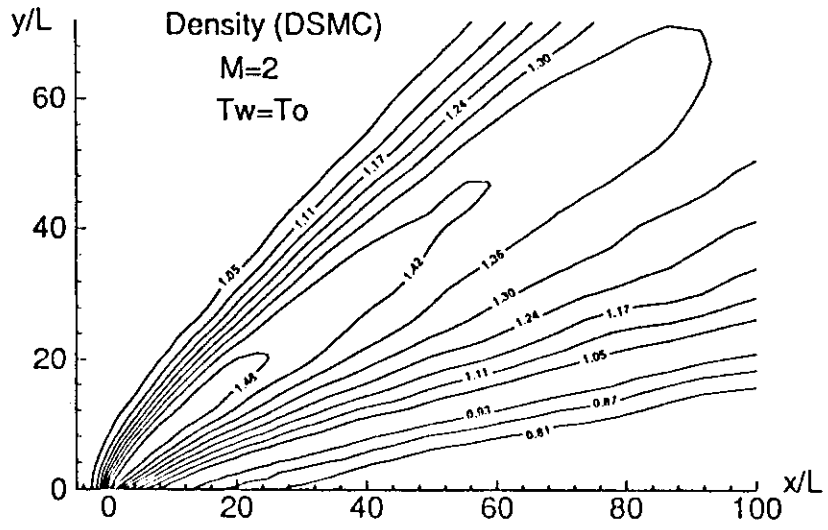
Density (DSMC)
M=2
Tw=To
y/L
x/L
0
20
40
60
80
100

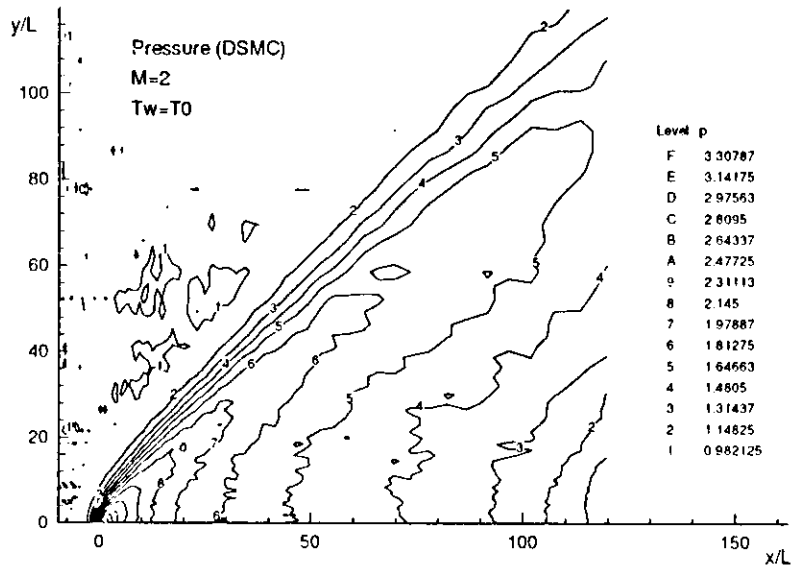
Pressure (DSMC)
M=2
Tw=T0
y/L
x/L
Level p
F 3.30787
E 3.14175
D 2.97563
C 2.8095
B 2.64337
A 2.47725
9 2.31113
8 2.145
7 1.97887
6 1.81275
5 1.64663
4 1.4805
3 1.31437
2 1.14825
1 0.982125

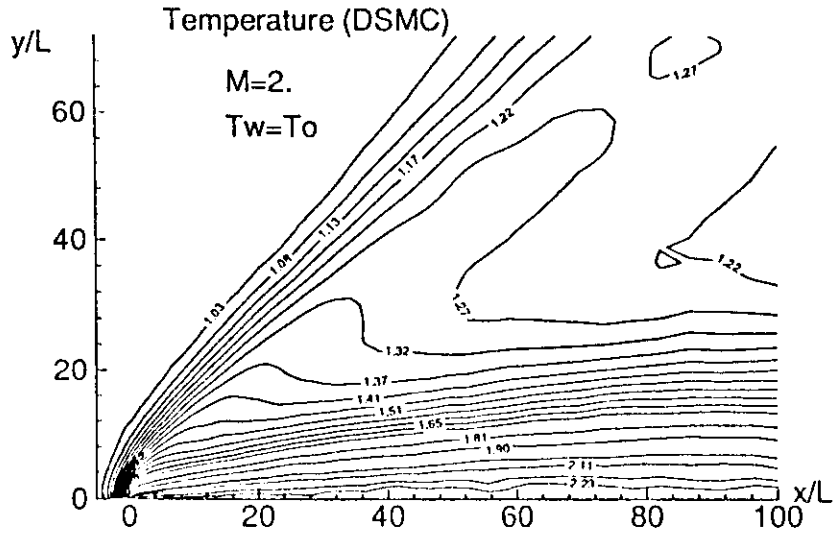
Temperature (DSMC)
M=2.
Tw=To
y/L
x/L

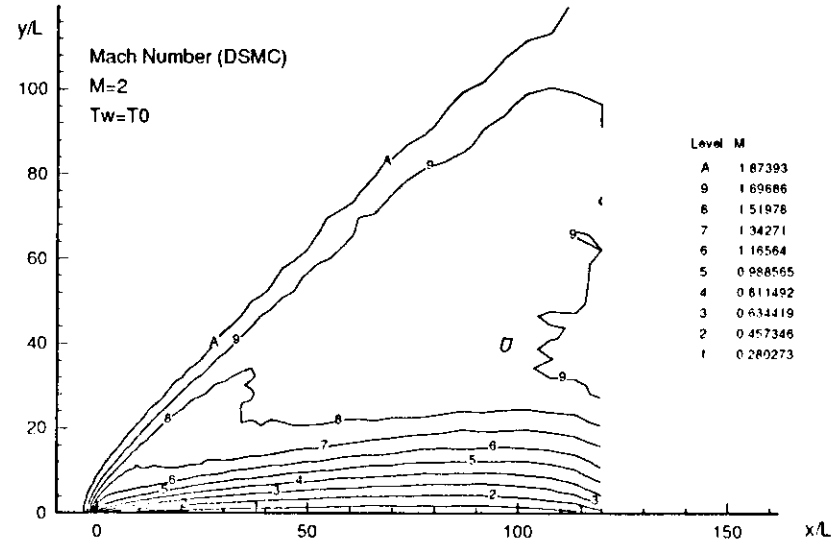
Mach Number (DSMC)
M=2
Tw=T0
y/L
x/L
Level M
A 1.87393
9 1.69686
8 1.51978
7 1.34271
6 1.16564
5 0.988565
4 0.811492
3 0.634419
2 0.457346
1 0.280273

Fig.39

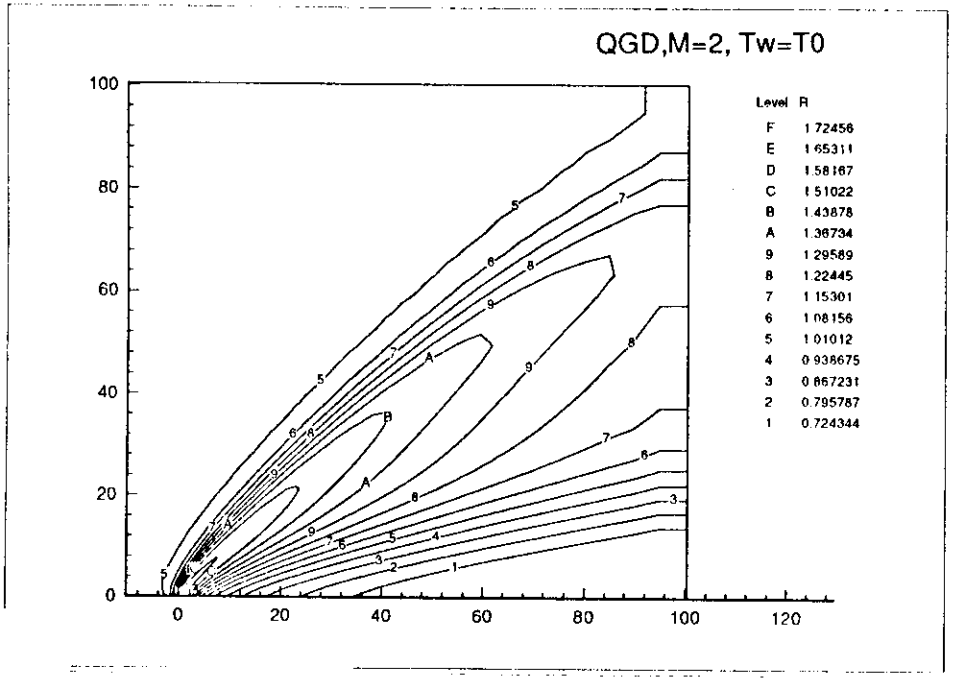
QGD,M=2, Tw=T0
Level R
F 1.72456
E 1.65311
D 1.58167
C 1.51022
B 1.43878
A 1.36734
9 1.29589
8 1.22445
7 1.15301
6 1.08156
5 1.01012
4 0.938675
3 0.867231
2 0.795787
1 0.724344

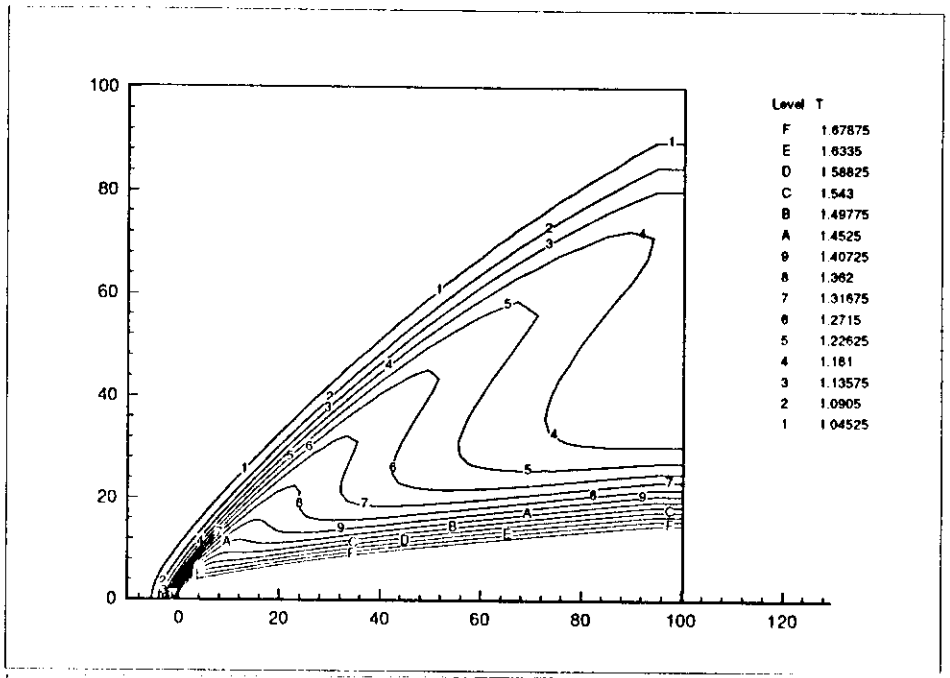
Level T
F 1.67875
E 1.6335
D 1.58825
C 1.543
B 1.49775
A 1.4525
9 1.40725
8 1.362
7 1.31675
6 1.2715
5 1.22625
4 1.181
3 1.13575
2 1.0905
1 1.04525

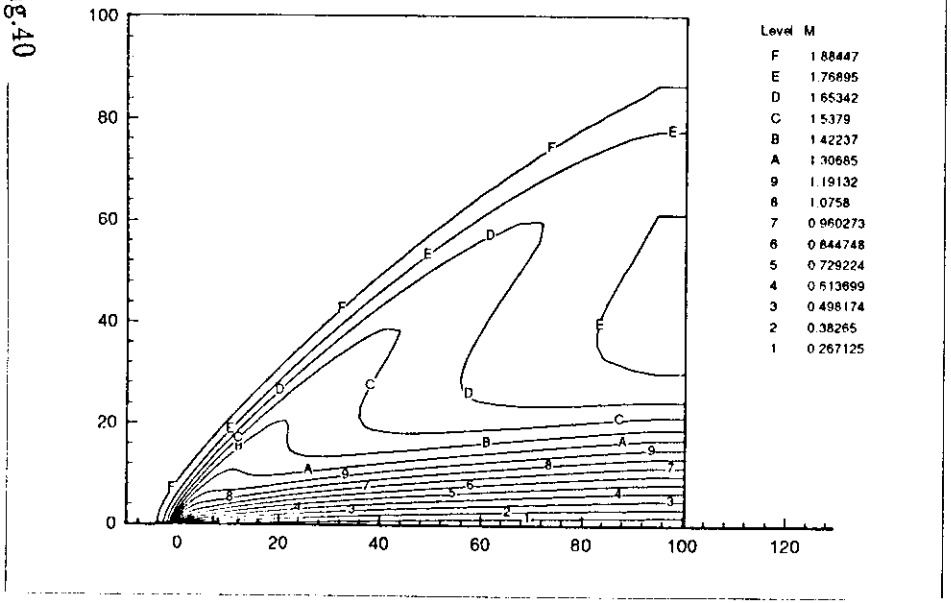
Level M
F 1.88447
E 1.76895
D 1.65342
C 1.5379
B 1.42237
A 1.30685
9 1.19132
8 1.0758
7 0.960273
6 0.844748
5 0.729224
4 0.613699
3 0.498174
2 0.38265
1 0.267125

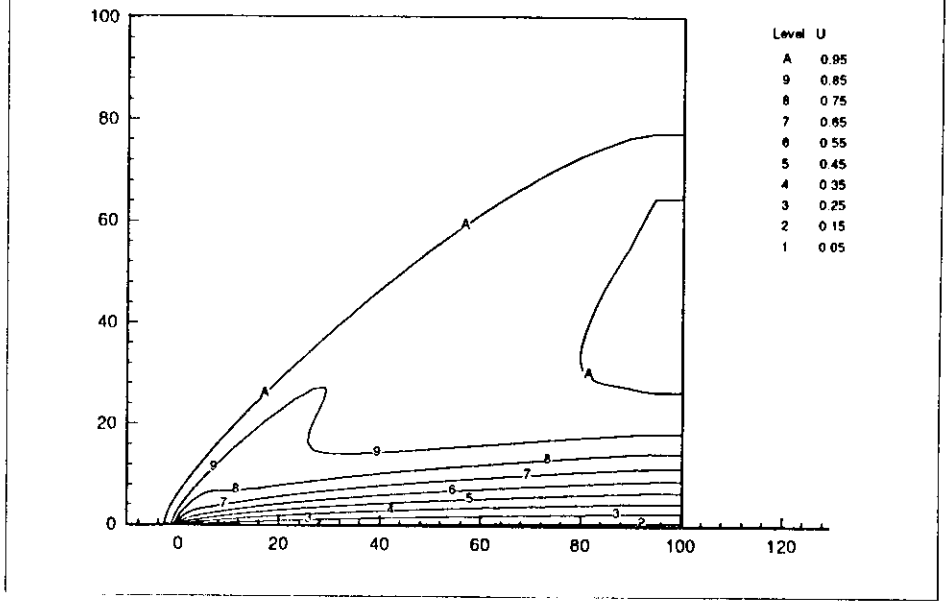
Level U
A 0.95
9 0.85
8 0.75
7 0.65
6 0.55
5 0.45
4 0.35
3 0.25
2 0.15
1 0.05

Fig.40

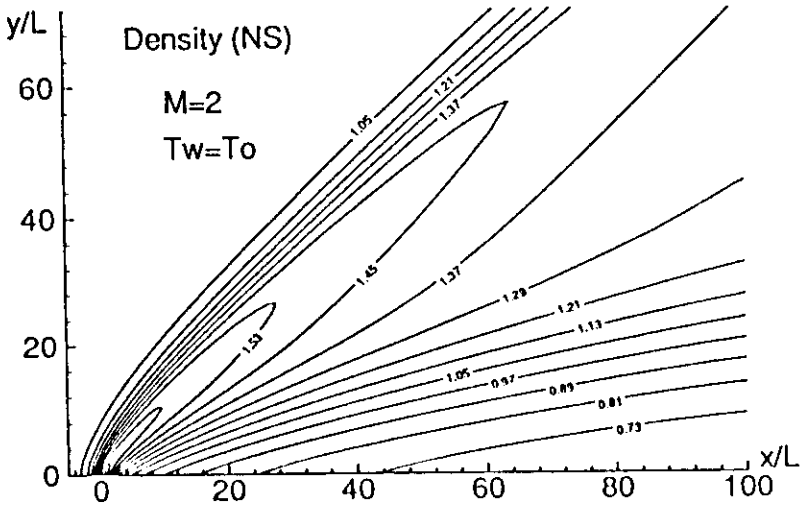
y/L
Density (NS)
M=2
Tw=To
60
40
20
0
0
20
40
60
80
100
x/L
1.05
1.21
1.37
1.45
1.53
1.37
1.29
1.21
1.13
1.05
0.97
0.89
0.81
0.73

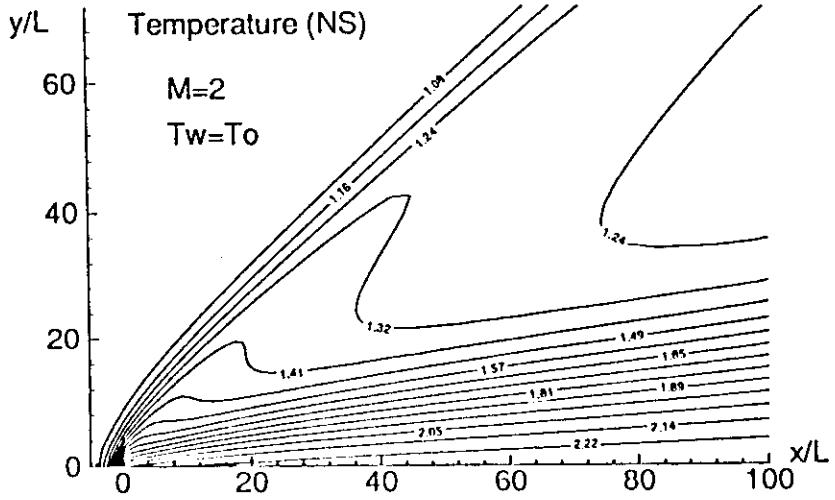
y/L
Temperature (NS)
M=2
Tw=To
60
40
20
0
0
20
40
60
80
100
x/L
1.08
1.24
1.16
1.24
1.32
1.41
1.49
1.57
1.65
1.81
1.89
2.05
2.14
2.22

Fig.41

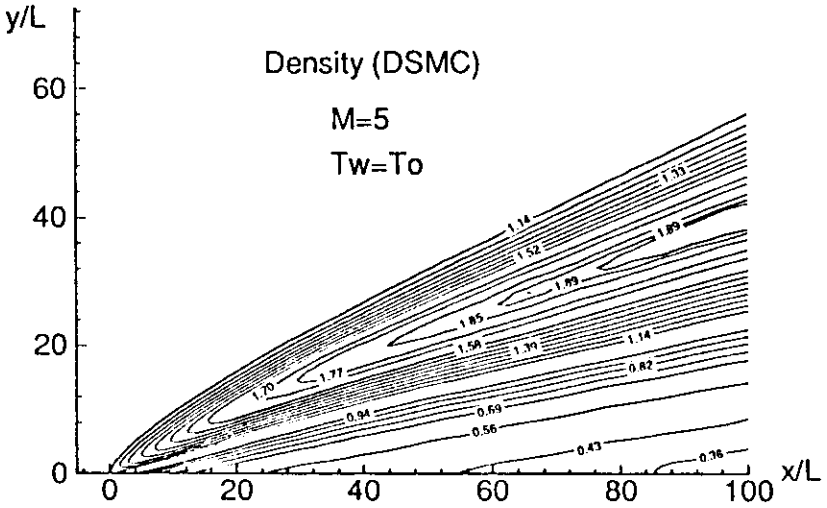
Density (DSMC)
M=5
Tw=To
y/L
x/L
0
20
40
60
80
100
1.70
1.77
1.85
1.92
1.99
2.06
2.13
1.14
1.52
1.89
1.59
1.39
1.14
0.82
0.94
0.69
0.56
0.43
0.36

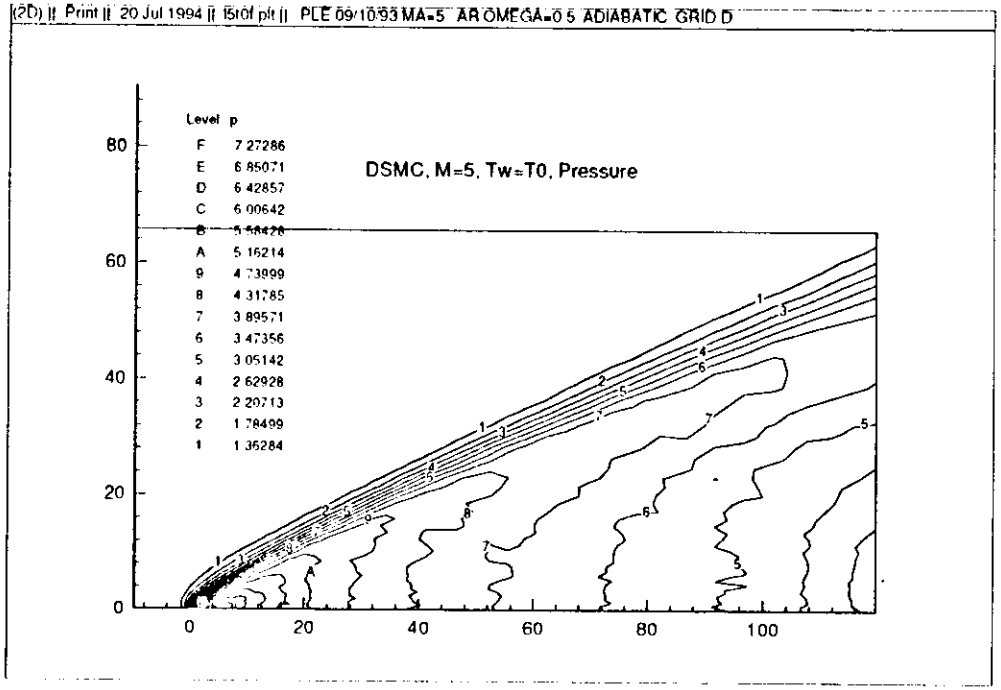
(2D) || Print || 20 Jul 1994 || Plot plt || PLE 09/10/93 MA=5 AR OMEGA=0.5 ADIABATIC GRID D
DSMC, M=5, Tw=T0, Pressure
Level p
F 7.27286
E 6.85071
D 6.42857
C 6.00642
B 5.58428
A 5.16214
9 4.73999
8 4.31785
7 3.89571
6 3.47356
5 3.05142
4 2.62928
3 2.20713
2 1.78499
1 1.36284
0
20
40
60
80
100

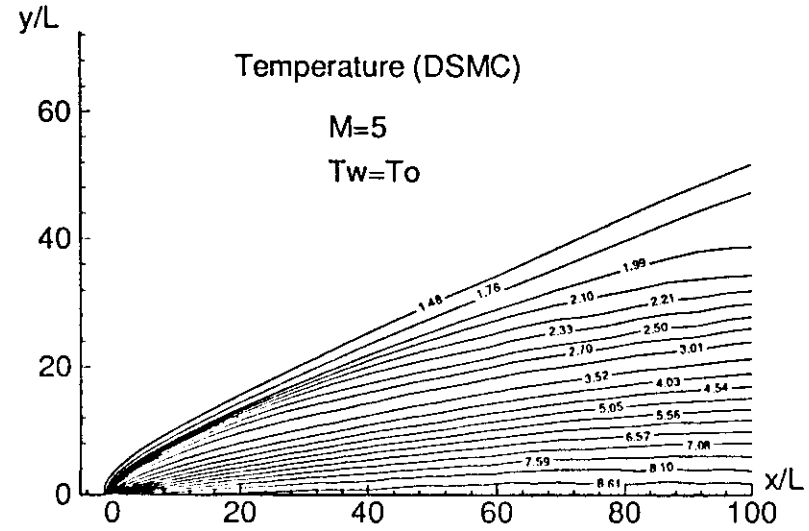
Temperature (DSMC)
M=5
Tw=To
y/L
x/L
0
20
40
60
80
100
1.48
1.76
1.99
2.10
2.21
2.33
2.50
2.70
3.01
3.52
4.03
4.54
5.05
5.56
6.57
7.08
7.59
8.10
8.61

Fig.42

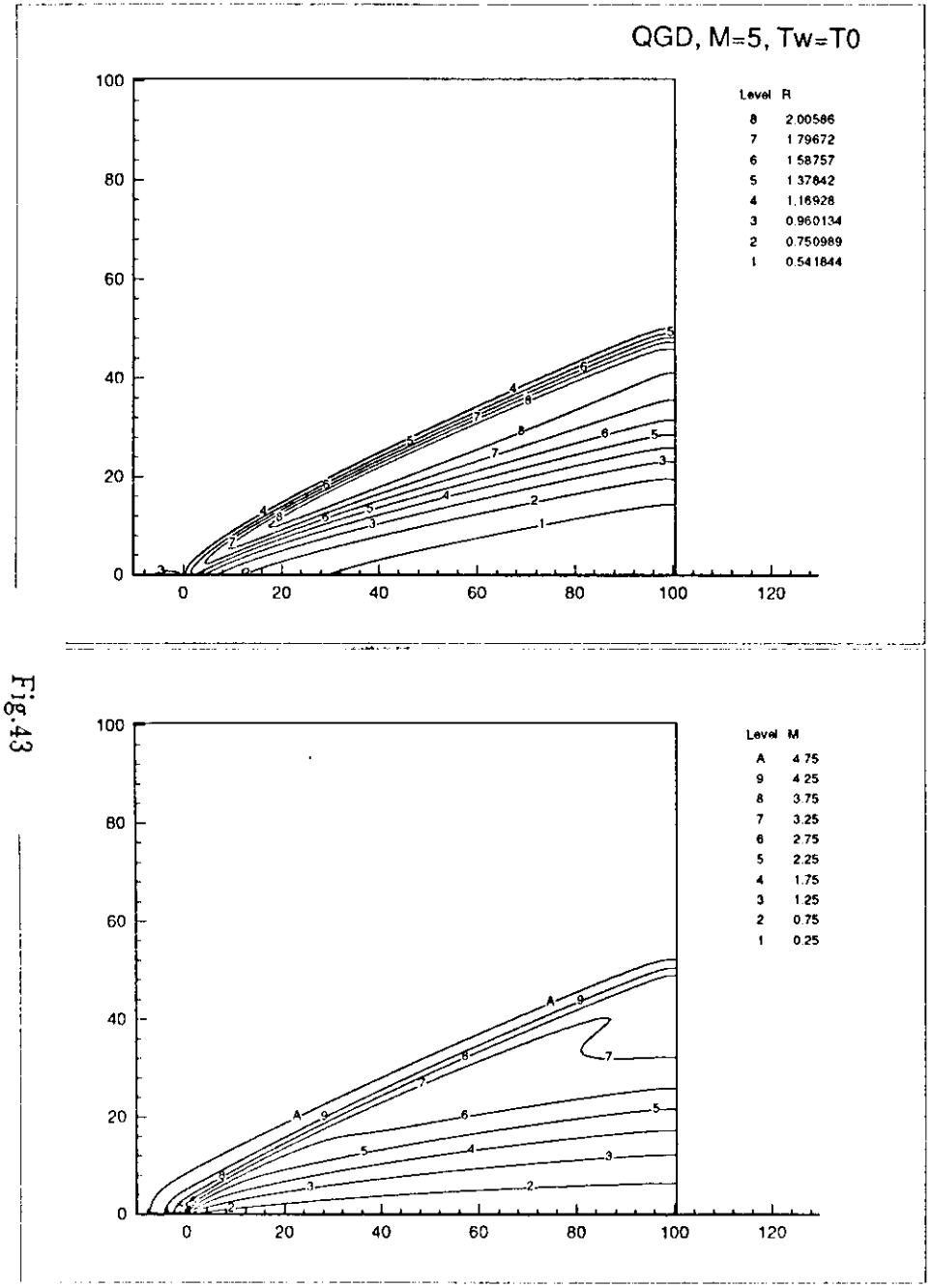
QGD, M=5, Tw=T0
Level R
8 2.00586
7 1.79672
6 1.58757
5 1.37842
4 1.16928
3 0.960134
2 0.750989
1 0.541844
Level T
8 7.81422
7 6.96244
6 6.11067
5 5.25889
4 4.40711
3 3.55533
2 2.70356
1 1.85178
Level M
A 4.75
9 4.25
8 3.75
7 3.25
6 2.75
5 2.25
4 1.75
3 1.25
2 0.75
1 0.25
Level U
A 0.95
9 0.85
8 0.75
7 0.65
6 0.55
5 0.45
4 0.35
3 0.25
2 0.15
1 0.05

Fig.43

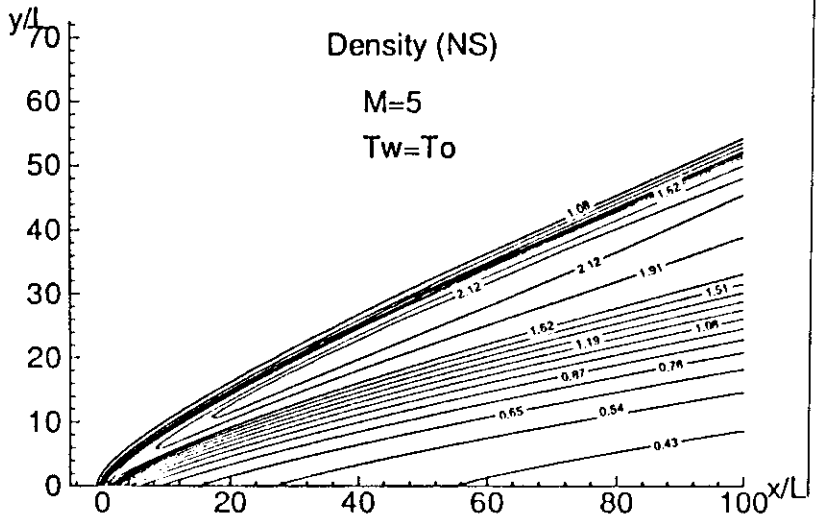
y/L
Density (NS)
M=5
Tw=To
x/L
0
20
40
60
80
100
10
30
50
70
1.08
1.52
2.12
1.91
1.51
1.62
1.19
1.08
0.97
0.76
0.65
0.54
0.43

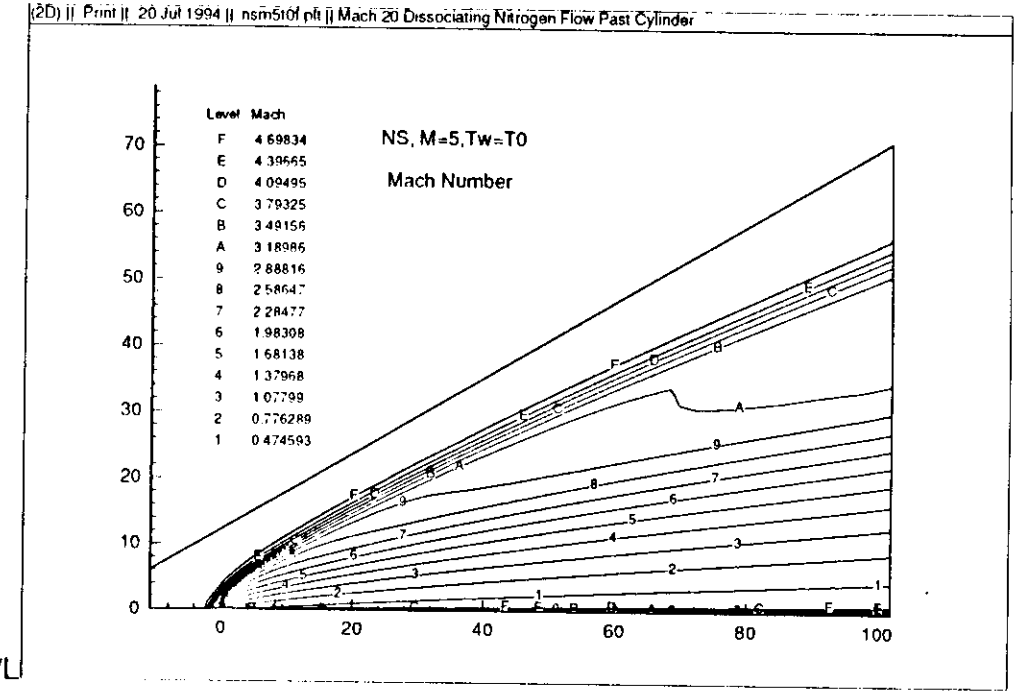
(2D) || Print || 20 Jul 1994 || nsm510f.plt || Mach 20 Dissociating Nitrogen Flow Past Cylinder
Level Mach
F 4.69834
E 4.39665
D 4.09495
C 3.79325
B 3.49156
A 3.18986
9 2.88816
8 2.58647
7 2.28477
6 1.98308
5 1.68138
4 1.37968
3 1.07799
2 0.776289
1 0.474593
NS, M=5,Tw=T0
Mach Number
0
20
40
60
80
100
10
30
50
70

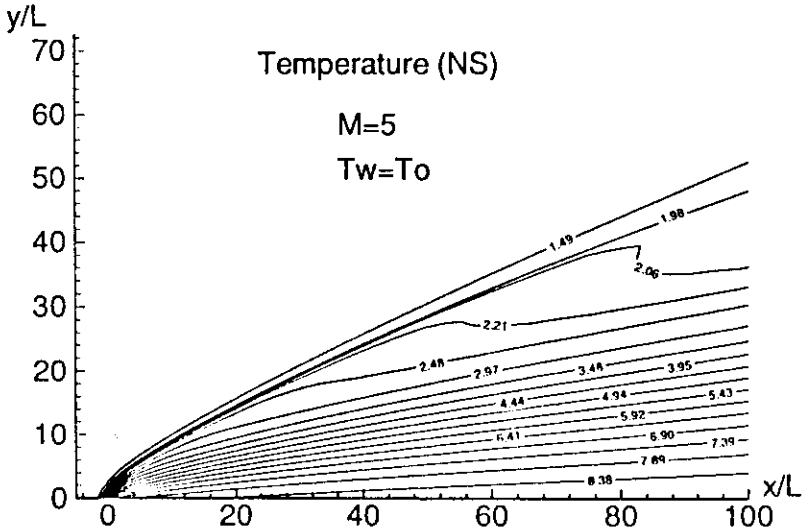
y/L
Temperature (NS)
M=5
Tw=To
x/L
0
20
40
60
80
100
10
30
50
70
1.49
1.98
2.06
2.21
2.48
2.97
3.46
3.95
4.44
4.94
5.43
5.92
6.41
6.90
7.39
7.89
8.38

Fig.44

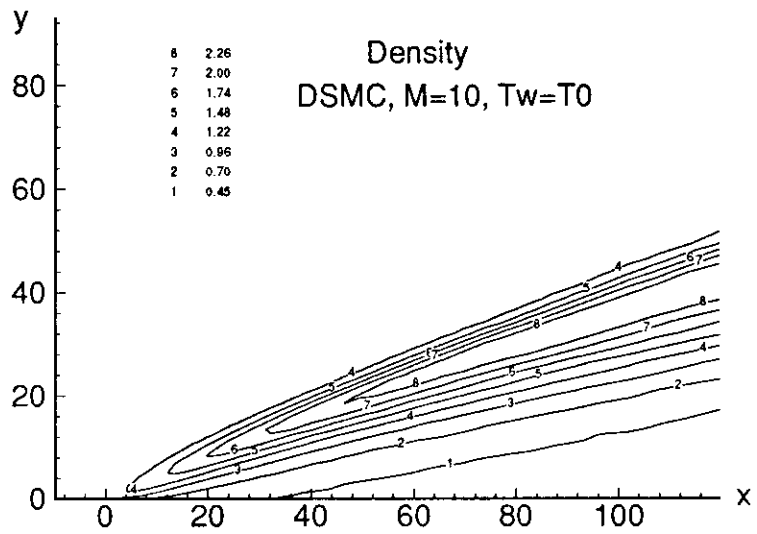
Density
DSMC, M=10, Tw=T0
8 2.26
7 2.00
6 1.74
5 1.48
4 1.22
3 0.96
2 0.70
1 0.45
y
x
0
20
40
60
80
100

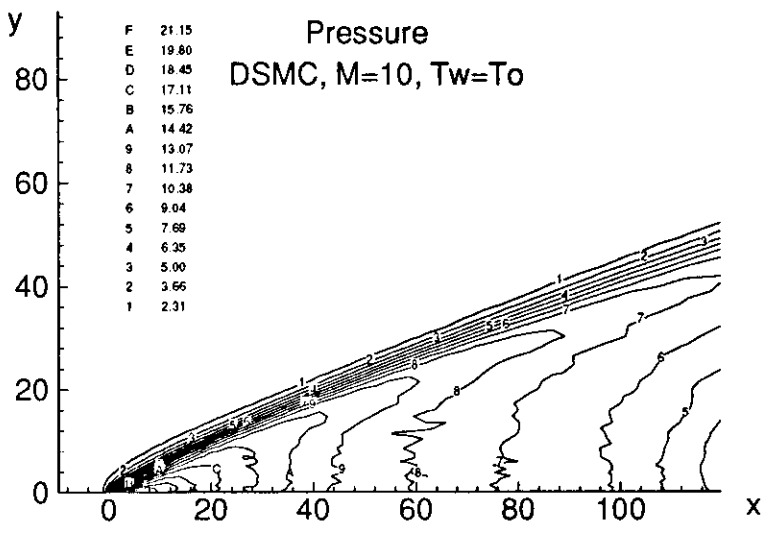
Pressure
DSMC, M=10, Tw=To
F 21.15
E 19.80
D 18.45
C 17.11
B 15.76
A 14.42
9 13.07
8 11.73
7 10.38
6 9.04
5 7.69
4 6.35
3 5.00
2 3.66
1 2.31
y
x
0
20
40
60
80
100

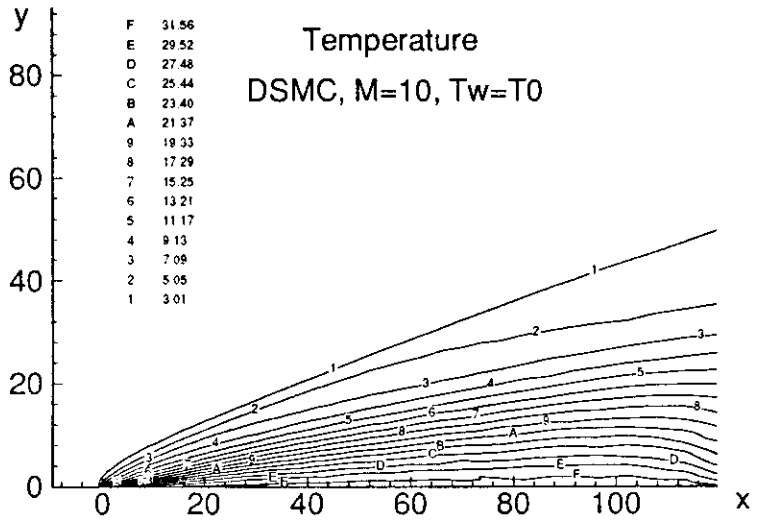
Temperature
DSMC, M=10, Tw=T0
F 31.56
E 29.52
D 27.48
C 25.44
B 23.40
A 21.37
9 19.33
8 17.29
7 15.25
6 13.21
5 11.17
4 9.13
3 7.09
2 5.05
1 3.01
y
x
0
20
40
60
80
100

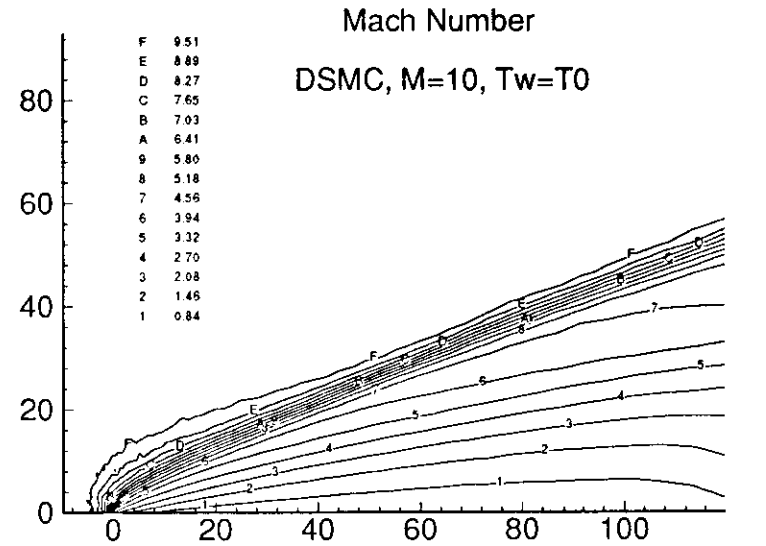
Mach Number
DSMC, M=10, Tw=T0
F 9.51
E 8.89
D 8.27
C 7.65
B 7.03
A 6.41
9 5.80
8 5.18
7 4.56
6 3.94
5 3.32
4 2.70
3 2.08
2 1.46
1 0.84
0
20
40
60
80
100

Fig.45

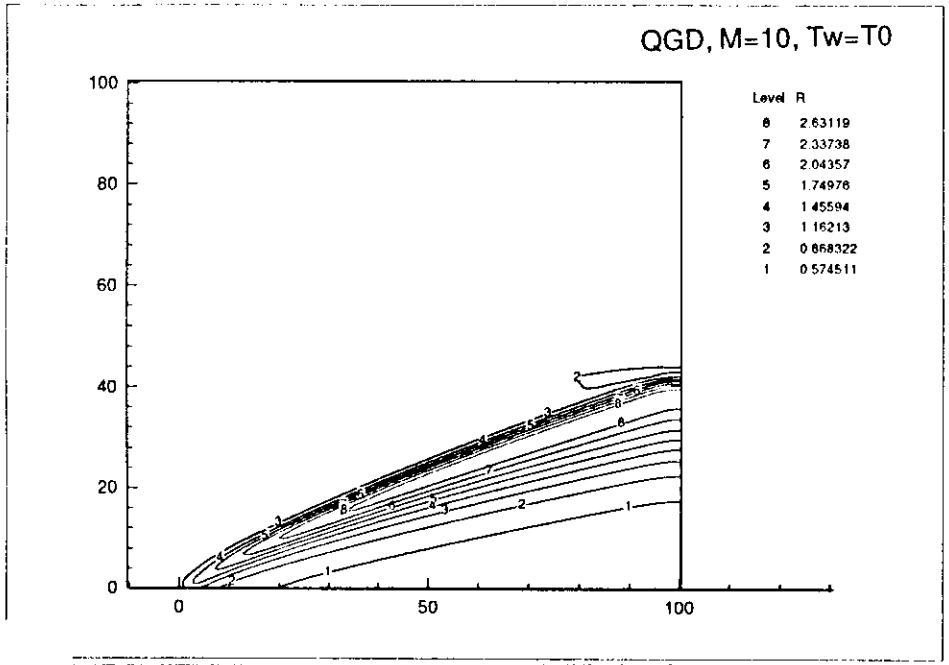
QGD, M=10, Tw=T0
Level R
8 2.63119
7 2.33738
6 2.04357
5 1.74976
4 1.45594
3 1.16213
2 0.868322
1 0.574511
0
20
40
60
80
100
0
50
100

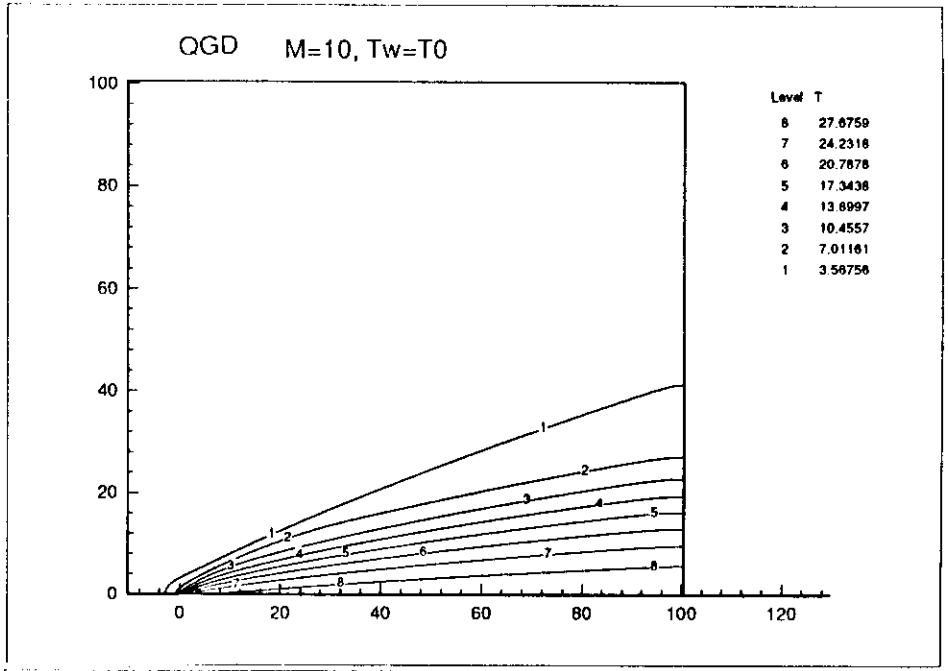
QGD M=10, Tw=T0
Level T
8 27.6759
7 24.2318
6 20.7878
5 17.3438
4 13.8997
3 10.4557
2 7.01161
1 3.56756
0
20
40
60
80
100
120

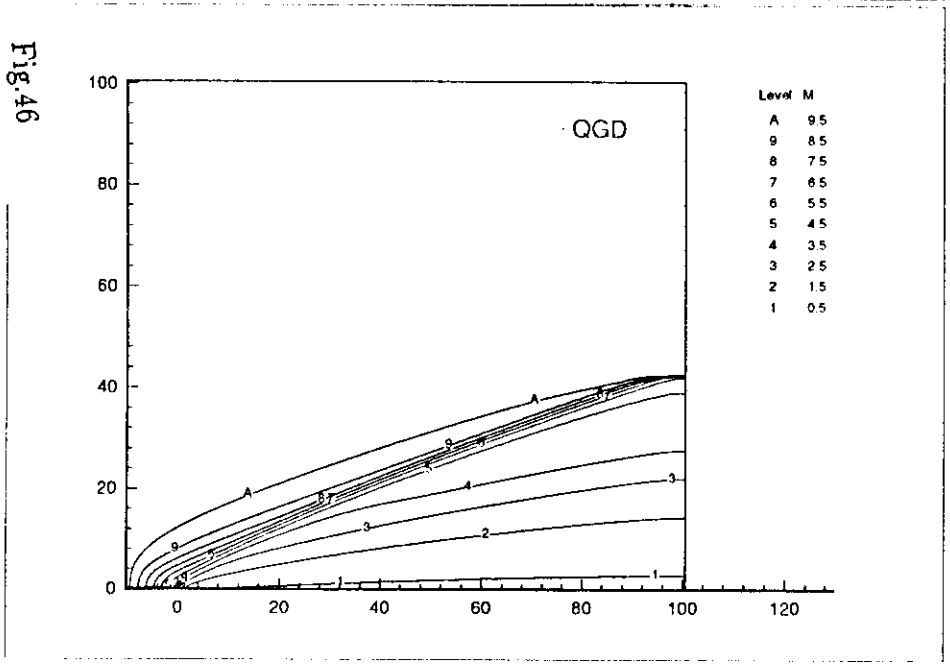
QGD
Level M
A 9.5
9 8.5
8 7.5
7 6.5
6 5.5
5 4.5
4 3.5
3 2.5
2 1.5
1 0.5
0
20
40
60
80
100
120

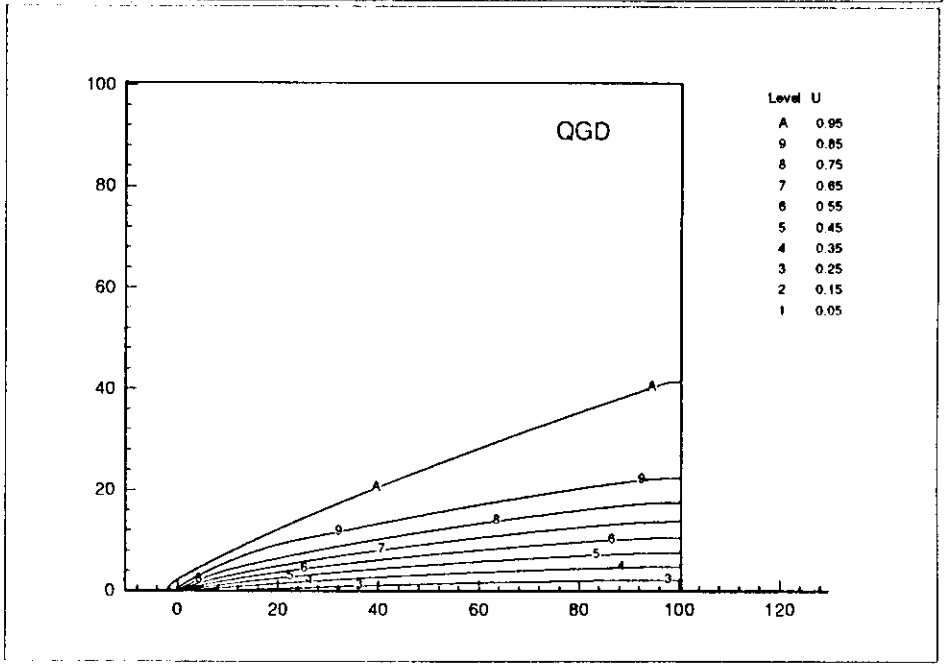
QGD
Level U
A 0.95
9 0.85
8 0.75
7 0.65
6 0.55
5 0.45
4 0.35
3 0.25
2 0.15
1 0.05
0
20
40
60
80
100
120

Fig.46

(2D) || Print || 20 Jul 1994 || nsm10t0f.plt || M 10, temperature paroi chaude

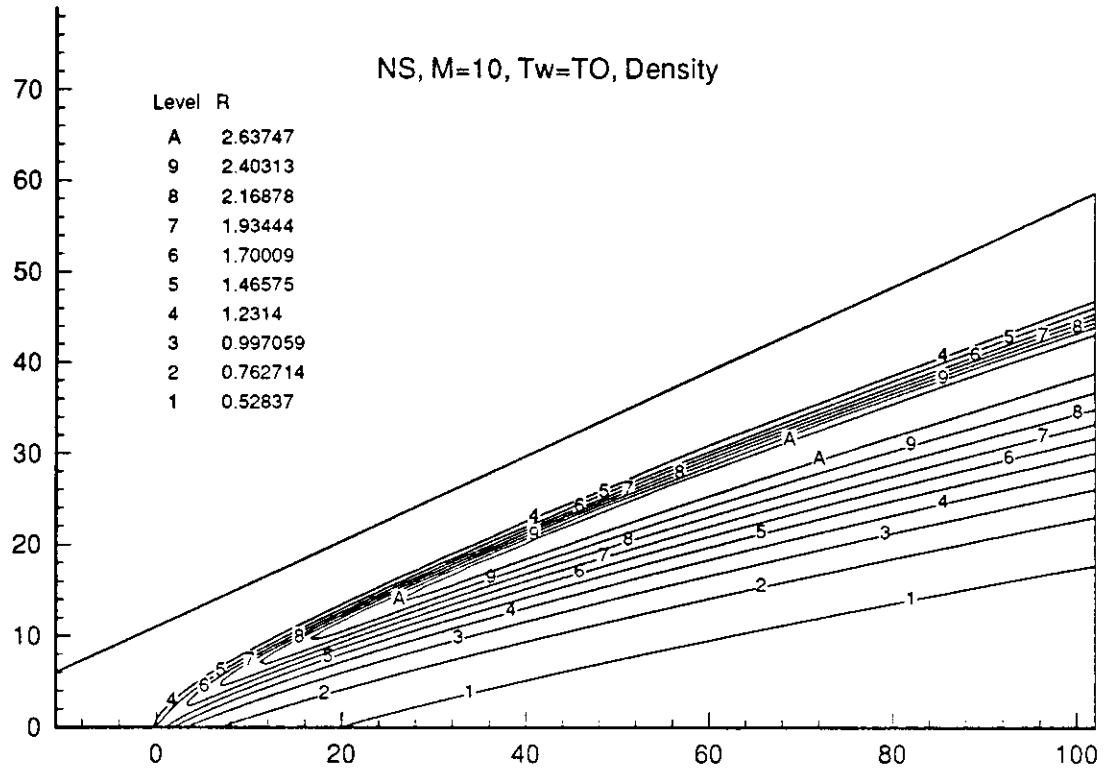

(2D) || Print || 20 Jul 1994 || nsm10t0f.plt || M 10, temperature paroi chaude

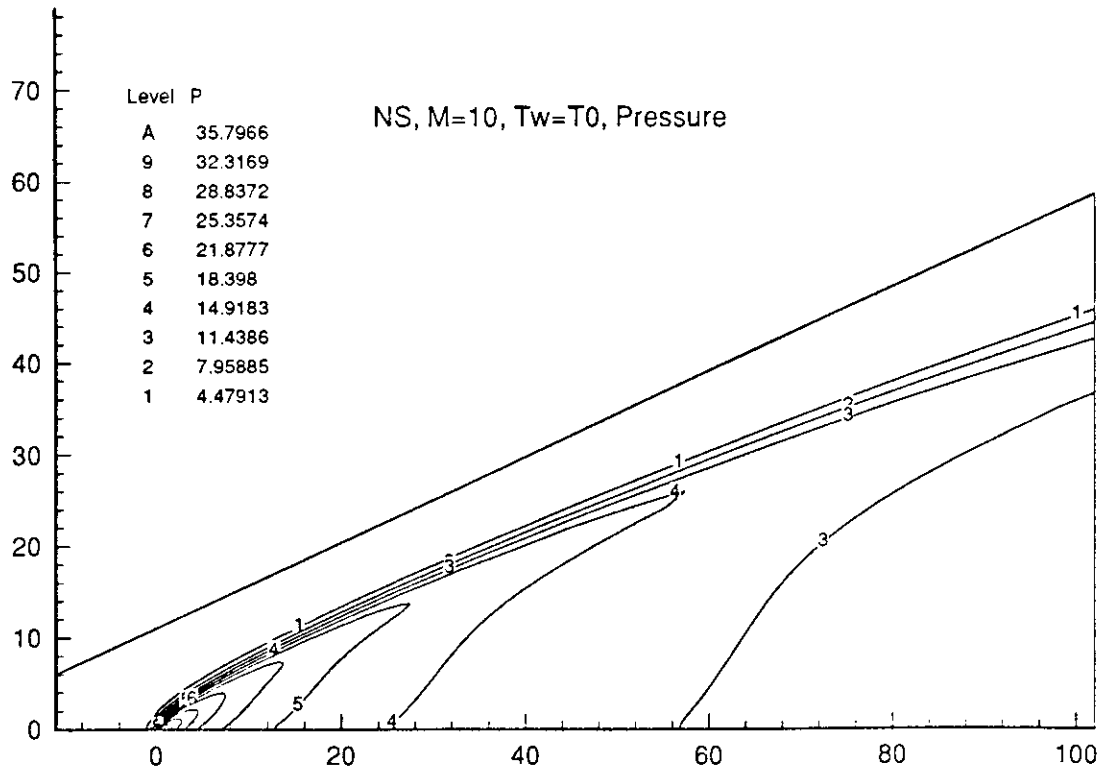

Fig.47

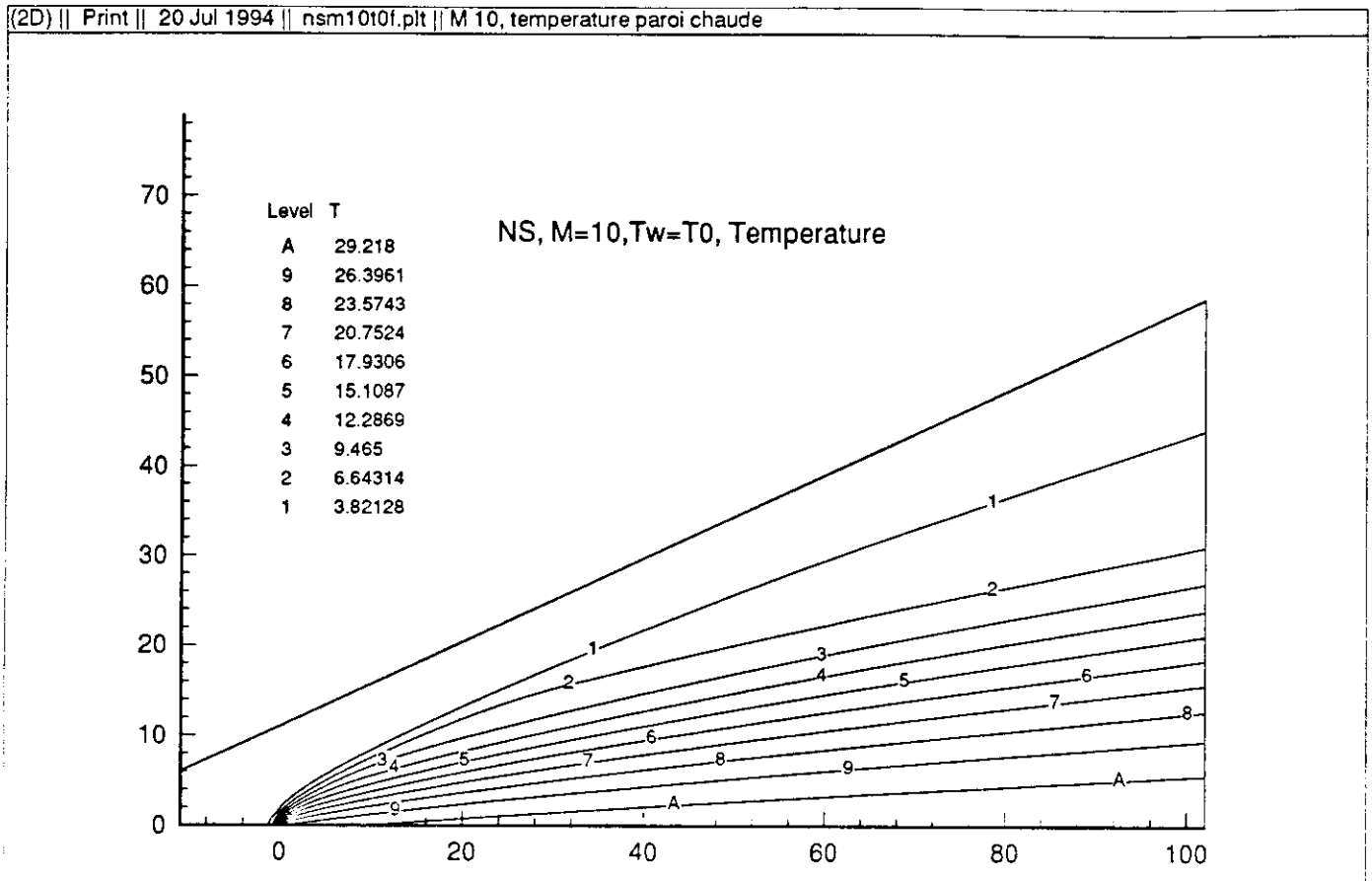
(2D) || Print || 20 Jul 1994 || nsm10t0f.plt || M 10, temperature paroi chaude
Level T
A 29.218
9 26.3961
8 23.5743
7 20.7524
6 17.9306
5 15.1087
4 12.2869
3 9.465
2 6.64314
1 3.82128
NS, M=10,Tw=T0, Temperature
0
10
20
30
40
50
60
70
0
20
40
60
80
100

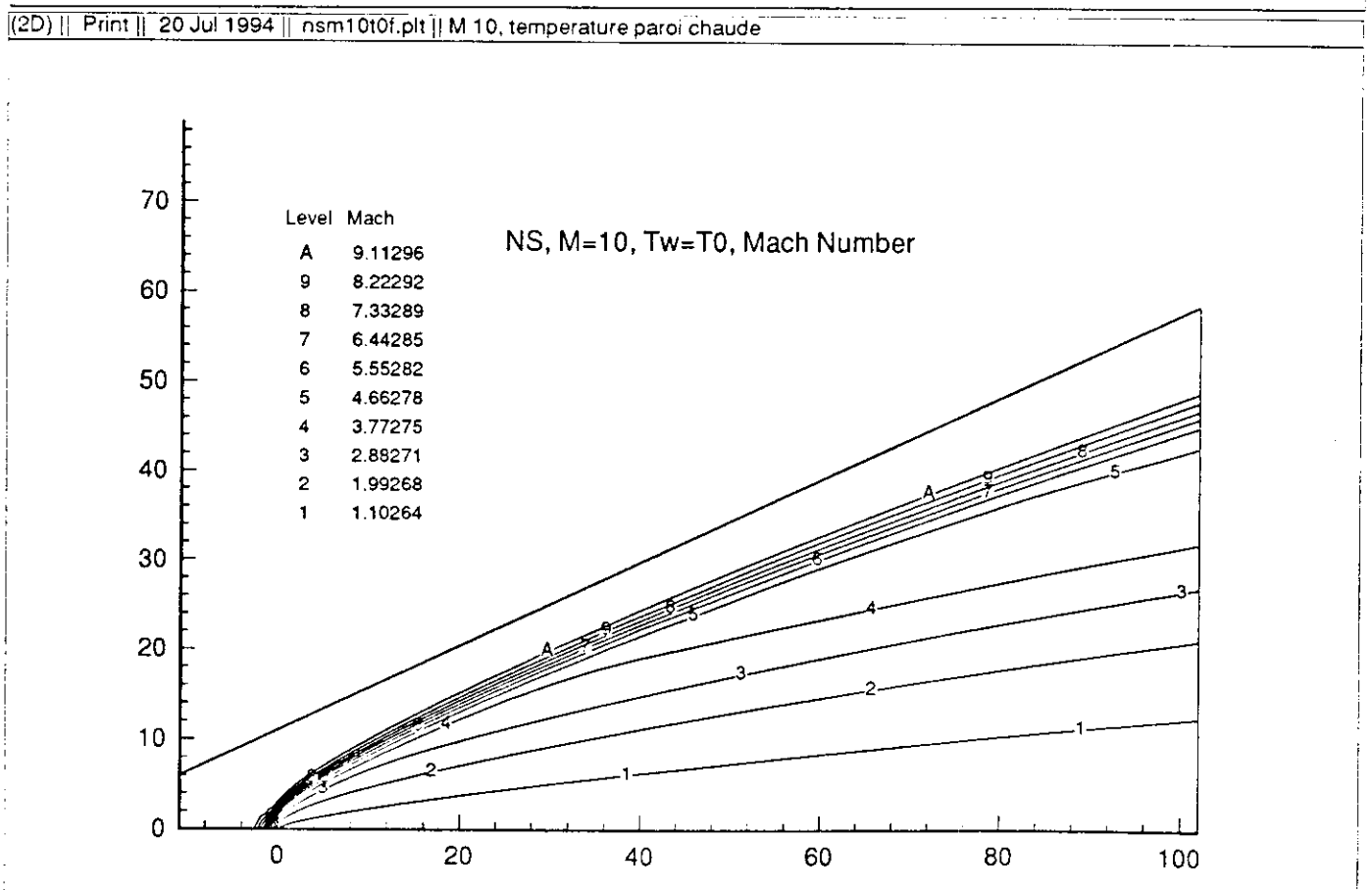
(2D) || Print || 20 Jul 1994 || nsm10t0f.plt || M 10, temperature paroi chaude
Level Mach
A 9.11296
9 8.22292
8 7.33289
7 6.44285
6 5.55282
5 4.66278
4 3.77275
3 2.88271
2 1.99268
1 1.10264
NS, M=10, Tw=T0, Mach Number
0
10
20
30
40
50
60
70
0
20
40
60
80
100

Fig.48

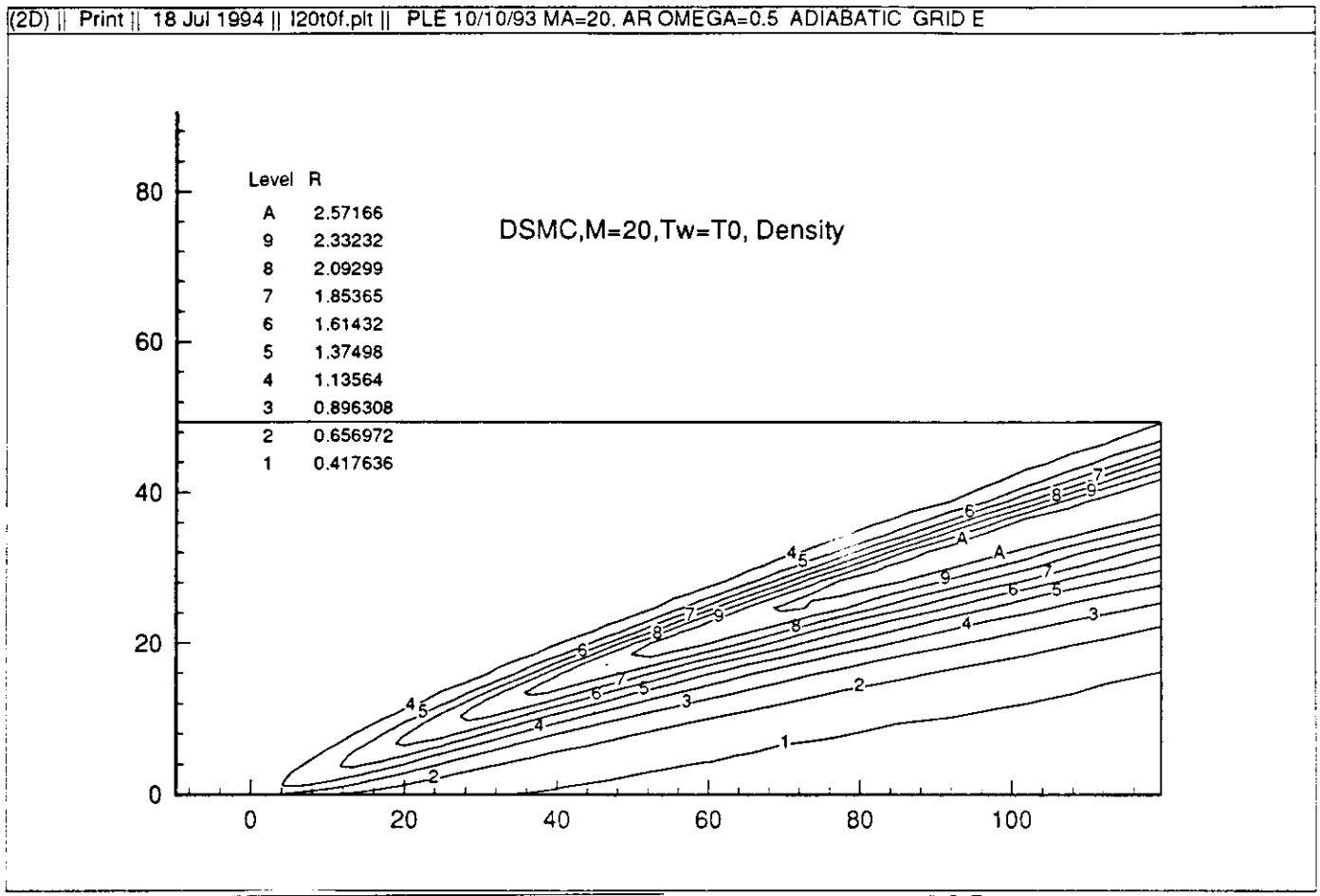
(2D) || Print || 18 Jul 1994 || I20t0f.plt || PLE 10/10/93 MA=20. AR OMEGA=0.5 ADIABATIC GRID E
Level R
A 2.57166
9 2.33232
8 2.09299
7 1.85365
6 1.61432
5 1.37498
4 1.13564
3 0.896308
2 0.656972
1 0.417636
DSMC,M=20,Tw=T0, Density
0
20
40
60
80
0
20
40
60
80
100

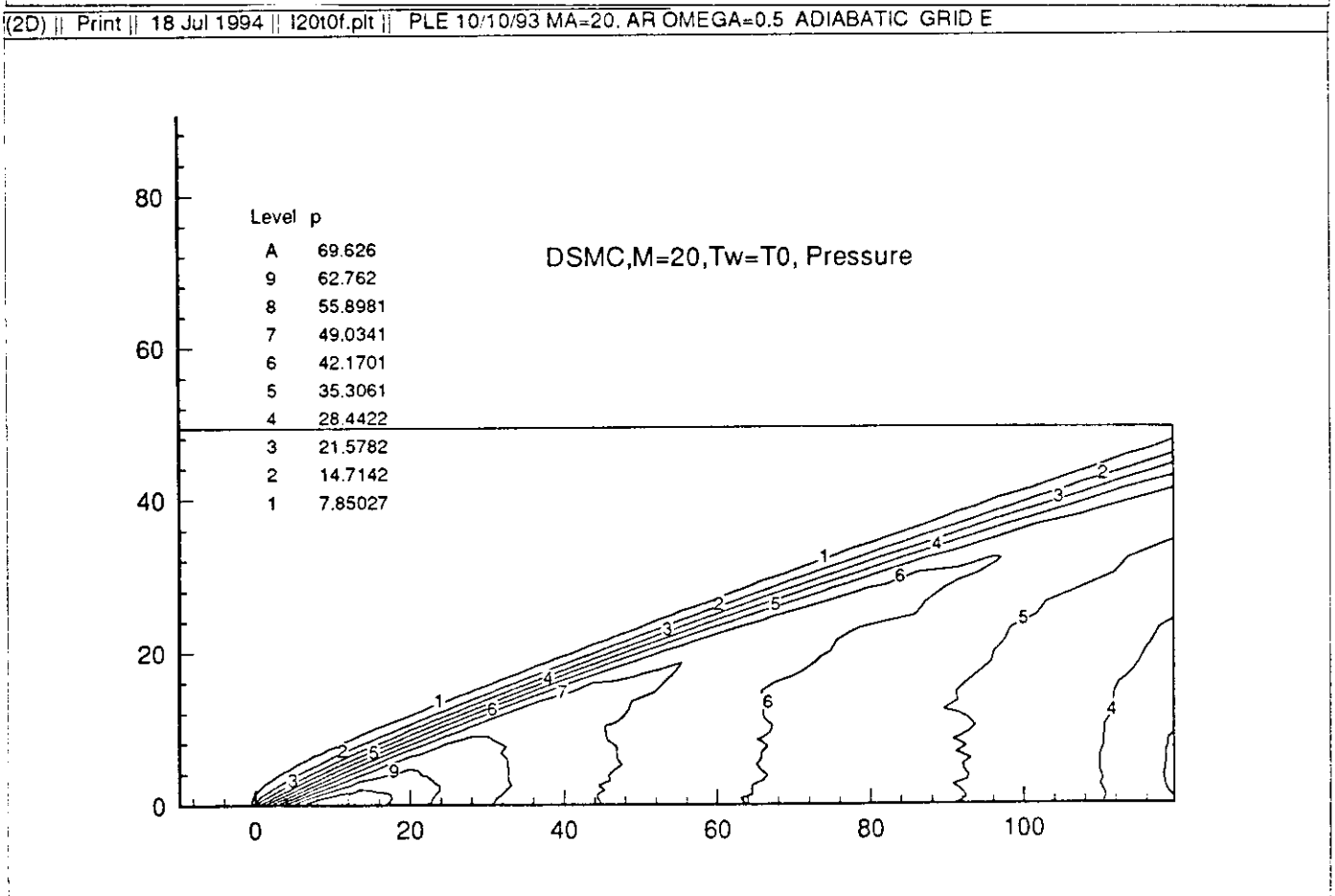
(2D) || Print || 18 Jul 1994 || I20t0f.plt || PLE 10/10/93 MA=20. AR OMEGA=0.5 ADIABATIC GRID E
Level p
A 69.626
9 62.762
8 55.8981
7 49.0341
6 42.1701
5 35.3061
4 28.4422
3 21.5782
2 14.7142
1 7.85027
DSMC,M=20,Tw=T0, Pressure
0
20
40
60
80
0
20
40
60
80
100

Fig.49

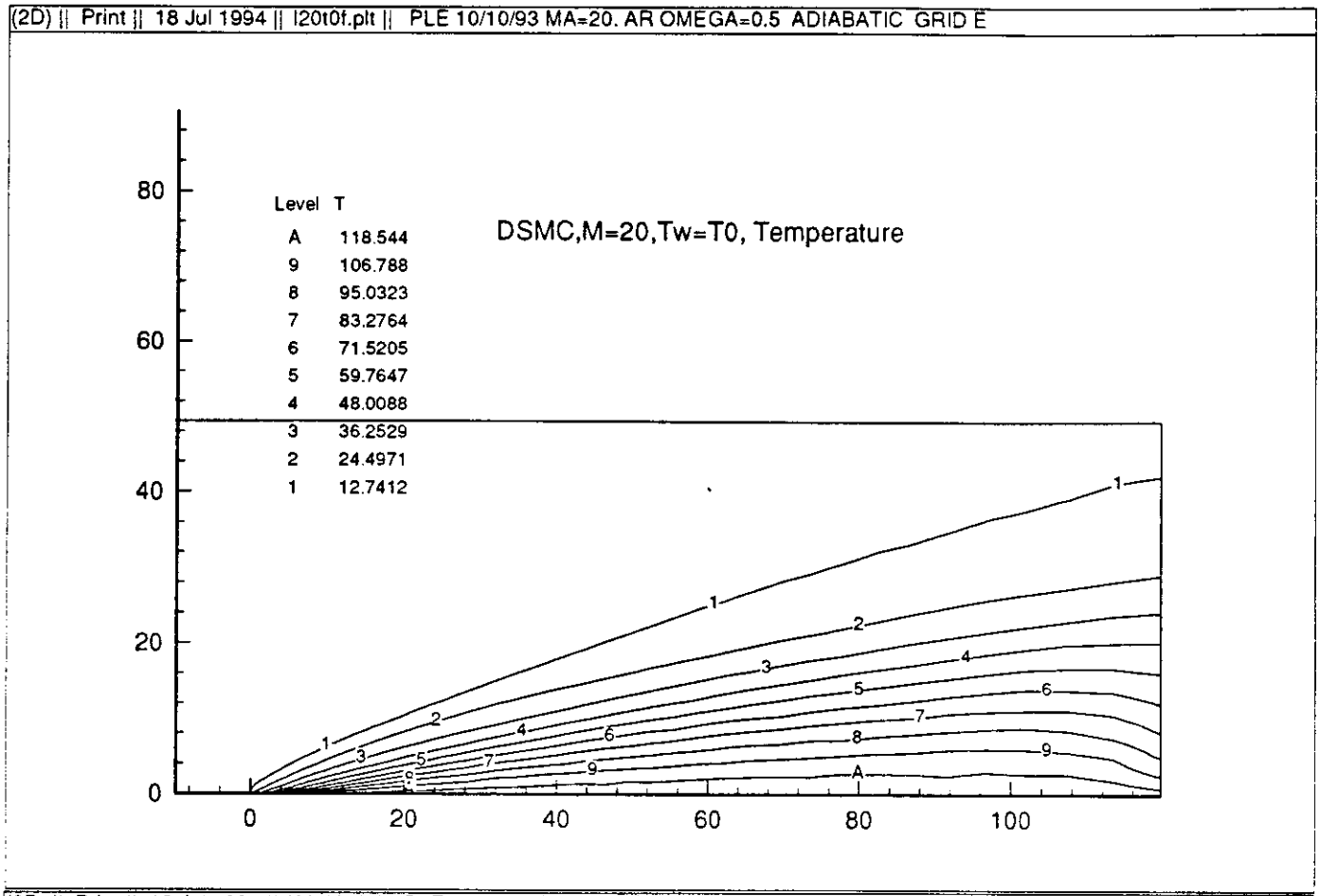
(2D) || Print || 18 Jul 1994 || I20t0f.plt || PLE 10/10/93 MA=20. AR OMEGA=0.5 ADIABATIC GRID E
Level T
A 118.544
9 106.788
8 95.0323
7 83.2764
6 71.5205
5 59.7647
4 48.0088
3 36.2529
2 24.4971
1 12.7412
DSMC,M=20,Tw=T0, Temperature
0
20
40
60
80
0
20
40
60
80
100

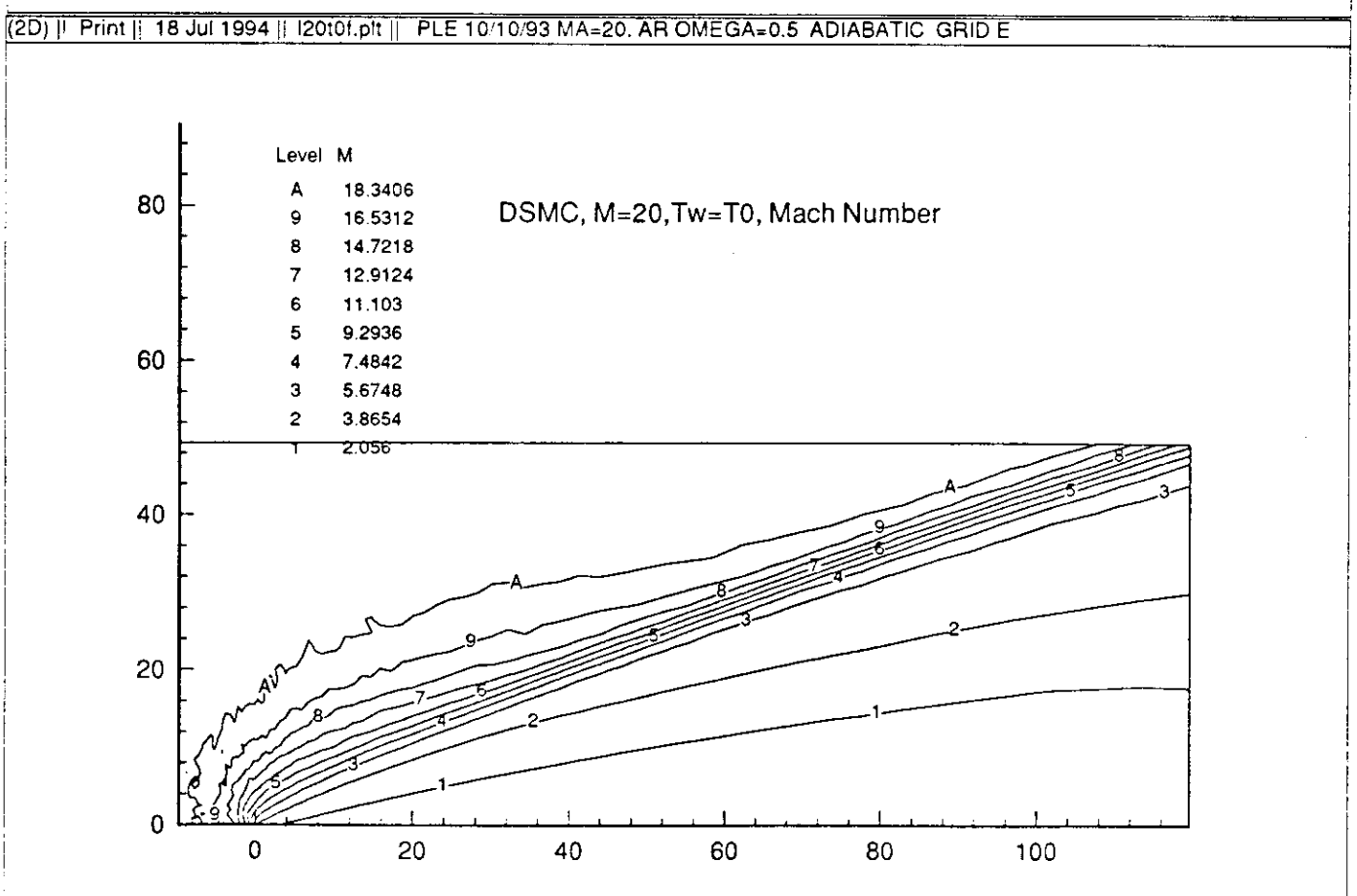
(2D) || Print || 18 Jul 1994 || I20t0f.plt || PLE 10/10/93 MA=20. AR OMEGA=0.5 ADIABATIC GRID E
Level M
A 18.3406
9 16.5312
8 14.7218
7 12.9124
6 11.103
5 9.2936
4 7.4842
3 5.6748
2 3.8654
1 2.056
DSMC, M=20,Tw=T0, Mach Number
0
20
40
60
80
0
20
40
60
80
100

Fig.50

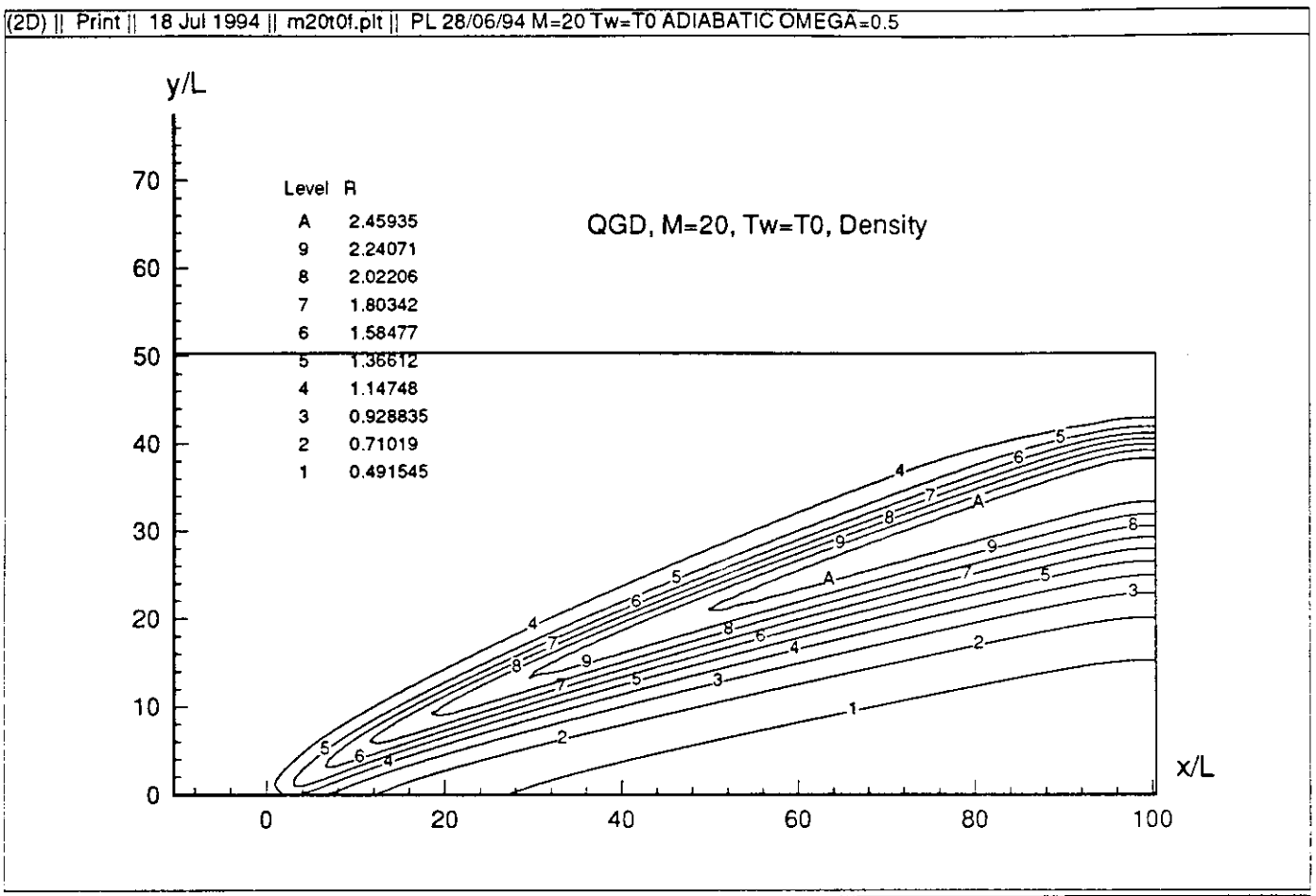
(2D) || Print || 18 Jul 1994 || m20t0f.plt || PL 28/06/94 M=20 Tw=T0 ADIABATIC OMEGA=0.5
y/L
Level R
A 2.45935
9 2.24071
8 2.02206
7 1.80342
6 1.58477
5 1.36612
4 1.14748
3 0.928835
2 0.71019
1 0.491545
QGD, M=20, Tw=T0, Density
x/L
0
10
20
30
40
50
60
70
0
20
40
60
80
100

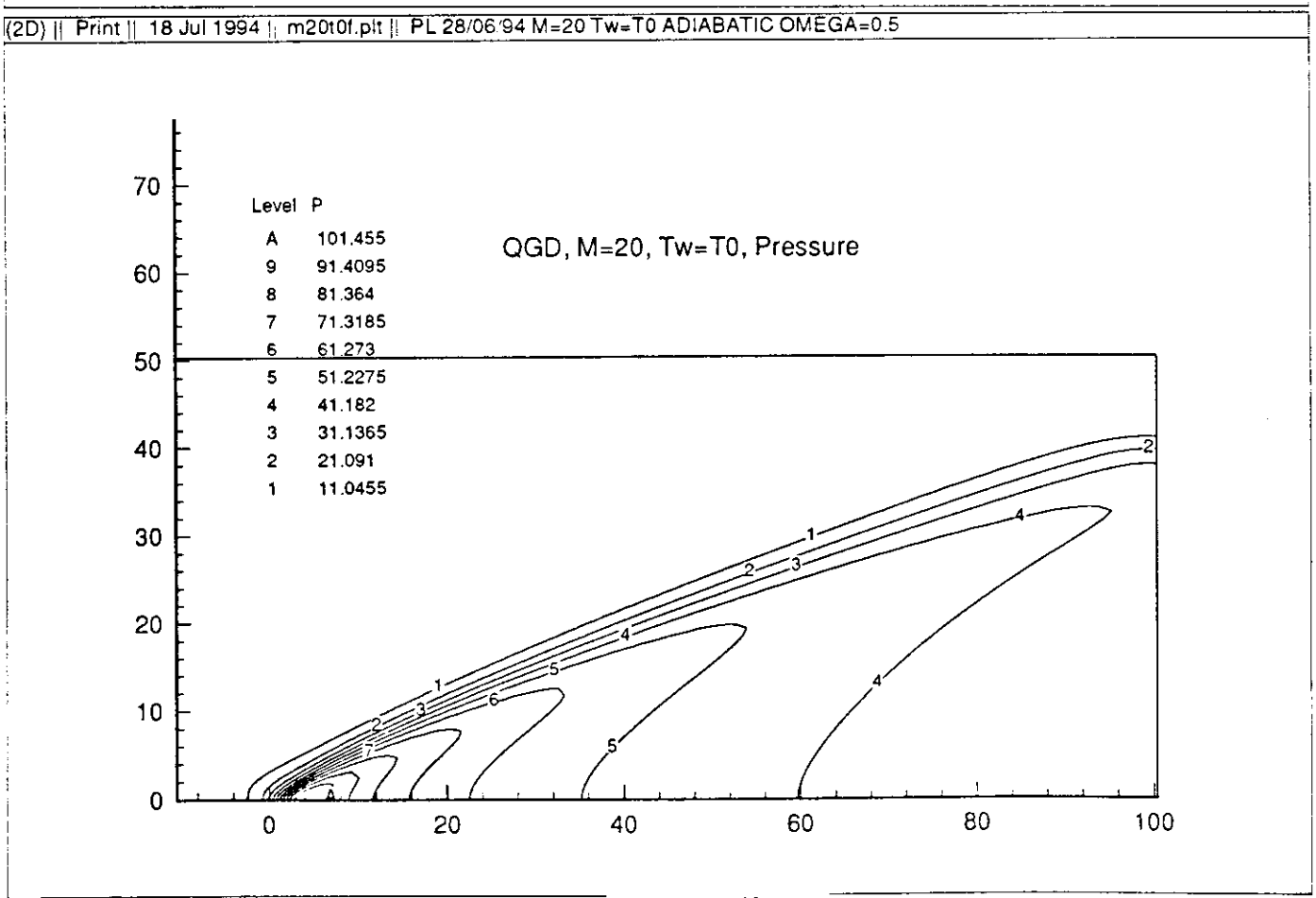
(2D) || Print || 18 Jul 1994 || m20t0f.plt || PL 28/06/94 M=20 Tw=T0 ADIABATIC OMEGA=0.5
Level P
A 101.455
9 91.4095
8 81.364
7 71.3185
6 61.273
5 51.2275
4 41.182
3 31.1365
2 21.091
1 11.0455
QGD, M=20, Tw=T0, Pressure
0
10
20
30
40
50
60
70
0
20
40
60
80
100

Fig.51

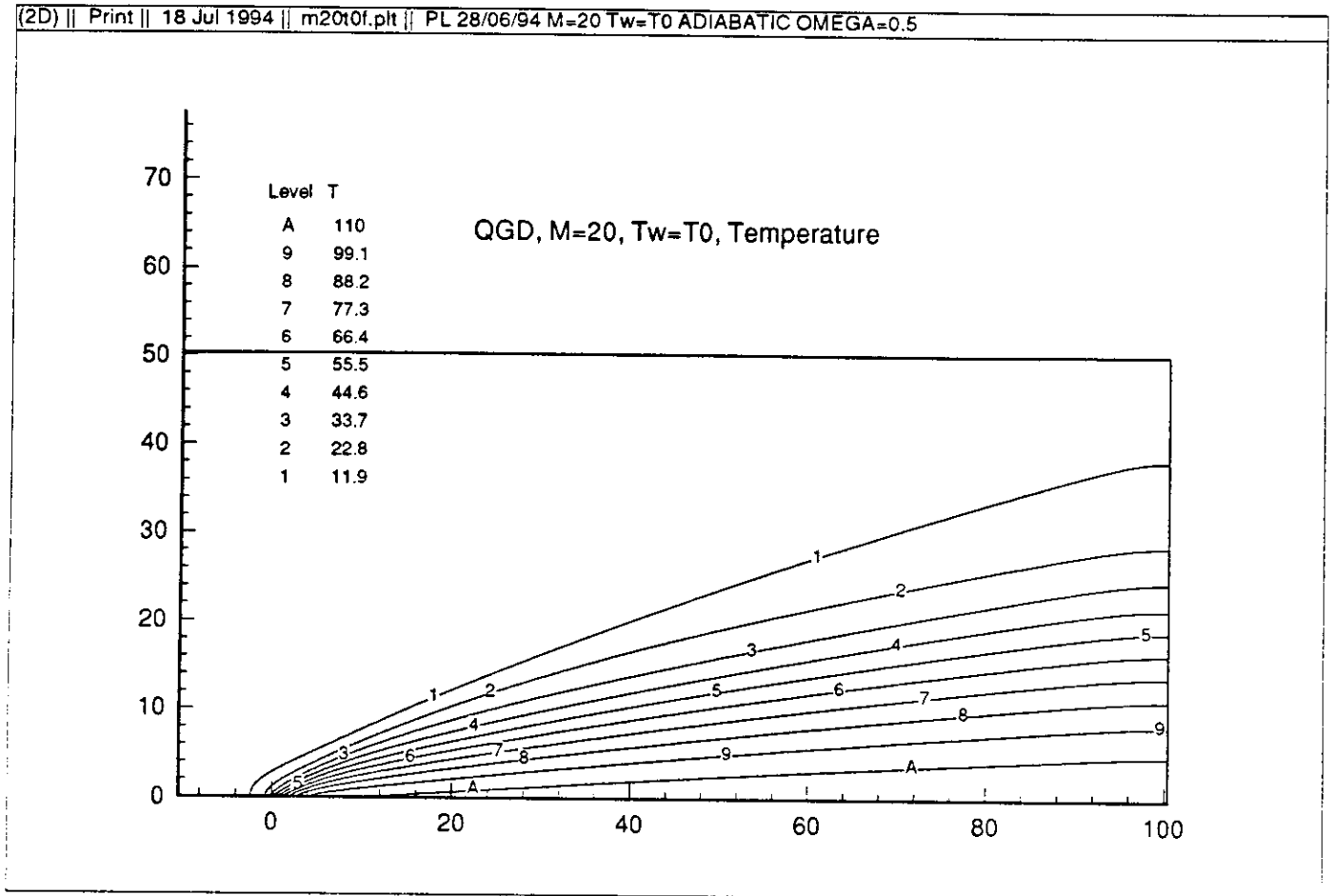
(2D) || Print || 18 Jul 1994 || m20t0f.plt || PL 28/06/94 M=20 Tw=T0 ADIABATIC OMEGA=0.5
Level T
A 110
9 99.1
8 88.2
7 77.3
6 66.4
5 55.5
4 44.6
3 33.7
2 22.8
1 11.9
QGD, M=20, Tw=T0, Temperature
0
10
20
30
40
50
60
70
0
20
40
60
80
100

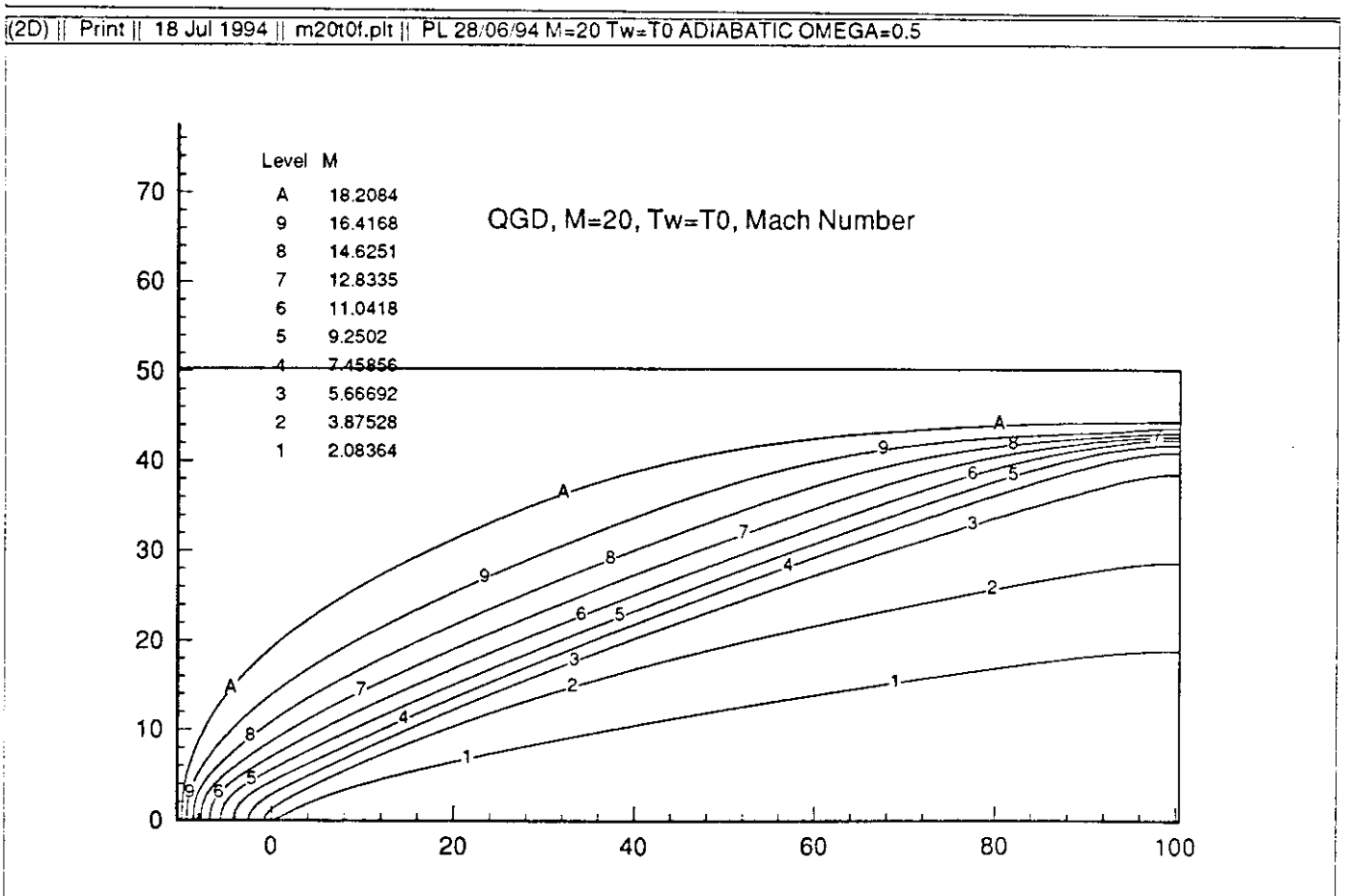
(2D) || Print || 18 Jul 1994 || m20t0f.plt || PL 28/06/94 M=20 Tw=T0 ADIABATIC OMEGA=0.5
Level M
A 18.2084
9 16.4168
8 14.6251
7 12.8335
6 11.0418
5 9.2502
4 7.45856
3 5.66692
2 3.87528
1 2.08364
QGD, M=20, Tw=T0, Mach Number
0
10
20
30
40
50
60
70
0
20
40
60
80
100

Fig.52

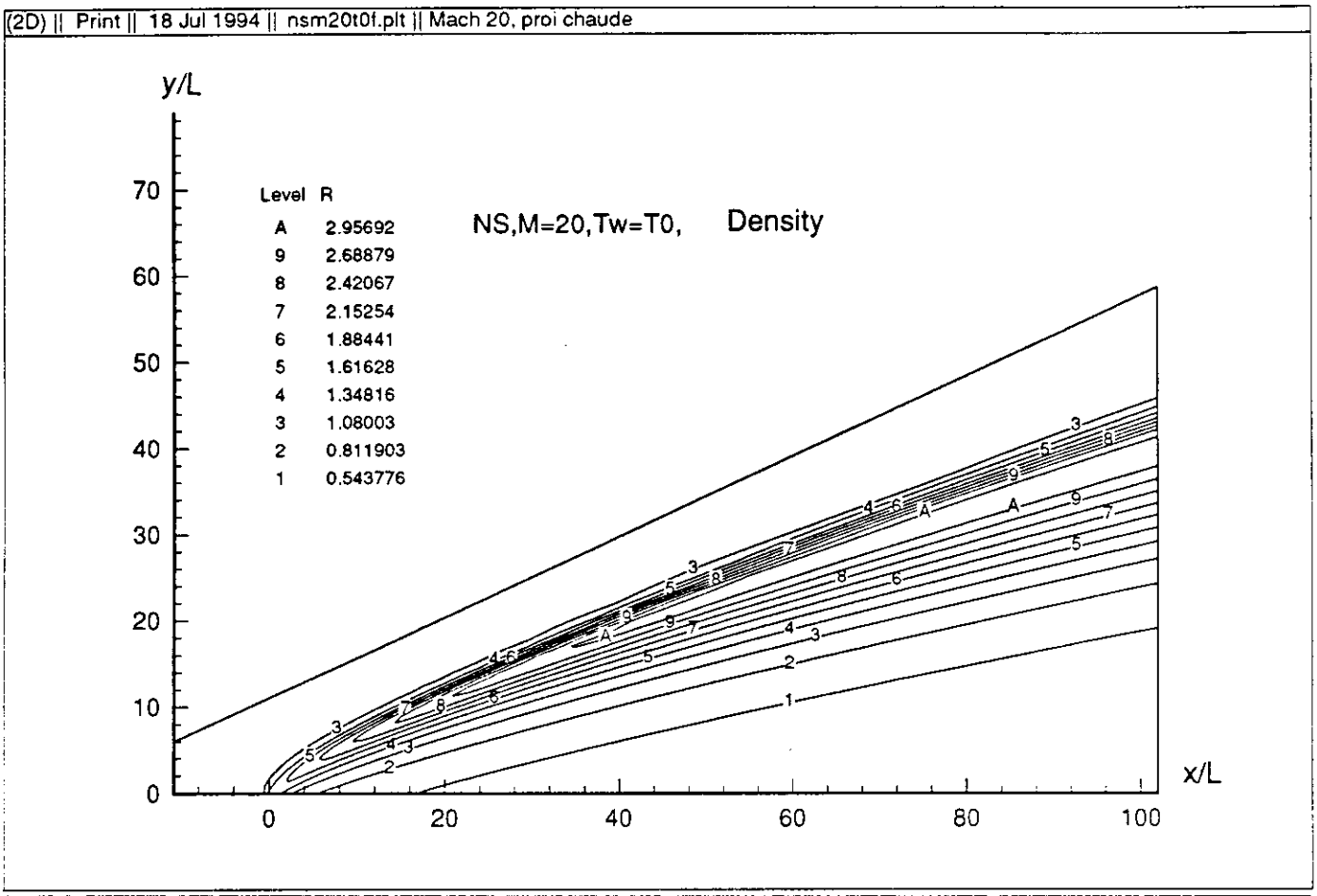
(2D) || Print || 18 Jul 1994 || nsm20t0f.plt || Mach 20, proi chaude
y/L
Level R
A 2.95692
9 2.68879
8 2.42067
7 2.15254
6 1.88441
5 1.61628
4 1.34816
3 1.08003
2 0.811903
1 0.543776
NS,M=20,Tw=T0, Density
x/L
0
10
20
30
40
50
60
70
0
20
40
60
80
100

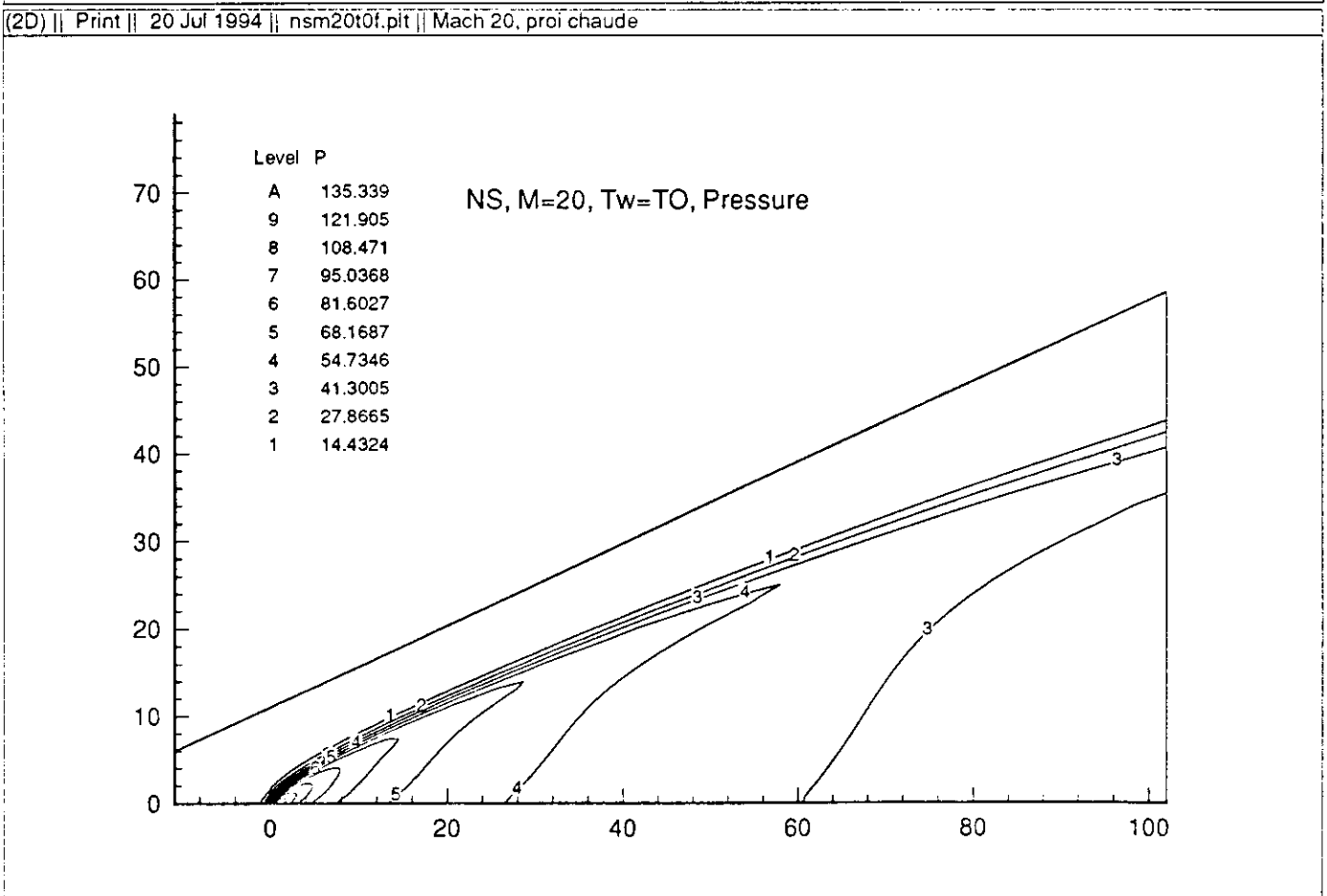
(2D) || Print || 20 Jul 1994 || nsm20t0f.plt || Mach 20, proi chaude
Level P
A 135.339
9 121.905
8 108.471
7 95.0368
6 81.6027
5 68.1687
4 54.7346
3 41.3005
2 27.8665
1 14.4324
NS, M=20, Tw=TO, Pressure
0
10
20
30
40
50
60
70
0
20
40
60
80
100

Fig.53

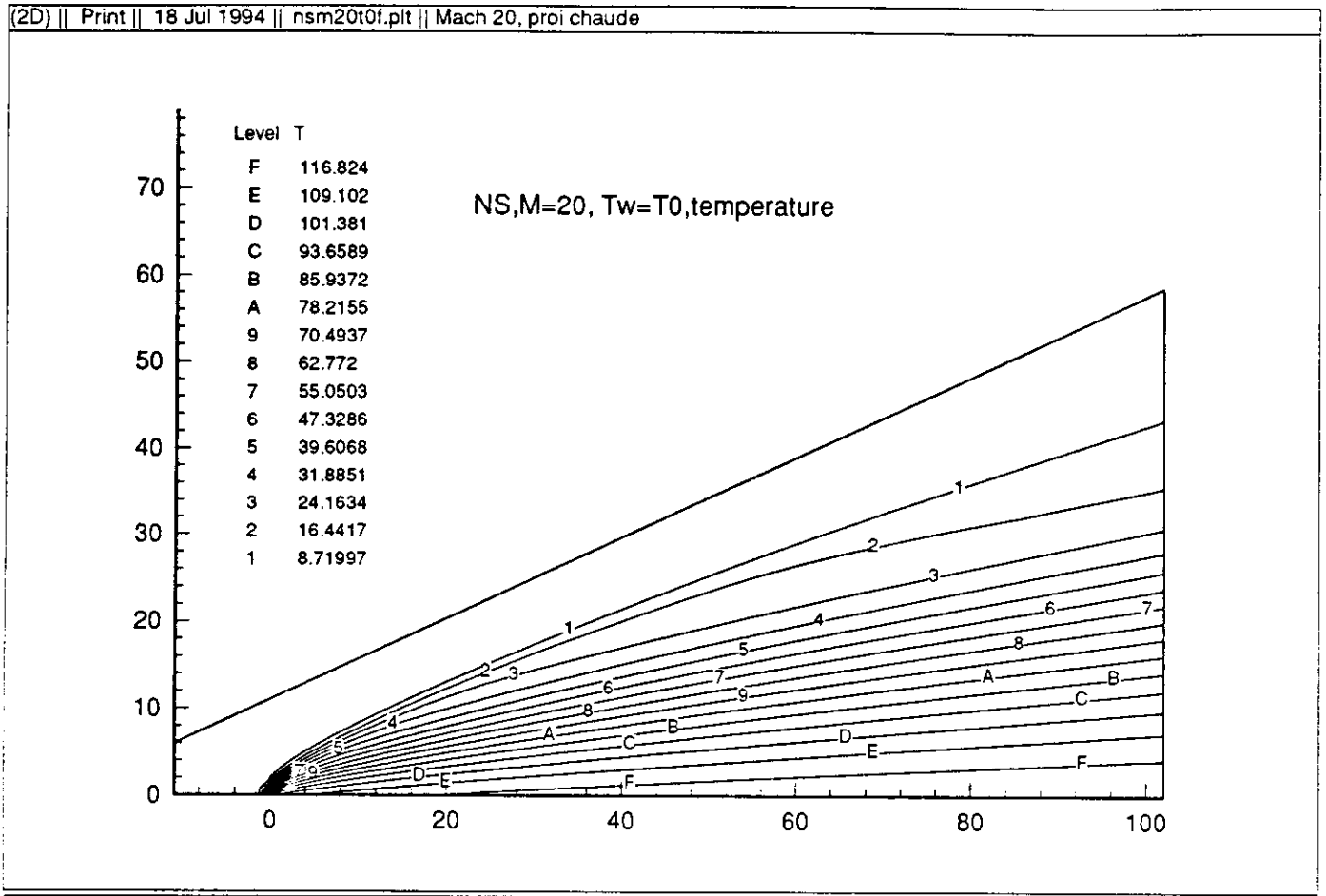
(2D) || Print || 18 Jul 1994 || nsm20t0f.plt || Mach 20, proi chaude
NS,M=20, Tw=T0,temperature
Level T
F 116.824
E 109.102
D 101.381
C 93.6589
B 85.9372
A 78.2155
9 70.4937
8 62.772
7 55.0503
6 47.3286
5 39.6068
4 31.8851
3 24.1634
2 16.4417
1 8.71997
0
10
20
30
40
50
60
70
0
20
40
60
80
100

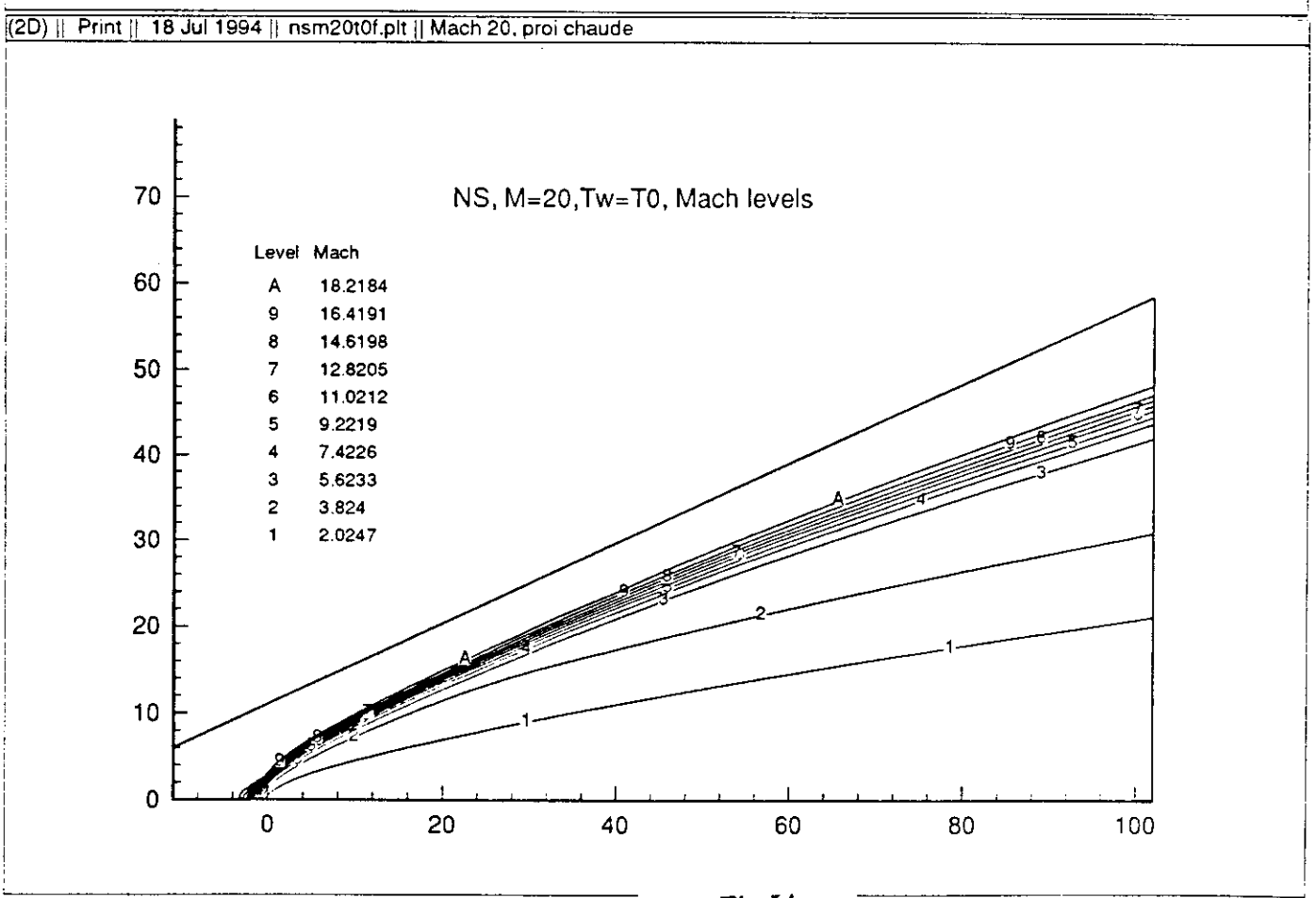
(2D) || Print || 18 Jul 1994 || nsm20t0f.plt || Mach 20, proi chaude
NS, M=20,Tw=T0, Mach levels
Level Mach
A 18.2184
9 16.4191
8 14.6198
7 12.8205
6 11.0212
5 9.2219
4 7.4226
3 5.6233
2 3.824
1 2.0247
0
10
20
30
40
50
60
70
0
20
40
60
80
100

Fig.54

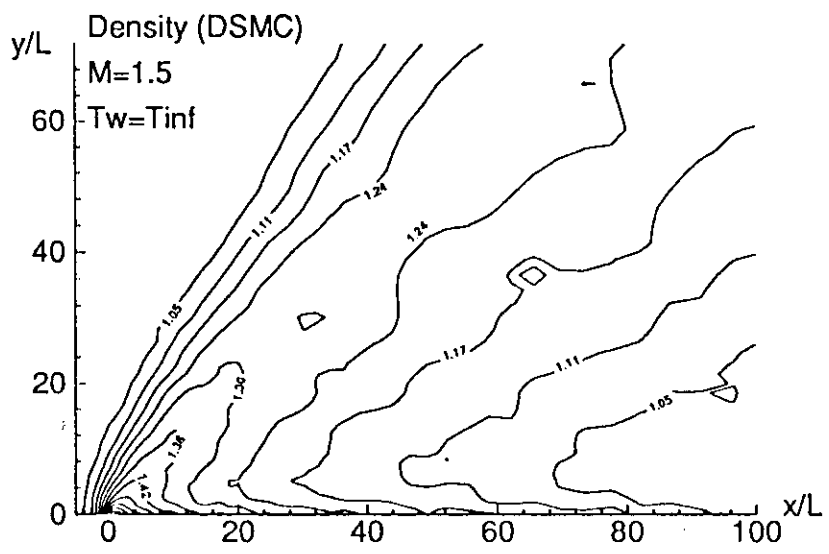
Density (DSMC)
M=1.5
Tw=Tinf
y/L
x/L
0
20
40
60
80
100

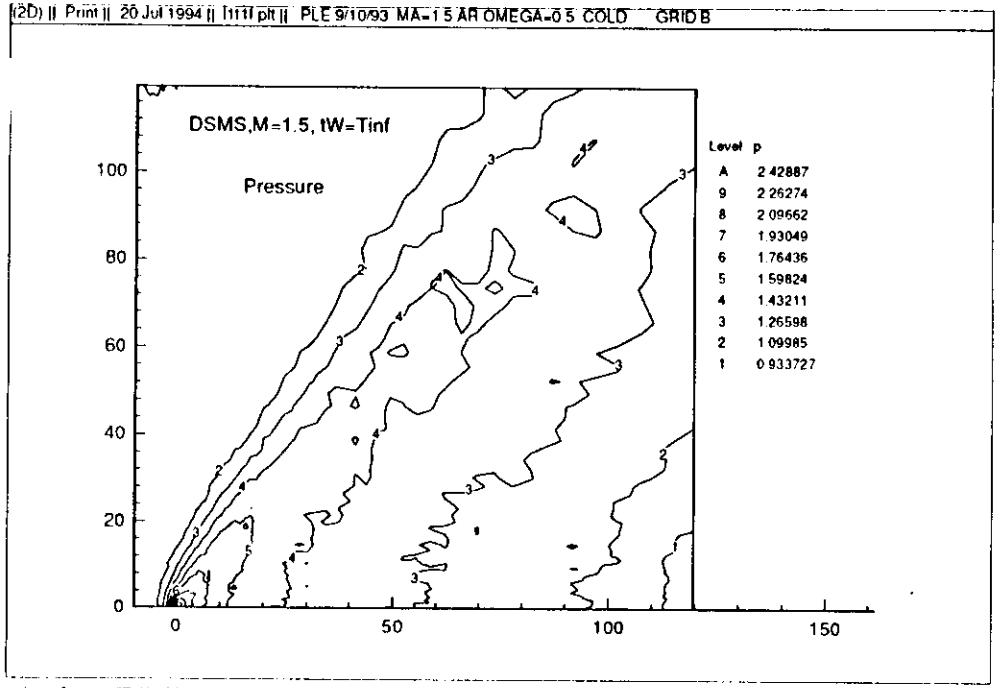
(2D) || Print || 20 Jul 1994 || 1111 plt || PLE 9/10/93 MA=1.5 AR OMEGA=0.5 COLD GRID B
DSMS,M=1.5, tW=Tinf
Pressure
Level p
A 2.42887
9 2.26274
8 2.09662
7 1.93049
6 1.76436
5 1.59824
4 1.43211
3 1.26598
2 1.09985
1 0.933727
0
20
40
60
80
100
0
50
100
150

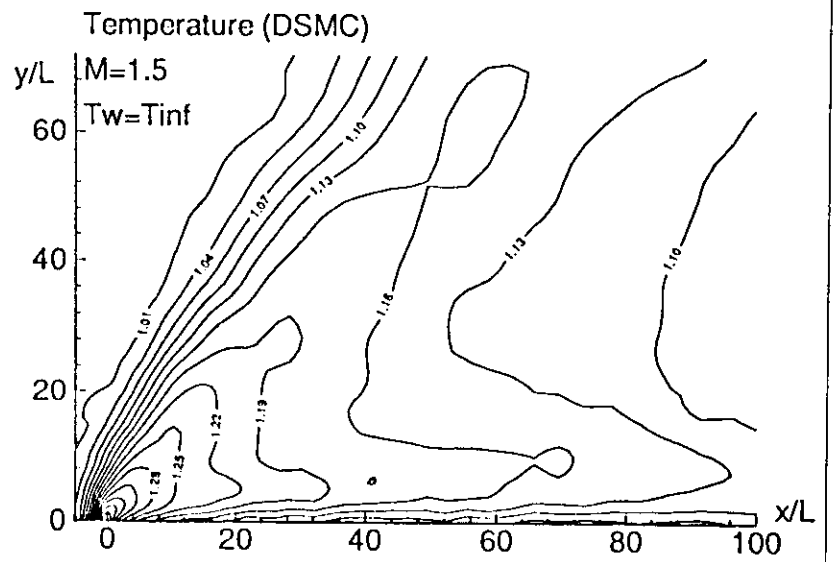
Temperature (DSMC)
M=1.5
Tw=Tinf
y/L
x/L
0
20
40
60
80
100

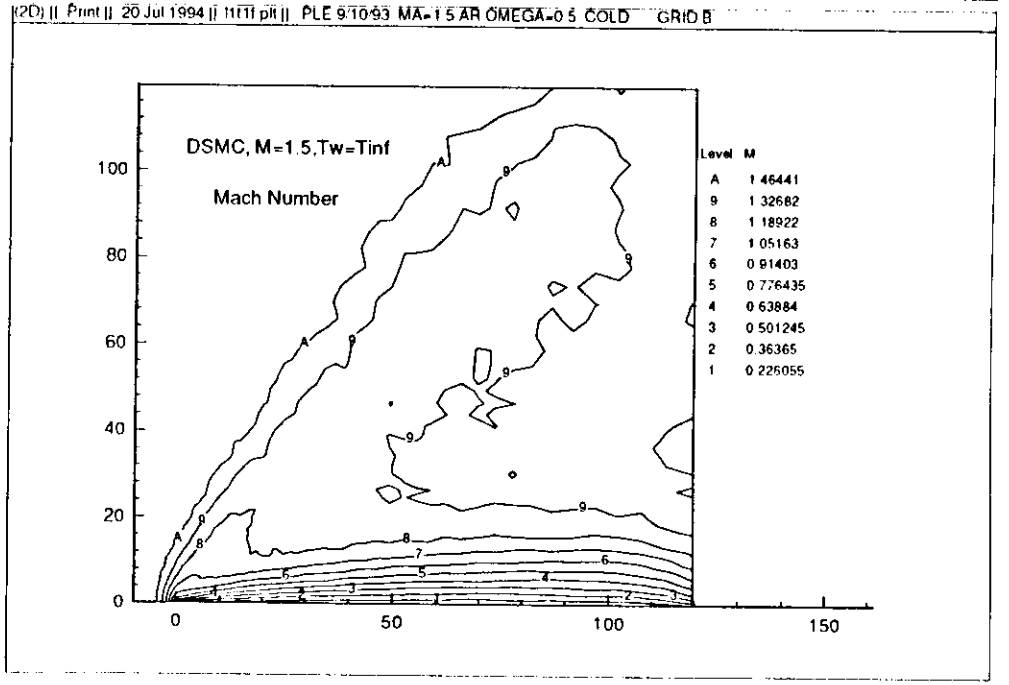
(2D) || Print || 20 Jul 1994 || 1111 plt || PLE 9/10/93 MA=1.5 AR OMEGA=0.5 COLD GRID B
DSMC, M=1.5,Tw=Tinf
Mach Number
Level M
A 1.46441
9 1.32682
8 1.18922
7 1.05163
6 0.91403
5 0.776435
4 0.63884
3 0.501245
2 0.36365
1 0.226055
0
20
40
60
80
100
0
50
100
150

Fig.55

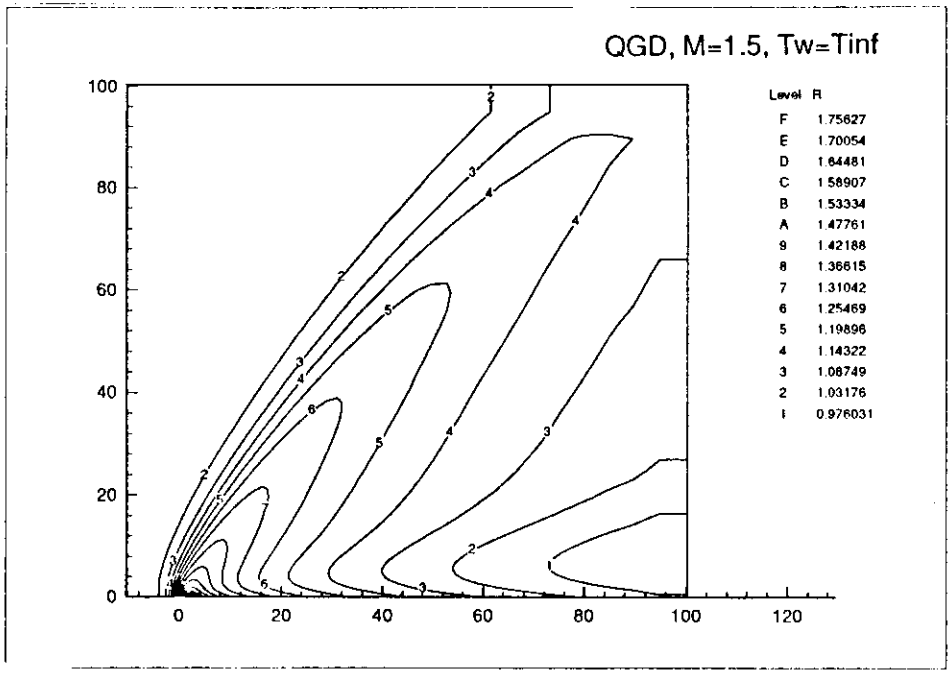
QGD, M=1.5, Tw=Tinf
Level R
F 1.75627
E 1.70054
D 1.64481
C 1.58907
B 1.53334
A 1.47761
9 1.42188
8 1.36615
7 1.31042
6 1.25469
5 1.19896
4 1.14322
3 1.08749
2 1.03176
1 0.976031

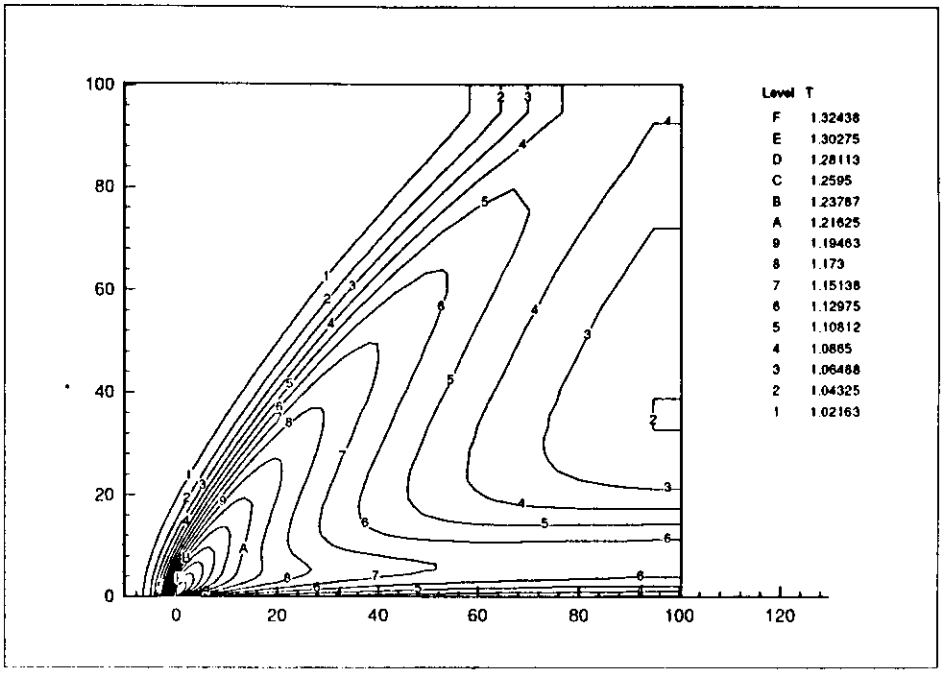
Level T
F 1.32438
E 1.30275
D 1.28113
C 1.2595
B 1.23787
A 1.21625
9 1.19463
8 1.173
7 1.15138
6 1.12975
5 1.10812
4 1.0865
3 1.06488
2 1.04325
1 1.02163

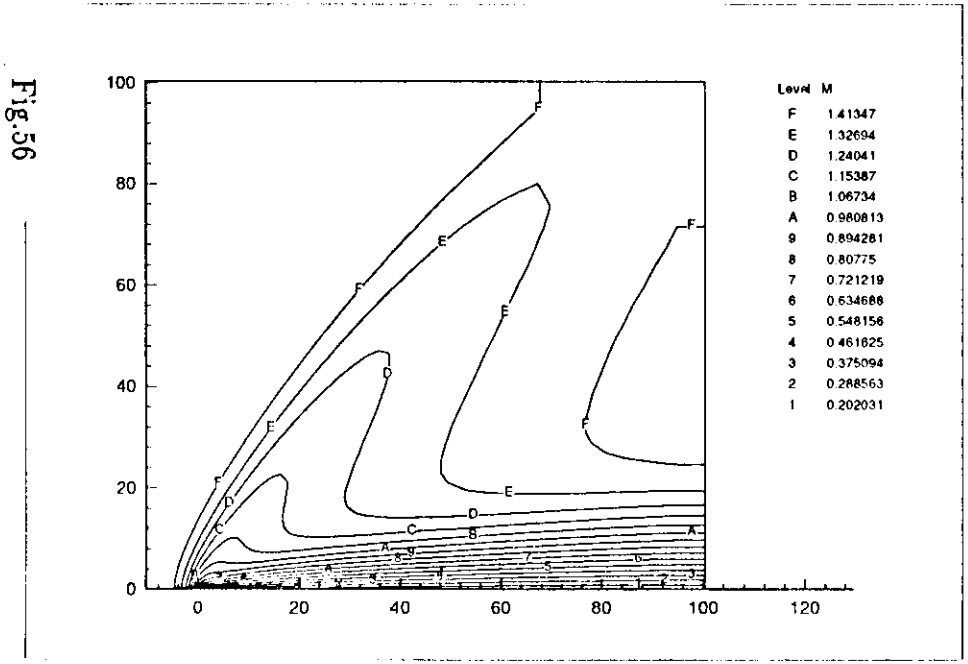
Level M
F 1.41347
E 1.32694
D 1.24041
C 1.15387
B 1.06734
A 0.980813
9 0.894281
8 0.80775
7 0.721219
6 0.634688
5 0.548156
4 0.461625
3 0.375094
2 0.288563
1 0.202031

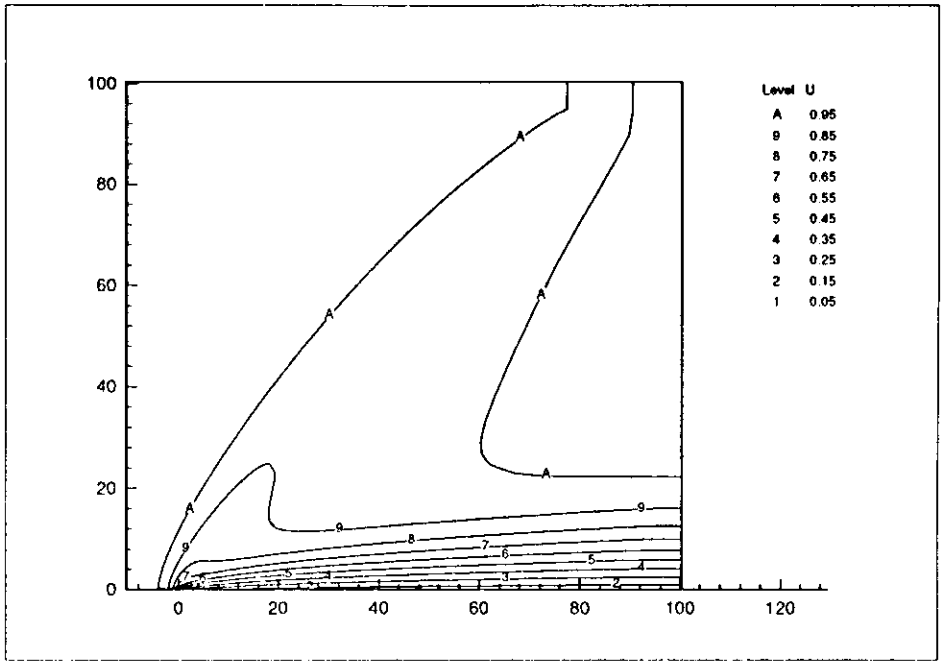
Level U
A 0.95
9 0.85
8 0.75
7 0.65
6 0.55
5 0.45
4 0.35
3 0.25
2 0.15
1 0.05

Fig.56

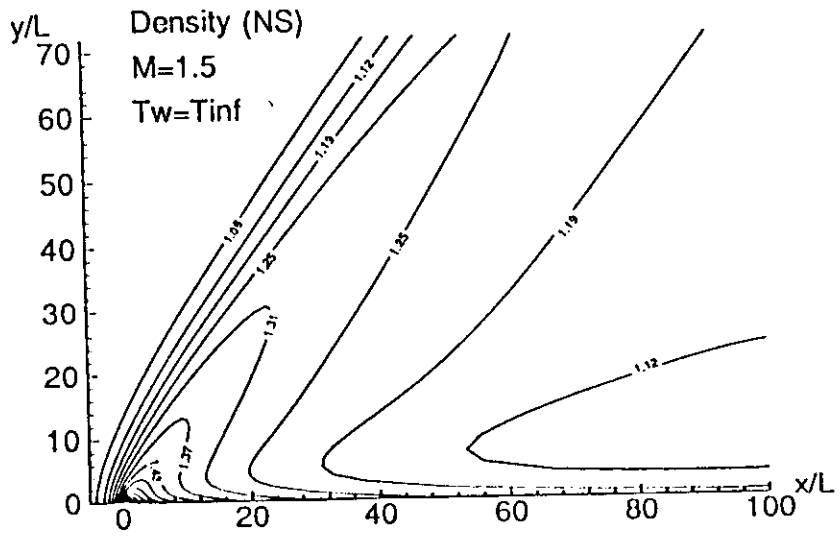
Density (NS)
M=1.5
Tw=Tinf
y/L
x/L
0
10
20
30
40
50
60
70
0
20
40
60
80
100

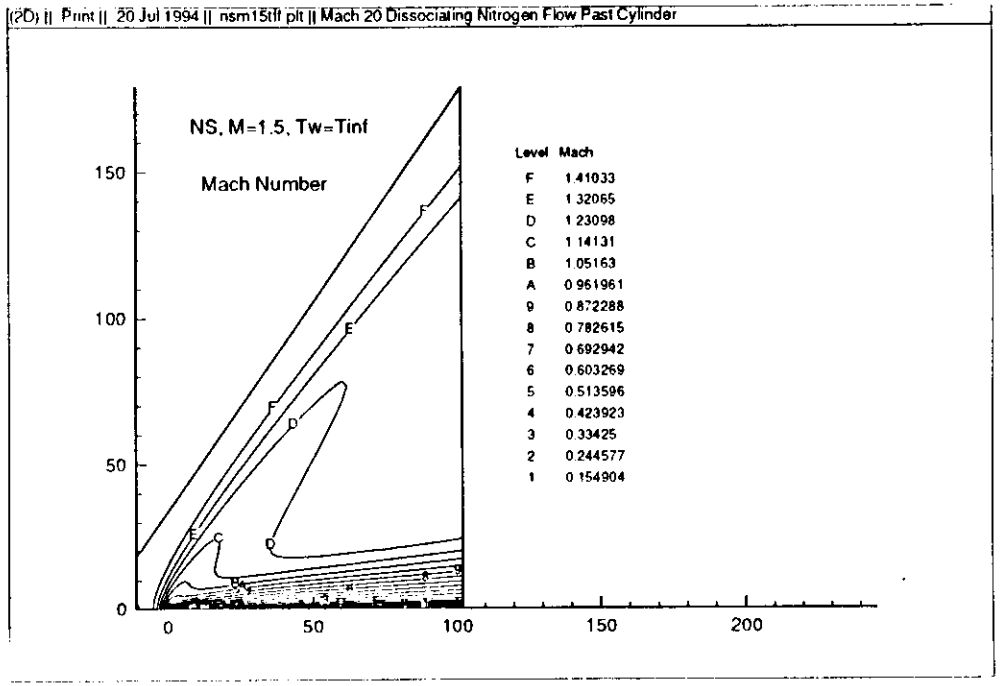
(2D) || Print || 20 Jul 1994 || nsm15tlf plt || Mach 20 Dissociating Nitrogen Flow Past Cylinder
NS, M=1.5, Tw=Tinf
Mach Number
Level Mach
F 1.41033
E 1.32065
D 1.23098
C 1.14131
B 1.05163
A 0.961961
9 0.872288
8 0.782615
7 0.692942
6 0.603269
5 0.513596
4 0.423923
3 0.33425
2 0.244577
1 0.154904
0
50
100
150
200

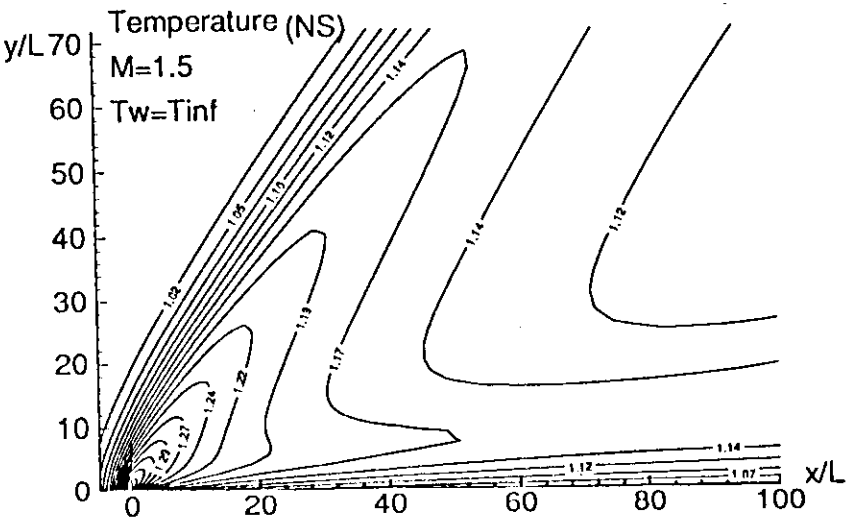
Temperature (NS)
M=1.5
Tw=Tinf
y/L
x/L
0
10
20
30
40
50
60
70
0
20
40
60
80
100

Fig.57

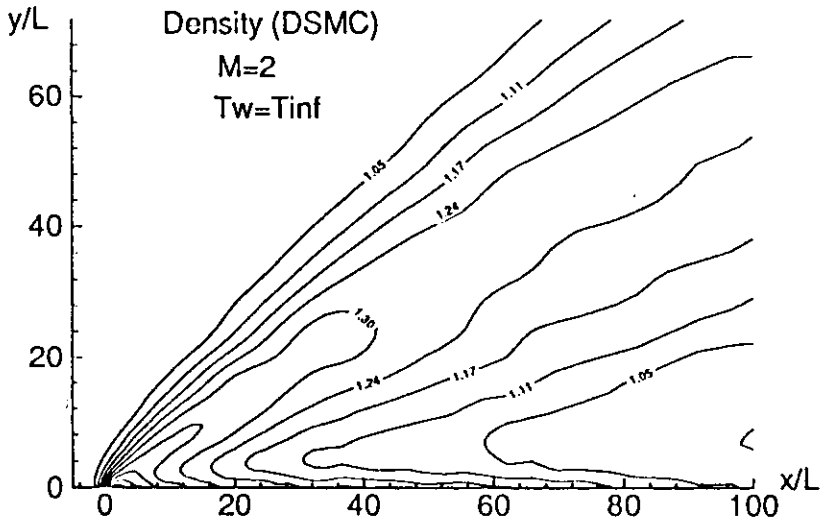
Density (DSMC)
M=2
Tw=Tinf
y/L
x/L
0
20
40
60
80
100
1.05
1.11
1.17
1.24
1.30

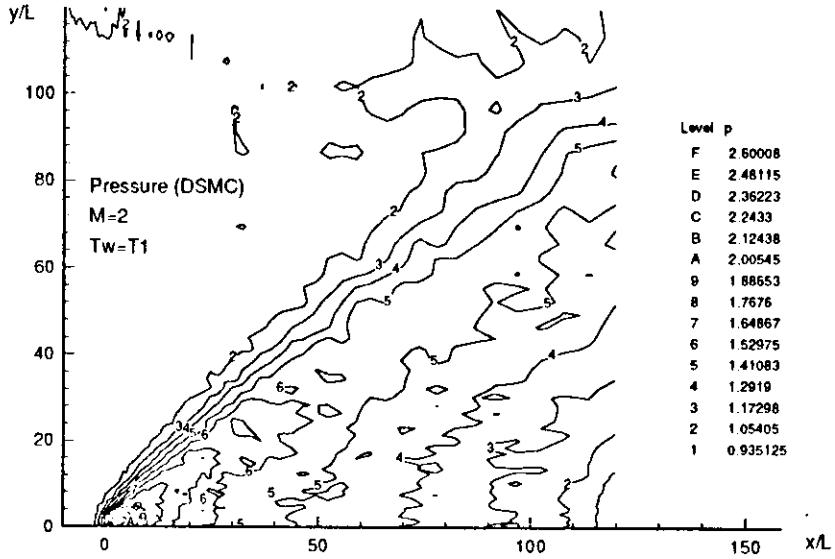
Pressure (DSMC)
M=2
Tw=T1
y/L
x/L
Level p
F 2.60008
E 2.48115
D 2.36223
C 2.2433
B 2.12438
A 2.00545
9 1.88653
8 1.7676
7 1.64867
6 1.52975
5 1.41083
4 1.2919
3 1.17298
2 1.05405
1 0.935125

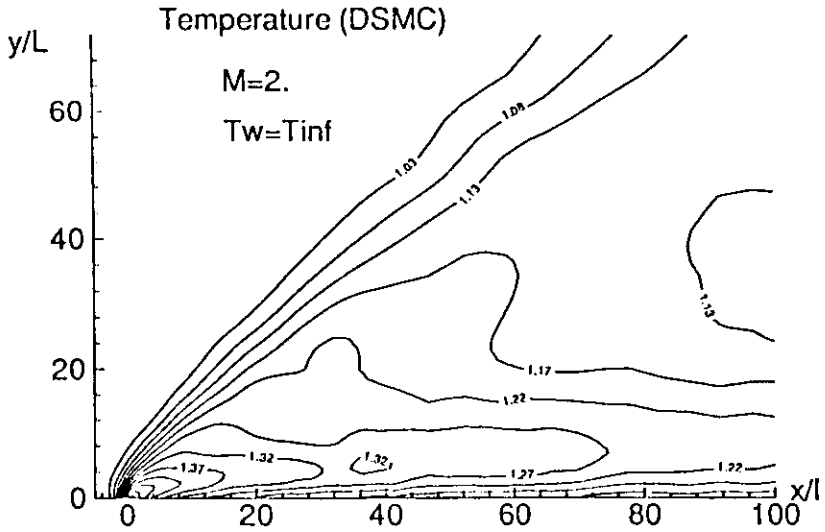
Temperature (DSMC)
M=2.
Tw=Tinf
y/L
x/l
1.03
1.08
1.13
1.17
1.22
1.27
1.32
1.37

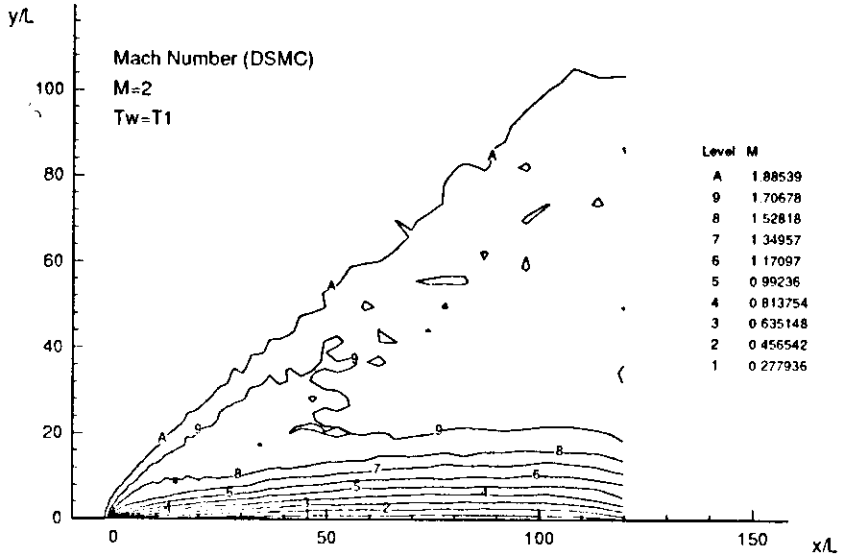
Mach Number (DSMC)
M=2
Tw=T1
y/L
x/L
Level M
A 1.88539
9 1.70678
8 1.52818
7 1.34957
6 1.17097
5 0.99236
4 0.813754
3 0.635148
2 0.456542
1 0.277936

Fig.58

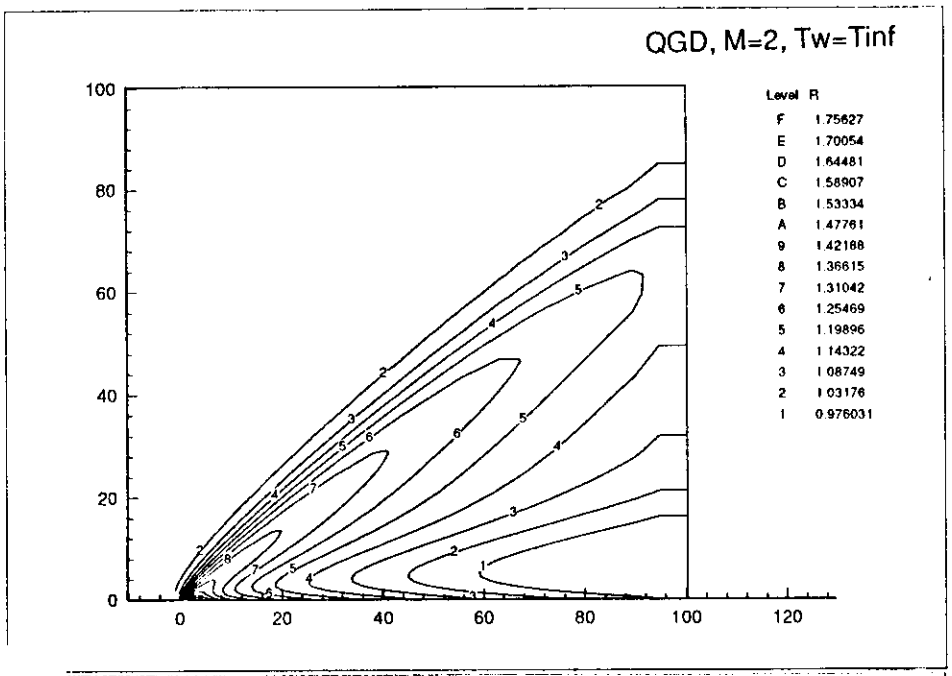
QGD, M=2, Tw=Tinf
Level R
F 1.75627
E 1.70054
D 1.64481
C 1.58907
B 1.53334
A 1.47761
9 1.42188
8 1.36615
7 1.31042
6 1.25469
5 1.19896
4 1.14322
3 1.08749
2 1.03176
1 0.976031

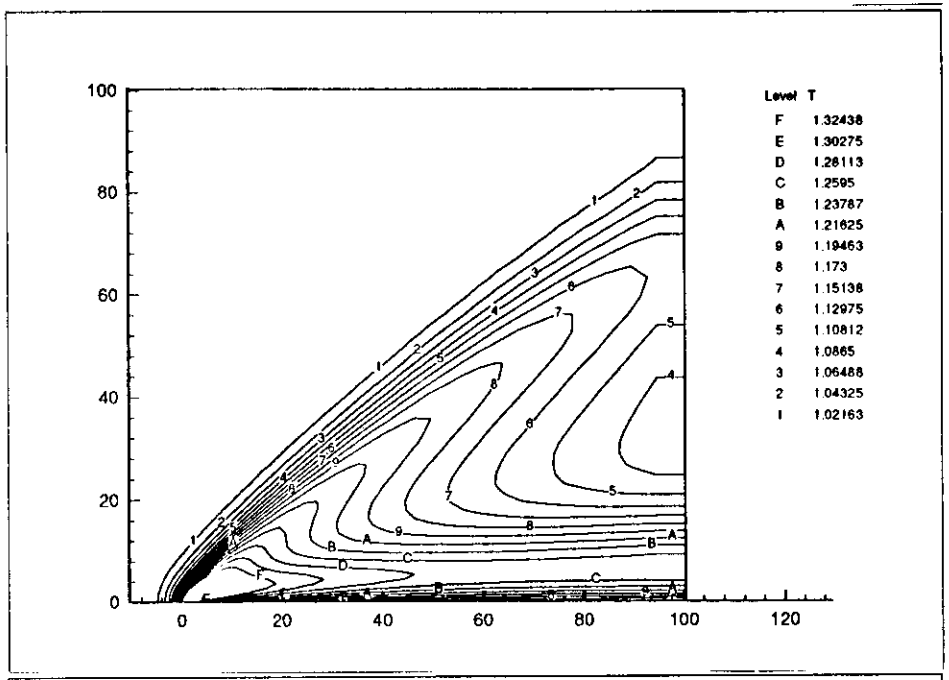
Level T
F 1.32438
E 1.30275
D 1.28113
C 1.2595
B 1.23787
A 1.21625
9 1.19463
8 1.173
7 1.15138
6 1.12975
5 1.10812
4 1.0865
3 1.06488
2 1.04325
1 1.02163

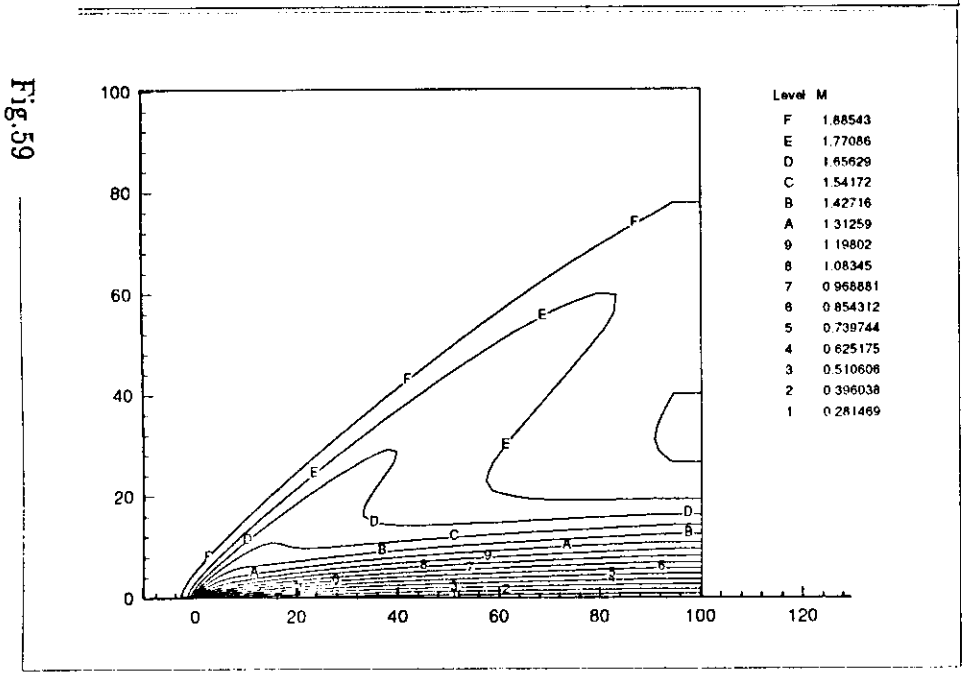
Level M
F 1.88543
E 1.77086
D 1.65629
C 1.54172
B 1.42716
A 1.31259
9 1.19802
8 1.08345
7 0.968881
6 0.854312
5 0.739744
4 0.625175
3 0.510606
2 0.396038
1 0.281469

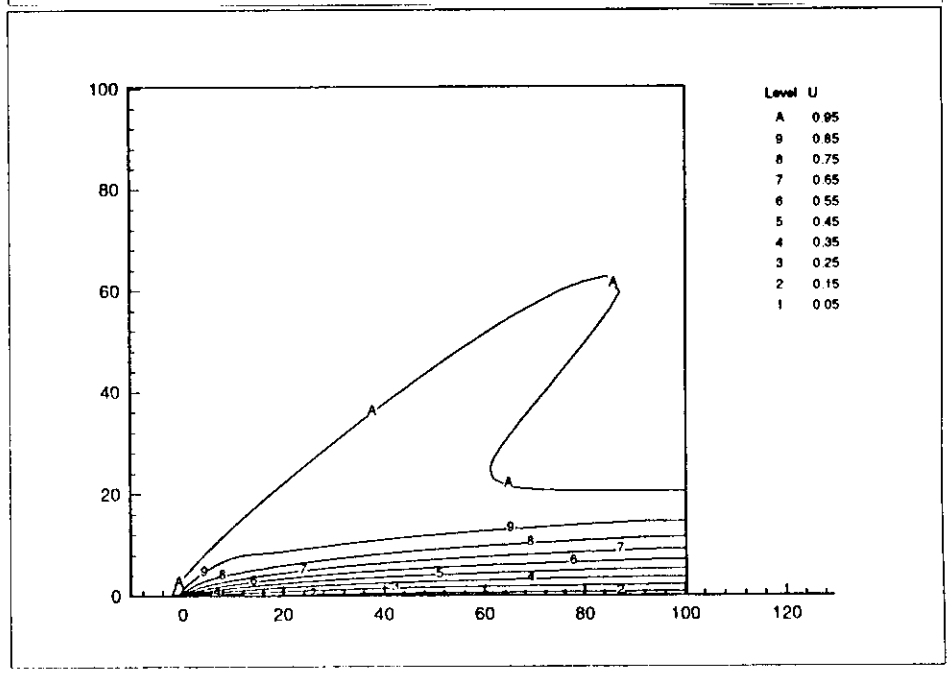
Level U
A 0.95
9 0.85
8 0.75
7 0.65
6 0.55
5 0.45
4 0.35
3 0.25
2 0.15
1 0.05

Fig.59

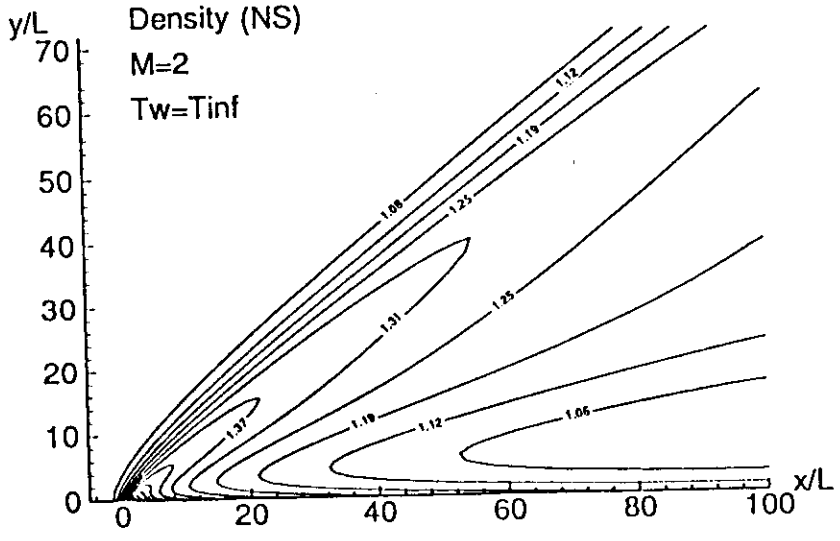
Density (NS)
M=2
Tw=Tinf
y/L
x/L
70
60
50
40
30
20
10
0
0
20
40
60
80
100

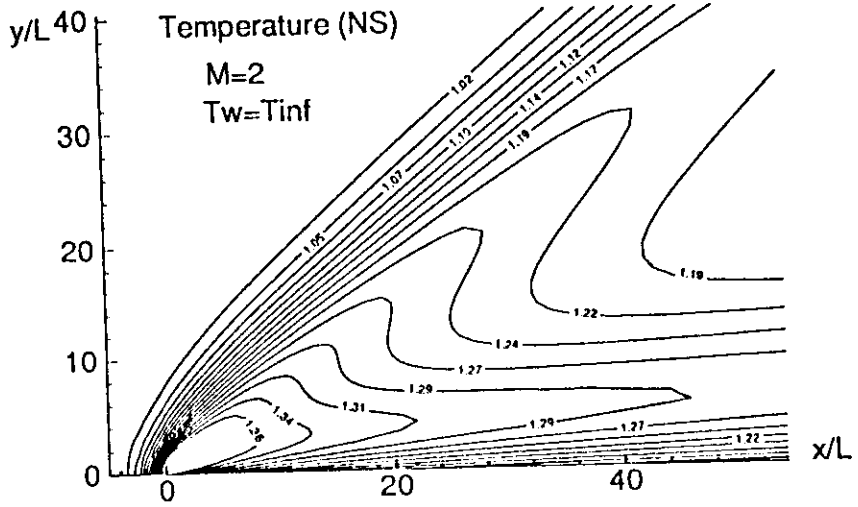
Temperature (NS)
M=2
Tw=Tinf
y/L
x/L
40
30
20
10
0
0
20
40

Fig.60

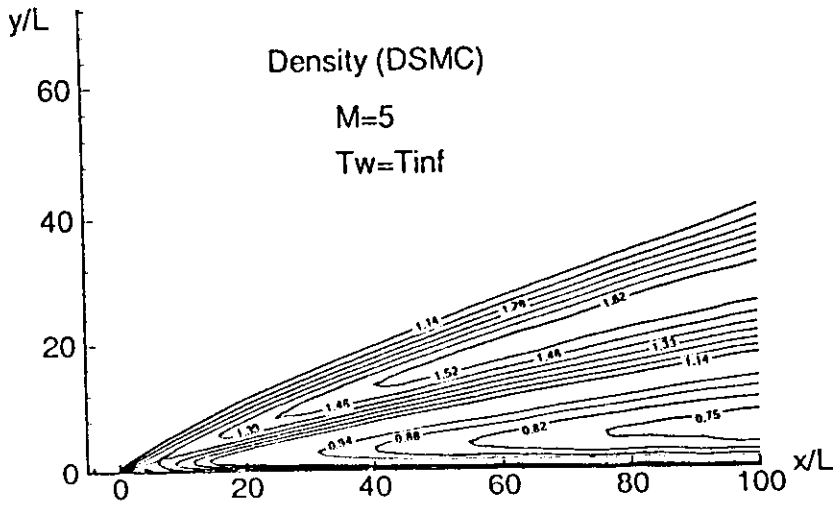
Density (DSMC)
M=5
Tw=Tinf
y/L
x/L
0
20
40
60
80
100

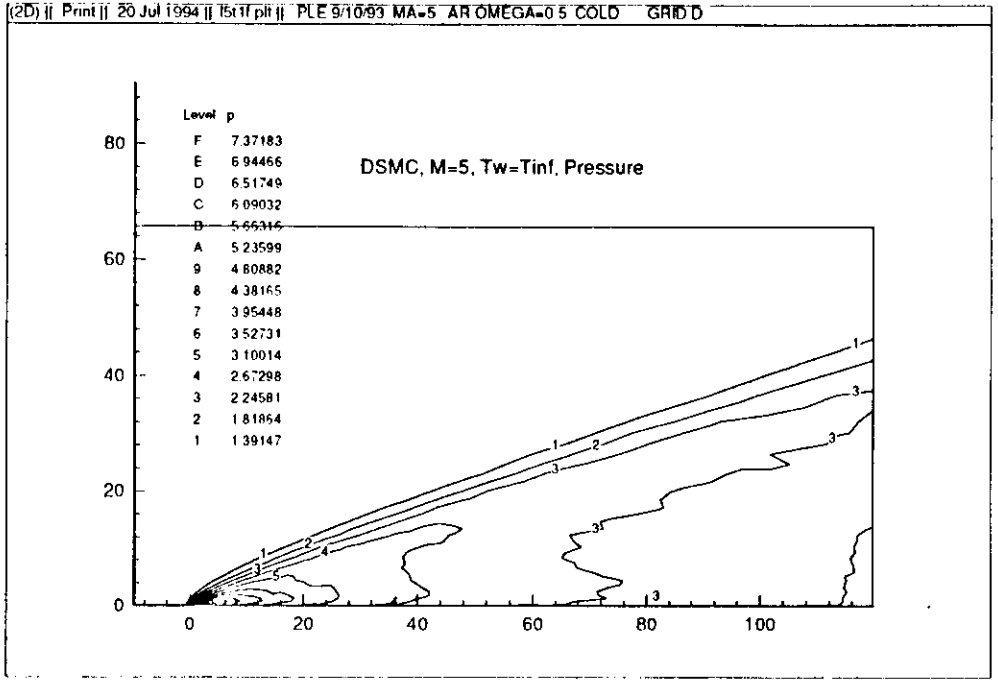
(2D) || Print || 20 Jul 1994 || l5t1f.plt || PLE 9/10/93 MA=5 AR OMEGA=0 5 COLD GRID D
Level p
F 7.37183
E 6.94466
D 6.51749
C 6.09032
B 5.66315
A 5.23599
9 4.80882
8 4.38165
7 3.95448
6 3.52731
5 3.10014
4 2.67298
3 2.24581
2 1.81864
1 1.39147
DSMC, M=5, Tw=Tinf, Pressure

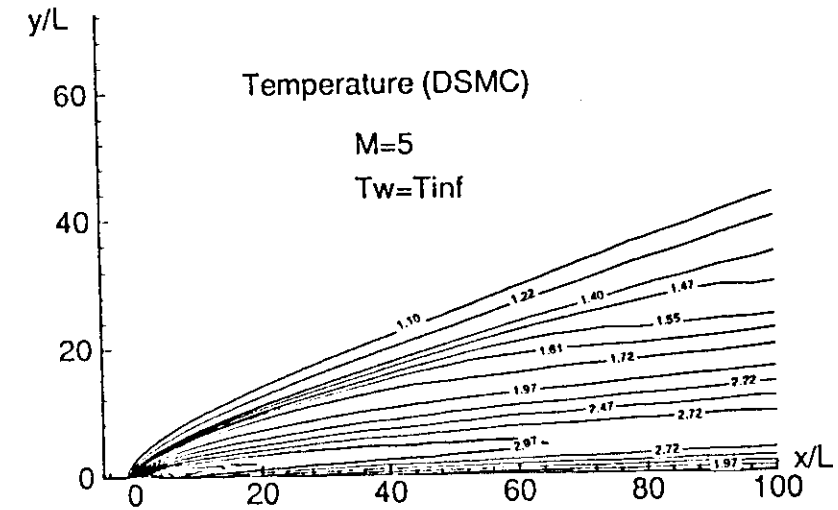
Temperature (DSMC)
M=5
Tw=Tinf
y/L
x/L
0
20
40
60
80
100

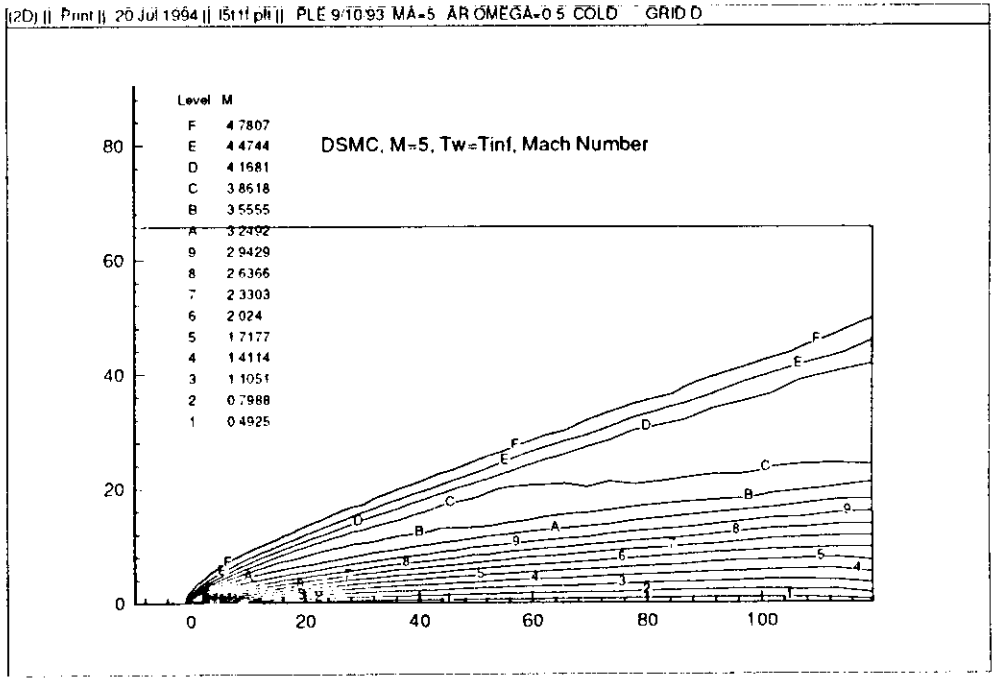
(2D) || Print || 20 Jul 1994 || l5t1f.plt || PLE 9/10/93 MA=5 AR OMEGA=0 5 COLD GRID D
Level M
F 4.7807
E 4.4744
D 4.1681
C 3.8618
B 3.5555
A 3.2492
9 2.9429
8 2.6366
7 2.3303
6 2.024
5 1.7177
4 1.4114
3 1.1051
2 0.7988
1 0.4925
DSMC, M=5, Tw=Tinf, Mach Number

Fig.61

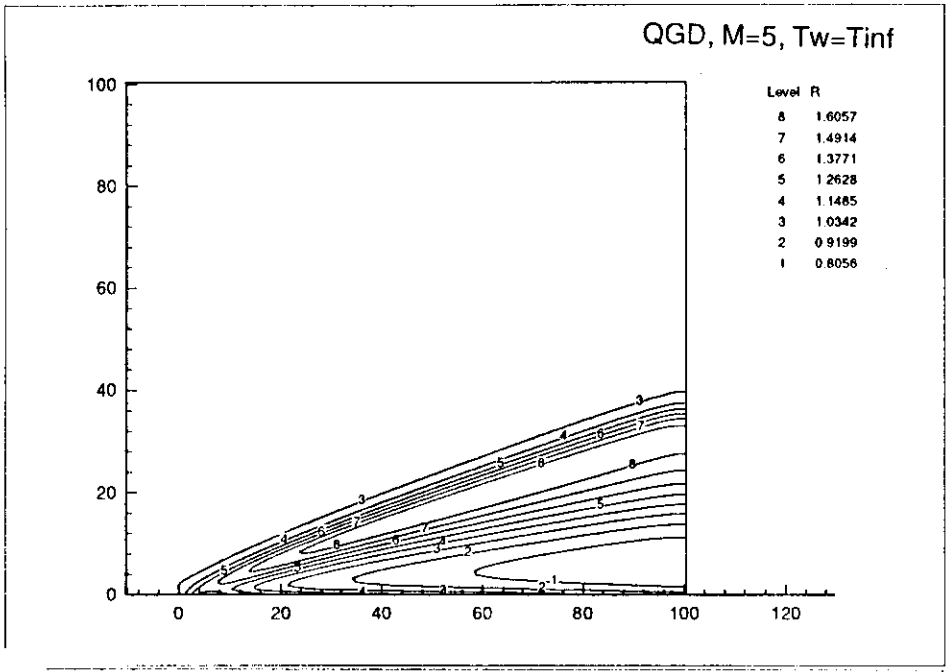
QGD, M=5, Tw=Tinf
Level R
8 1.6057
7 1.4914
6 1.3771
5 1.2628
4 1.1485
3 1.0342
2 0.9199
1 0.8056

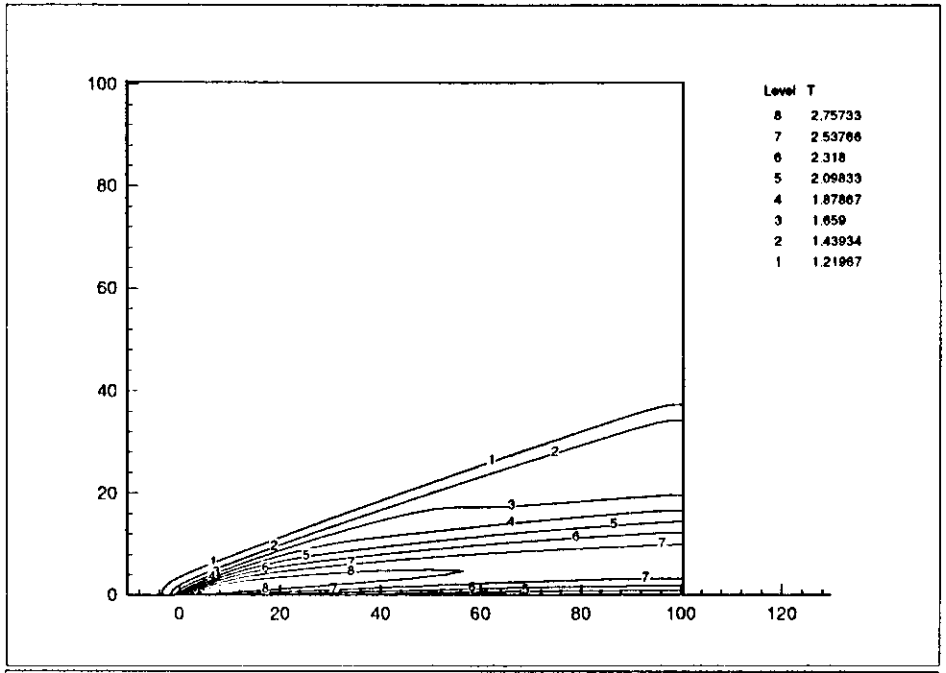
Level T
8 2.75733
7 2.53766
6 2.318
5 2.09833
4 1.87867
3 1.659
2 1.43934
1 1.21967

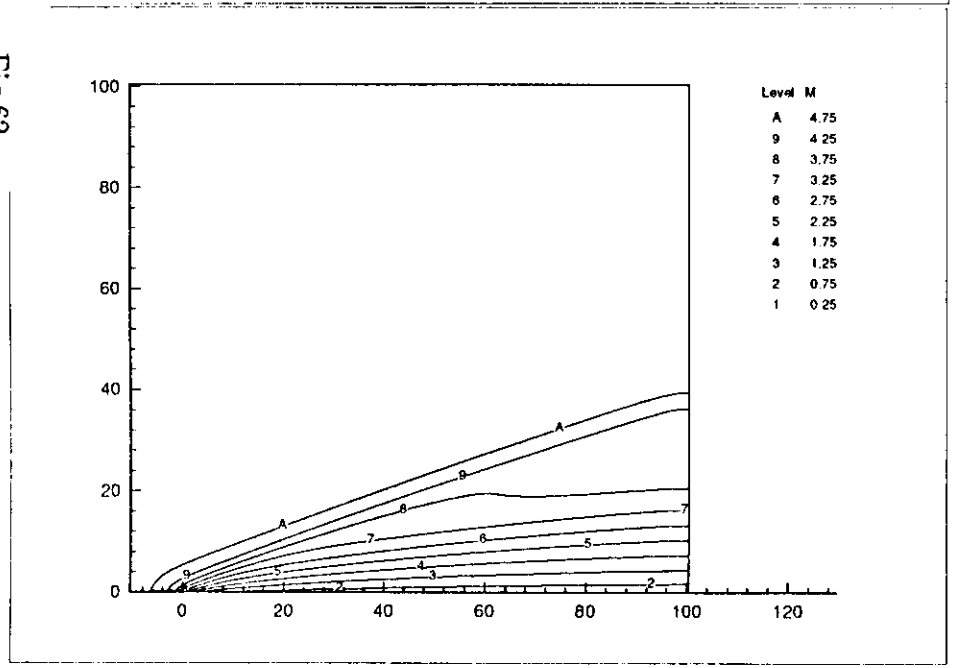
Level M
A 4.75
9 4.25
8 3.75
7 3.25
6 2.75
5 2.25
4 1.75
3 1.25
2 0.75
1 0.25

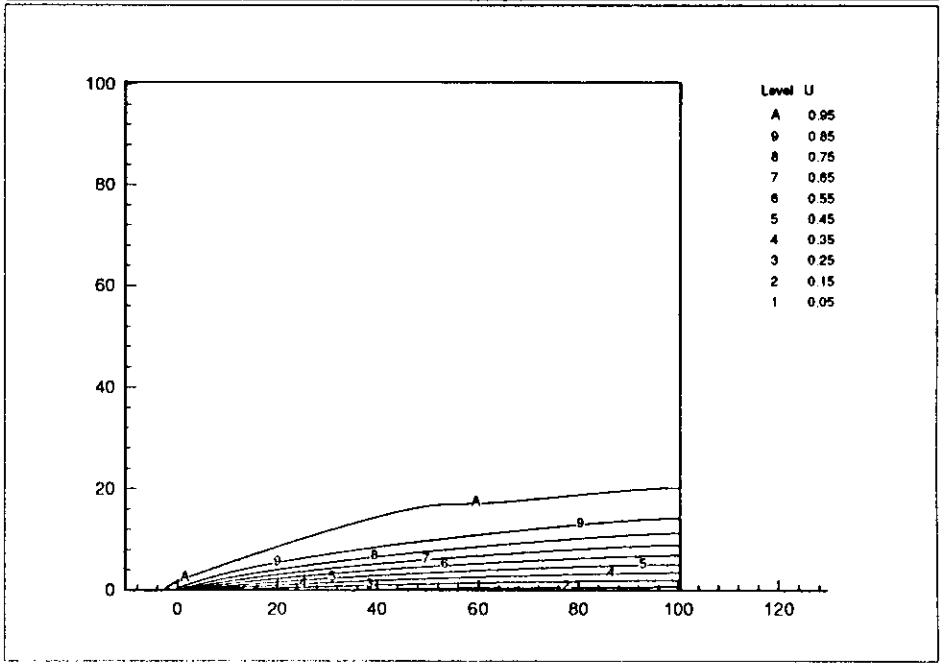
Level U
A 0.95
9 0.85
8 0.75
7 0.65
6 0.55
5 0.45
4 0.35
3 0.25
2 0.15
1 0.05

Fig.62

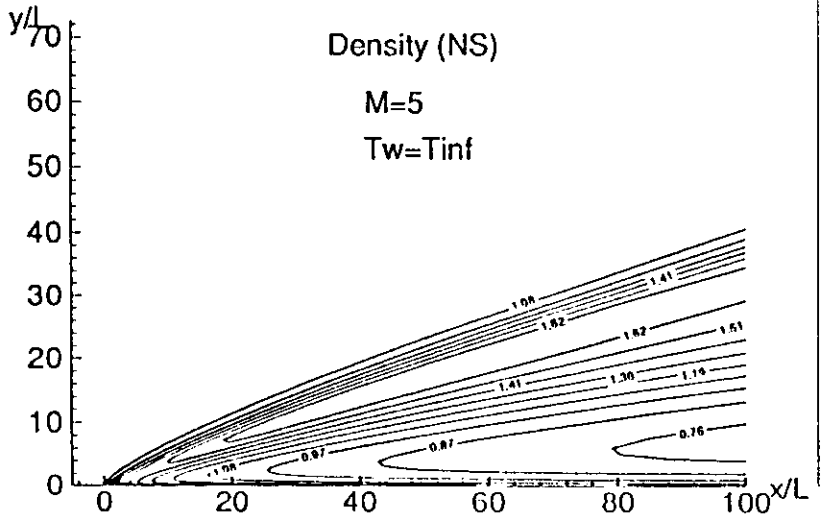
Density (NS)
M=5
Tw=Tinf
y/L
x/L
0
10
20
30
40
50
60
70
0
20
40
60
80
100

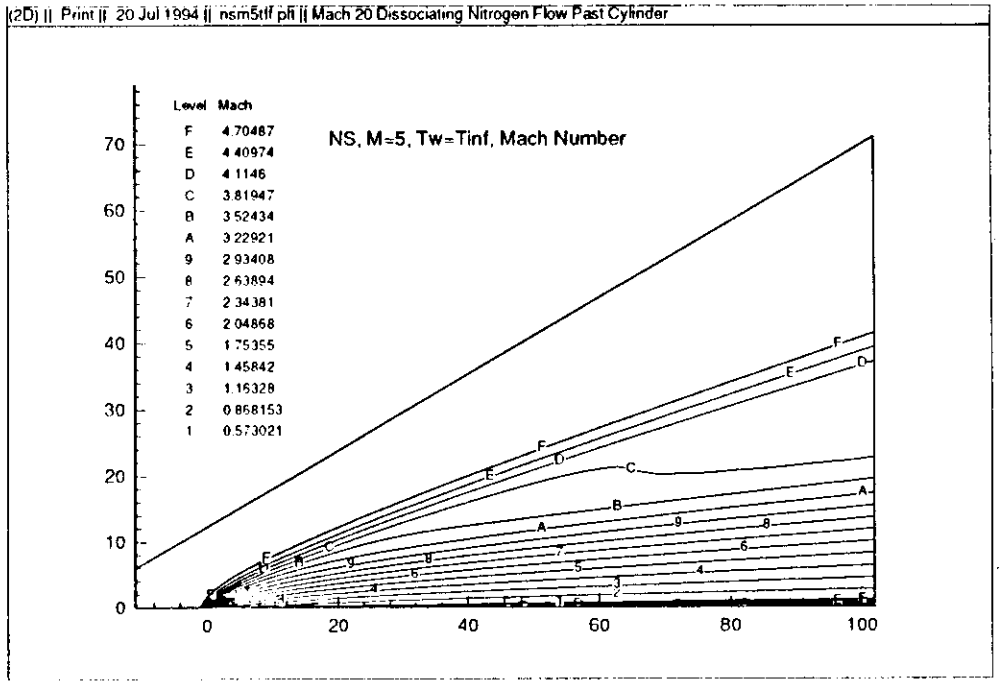
(2D) || Print || 20 Jul 1994 || nsm5tlf.plt || Mach 20 Dissociating Nitrogen Flow Past Cylinder
NS, M=5, Tw=Tinf, Mach Number
Level Mach
F 4.70487
E 4.40974
D 4.1146
C 3.81947
B 3.52434
A 3.22921
9 2.93408
8 2.63894
7 2.34381
6 2.04868
5 1.75355
4 1.45842
3 1.16328
2 0.868153
1 0.573021

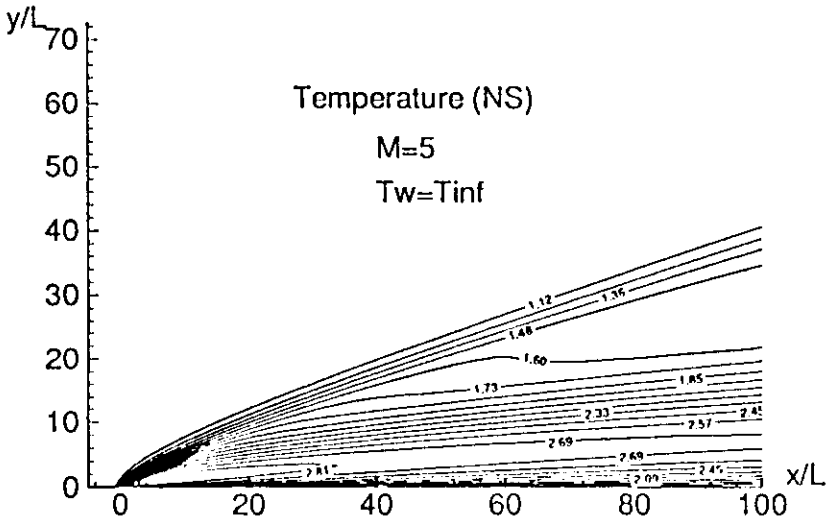
Temperature (NS)
M=5
Tw=Tinf
y/L
x/L
0
10
20
30
40
50
60
70
0
20
40
60
80
100

Fig.63

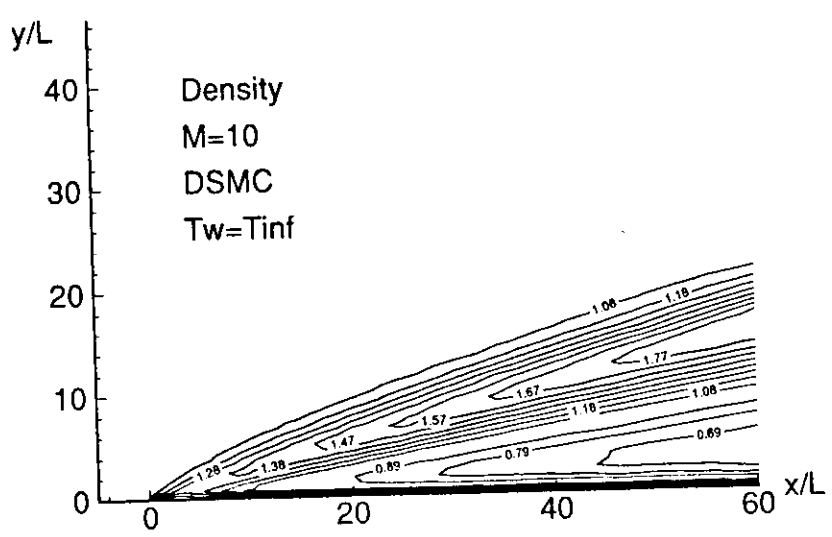
y/L
40
30
20
10
0
Density
M=10
DSMC
Tw=Tinf
1.08
1.18
1.77
1.67
1.57
1.18
1.08
0.69
0.79
0.89
1.28
1.38
1.47
0
20
40
60
x/L

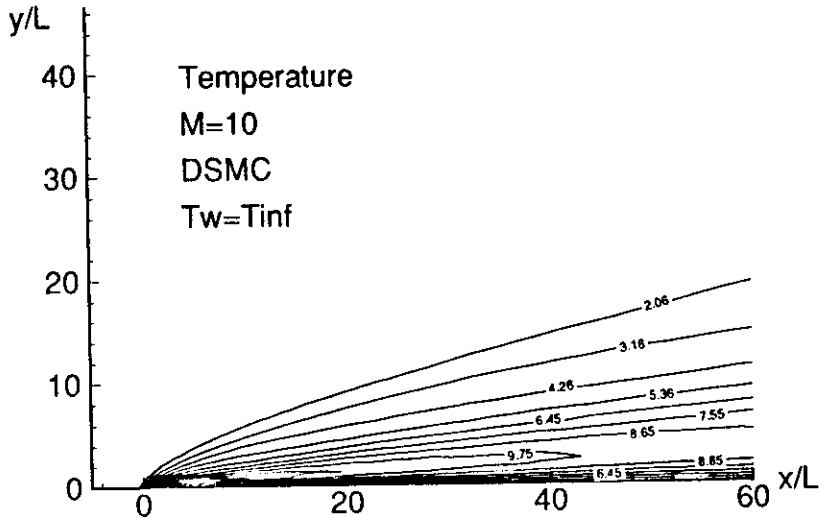
y/L
40
30
20
10
0
Temperature
M=10
DSMC
Tw=Tinf
2.06
3.16
4.26
5.36
6.45
7.55
8.65
9.75
8.85
6.45
0
20
40
60
x/L

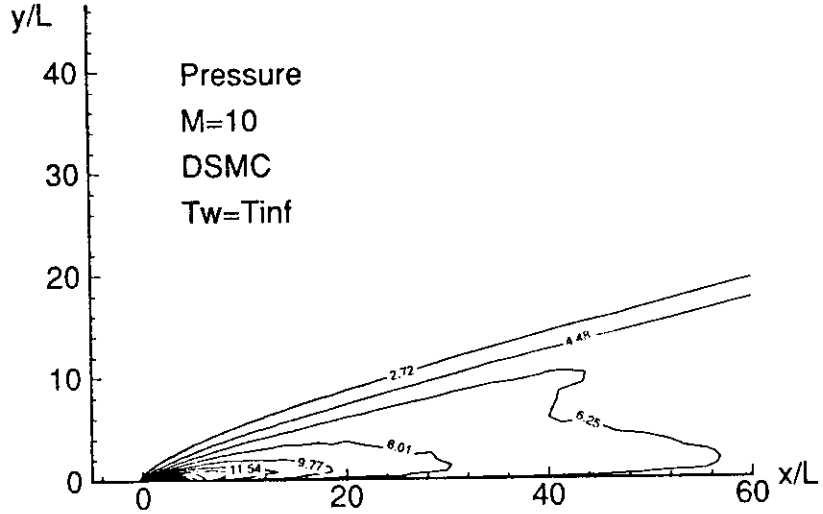
y/L
40
30
20
10
0
Pressure
M=10
DSMC
Tw=Tinf
8.48
2.72
6.25
8.01
9.77
11.54
0
20
40
60
x/L

Fig.64

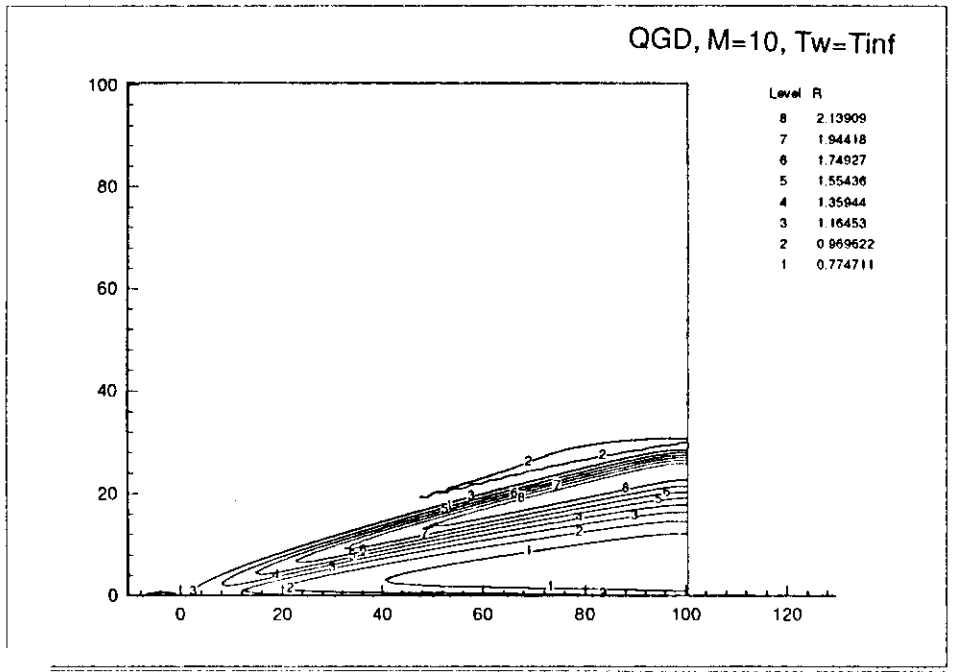

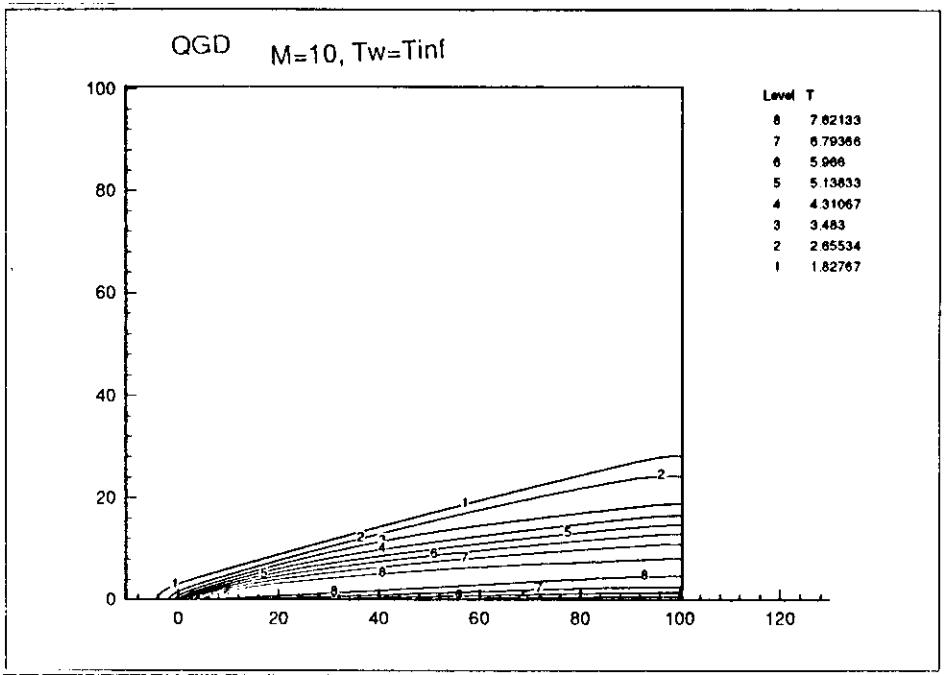

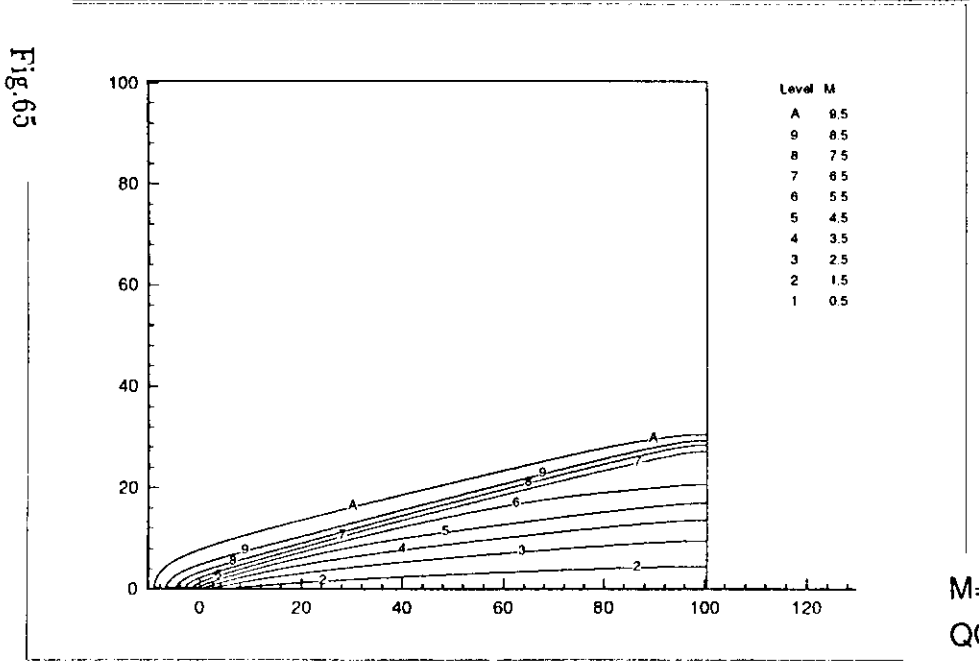

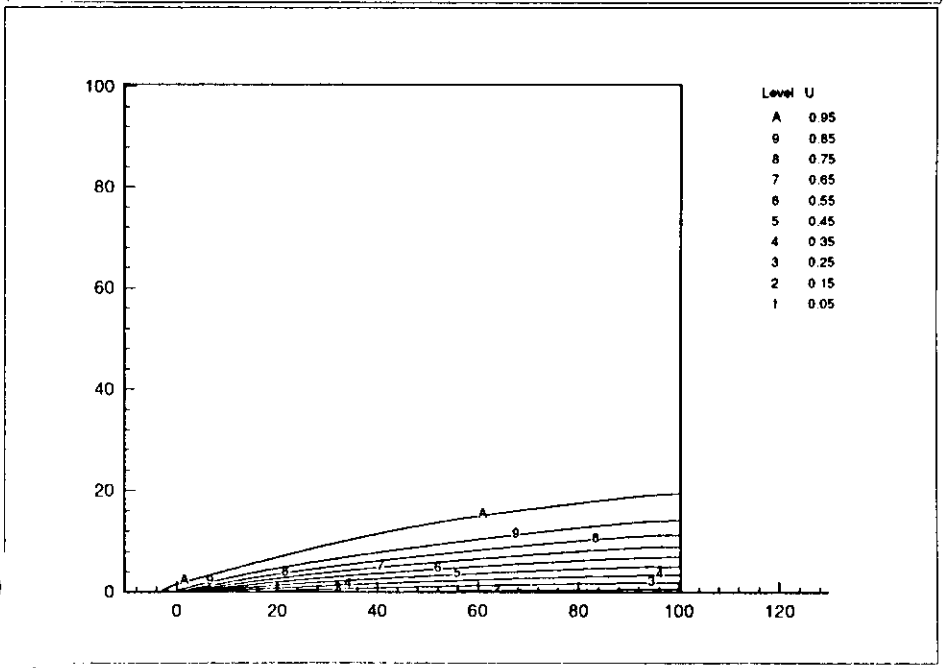

Fig.65

M=10
QGD
Tw=Tinf

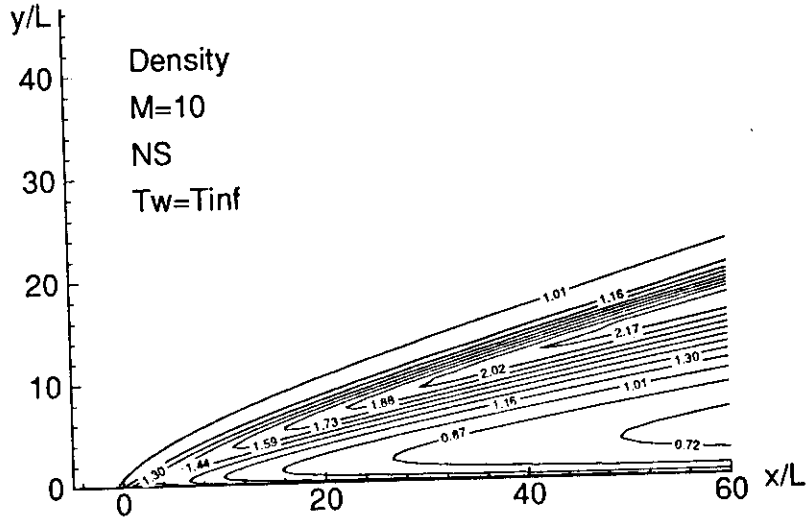
y/L
Density
M=10
NS
Tw=Tinf
x/L
0
20
40
60
10
30
1.01
1.16
2.17
2.02
1.30
1.88
1.73
1.59
1.44
1.30
0.87
0.72

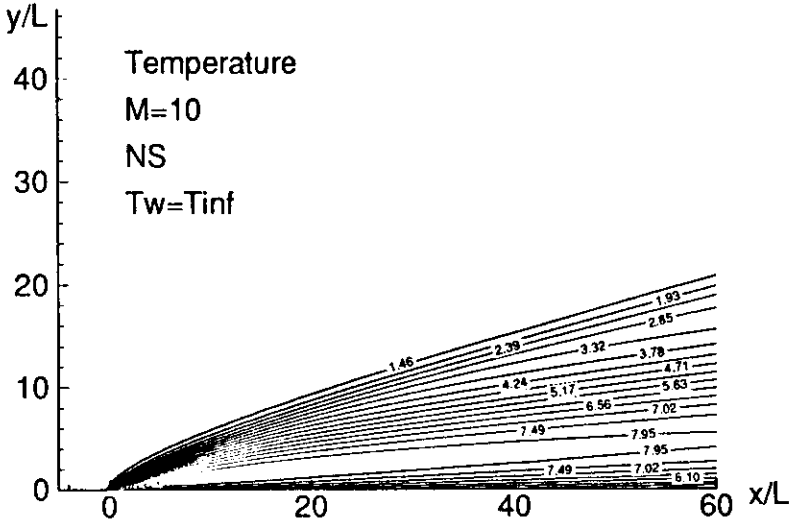
y/L
Temperature
M=10
NS
Tw=Tinf
x/L
0
20
40
60
10
30
1.93
2.85
2.39
3.32
3.78
4.71
5.63
7.02
7.95
6.10

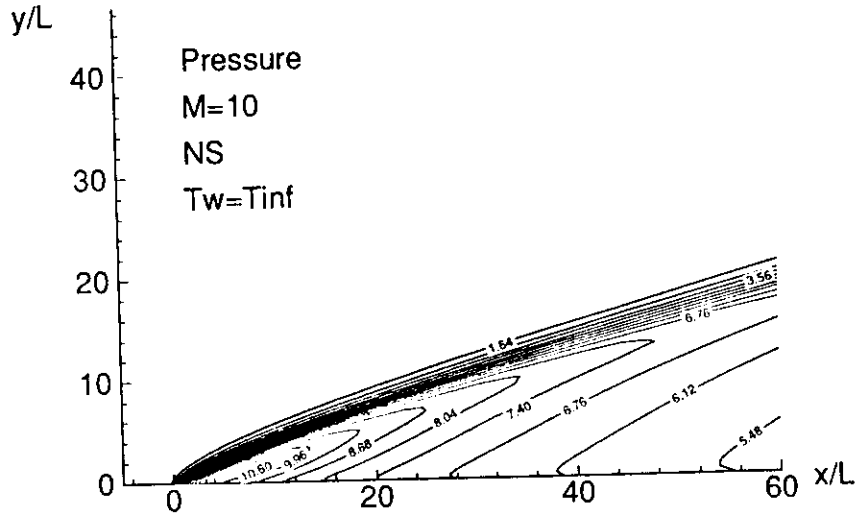
y/L
Pressure
M=10
NS
Tw=Tinf
x/L
0
20
40
60
10
30
1.64
6.76
8.04
7.40
6.76
6.12
5.48
8.88
9.96
10.60

Fig.66

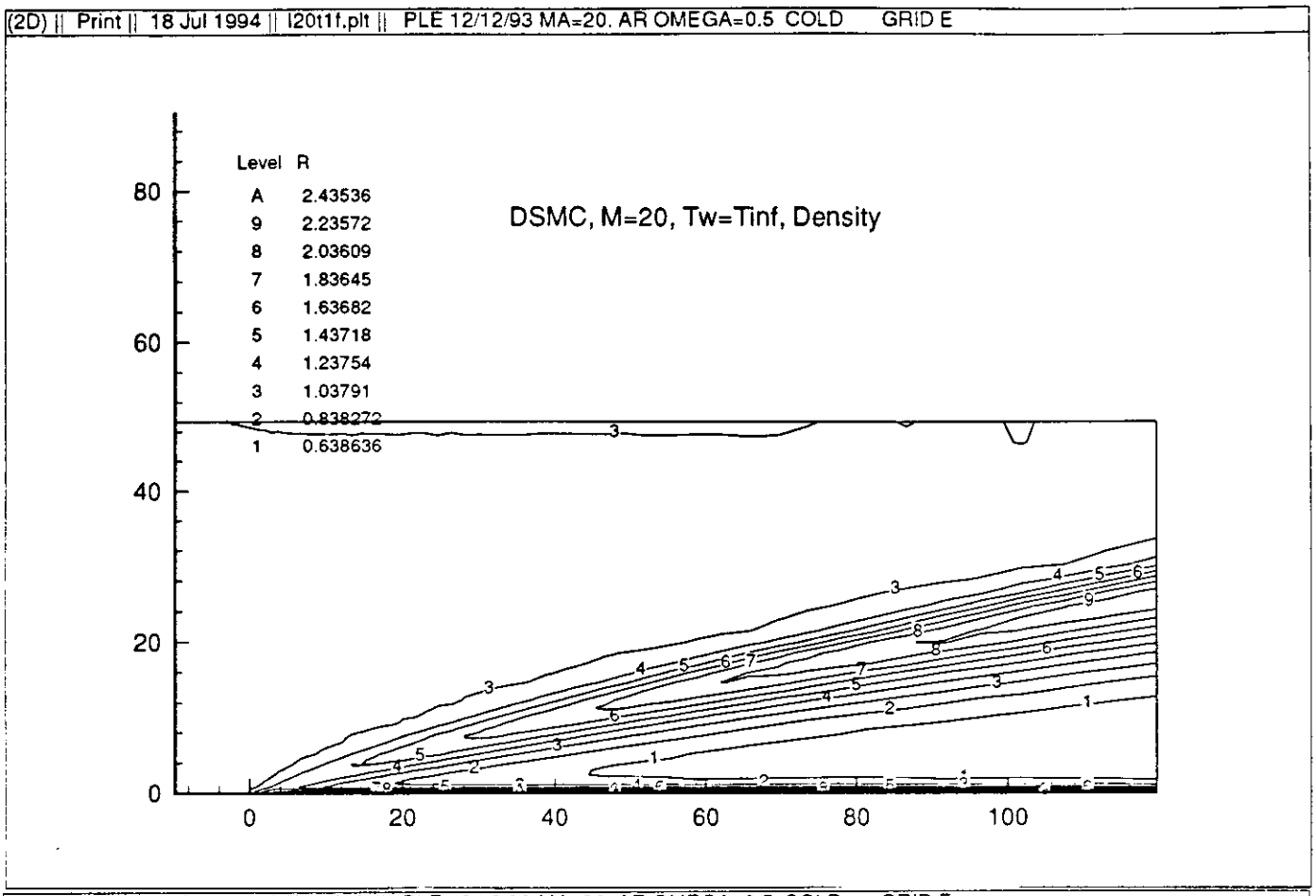
(2D) || Print || 18 Jul 1994 || I20t1f.plt || PLE 12/12/93 MA=20. AR OMEGA=0.5 COLD GRID E
Level R
A 2.43536
9 2.23572
8 2.03609
7 1.83645
6 1.63682
5 1.43718
4 1.23754
3 1.03791
2 0.838272
1 0.638636
DSMC, M=20, Tw=Tinf, Density
0
20
40
60
80
0
20
40
60
80
100

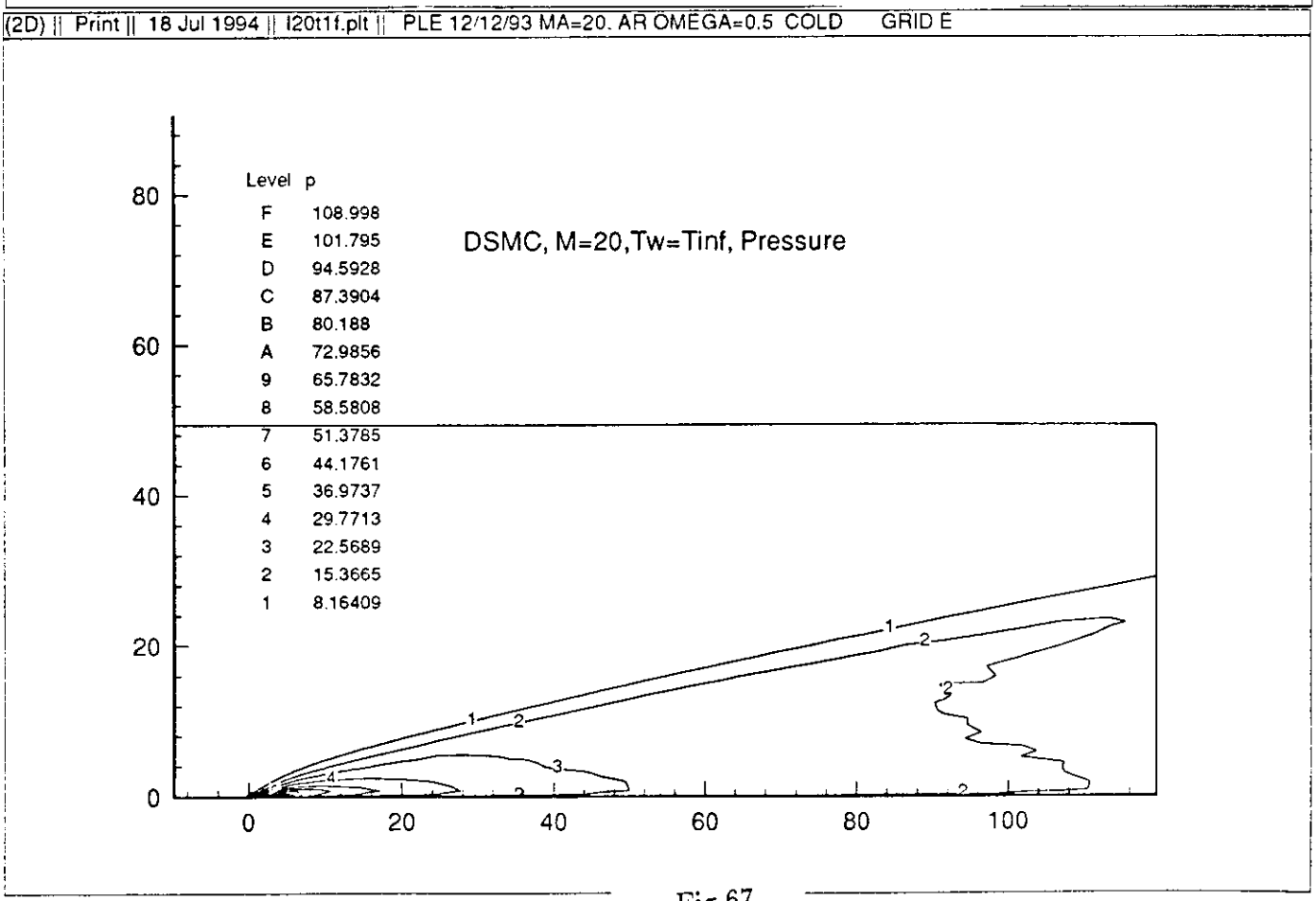
(2D) || Print || 18 Jul 1994 || I20t1f.plt || PLE 12/12/93 MA=20. AR OMEGA=0.5 COLD GRID E
Level p
F 108.998
E 101.795
D 94.5928
C 87.3904
B 80.188
A 72.9856
9 65.7832
8 58.5808
7 51.3785
6 44.1761
5 36.9737
4 29.7713
3 22.5689
2 15.3665
1 8.16409
DSMC, M=20,Tw=Tinf, Pressure
0
20
40
60
80
0
20
40
60
80
100

Fig.67

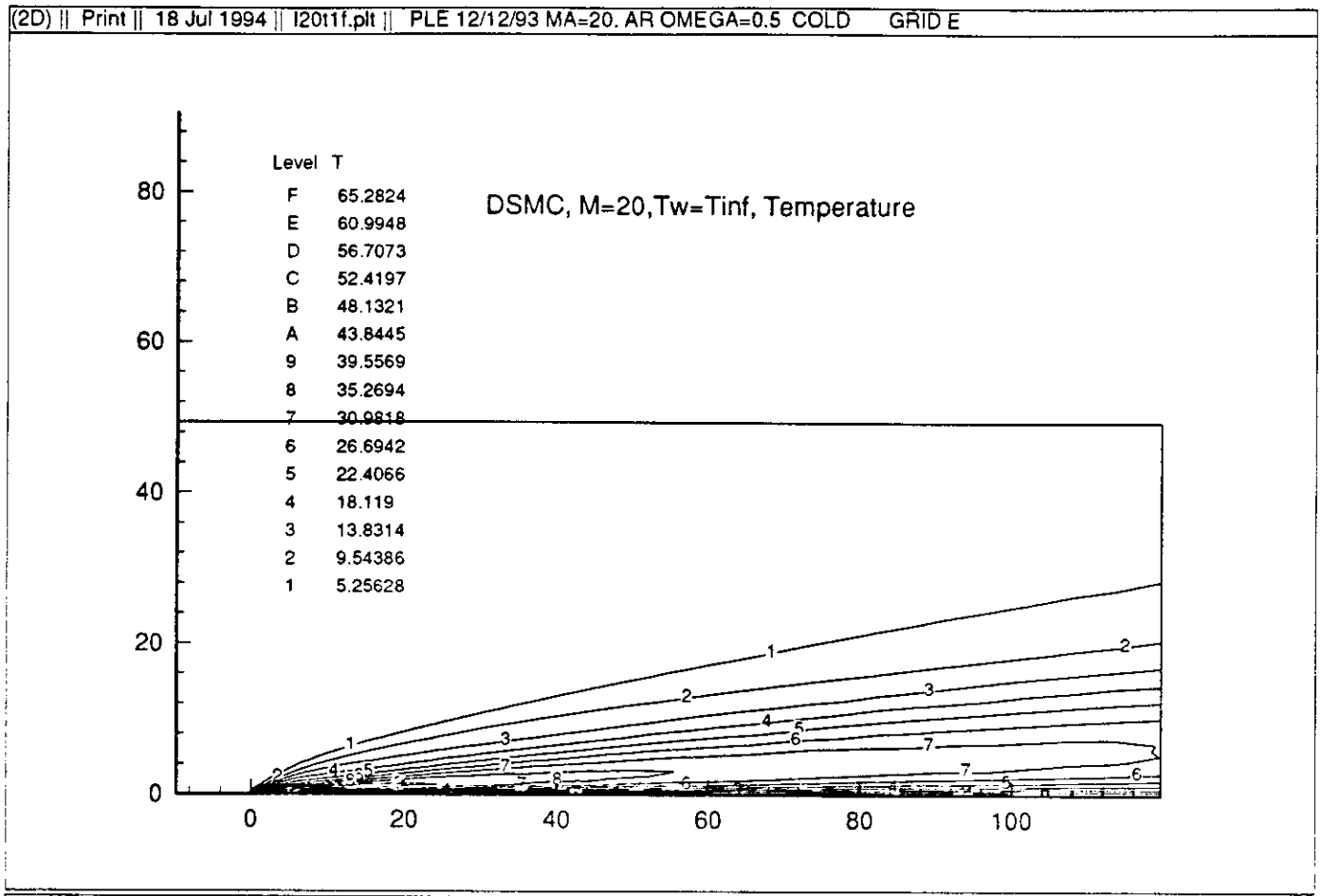
(2D) || Print || 18 Jul 1994 || I2011f.plt || PLE 12/12/93 MA=20. AR OMEGA=0.5 COLD GRID E
Level T
F 65.2824
E 60.9948
D 56.7073
C 52.4197
B 48.1321
A 43.8445
9 39.5569
8 35.2694
7 30.9818
6 26.6942
5 22.4066
4 18.119
3 13.8314
2 9.54386
1 5.25628
DSMC, M=20,Tw=Tinf, Temperature
0
20
40
60
80
100

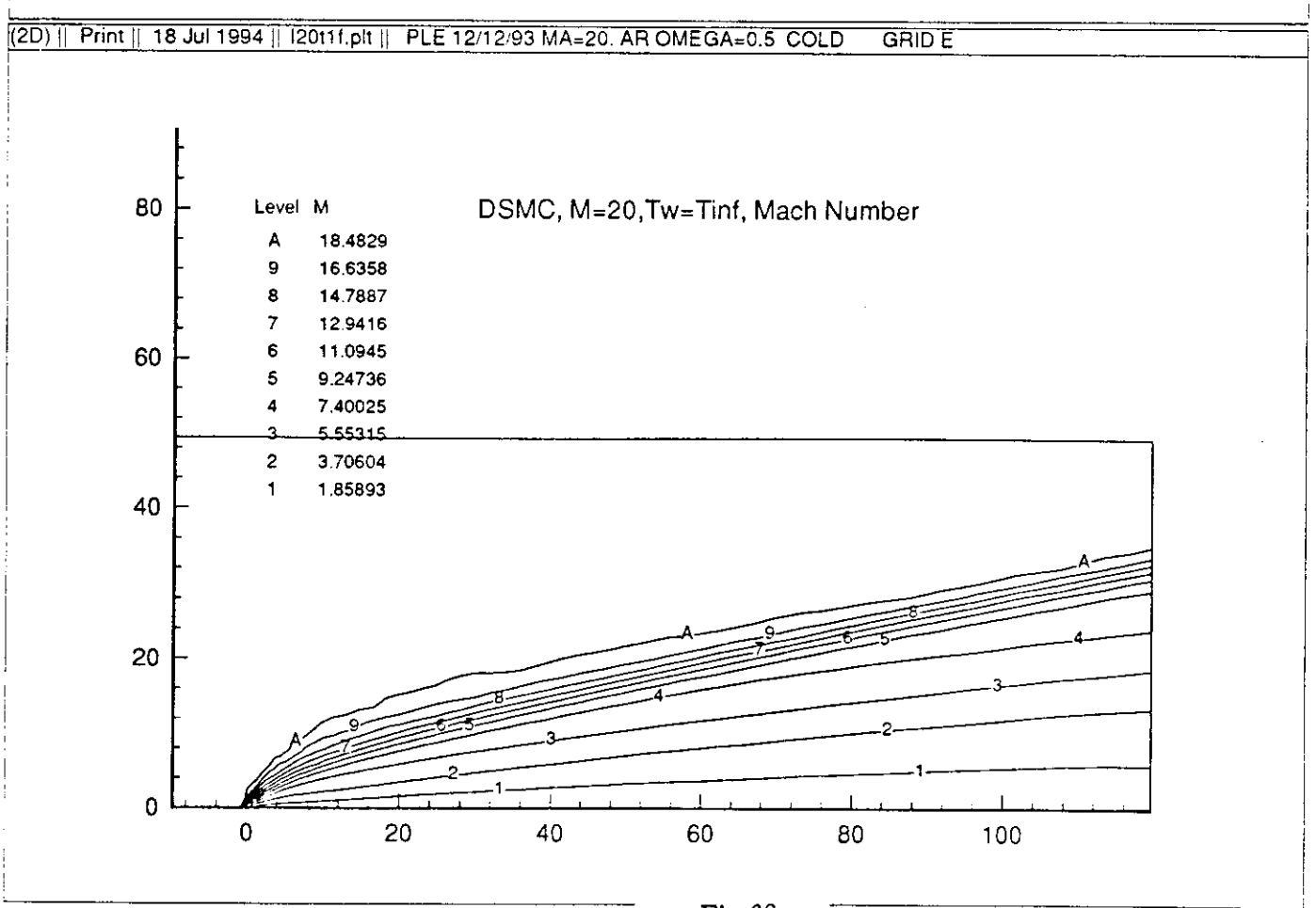
(2D) || Print || 18 Jul 1994 || I2011f.plt || PLE 12/12/93 MA=20. AR OMEGA=0.5 COLD GRID E
Level M
A 18.4829
9 16.6358
8 14.7887
7 12.9416
6 11.0945
5 9.24736
4 7.40025
3 5.55315
2 3.70604
1 1.85893
DSMC, M=20,Tw=Tinf, Mach Number
0
20
40
60
80
100

Fig.68

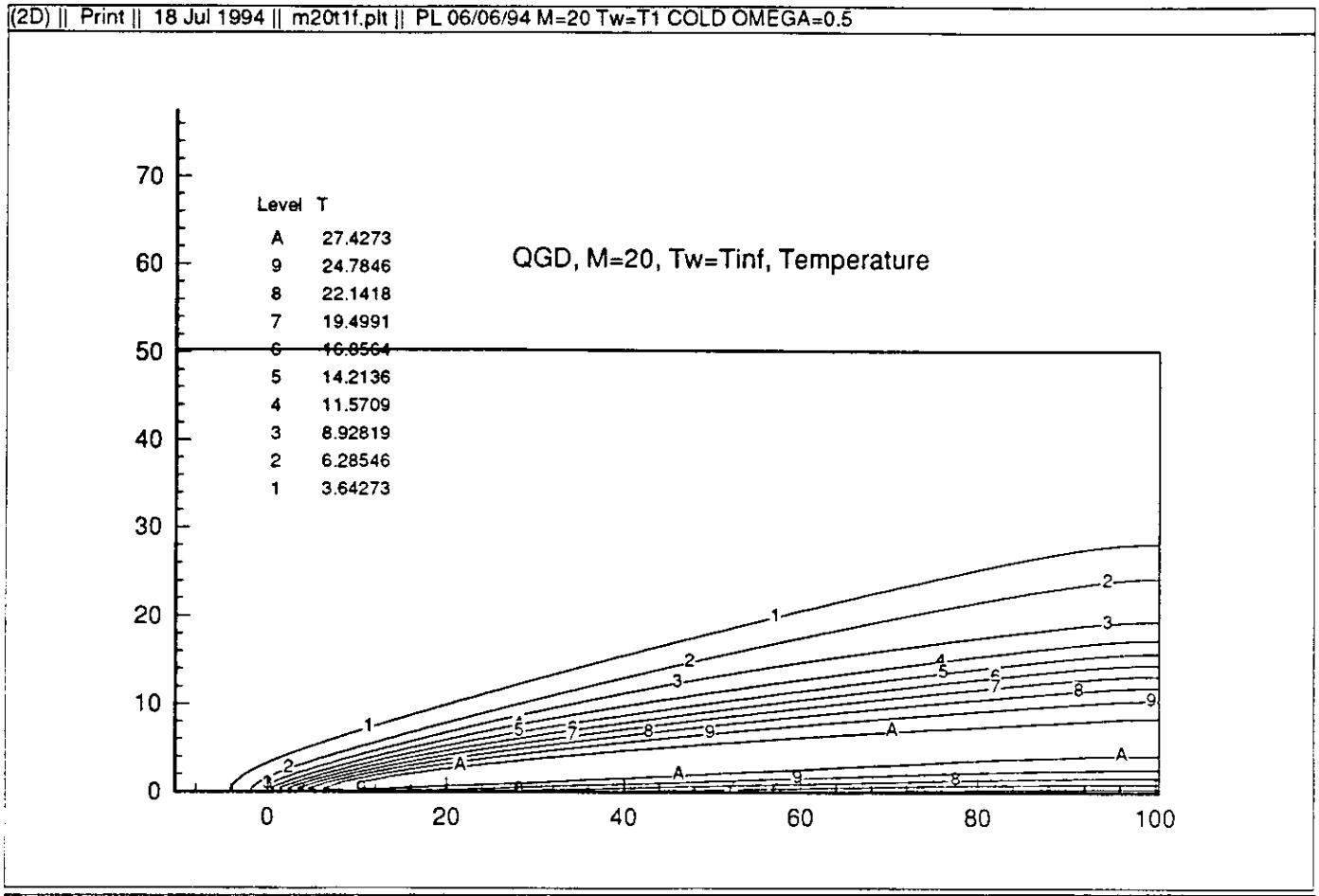
(2D) || Print || 18 Jul 1994 || m20t1f.plt || PL 06/06/94 M=20 Tw=T1 COLD OMEGA=0.5
Level T
A 27.4273
9 24.7846
8 22.1418
7 19.4991
6 16.8564
5 14.2136
4 11.5709
3 8.92819
2 6.28546
1 3.64273
QGD, M=20, Tw=Tinf, Temperature
0
10
20
30
40
50
60
70
0
20
40
60
80
100

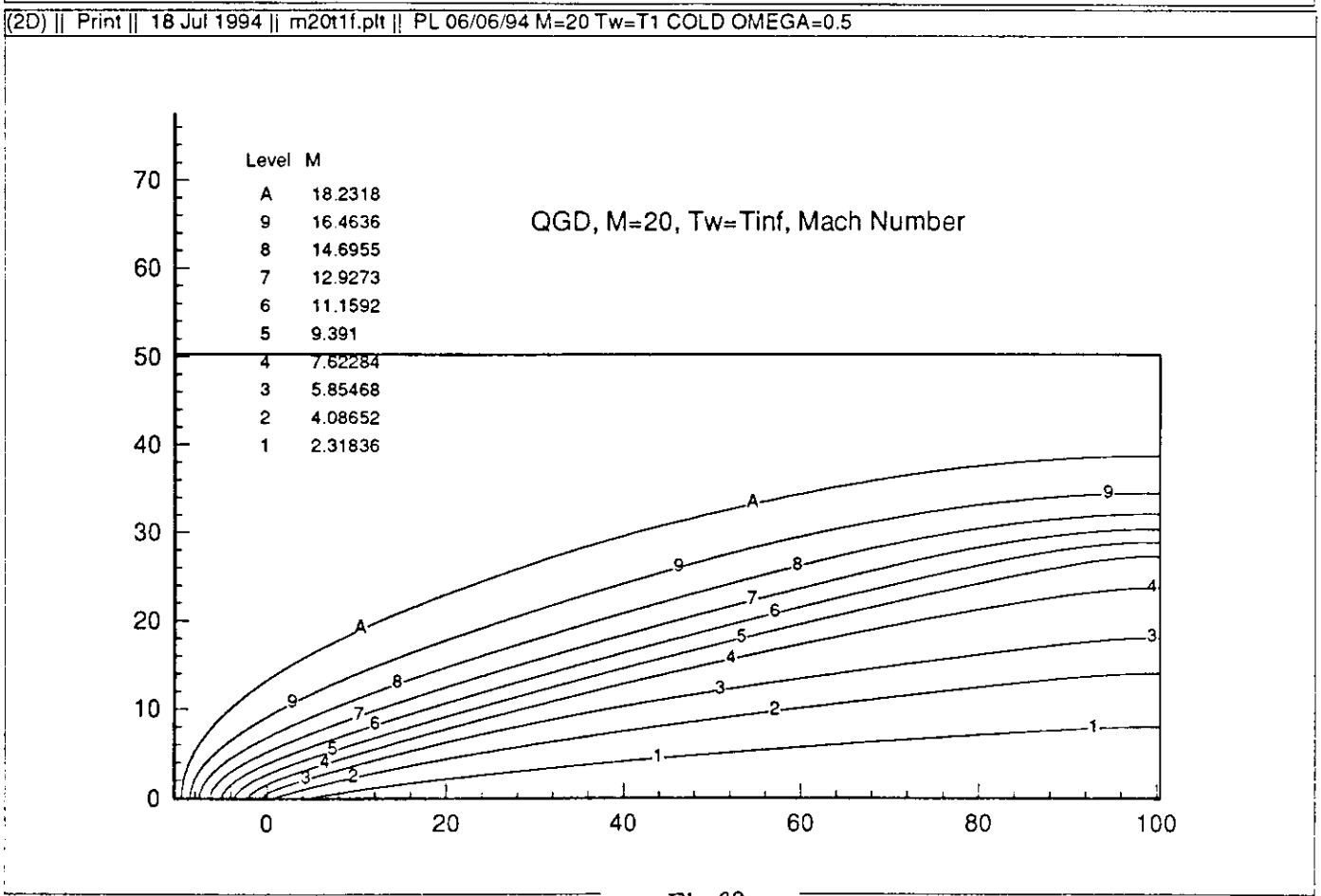
(2D) || Print || 18 Jul 1994 || m20t1f.plt || PL 06/06/94 M=20 Tw=T1 COLD OMEGA=0.5
Level M
A 18.2318
9 16.4636
8 14.6955
7 12.9273
6 11.1592
5 9.391
4 7.62284
3 5.85468
2 4.08652
1 2.31836
QGD, M=20, Tw=Tinf, Mach Number
0
10
20
30
40
50
60
70
0
20
40
60
80
100

Fig.69

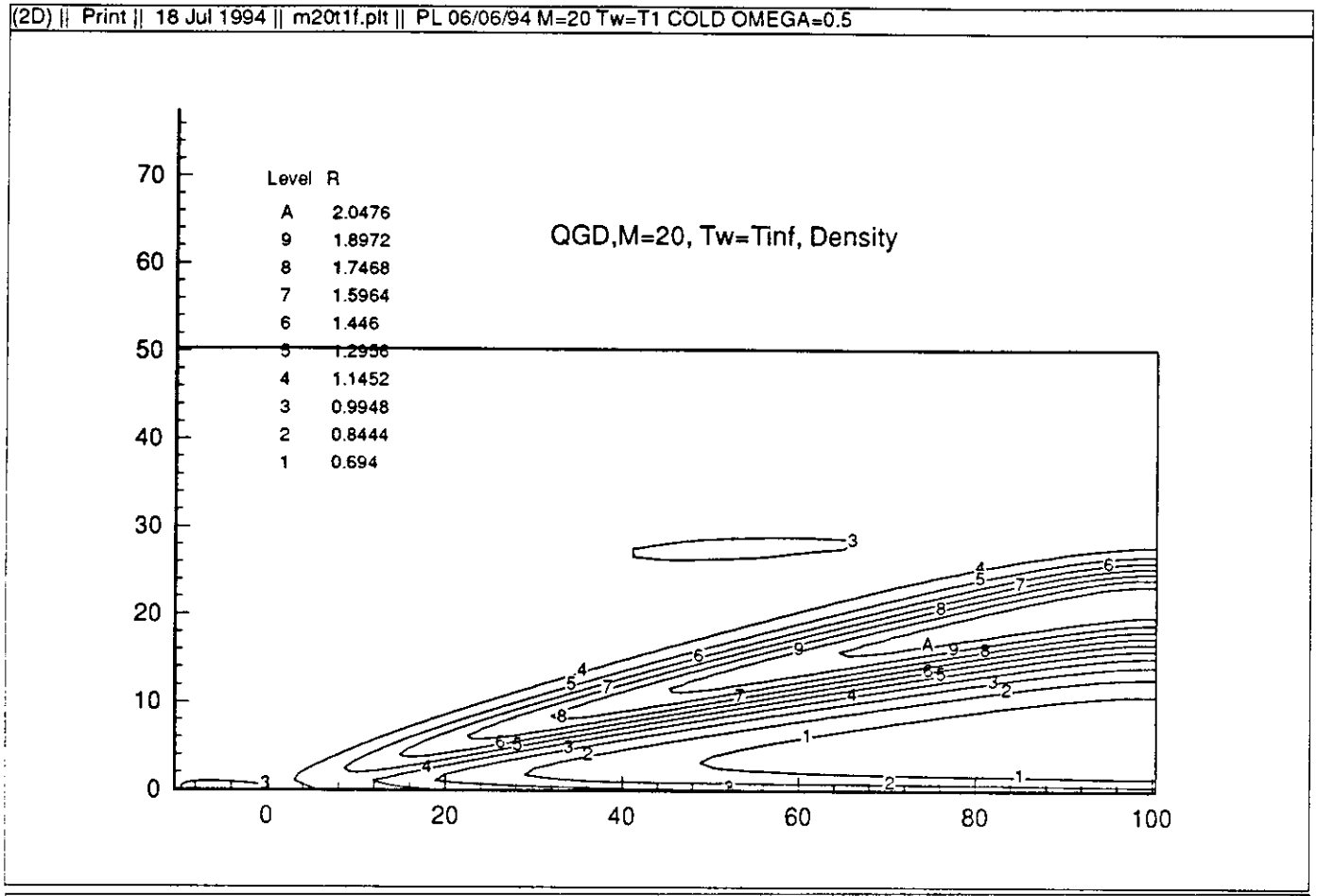
(2D) || Print || 18 Jul 1994 || m20t1f.plt || PL 06/06/94 M=20 Tw=T1 COLD OMEGA=0.5
Level R
A 2.0476
9 1.8972
8 1.7468
7 1.5964
6 1.446
5 1.2956
4 1.1452
3 0.9948
2 0.8444
1 0.694
QGD,M=20, Tw=Tinf, Density
0
10
20
30
40
50
60
70
0
20
40
60
80
100

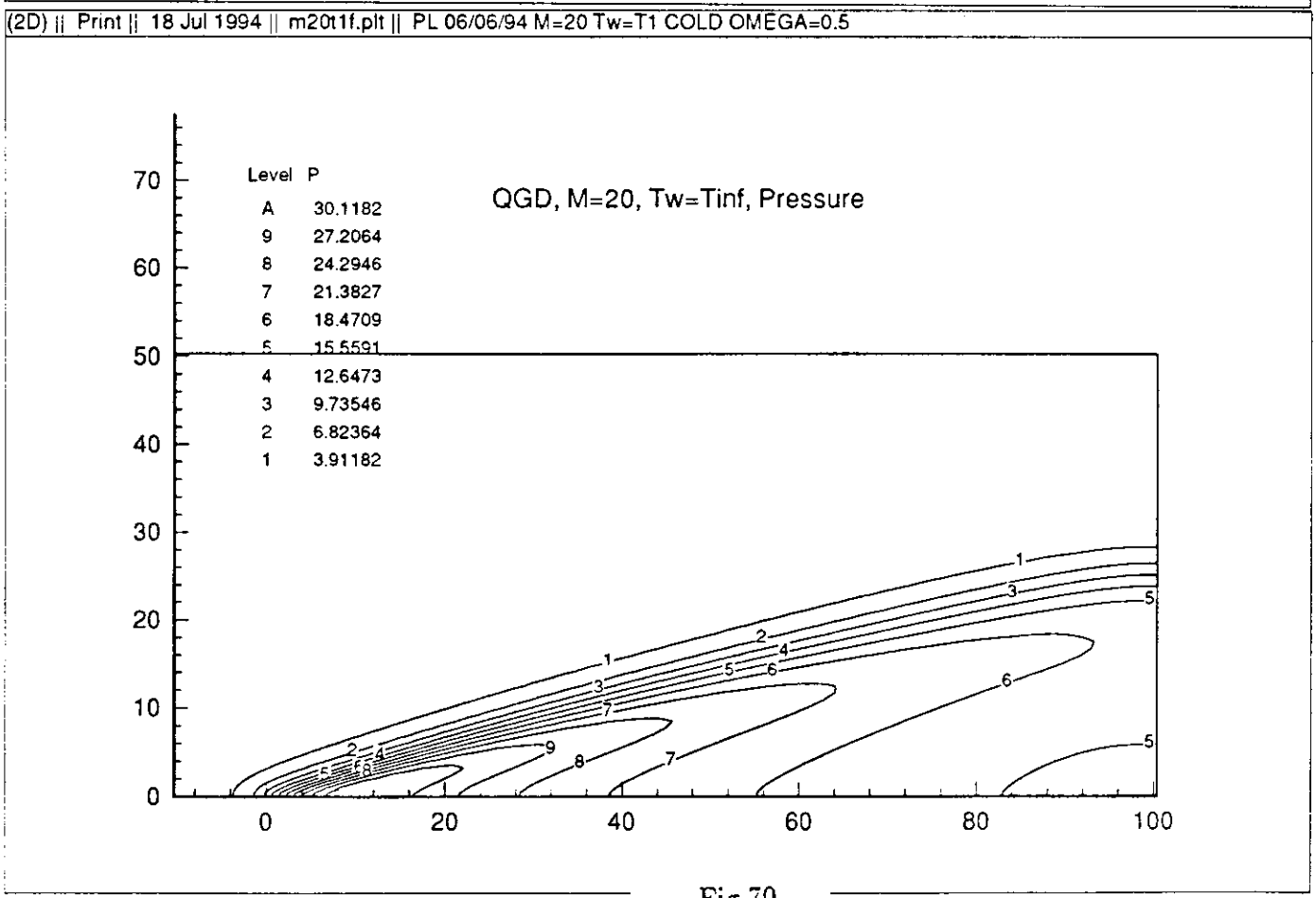
(2D) || Print || 18 Jul 1994 || m20t1f.plt || PL 06/06/94 M=20 Tw=T1 COLD OMEGA=0.5
Level P
A 30.1182
9 27.2064
8 24.2946
7 21.3827
6 18.4709
5 15.5591
4 12.6473
3 9.73546
2 6.82364
1 3.91182
QGD, M=20, Tw=Tinf, Pressure
0
10
20
30
40
50
60
70
0
20
40
60
80
100

Fig.70

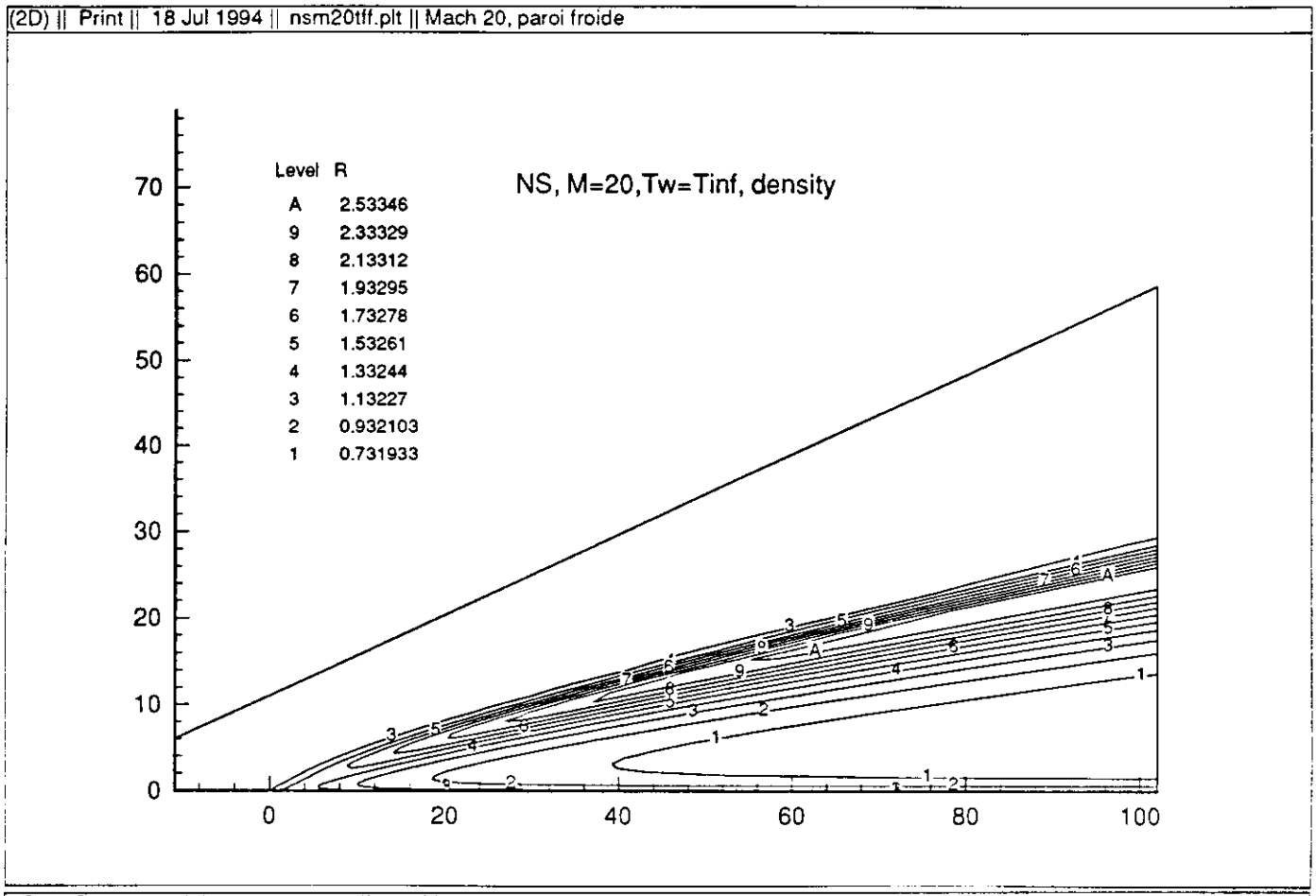
(2D) || Print || 18 Jul 1994 || nsm20tff.plt || Mach 20, paroi froide
Level R
A 2.53346
9 2.33329
8 2.13312
7 1.93295
6 1.73278
5 1.53261
4 1.33244
3 1.13227
2 0.932103
1 0.731933
NS, M=20,Tw=Tinf, density
0
10
20
30
40
50
60
70
0
20
40
60
80
100

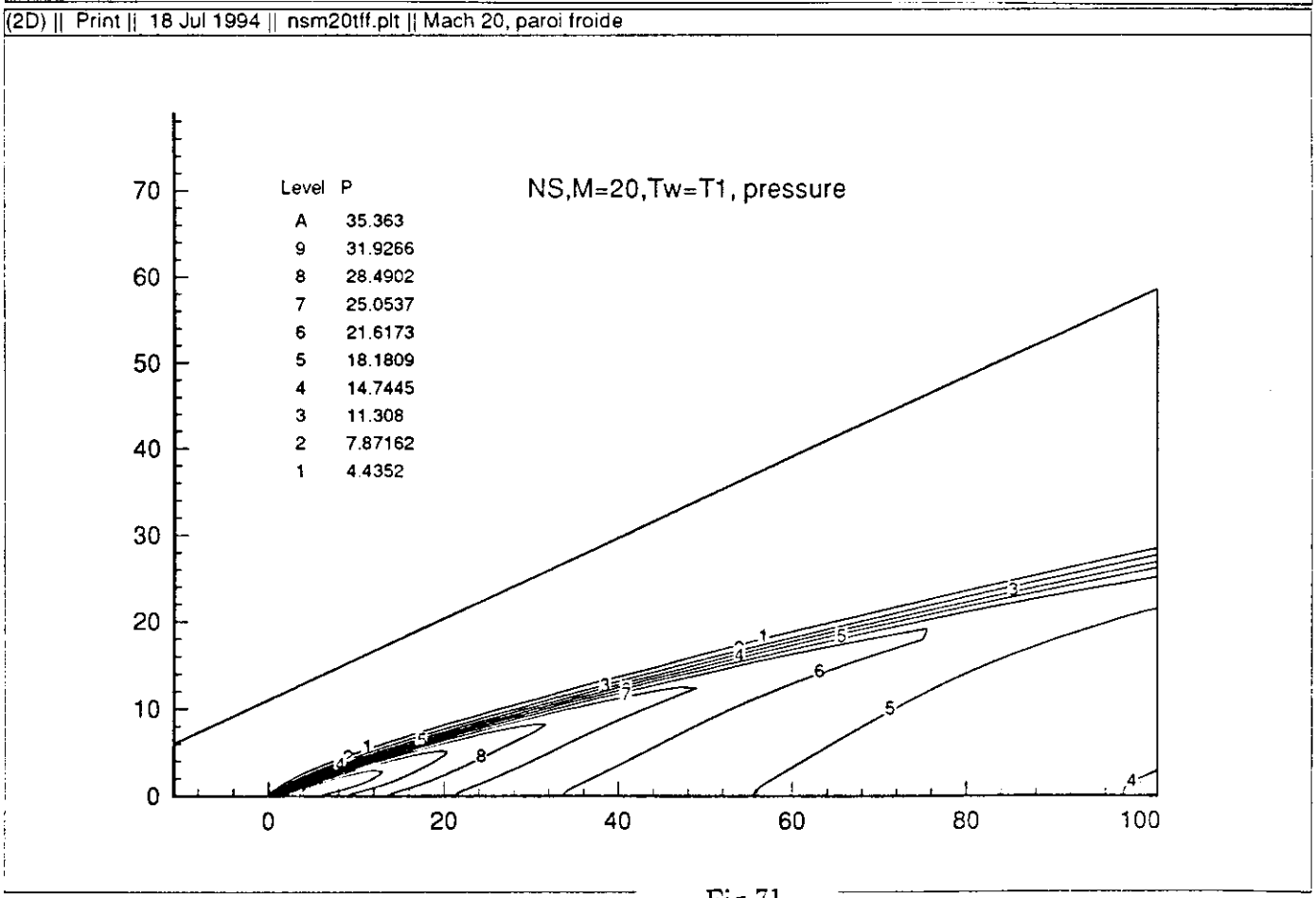
(2D) || Print || 18 Jul 1994 || nsm20tff.plt || Mach 20, paroi froide
Level P
A 35.363
9 31.9266
8 28.4902
7 25.0537
6 21.6173
5 18.1809
4 14.7445
3 11.308
2 7.87162
1 4.4352
NS,M=20,Tw=T1, pressure
0
10
20
30
40
50
60
70
0
20
40
60
80
100

Fig.71

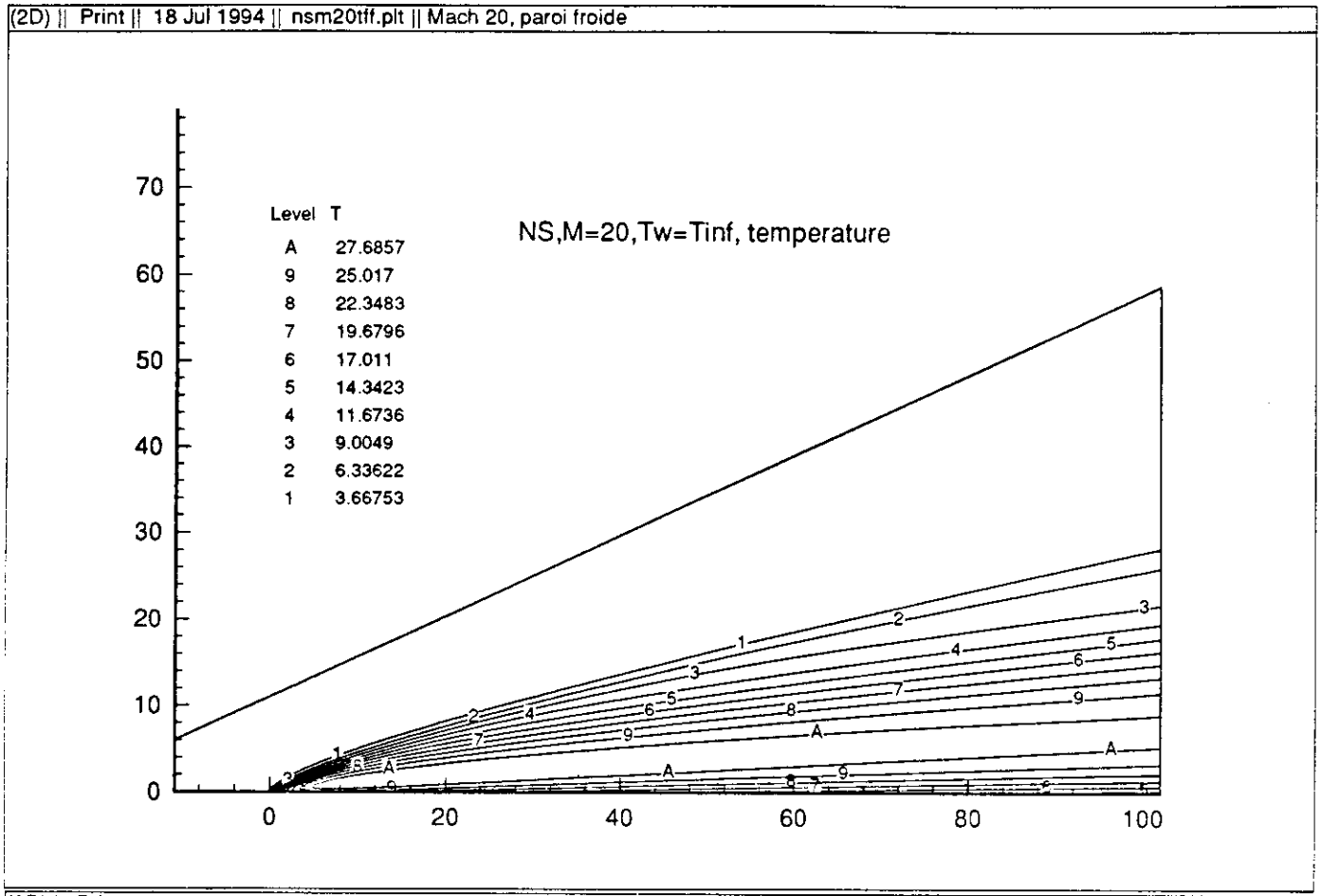
(2D) || Print || 18 Jul 1994 || nsm20tff.plt || Mach 20, paroi froide
NS,M=20,Tw=Tinf, temperature
Level T
A 27.6857
9 25.017
8 22.3483
7 19.6796
6 17.011
5 14.3423
4 11.6736
3 9.0049
2 6.33622
1 3.66753
0
10
20
30
40
50
60
70
0
20
40
60
80
100

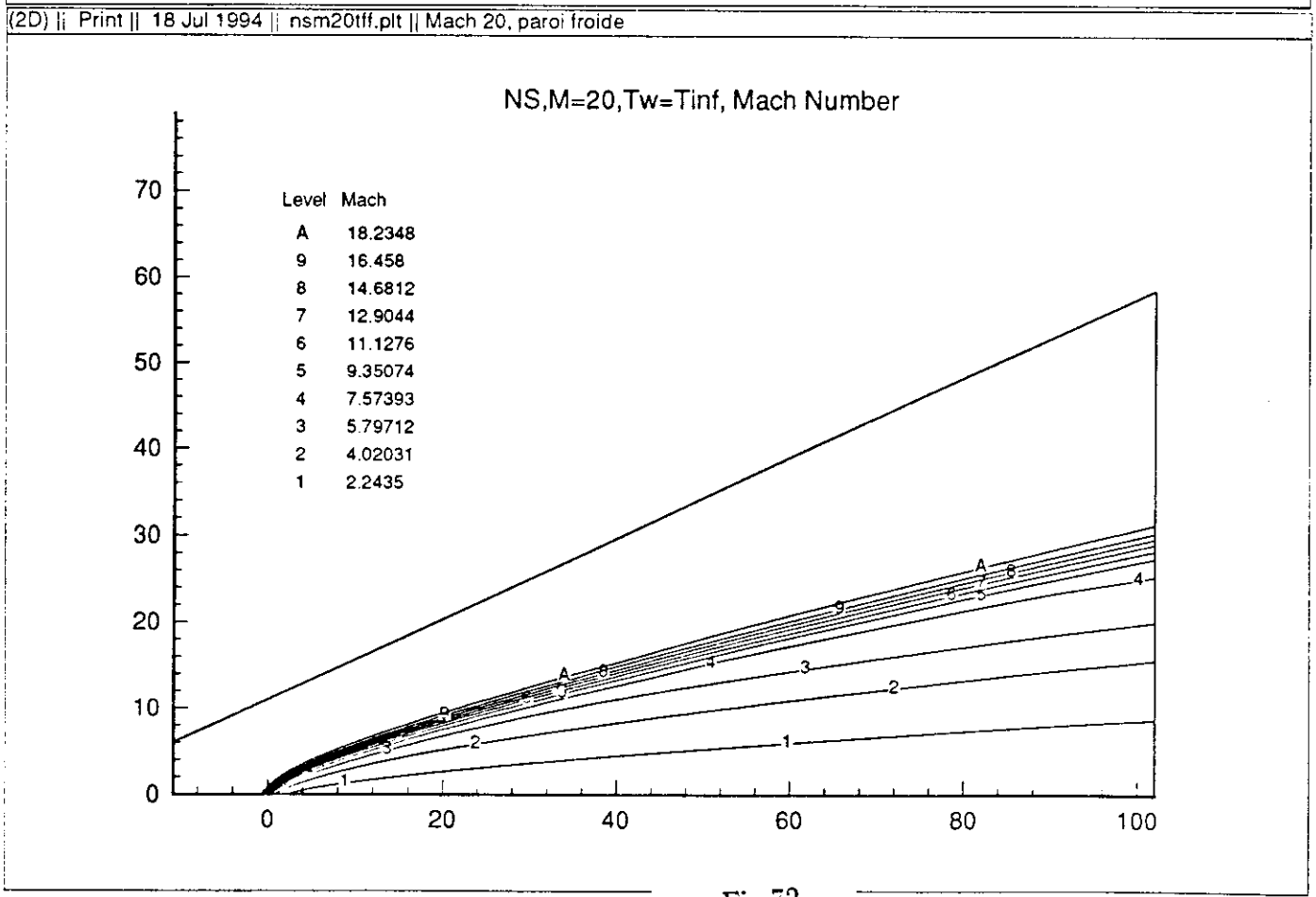
(2D) || Print || 18 Jul 1994 || nsm20tff.plt || Mach 20, paroi froide
NS,M=20,Tw=Tinf, Mach Number
Level Mach
A 18.2348
9 16.458
8 14.6812
7 12.9044
6 11.1276
5 9.35074
4 7.57393
3 5.79712
2 4.02031
1 2.2435
0
10
20
30
40
50
60
70
0
20
40
60
80
100

Fig.72

Sensitivity studies

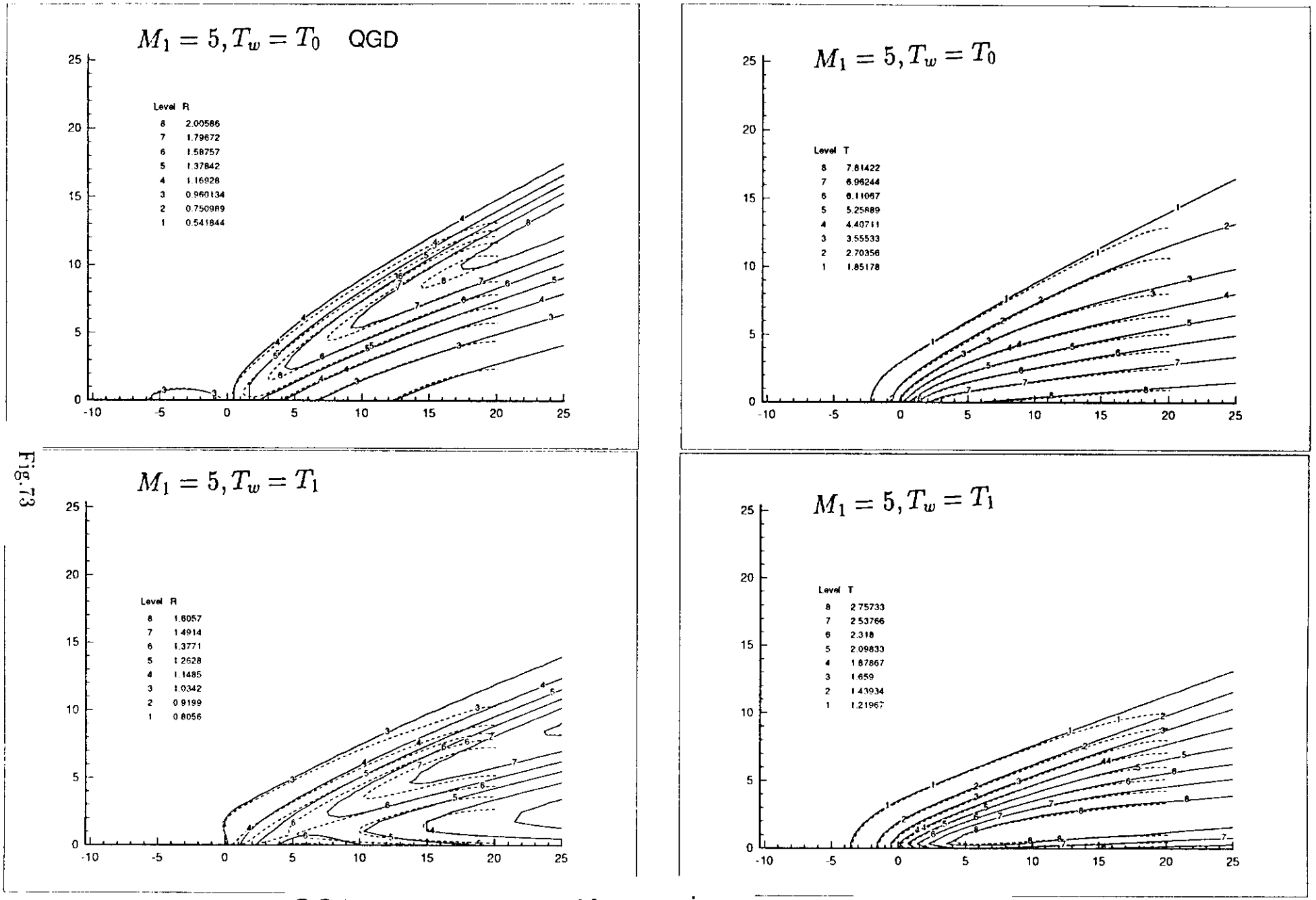

Fig. 73

QGD Coarse vs fine grid comparison

—— coarse

····· fine

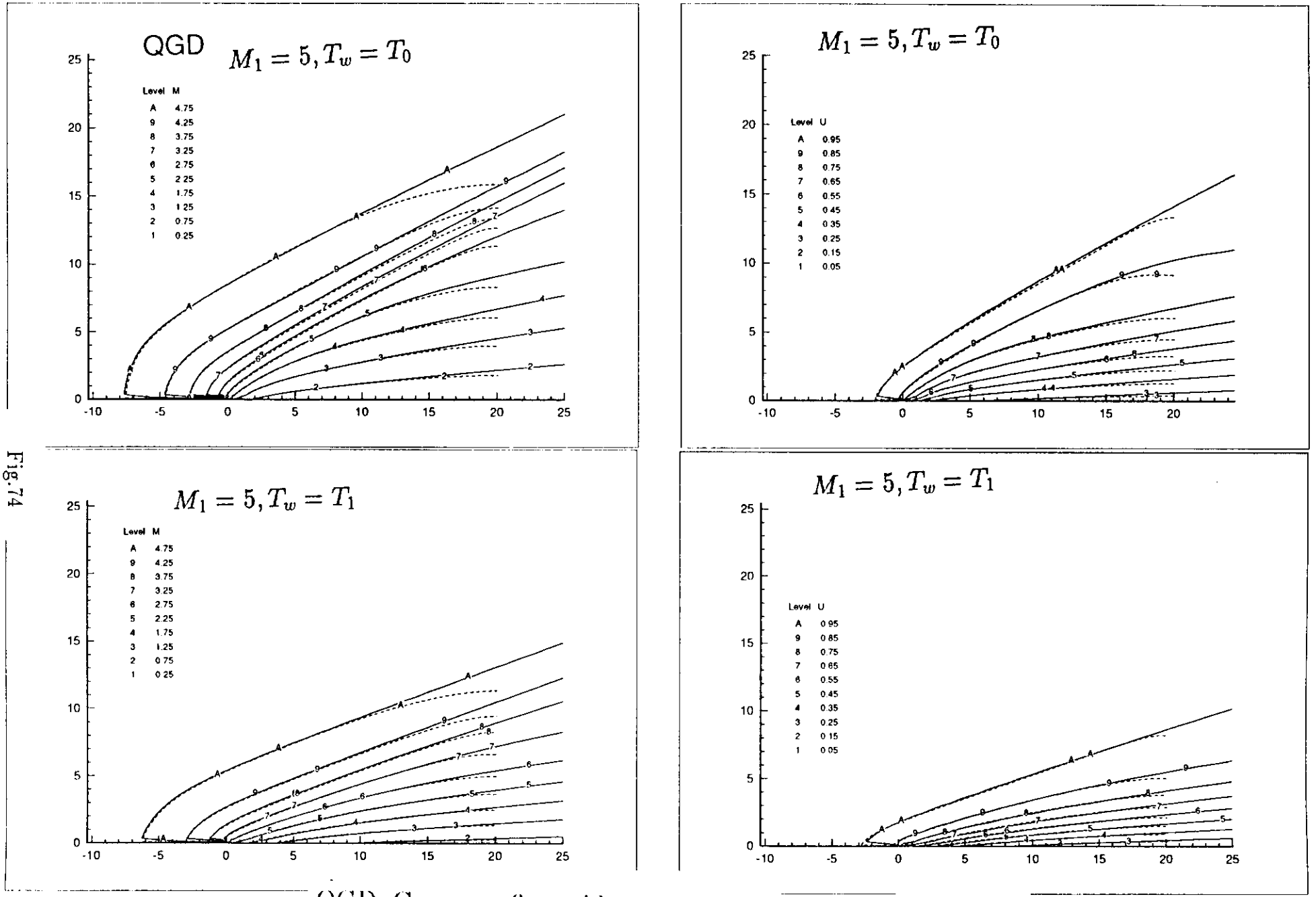

Fig. 74

QGD Coarse vs fine grid comparison

—— coarse

..... fine

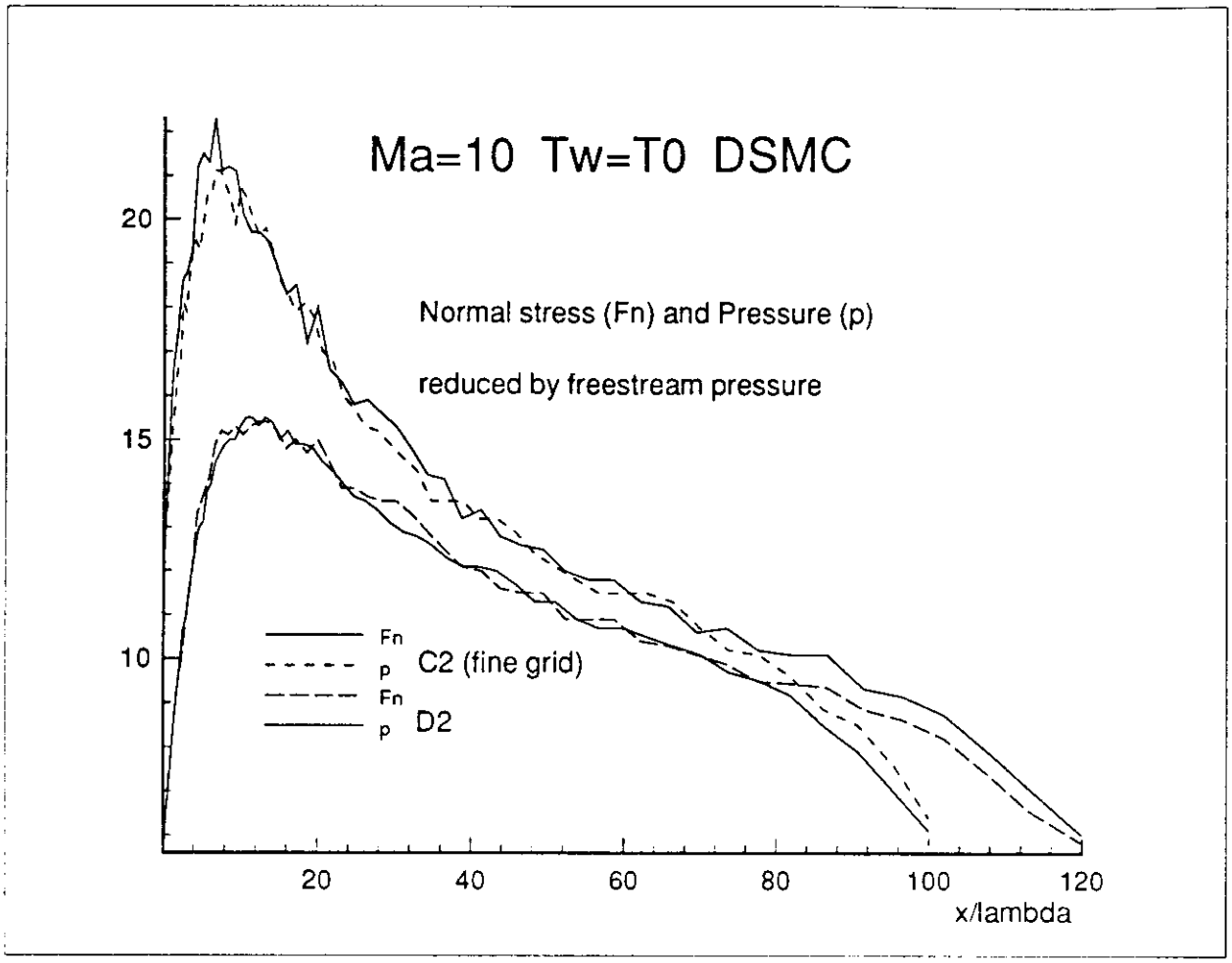
Ma=10 Tw=T0 DSMC
Normal stress (Fn) and Pressure (p)
reduced by freestream pressure
Fn
p
C2 (fine grid)
Fn
p
D2
20
15
10
20
40
60
80
100
120
x/lambda

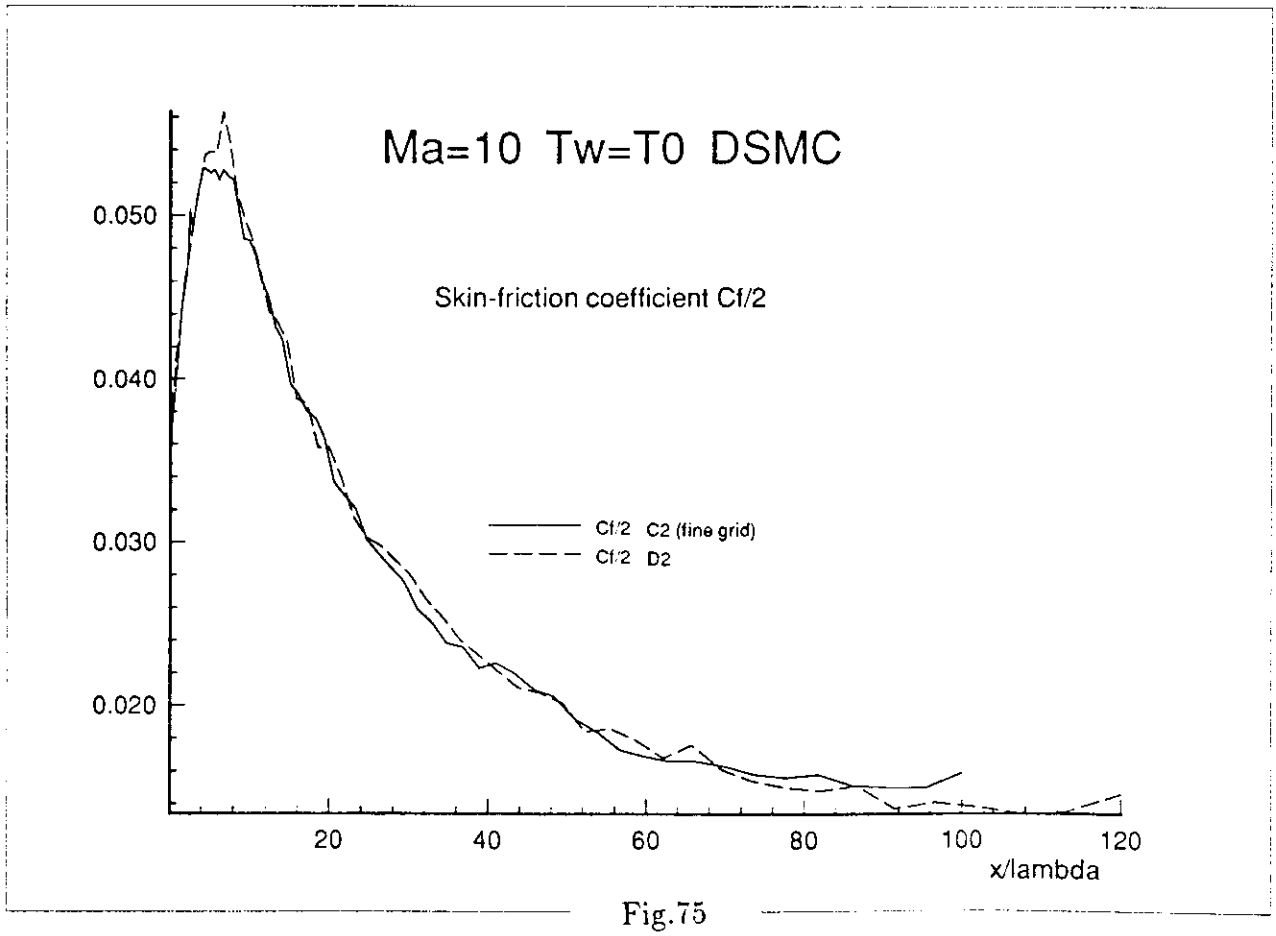
Ma=10 Tw=T0 DSMC
Skin-friction coefficient Cf/2
Cf/2 C2 (fine grid)
Cf/2 D2
0.050
0.040
0.030
0.020
20
40
60
80
100
120
x/lambda

Fig.75

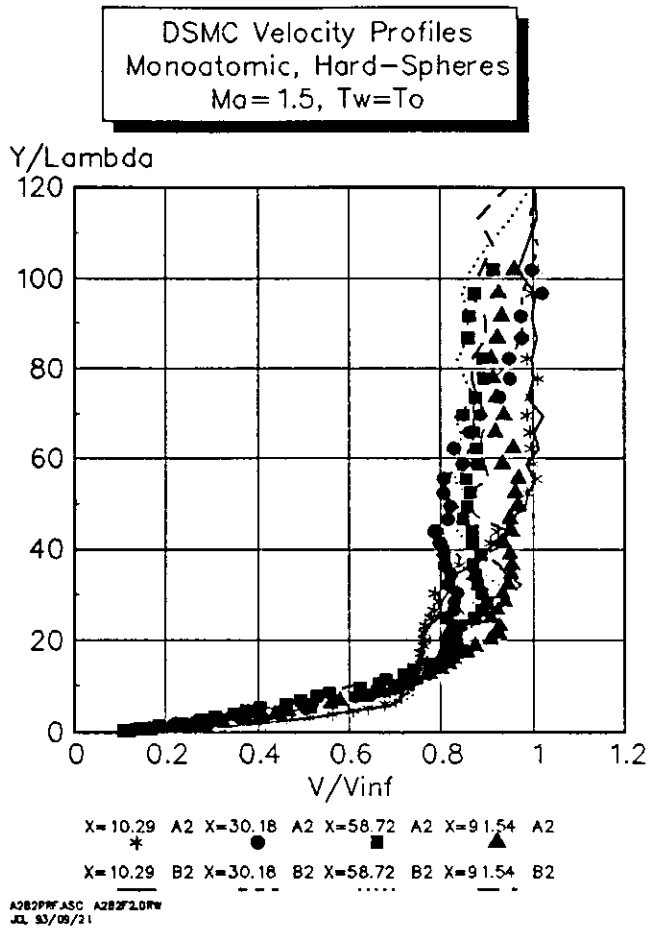
DSMC Velocity Profiles
Monoatomic, Hard-Spheres
Ma=1.5, Tw=To
Y/Lambda
V/Vinf
X=10.29 A2 X=30.18 A2 X=58.72 A2 X=91.54 A2
X=10.29 B2 X=30.18 B2 X=58.72 B2 X=91.54 B2

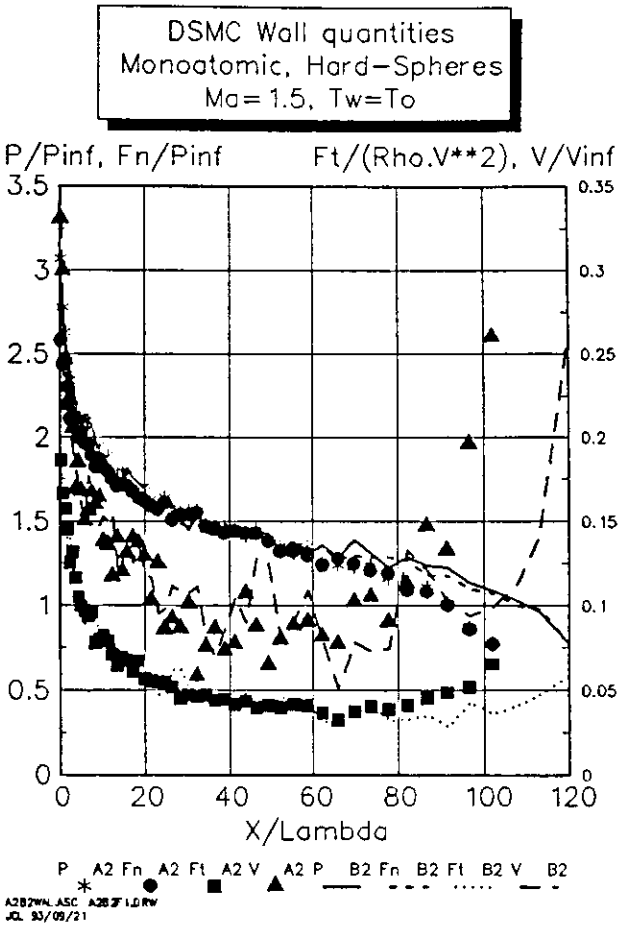
DSMC Wall quantities
Monoatomic, Hard-Spheres
Ma=1.5, Tw=To
P/Pinf, Fn/Pinf
Ft/(Rho.V**2), V/Vinf
X/Lambda
P A2 Fn A2 Ft A2 V A2 P B2 Fn B2 Ft B2 V B2

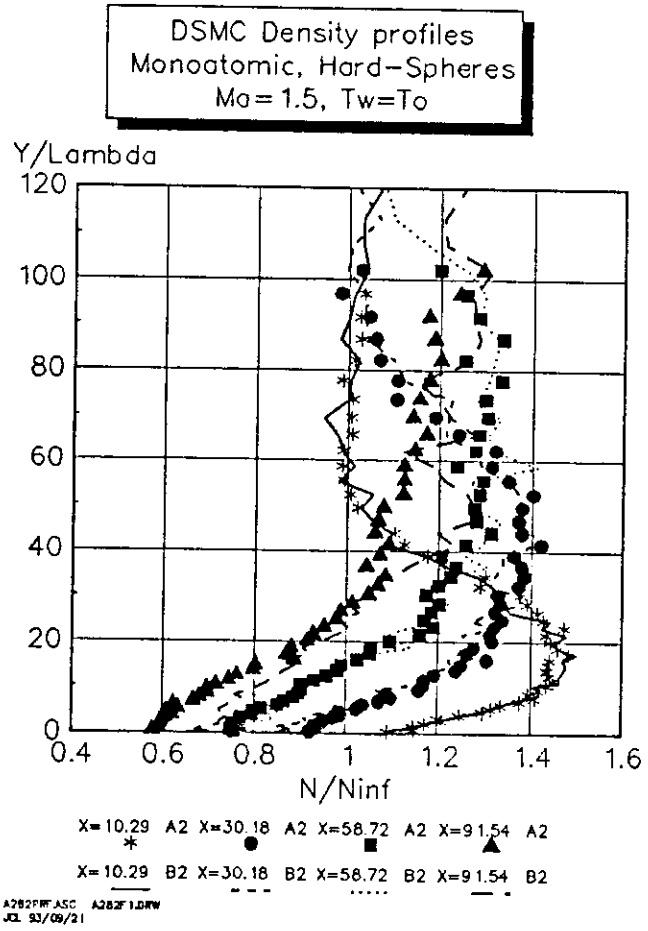
DSMC Density profiles
Monoatomic, Hard-Spheres
Ma=1.5, Tw=To
Y/Lambda
N/Ninf
X=10.29 A2 X=30.18 A2 X=58.72 A2 X=91.54 A2
X=10.29 B2 X=30.18 B2 X=58.72 B2 X=91.54 B2

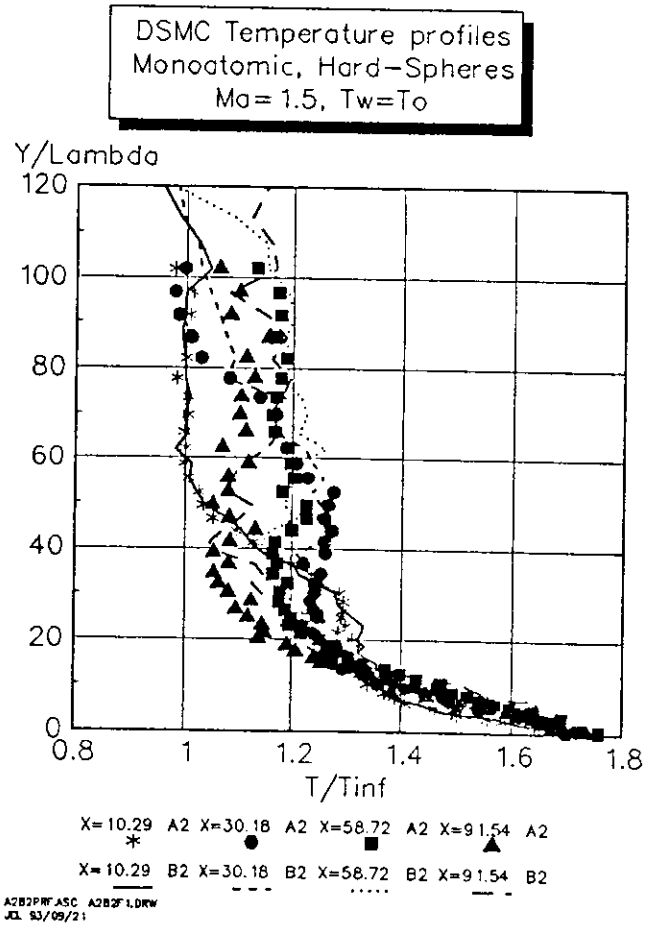
DSMC Temperature profiles
Monoatomic, Hard-Spheres
Ma=1.5, Tw=To
Y/Lambda
T/Tinf
X=10.29 A2 X=30.18 A2 X=58.72 A2 X=91.54 A2
X=10.29 B2 X=30.18 B2 X=58.72 B2 X=91.54 B2

Fig.76

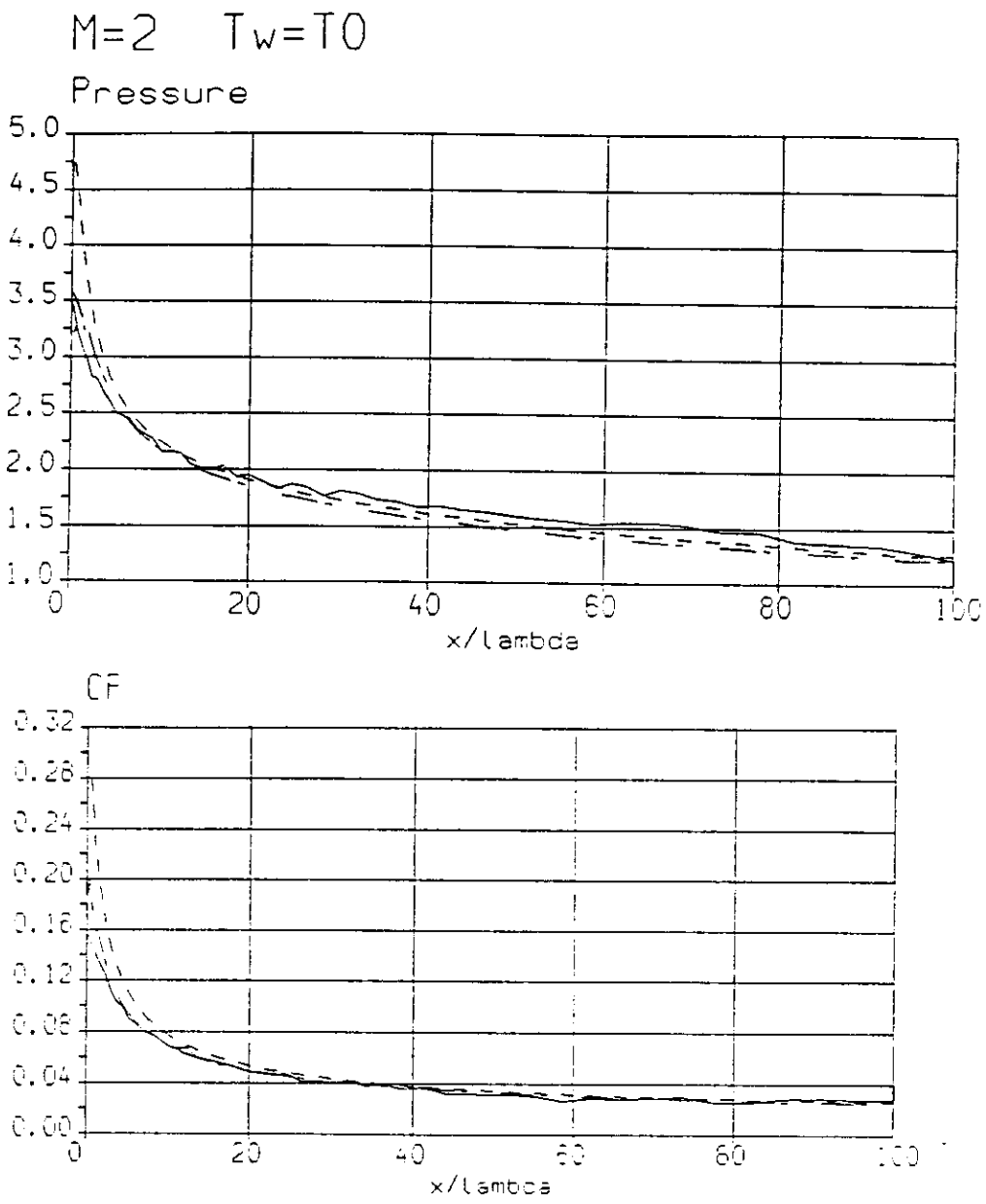

QGD Slip vs no-slip BC comparison

——— DSMC
– – – QGD no-slip BC
— · — · QGD slip BC

Fig.77

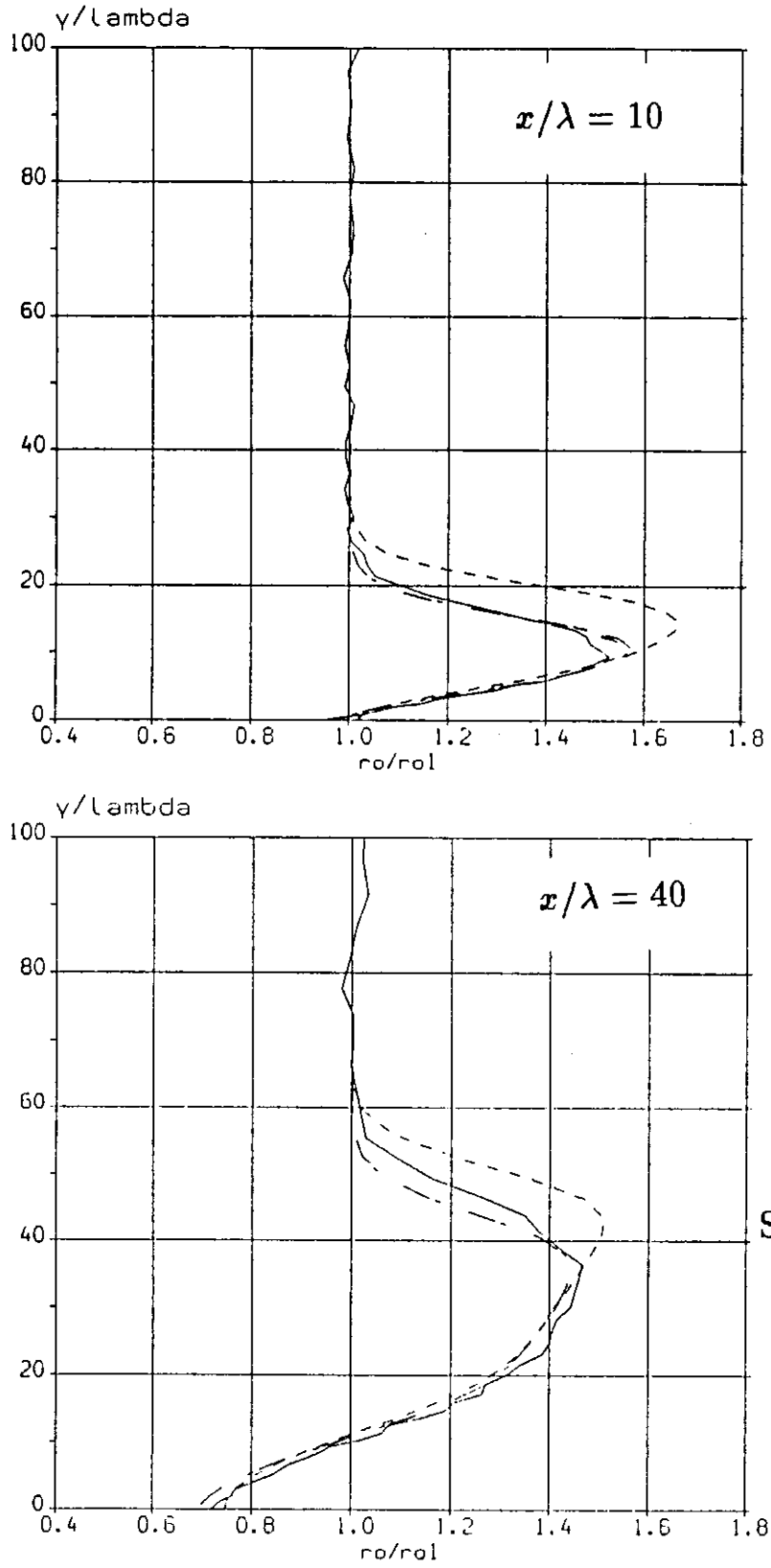
Density profiles
M=2 Tw=T0
y/lambda
$x/\lambda = 10$
$x/\lambda = 40$
ro/ro1
Slip vs no-slip BC comparison
DSMC
QGD no-slip BC
QGD slip BC

Fig.78

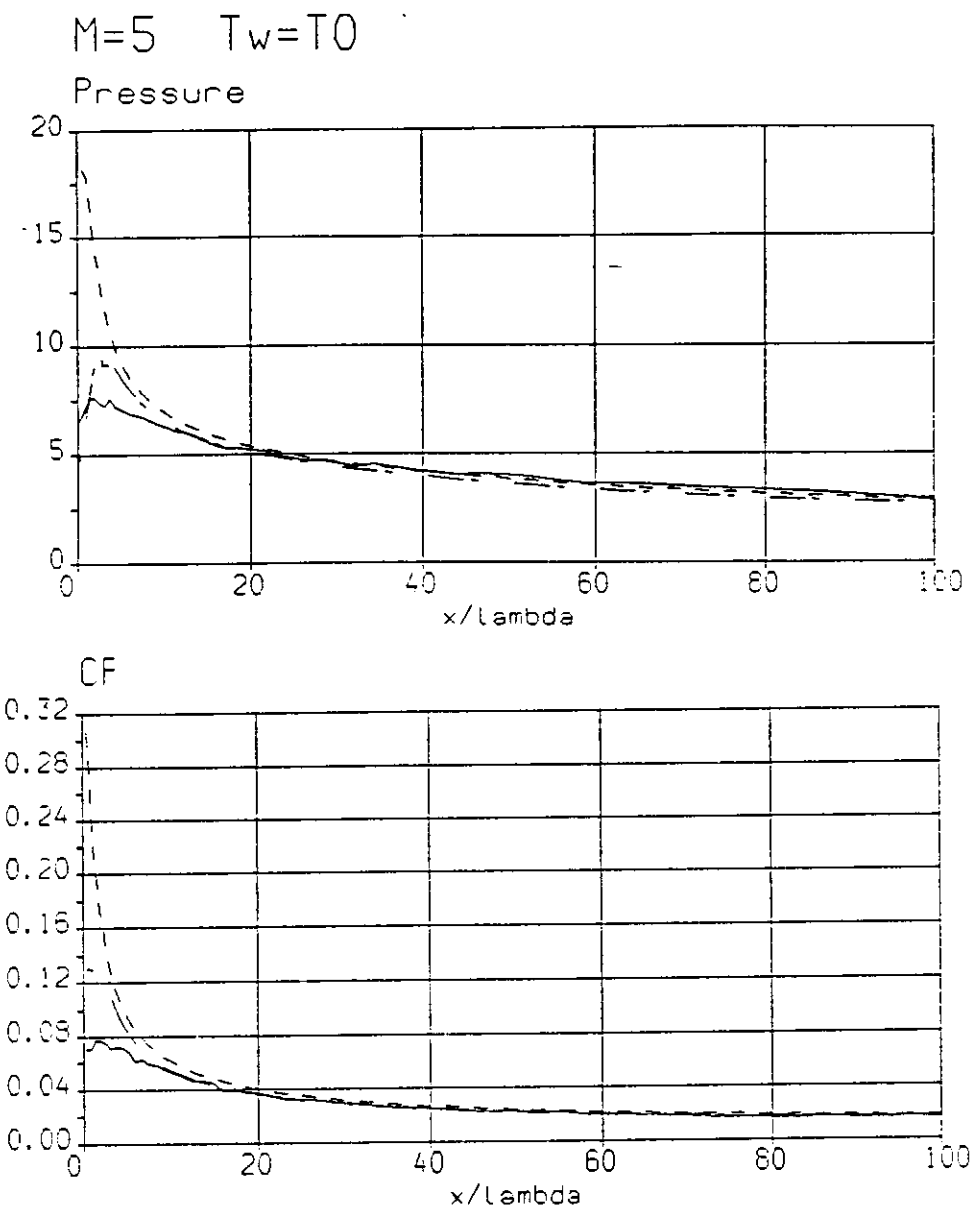

Slip vs no-slip BC comparison

——— DSMC
– – – QGD no-slip BC
—·—· QGD slip BC

Fig.79

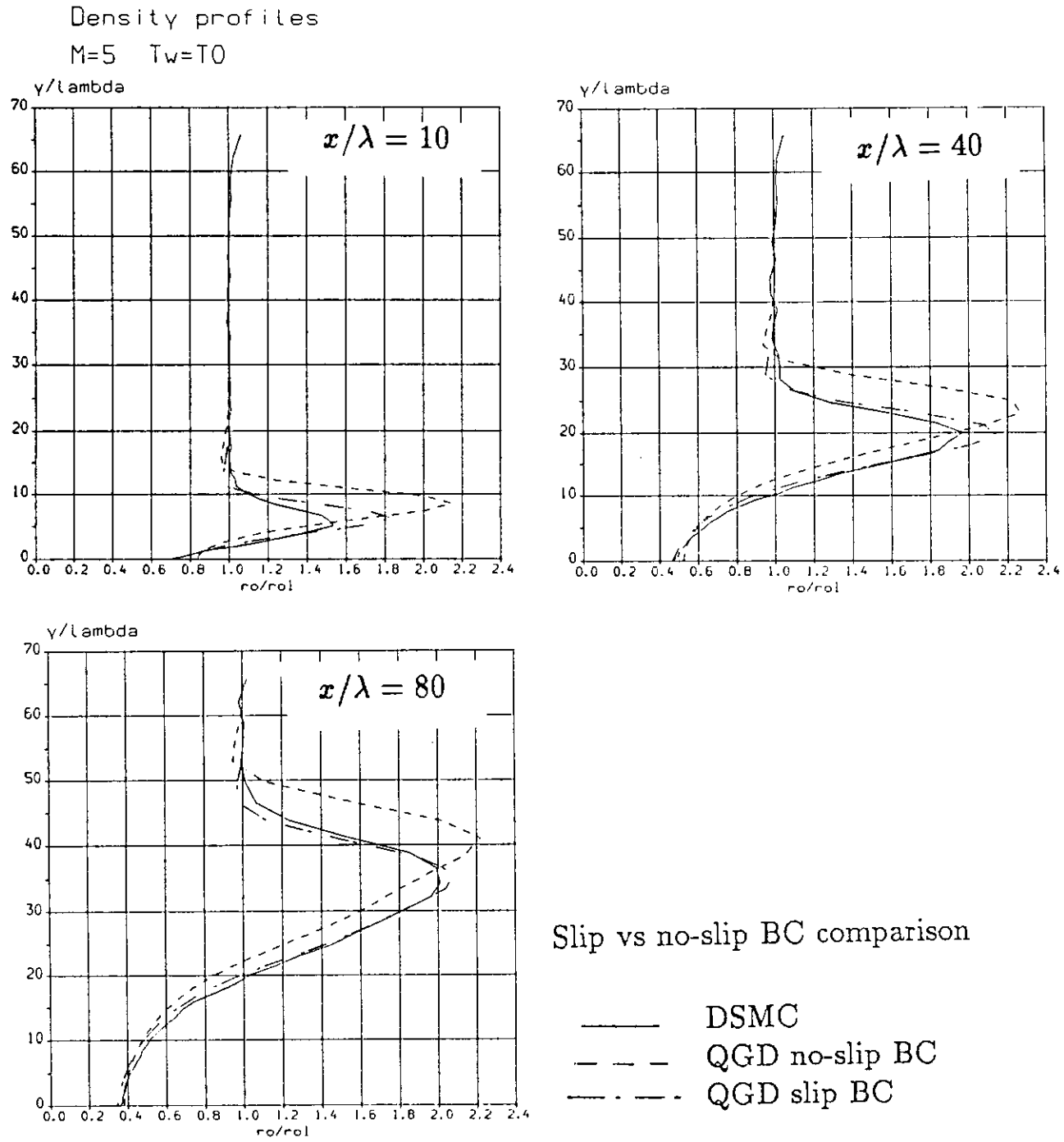
Density profiles
M=5 Tw=T0
y/lambda
$x/\lambda = 10$
$x/\lambda = 40$
$x/\lambda = 80$
ro/ro1
Slip vs no-slip BC comparison
DSMC
QGD no-slip BC
QGD slip BC

Fig.80

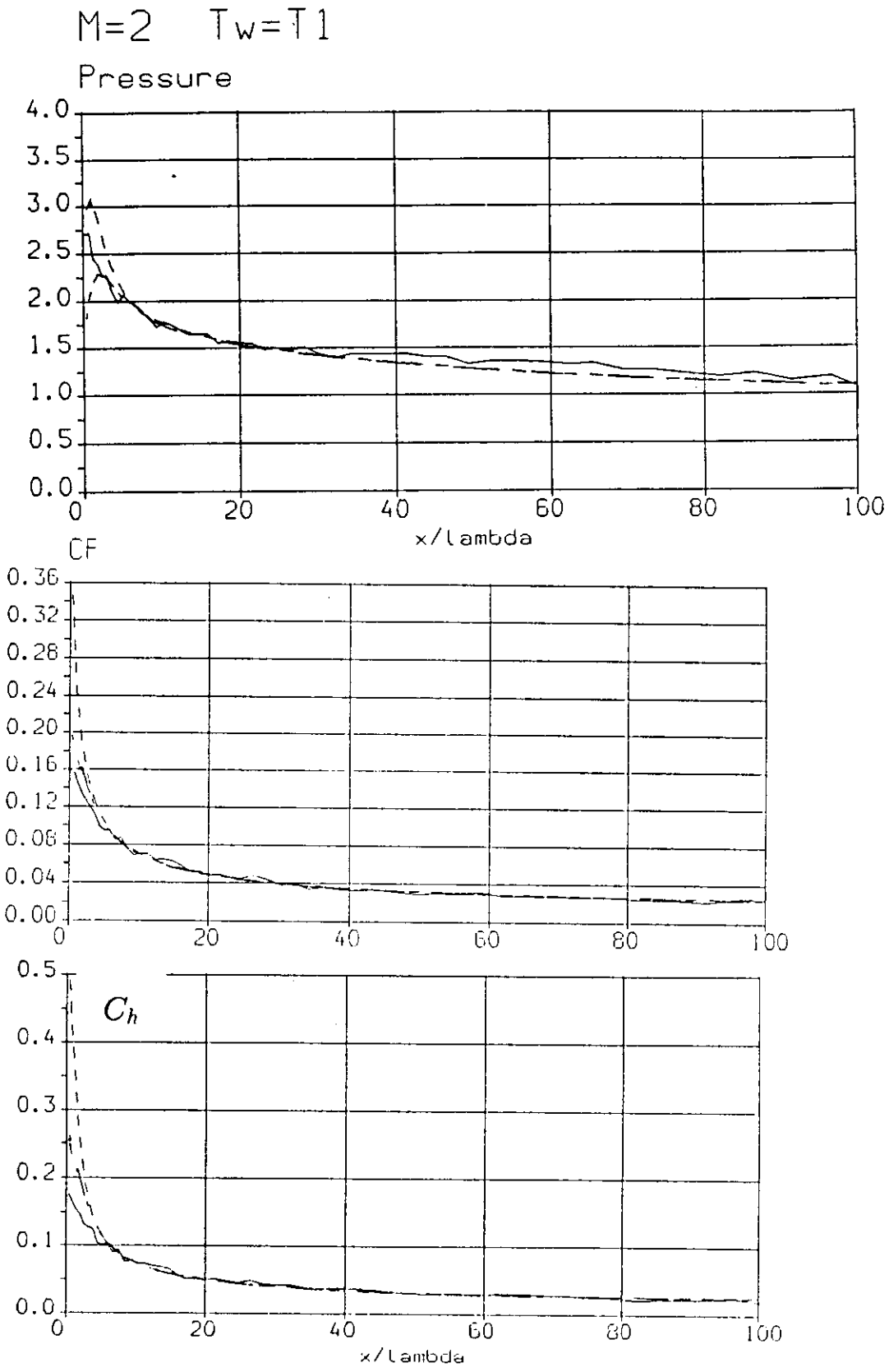

Fig.81 Slip vs no-slip BC comparison

——— DSMC
– – – QGD no-slip BC
—·—· QGD slip BC

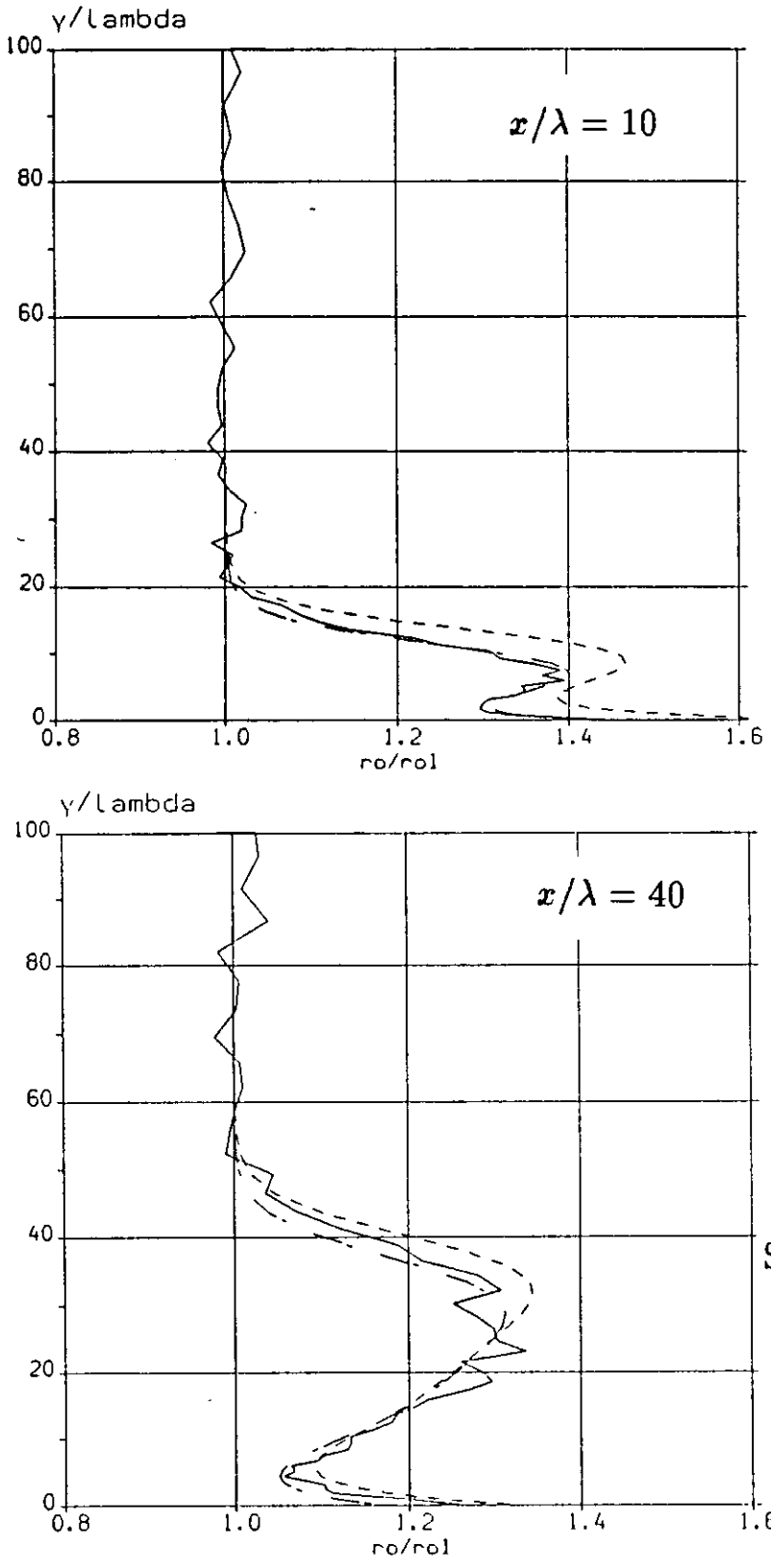
Density profiles
M=2 Tw=T1
y/lambda
100
80
60
40
20
0
0.8
1.0
1.2
1.4
1.6
ro/rol
$x/\lambda = 10$
y/lambda
100
80
60
40
20
0
0.8
1.0
1.2
1.4
1.6
ro/rol
$x/\lambda = 40$
Slip vs no-slip BC comparison
DSMC
QGD no-slip BC
QGD slip BC

Fig.82

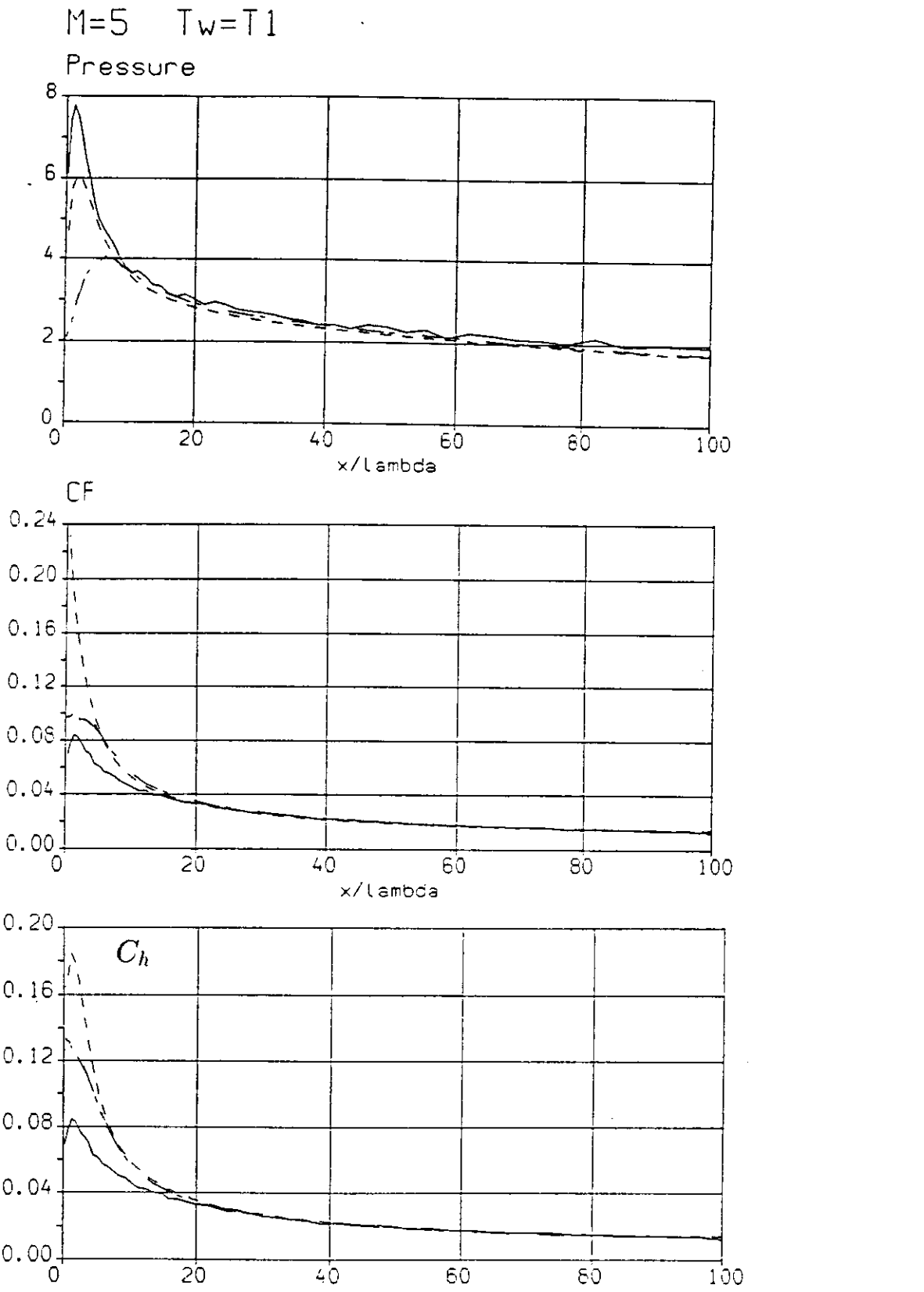

Slip vs no-slip BC comparison

Fig.83

——— DSMC

– – – QGD no-slip BC

—·—· QGD slip BC

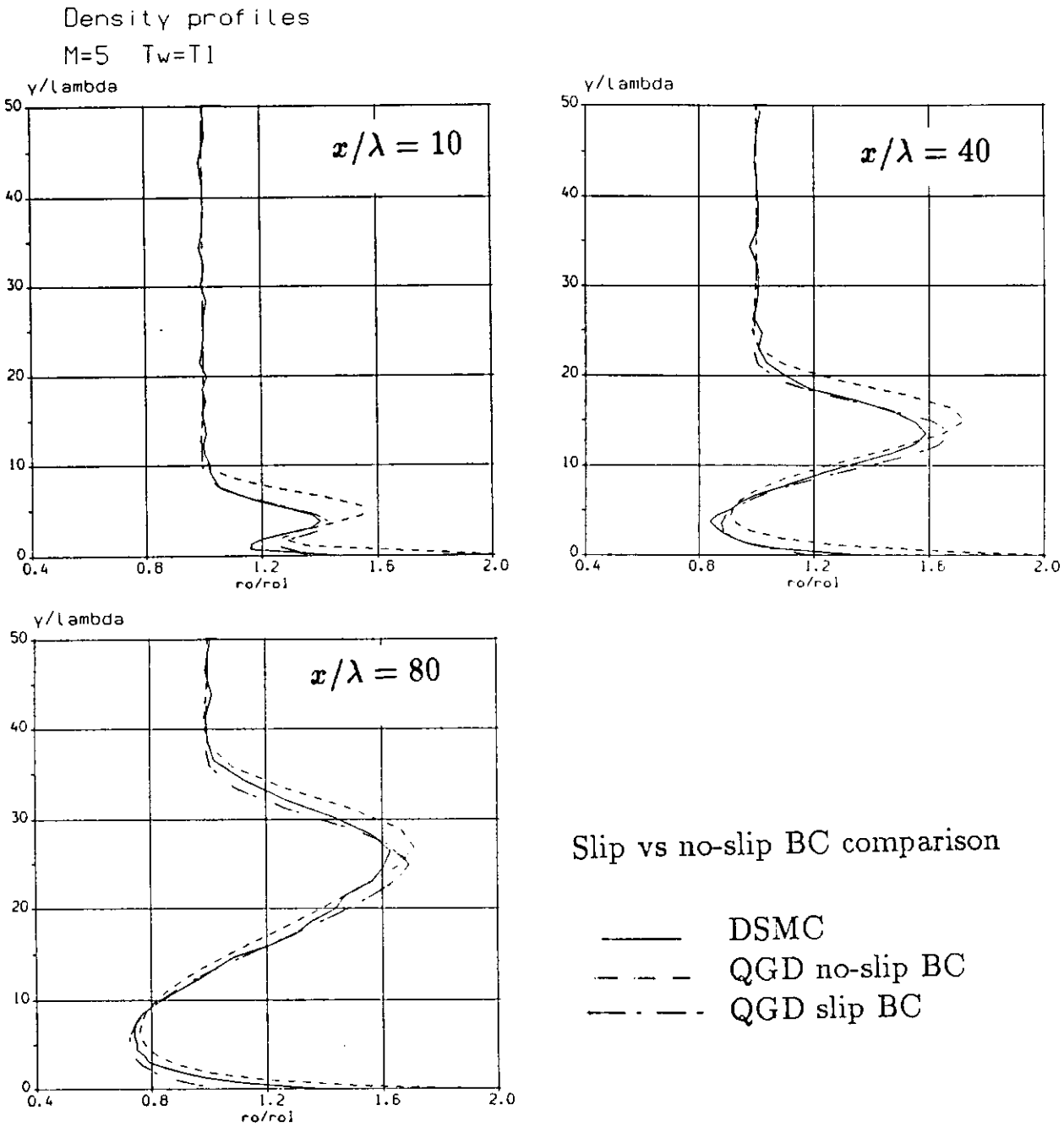
Density profiles
M=5 Tw=T1
y/lambda
$x/\lambda = 10$
$x/\lambda = 40$
$x/\lambda = 80$
ro/ro1
0.4
0.8
1.2
1.6
2.0
0
10
20
30
40
50
Slip vs no-slip BC comparison
DSMC
QGD no-slip BC
QGD slip BC

Fig.84

Réalisé avec le concours du Service Imprimerie de la
DELEGATION REGIONALE ILE DE FRANCE - Secteur Ouest et Nord
1, Place Aristide Briand - 92195 Meudon Cédex - Tél 45 07 50 50 - Télex 634002 F